DOE/PC/90054--T17

Novel Nanodispersed Coal Liquefaction Catalysts: Molecular Design Via Microemulsion-Based Synthesis

Final Technical Report
October 1990 - December 1994

by

K. Osseo-Asare, E. Boakye, M. Vittal and L. R. Radovic

Department of Materials Science and Engineering
The Pennsylvania State University
University Park, PA 16802

April 1995

DISCLAIMER

TABLE OF CONTENTS

LIST OF FIGURES

LIST OF TABLES

CHAPTER 1

INTRODUCTION AND OBJECTIVES

1.1 SOME ASPECTS OF HETEROGENEOUS CATALYSIS

In the United States, about 90% of the industrial production of fuels and chemicals involves the use of catalysts (1). The recent emphasis on environmental issues has provided another area in which catalysis can have an impact. Thus, interest in catalyst research and development is ever on the increase.

It is well recognized that the performance of a heterogeneous metal catalyst is directly related to its dispersion. The term *dispersion* refers to the percentage of metal atoms exposed to reactants. Catalyst dispersion may be increased by spreading the metal on a solid carrier to produce what is known as a *supported catalyst*. In applications such as direct coal liquefaction, supported catalysts cannot achieve intimate contact with the coal; and in the thermocatalytic hydroconversion of heavy petroleum feedstocks, they suffer from deactivation problems. This difficulty has spawned the development of *unsupported (or dispersed) catalysts* for these processes.

Of fundamental importance to catalysis is the influence of particle size on catalytic properties. For supported metals, a review of the literature in this area has been given recently by Che and Bennett (2). However, for unsupported catalysts, the literature on correlations between catalyst particle size and activity is scarce. One reason for this is the paucity – until recently – of simple, reproducible means of fabricating ultrafine, monodispersed inorganic solids in the laboratory. However, this situation has been somewhat ameliorated by recent advances in colloid science.

Various methods have been used to synthesize particles of large specific surface area for catalysis applications (3-5). Most of these methods are based on hydrocolloids (3) and aerosols (4). Recently a novel synthesis method based on metal-loaded water-in-oil microemulsions has attracted the attention of catalyst preparation scientists (5). Water-in-oil microemulsions are characterized by the presence of aqueous nanodrops stabilized by surfactant molecules and dispersed in an external oil phase. Due to the cage-like nature of the water pools, particle aggregation is limited when particle precipitation is effected in them.

Molybdenum sulfide is a potential coal liquefaction catalyst (6). In this report the physico-chemical parameters underlying the synthesis of nanosize molybdenum sulfide particles in water-in-oil (w/o) microemulsions by acidification of ammonium tetrathiomolybdate are investigated. The formation of submicron-sized molybdenum sulfide particles should provide a large surface area that will increase the reactive site/mass ratio and thus enhance the dissolution stage of coal liquefaction. Of specific interest is the relationship between the molybdenum sulfide particle dispersion and liquefaction yields.

1.2 SOME ASPECTS OF MOLYBDENUM SOLUTION CHEMISTRY

Among the synthesis routes of molybdenum trisulfide is acidification of tetrathiomolybdate ions (MoS_4^{2-}). The overall reaction is given by:

$$MoS_4^{2-} + 2H^+ = MoS_3(s) + H_2S \qquad [1.1]$$

Generally, the tetrathiomolybdate precursor reagent is prepared by reacting ammonium molybdate, $(NH_4)_2MoO_4$, with hydrogen sulfide at pH<10 (7,8). The

formation of MoS_4^{2-} by reacting MoO_4^{2-} and H_2S proceeds via successive replacement of O^{2-} by S^{2-} (9). That is,

$$[MoO_{4-n}S_n]^{2-} + H_2S = [MoO_{3-n}S_{n+1}]^{2-} + H_2O \quad [1.2]$$

where n=0,1,2,3. The rate of sequential replacement of O^{2-} by S^{2-} decreases in the order $MoO_3S^{2-} > MoO_2S_2^{2-} > MoOS_3^{2-} > MoS_4^{2-}$ (10). Extensive formation of the tetrathiomolybdate species has been shown to depend on the S/Mo molar ratio and on the solution pH (10,11). Clarke et al. (10) reported that the formation of the tetrathiomolybdate species is complete at S/Mo > 300 and pH=6. On acidification of tetrathiomolybdate ions to pH below 3, molybdenum trisulfide forms.

1.3 COLLOIDAL SYSTEMS

1.3.1 Brief Overview

Any particle which has some linear dimension between 10^{-8} m and 10^{-6} m is considered a colloid. Table 1.1 gives a summary of some of the names used to designate colloidal systems (12). In this work, the primary concern is with emulsions, and, in particular, with oil-water emulsions. Based primarily on droplet size and long-term stability, emulsions are classified as either macroemulsions (low stability; large, polydispersed droplets) or microemulsions (high stability; fine, monodispersed droplets). Macroemulsions are formed by applying large shear forces to mixtures of immiscible liquids. Microemulsions are formed rather differently and thus warrant an independent discussion.

Table 1.1

Summary of Some of the Descriptive Names Used to Designate Colloidal Systems (12).

Continuous Phase	Dispersed Phase	Descriptive Names
Gas	Liquid	Fog, mist, aerosol
Gas	Solid	Smoke, aerosol
Liquid	Gas	Foam
Liquid	**Liquid**	**Emulsion**
Liquid	Solid	Sol, colloidal solution, gel, suspension
Solid	Gas	Solid foam
Solid	Liquid	Gel, solid emulsion
Solid	Solid	Alloy

1.3.2 Microemulsions

It is well known that oil and water do not mix. However, if a dispersing agent (surfactant) is added, then a clear, homogeneous mixture of oil and water can form. It is usual to represent this by a ternary phase diagram, a schematic of which is shown in Figure 1.1 (13).

A surfactant molecule is one that has (a) distinct hydrophobic and hydrophilic regions, and (b) an appropriate balance between them. In both apolar (hydrocarbon) and polar (aqueous) media, surfactant molecules undergo spontaneous self-association by a sequential process as their concentration increases. Above a certain concentration level, closed aggregates – called micelles – are formed. *Normal micelles* are formed in water/surfactant solutions, while *inverse micelles* are formed in oil/surfactant solutions. In the former, the hydrophilic groups of the surfactant molecules point away from the center of the aggregate, while the situation is reversed in the latter.

If water molecules are added to an oil/surfactant solution containing inverse micelles, they interact with the hydrophilic part of the surfactant molecules, so that inverse micelles containing immobilized water molecules are formed (swollen micelles). The addition of more water results in larger aggregates containing free water, and the system is now referred to as a water-in-oil microemulsion. The microdrops of aqueous phase are typically 3–30 nm in size.

In certain cases, a co-surfactant may be added to the system. Generally, the addition of co-surfactant decreases the oil/water interfacial tension and changes the balance between the hydrophilic and hydrophobic regions of the surfactant, so as to favor the spontaneous formation of microemulsions.

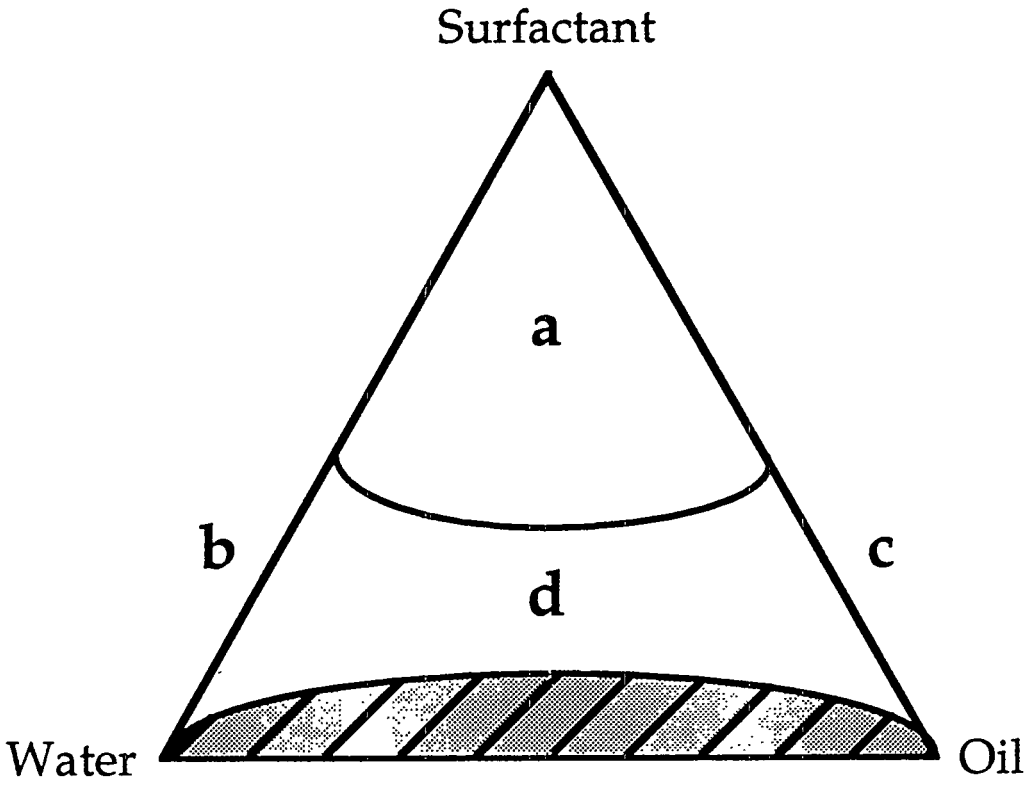

Figure 1.1

Schematic ternary phase diagram of an oil-water-surfactant system.

Shaded region represents the water-oil immiscibility (2-phase) region (13).

a, liquid-crystalline phases;

b, micelles in aqueous solution;

c, inverse micelles in oil;

d, concentrated single-phase microemulsion domain.

At certain oil/water compositions, if a surfactant is added to the mixture, a thermodynamically stable transparent liquid dispersion is thus obtained. Examples of some typical surfactants that are used in microemulsion formulation are shown in Figure 1.2. A microemulsion is therefore defined as a thermodynamically stable, optically transparent dispersion of oil-in-water (o/w) or water-in-oil (w/o) nanodroplets which are stabilized by surfactant molecules (14-22). The continuous or external phase for these o/w and w/o dispersions are water and oil, respectively. Although the microemulsion droplets have been described as spherical, neutron scattering studies show that, depending on the microemulsion composition, the droplets may be cubic or bicontinuous (13,23,24).

Among the necessary conditions for microemulsion formation is the adsorption of surfactant molecules at the water/oil interface. The adsorption dramatically lowers the interfacial tension to ultra low values, e.g., $\gamma < 10^{-2}$ mN/m (9). As a result, the interface expands and microemulsion droplets form spontaneously. In addition to the surface tension term, other factors such as the bending instability of the interface and the entropic dispersion of the microemulsion droplets have been shown to contribute to spontaneous emulsification (14,25,26). Safran and Turkevich (25) have expressed the sum of the interfacial and bending energy emulsification terms as:

$$F = n[4\pi R^2\gamma + 16\pi K(1-R/R^\circ)^2] \qquad [1.3]$$

where R° is the radius of spontaneous curvature (also referred to as natural radius of the water pool, i.e., the observed curvature when the w/o microemulsion phase is in equilibrium with the conjugate aqueous phase), R is the equilibrium radius of the swollen inverse micelles, γ is the surface tension of the interface, n is the

NP-5 = Polyoxyethylene(5)nonylphenyl ether

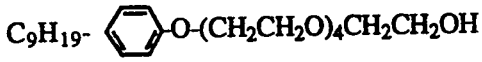

Triton X-100 = Polyoxyethylene(9-10)octylphenyl ether

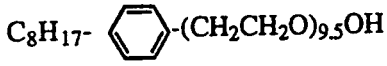

Aerosol OT = Sodium bis(2-ethylhexyl) sulfonate

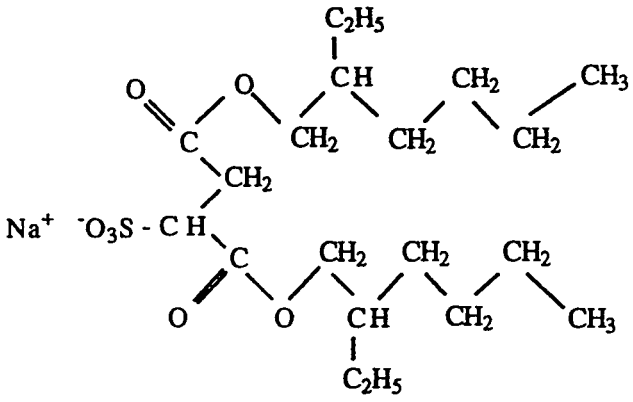

DDAB = Didodecyldimethyl ammonium bromide

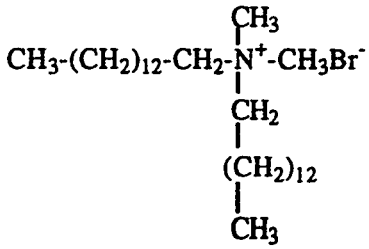

Figure 1.2

Molecular structure of surfactants:

(a) polyoxyethylene(5)nonylphenyl ether (NP-5);

(b) polyoxyethylene(9-10)octylphenyl ether (TX-100);

(c) sodium bis(2-ethylhexyl) sulfonate (AOT);

(d) didodecyldimethyl ammonium bromide (DDAB).

number of swollen inverse micelles per unit volume of microemulsion and K is the curvature elasticity or "rigidity" constant.

In Equation 1.3, the first and second terms represent the interfacial tension and bending energy terms, respectively. High and low values of K correspond to rigid and fluid interfaces, respectively. The value of K is of the order of 10^{-21} joules; thus the bending energy term becomes important only when γ is close to zero. When $K \sim k_b T$ (where k_b is the Boltzmann constant), the interface is subjected to bending instability that results from thermal fluctuations. Under these conditions, the decrease in free energy due to the dispersion entropy of the microemulsion droplets (which originates from the thermal instability of the interfacial film) may exceed the increase in free energy caused by the newly created interfacial area (14).

1.3.3 Microstructure of Microemulsions

Figure 1.3 is a more detailed sketch of a ternary phase diagram for a microemulsion system composed of oil, surfactant and water. The surfactant associated structures in Figure 1.3 include normal micelles, inverse micelles, o/w microemulsions, w/o microemulsions and liquid crystals. Depending on the hydrophile-lipophile balance (HLB) and the geometrical packing requirements of the surfactant molecules, the molecules self-associate to form normal micelles and inverse micelles. The HLB is an empirical quantity that measures the relative contributions of the surfactant tail and headgroup in micellization. The packing requirements emphasize the importance of geometrical constraints in packing the surfactant molecules at the oil/water interface. The key parameter for describing the packing of the surfactant molecules at the water/oil interface is the packing ratio (14). This is defined as the ratio of the cross-sectional area of the hydrocarbon chain of the surfactant molecule to that of the headgroup, i.e., $V_o/a_o l_c$, where V_o is the

volume of the surfactant hydrocarbon chain, a_o is the cross-sectional area of the surfactant headgroup, and l_c is 80-90% of the fully extended hydrocarbon portion of the surfactant chain. The packing ratio can be used to predict the microstructure of a surfactant aggregate. In this connection, it qualitatively accounts for the HLB of the surfactant molecule. For a surfactant with a low HLB, the ratio $V_o/a_o l_c$ is greater than 1, i.e., the tail area is greater than the head area. In this case inverse micelles form. On the other hand for surfactants with high HLB, i.e., when $V_o/a_o l_c < 1$, normal micelles are obtained. Above a certain oil-to-surfactant and water-to-surfactant molar ratio, the normal micelles and the inverse micelles swell and form o/w and w/o microemulsions, respectively.

Studies based on calorimetry (27) and spectroscopy (28,29) suggest that for microemulsions formulated with AOT as the amphiphilic agent, the transition from inverse micelles to w/o microemulsions occurs at a water-to-surfactant molar ratio (R) of 6-10. At a fixed oil-to-surfactant molar ratio (W), it is possible to effect a change from w/o to o/w microemulsion by increasing the microemulsion water content. Using conductivity, birefringence and NMR measurements, Shah and coworkers (30) postulated that the transition from w/o to o/w microemulsions occurs through the following structural changes as the water content increases: spherical w/o microemulsions -> cylindrical w/o microemulsions -> lamellar structures of surfactants, oil and water -> o/w microemulsions.

1.3.4 Particle Formation in Microemulsions

The compartmentalized nature of w/o microemulsions makes them useful as microreactors for the synthesis of ultrafine particles. The water pools provide a large number of nucleation sites that are isolated from each other by the apolar organic phase and hence limit particle aggregation. The w/o microemulsion

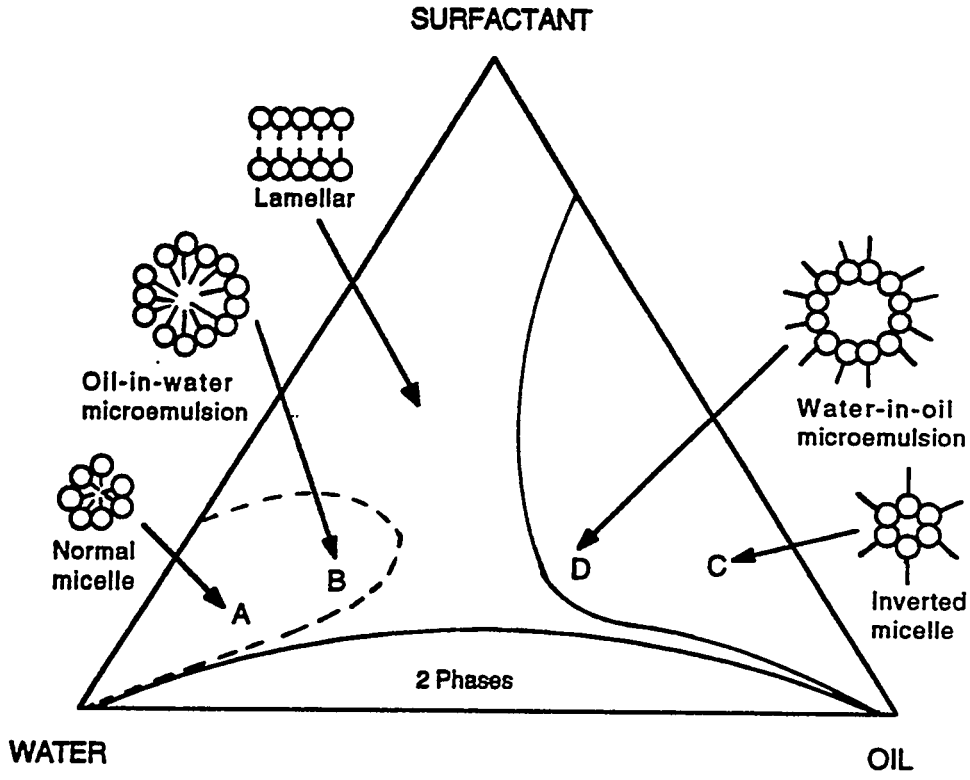

Figure 1.3

Schematic ternary-phase diagram of an oil-water-surfactant microemulsion system consisting of various associated structures:

(A) normal micelles; (B) o/w microemulsions; (C) inverse micelles;

(D) w/o microemulsions.

(Adapted from Reference 22.)

droplets are capable of solubilizing inorganic salts which serve as precursor reagents for particle formation (15,31-34). In addition, the w/o microemulsions exchange their droplet contents in a time scale of the order of milliseconds via collision, fusion and fission (35-38). These properties of the inverse micelles offer the opportunity of making nanosize monodispersed materials in their water cores. The successful synthesis of nanosize particles using inverse micelles has been reported for a wide variety of materials (32-34,39-58), among which are the hydrogenation catalysts of nickel and cobalt borides (31), noble metals (34,39), and platinum-group metals (40-42). Other materials such as cadmium sulfide (43-49), copper, lead and indium sulfides (45,50), cadmium selenide (51), silica (32,33,52-54), silver halides (55,56), barium ferrite (57), and molybdenum sulfide (58) have also been made in microemulsions.

The particle synthesis protocols that have been used can be classified into three main groups: (a) microemulsion plus trigger, (b) two microemulsions, and (c) microemulsion plus a second reactant (33). Figure 1.4 shows how the synthesis reactions may be implemented in each case.

1.3.5 Microemulsion Droplet Dynamics and Particle Growth

It is generally accepted that the microemulsion droplet contents rapidly exchange in the time scale of microseconds to milliseconds (35-38). The mechanism of solute exchange is said to involve the formation of transient droplet dimers, followed by fusion and fission (59). The rate of exchange of material between the water pools is represented by a constant, K_{ex}. Although the microemulsion droplets constantly collide with one another, not all the collisions lead to solute transfer. Robinson and coworkers (59) have shown that for the AOT/heptane/water microemulsion, the second-order rate constant for collision between two

microemulsion droplets (K_c) and that of solute exchange (K_{ex}) are, respectively, of the order of 10^{10} and 10^7 L mol^{-1} s^{-1}. From the ratio, K_c/K_{ex}, it is inferred that only one out of 10^3 collisions leads to solute exchange.

The importance of the relationship between the microemulsion dynamics (i.e., K_{ex}) and particle growth in the microemulsion water cores is noteworthy. Robinson and coworkers (43,59) and Shah and coworkers (56,60,61) have shown that the exchange rate of solute species and the growth rate of cadmium sulfide and silver halide particles synthesized in AOT microemulsions concurrently increase with the carbon number of the oil. This relationship between solute exchange (dynamics) and particle growth suggests the need to consider the dynamics of the microemulsion droplets if particle growth and polydispersity are to be controlled.

1.3.6 Catalyst Particle Synthesis in Microemulsions

It is natural that the above method has also been used to produce catalytic materials. As stated in Section 1.3.5, these include nickel and cobalt borides (62,63), noble metals (39), platinum-group metals (42,64-66), and molybdenum sulfide (58). In all cases, the particles produced were reported to be of nanometer size and to possess low polydispersity.

While a considerable amount of effort has been directed towards understanding the mechanisms of particle nucleation and growth in microemulsions, very little attention has been focused on the end use of such particles. Indeed, a majority of the publications in the field do not venture beyond the particle synthesis and characterization stages. This is unfortunate because many of the issues involved – insofar as actually using the particles for some function is concerned – remain a mystery.

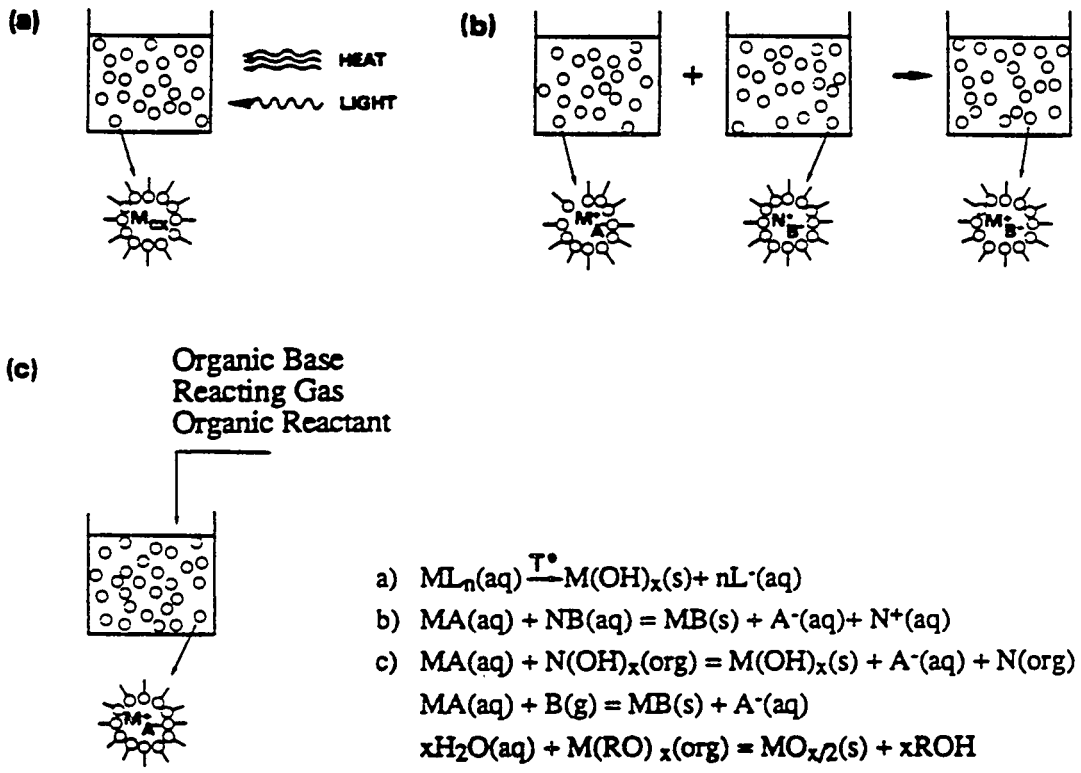

Figure 1.4

Powder synthesis methods in inverse microemulsions:

(a) microemulsion plus trigger;

(b) two microemulsions;

(c) microemulsion plus second reactant (33).

With regard to catalyst particles, the above statements are especially true. Microemulsion-synthesized catalyst particles have been tested for activity in only a few catalytic reactions and in a variety of ways (see Section 1.4). The activities of catalysts prepared from microemulsions were found to be similar or lower when compared to those of catalysts prepared by conventional means (42,65,66). It was also found that catalytic activity depended strongly on the fashion in which the particles were employed as catalysts (62,63). Thus, no systematic study has been conducted that can build a much-needed bridge between the particle synthesis and testing stages.

1.4 OPTIONS FOR TESTING CATALYST PARTICLES SYNTHESIZED IN MICROEMULSIONS

From a survey of the literature, three modes of employing catalyst particles synthesized in microemulsions were identified. They are discussed below.

1.4.1 *In Situ* Mode

The catalyst particles may be employed while they are suspended in a microemulsion. Boutonnet et al. (64) used this approach to test the activity of platinum particles prepared in various microemulsions for the hydrogenation/isomerization reactions of 1-butene. In terms of microemulsion stability and catalyst particle coagulation, the systems most stable were those based on nonionic surfactant, n-alkane and water. The particles were found to be active for this reaction. However, in a subsequent publication (65), the activity of the same particles for the same reaction was reported to be ten times greater when they were

transferred onto supports and washed and heat-treated to remove the surfactant molecules adsorbed on them. Thus, the relatively lower activity reported in the earlier publication was attributed to surfactant inhibition of reactant access to catalyst active sites (65).

Ravet et al. (62) and Nagy et al. (63) have reported the preparation of monodispersed nickel boride, cobalt boride and bimetallic Ni-Co boride in an inverse micellar system composed of cetyltrimethylammonium boride (CTAB), 1-hexanol and water. The particles were tested for catalytic activity in hydrogenation of crotonaldehyde. The activities of the particles in suspension were compared against those extracted from the inverse micelles and cleaned to remove adsorbed species. Not surprisingly, the latter were found to be more active, despite the possible loss of dispersion.

It is clear then that activity data for particles suspended in microemulsions can be of limited value. Interpretation of such data is very likely to be confounded by such factors as emulsion stability, adsorbed surfactant, etc., making the determination of specific activity of catalysts difficult or impossible.

Before discussing the next option for employing catalysts prepared by a microemulsion method, it is instructive to consider one more example - that of the emulsion catalyst developed by the Dow Chemical Co. during the 1970s for the hydrogenation of coal and heavy petroleum fractions (67,68). In this process, the catalyst is introduced as an emulsion of an aqueous solution of ammonium paramolybdate ($(NH_4)_6Mo_7O_{24}.4H_2O$) in either coal-derived oil, or petroleum distillation residue. Under reaction conditions, the metal compound is converted to highly dispersed particles of MoS_2, later determined to be of nanometer scale (69). The stability of the emulsion in this process was deemed to be unimportant since the emulsion was employed soon after preparation. For this reason, surfactants were not *deliberately* added to the reaction mixture. However, it is significant that

both coal liquids and heavy petroleum fractions contain asphaltenes, some of which have the ability to form water-in-oil emulsions (70,71). (In fact, the formation of stable water-petroleum emulsions is an unwanted effect that often occurs when crude oils are treated with water during oil production and refining (72).) Since emulsifiers "native" to the reaction mixture may have contributed to water-droplet stabilization, in retrospect this must be considered a possible case of microemulsion-based catalyst synthesis.

1.4.2 Transfer Onto Supports

After preparation, the catalyst particles may be transferred onto supports, followed by removal of the micellar solution, and thorough washing. In essence, this is a novel method of preparing supported catalysts. It is novel in that catalyst particles are synthesized in non-aqueous media and transferred onto supports, while most conventional catalyst preparation methods call for the impregnation of supports from aqueous salt solutions.

There are basically two problems associated with this method of catalyst synthesis. The first pertains to the transfer of particles onto the support. This must be achieved with minimal particle agglomeration attending. Second, extreme care must be taken to ensure that surfactant molecules are completely removed from the catalyst prior to application. Since many conventional catalyst supports are also good adsorbents for surface-active agents (73), surfactant molecules are likely to be present on the surface of the support also.

Boutonnet and coworkers (42,65,66) have developed and used a process in which the transfer of particles is effected by breaking the emulsion (after the particles have formed) in the presence of the carrier. The emulsion was destroyed either by adding an emulsion-breaker (for example, tetrahydrofuran (THF)), or by raising the

temperature. In this fashion, a Pt/Al_2O_3 catalyst was prepared by adding alumina to a stable suspension of Pt particles in a pentaethyleneglycoldodecylether (PEGDE)/n-hexadecane/water microemulsion and inducing destabilization via addition of an excess of tetrahydrofuran under vigorous stirring (66). Electron microscopy revealed that the particles were well-dispersed on the support, with an average particle size of around 2 nm.

Along similar lines, supported Pt, Pd and Rh catalysts were also prepared by Boutonnet et al. by depositing either Pt, Pd or Rh particles synthesized in microemulsions on pumice (66). Touroude et al. have also synthesized Pt/Pd (42) alloy particles in microemulsions and deposited them onto alumina.

It is interesting to note that the above catalysts from microemulsions exhibited very similar activities to those of catalysts synthesized by conventional means. This was observed despite the fact that the former were more highly dispersed. In fact, in some cases the activities were even lower than those of "classical catalysts" (66). The authors speculated that this was due to the poisoning effect of surfactant molecules that were not removed during catalyst preparation.

With regard to the transfer of particles onto supports, a few concluding remarks are in order. Turkevich and Kim (74) prepared a Pd/alumina catalyst by adsorbing palladium particles from an *aqueous* sol of the metal onto gamma alumina. They reported that the palladium was adsorbed as individual particles on the support. It is possible to rationalize this in terms of the tendency for some minerals (75) and ion-exchange resins (76) to adsorb colloids, which is an example of a well-studied phenomenon called heterocoagulation. However, the adsorption of colloidal particles from *nonaqueous* solutions has not been studied. This bears further investigation at least from the point of view of preparing supported catalysts via inverse micelle synthesis of inorganic particles.

1.4.3 Harvesting of Particles

The third alternative is to extract the particles from the microemulsion fluid phase after synthesis. Inorganic powders have been prepared in this fashion by a number of workers (77-80). As a method of synthesizing bulk inorganic materials, it must be compared and contrasted with other liquid-phase particle synthesis methods. The use of chemical reactions in microemulsions offers several advantages. It is relatively simple and versatile and also offers the possibility of controlling the particle size and size distribution within narrow limits.

An important consideration governing all liquid-phase methods of particle synthesis is the quantity of particles produced per unit volume (or weight) of solution (hereafter referred to as the yield). For microemulsions, the particle yield-controlling factor is the water-to-surfactant molar ratio, R. Generally, increasing the water content (i.e., R) leads to an increase in the particle size and polydispersity. However, to obtain a high yield of particles, it is necessary to solubilize a correspondingly large quantity of metal salt (and, thus, water) in the microemulsion. In addition, both salt concentration and water content must of course be kept within the bounds set by the phase behavior of the microemulsion system.

The above statements point to the necessity of a trade-off between particle yield on the one hand, and particle size and polydispersity on the other. Thus, there are two regimes in which microemulsions may be used for particle synthesis: low R and high R. Generally, in producing relatively small quantities of ultrafine particles with narrow size distribution, working in the low R regime recommends itself. On the other hand, to obtain high particle yields, it is necessary to work in the region of high R values.

Darab et al. (81) have produced nanoscale nickel- and iron oxyhydroxide powder in yields of approximately 10 g/L by a modified reverse micelle (MRM) method. The powders were found to be catalytically active for the hydroliquefaction of coal. Martino et al. (82) have produced iron-based clusters in inverse micelles and used them as coal liquefaction catalysts, both *in situ* and as powders recovered from the microemulsion medium. Only in the latter case did the catalyst particles show any activity for coal liquefaction.

1.5. RESEARCH SCOPE AND OBJECTIVES

The overall objective of this project was to develop an approach for the synthesis of direct liquefaction catalysts of nanometer size. The emphasis is on molybdenum- and iron-based catalysts, but the techniques developed for the dispersion of these unsupported catalysts are thought to have general applicability. Furthermore, an additional goal was to determine quantitatively the effect of catalyst particle size on the product yield and the product distribution from liquefaction of bituminous and subbituminous coals.

Although the microemulsion fluid phase has been used by many scientists to prepare solid materials, the primary emphasis in previous work has been to demonstrate the success of making specific materials in this medium. In other words, only a limited number of studies have been systematic investigations of the influence of the microemulsion properties on the particle characteristics (e.g., particle size and distribution). Among the factors that may affect the particle size and distribution are: (a) type of surfactant, (b) type of co-surfactant, (c) nature of oil, (d) proportion of water, (e) concentration of reactant species, and (f) synthesis protocol. Knowledge of how these factors affect particle size is vital in designing the

optimal conditions needed to generate ultrafine particles in microemulsions. Our progress in this direction is described in Chapters 2-5.

In particular, the work reported herein seeks to advance our understanding of how the microemulsion properties and/or components affect the particle size at the molecular level. For example, it seeks to elucidate the manner in which microemulsion microstructure (e.g., droplet size), microemulsion phase behavior, micellar dynamics (solute exchange rates), the water content, the molybdate occupancy number (the number of ammonium tetrathiomolybdate molecules per inverse micelle) and the synthesis protocol affect the particle size and polydispersity. On a more practical level, it seeks answers to the question of how the particle size and polydispersity could be controlled by manipulating the microemulsion components and/or properties.

At the same time, the work reported here (Chapters 6-8) includes meaningful catalytic liquefaction tests on coals and under conditions that are of interest to DOE. On one hand, it was sought to optimize the traditional aqueous impregnation method of dispersing catalysts on coal surfaces. By controlling the solution chemistry, the uptake of metallic species by coal surfaces can, in theory, be optimized. At the same time, a novel microemulsion method was developed in an attempt to gain greater control over catalyst dispersion. Molybdenum sulfide catalyst particles were synthesized in microemulsions and tested *in situ* (i.e., while suspended in the microemulsion medium) for activity in the liquefaction of a bituminous and a subbituminous coal. Finally, a bridge was sought between the synthesis of ultrafine inorganic solids in microemulsion media and their subsequent employment as catalytic materials (see Appendix V). One viable option is to harvest the particles from the microemulsion medium before use.

1.6 REFERENCES

1. Roth, J.F. *Catalysis - A Critical Technology of the Future*, Houdry Award Lecture, 12th North American Meeting of The Catalysis Society, Lexington, KY, 1991.
2. Che, M. and Bennett, C.O. *Adv. Catal.* **36**, 55, 1989.
3. Haruta, M., Lamaitre, J., Delannay, F., and Delmon, B., *J. Colloid Interface Sci.* **101,** 59 (1984).
4. Andres, M., Charcosset, H., Chiche, P., Davignon, L., Djega-Mariadassou, G., Joly, J.P., and Pregermain, S., *Fuel* **62,** 69 (1983).
5. Boutonnet-Kizling, M., Stenius, P., Anderson, S., Frestad, A., *Appl. Catal. B* **1,** 149 (1992).
6. Derbyshire, F.J., "Catalysis in Coal Liquefaction: New Directions for Research", IEA CR/08, London, 1988.
7. Harmer, M.A. and Sykes, G., *Inorg. Chem.* **19,** 2881 (1980).
8. Prasilova, J., and Burclova, J., *Radiochem. Radioanal. Lett.* **11,** 351 (1972).
9. Ayimonino, P.J., Ranade, A.C., Diemann, E., and Müller, A., *Z. Anorg. Allgem. Chem.* **371,** 300 (1969).
10. Clarke, N.J. and Laurie, S.H., *J. Inorg. Biochem.* **12,** 37 (1980).
11. Yatirajam, V., Ahuja, U., and Kakkar, L.R., *Talanta* **23,** 819 (1976).
12. Hiemenz, P.C. *Principles of Colloid and Surface Chemistry*, 2nd Ed. Marcel Dekker, New York, 1991, p. 11.
13. Robinson, B.H., *Nature* **320**, 376 (1986).
14. Leung, R., Hou, M.J., and Shah, D.O.," Surfactants in Chemical/Process Engineering" (D.T. Wasan, M.E. Ginn and D.O. Shah, Eds.), Surfactant Science Series, Vol. 28, Marcel Dekker, New York, 1988, p. 315.
15. Fendler, J.H., *Chem. Rev.* **87**, 877 (1987).

16. Ward, A.J.I. and Friberg, S.E., *Mater. Res. Bull.* **14**, 41(1989).

17. Sharma, M.K. and Shah, D.O., in "Macro- and Microemulsions Theory and Applications" (D.O. Shah, Ed.), ACS Symposium Series, Vol. 272, Washington D.C., 1985, p. 1.

18. Cazabat, A.M., Chatenay, D., Guering P., Urback, W., Langevin, D., and Meunier, J., in "Microemulsion Systems" (H.L. Rosano and M. Clausse, Eds.), Surfactant Science Series, Vol. 24, Marcel Dekker, New York, 1987, p. 183.

19. Ayyub, P., in "Progress in Microemulsions" (S. Martellucci and A.N. Chester, Eds.), Plenum Press, New York, 1989, p. 217.

20. Zana, R. and Lang, J., in " Microemulsions Structure and Dynamics" (S.E. Friberg and P. Bothorel, Eds.), CRC Press, Boca Raton, Florida, 1987, p. 153.

21. Cazabat, A.M., Chatenay, D., Guering P., Urback, W., Langevin, D., Meunier, J., and Sarba, D., in " Reverse Micelles" (P.L. Luisi and B.E. Straub, Eds.), Plenum Press, New York, 1984, p. 121.

22. Robinson, B.H., Khan-Lodhi, A.N., and Towey, T., in "Structure and Reactivity in Reverse Micelles" (M.P. Pileni, Ed.), Elsevier, New York, 1989, p. 198.

23. Tabony, J., *Nature* **319**, 400 (1986).

24. Tabony, J., *Nature* **320**, 338 (1986).

25. Safran, S.A. and Turkevich, L.A., *Phys. Rev. Lett.* **50**, 1930 (1983).

26. Bellocq, A.M., Biais, J., Botherel, P., Clin, B., Fourche, G., Lalanne, P., Lamaire, B., Lemanceau, B., and Roux, D., *Adv. Colloid Interface Sci.* **20**, 67 (1984).

27. Hauser, H., Haering, G., Pande, A., and Luisi, P.L., *J. Phys. Chem.* **93**, 7869 (1989).

28. Wong, M., Thomas, J.K., and Gratzel, M., *J. Am. Chem. Soc.* **98**, 2391 (1976).

29. Zulauf, M., and Eicke, H.F., *J. Phys. Chem.* **83**, 480 (1979).

30. Shah, D.O., Tamjeedi, A., Falcon, J.W., and Walker, R.D., *AIChE J.* **18,** 1116 (1972).

31. Nagy, J.B., *Colloids Surf.* **35,** 201 (1989).

32. Osseo-Asare K. and Arriagada, F.J., *Colloids Surf.* **50,** 321 (1990).

33. Osseo-Asare, K. and Arriagada, F.J., in "Ceramic Powder Science III" (G.L. Messing, S. Hirano and H. Hausner, Eds.), American Ceramic Society, Westerville, OH, 1990, p. 3.

34. Barnickel, P. and Wokaun, A., *Mol. Phys.* **69,** 1 (1990).

35. Atik, S.S. and Thomas, J.K., *Chem. Phys. Lett.* **79,** 351 (1981).

36. Clark, S., Fletcher, P.D.I., and Ye, X., *Langmuir* **6,** 1301 (1990).

37. Almgren, M., Stam, J.V., Swarup, S., and Lofroth, J.-E., *Langmuir* **2,** 432 (1986).

38. Bommarius, A.S., Holzwarth, J.F., Wang, D.I.C., and Hatton, T.A., *J. Phys. Chem.* **94,** 7232 (1990).

39. Barnickel, P., Wokaun, A., Sager, W., and Eicke, H.F., *J. Colloid Interface Sci.* **148,** 80 (1992).

40. Boutonnet, M., Kizling, J., Stenius P., and Maire, G., *Colloids Surf.* **5,** 209 (1982).

41. Claerbout A. and Nagy, J.B., in "Preparation of Catalysts V" (G. Poncelet, P.A. Jacobs, P. Grange and B. Delmon, Eds.), Elsevier, 1991, p. 705.

42. Touroude, R., Girard, P., Maire, G., Kizling, J., Boutonnet M., and Stenius, P., *Colloids Surf.* **67,** 19 (1992).

43. Towey, T.F., Khan-Lodhi, A., and Robinson, B.H., *J. Chem. Soc. Faraday Trans.* **86,** 3757 (1990).

44. Modes S. and Lianos, P., *J. Phys. Chem.* **93,** 5854 (1989).

45. Lianos P. and Thomas, J.K., in "Materials Science Forum", Vol. 25-26 (G.E. Murch and F.H. Wohlbier, Eds.), 1988, p. 369.

46. Petit C. and Pileni, M.P., *J. Phys. Chem.* **92,** 2282 (1988).

47. Motte, L., Petit, C., Boulanger, L., Lixon P., and Pileni, M.P., *Langmuir* **8,** 1049 (1992).

48. Pileni, M.P., Motte L., and Petit, C., *Chem. Mater.* **4,** 338 (1992).

49. Robinson, B.H., Towey, T.F., Zourab, S., Visser, A.J.W.G., and Hoek, A.V., *Colloids Surf.* **61,** 175 (1991).

50. Dannhausser, T., O'Neil, M., Johansson, K., Whitten D., and McLendon, G., *J. Phys. Chem.* **90,** 6074 (1986).

51. Steigerwald, M.L., Alivisatos, A.P., Gibson, J.M., Harris, T.D., Kortan, R., Müller, A. J., Thayer, A.M., Duncan, T.M., Douglas D.C., and Brus, L.E., *J. Am. Chem. Soc.* **110,** 3046 (1988).

52. Arriagada F.J., and Osseo-Asare, K., *Colloids Surf* **69,** 105 (1992).

53. Yamauchi, H., Ichikawa T., and Kondo, S., *Colloids Surf.* **37,** 71 (1989).

54. Yanagi, M., Asano, Y., Kandori, K., Kon-no K., and Kitahara, K., 1986 Shikizai Technical Conference (Osaka, Japan), 1986, p. 86.

55. Dvolaitzky, M., Ober, R., Taupin, C., Anthore, R., Auvray, K., Petipas C., and Williams, C., *J. Dispersion Sci. Technol.* **4,** 29 (1983).

56. Hou M.J. and Shah, D.O., in" Interfacial Phenomena in Biotechnology and Materials Processing" (Y.A. Attia, B.M. Moudgil and S. Chander, Eds.), Elsevier, 1988, p. 443.

57. Pillai, V., Kumar, P., Multani, M.S., and Shah, D.O., *Colloids Surf.* **80,** 69 (1993).

58. Boakye, E., Radovic, L.R., and Osseo-Asare, K., *J. Colloid Interface Sci.* **163,** 120 (1994).

59. Fletcher, D.I., Howe, A.M., and Robinson, B.H., *J. Chem Soc., Faraday Trans.* **183,** 985 (1987).

60. Chew, C.H., Gan, L.M., and Shah, D.O., *J. Dispersion Sci. Technol.* **11,** 593 (1990).

61. Hou, M.J. and Shah, D.O., *J. Colloid Interface Sci.* **123,** 398 (1988).

62. Ravet, I., Nagy, J.B., and Derouane, E.G., in *Preparation of Catalysts IV* (B. Delmon, P. Grange, P.A. Jacobs, and G. Poncelot, Eds.), Elsevier, Amsterdam 1987, p. 505.

63. Nagy, J.B., Bodart-Ravet, I., and Derouane, E.G., *Faraday Discuss. Chem. Soc.* **87**, 189 (1989).

64. Boutonnet, M., Kizling, J., Touroude, R., Maire, G., and Stenius, P., *Appl. Catal.* **20**, 163 (1986).

65. Boutonnet, M., Kizling, J., Mintsa-Eya, V., Choplin, A., Touroude, R., Maire, G., and Stenius, P., *J. Catal.* **103**, 95 (1987).

66. Boutonnet, M., Kizling, J., Touroude, R., Maire, G., and Stenius, P., *Catal. Lett.* **20**, 163 (1986).

67. Moll, N.G., and Quarderer, G.J., *U.S. Patent 4, 090, 943*, May 23, 1978.

68. Moll, N.G., and Quarderer, G.J., *Chem. Eng. Prog.* **75** (10), 46 (1979).

69. Krichko, A.A., Shpirt, M.Ya., Glazunov, M.P., Zekel, L.A., Krasnobaeva, N.V., Plavnik, G.M., Khrustaleva, G.N., and Aliev, A.D., *Khimiya Tverdogo Topliva* **22** (5), 62 (1988).

70. Papirer, E., Bourgeois, C., Siffert, B., and Balard, H., *Fuel* **61**, 732 (1982).

71. Siffert, B., Bourgeois, C., and Papirer, E., *Fuel* **63**, 834 (1984).

72. Speight, J.G. *The Chemistry and Technology of Petroleum*, 2nd Ed. Marcel Dekker, New York, 1991.

73. Clunie, J.S. and Ingram, B.T., *Adsorption from Solution at the Solid/Liquid Interface* (G.D. Parfitt and C.H. Rochester, Eds.), Academic Press, London, 1983.

74. Turkevich, J. and Kim, G., *Science* **169**, 873 (1970).

75. Thiessen, P.A., *Kolloid-Z.* **101**, 241 (1942).

76. Biddle, P. and Miles, J.H., *J. Inorg. Nucl. Chem.* **35**, 2555 (1973).

77. Ayyub, P., Multani, M., Barma, M., Palkar, V.R., and Vijayaraghavan, R., *J. Phys. C* **21**, 2229 (1988).

78. Dutta, P.K. and Robbins, D. *ACS Preprints, Div. Petroleum Chem.*, **34** (3), 461, 1989.

79. Pileni, M.P., *J. Phys. Chem.* **97**, 6961 (1993).

80. Kandori, K., Kon-no, K., and Kitahara, K., *J. Colloid Interf. Sci.* **122**, 78 (1988).

81. Darab, J.G., Fulton, J.L., and Linehan, J.C., *ACS Preprints, Div. Fuel Chem.* **38** (1), 27, 1993.

82. Martino, A., Wilcoxon, J.P., Sylwester, A.P., and Kawola, J.S., *ACS Preprints, Div. Fuel Chem.* **38** (1), 20, 1993.

CHAPTER 2

MICROEMULSION-MEDIATED SYNTHESIS OF NANOSIZE MOLYBDENUM SULFIDE PARTICLES

2.1 INTRODUCTION

As discussed in Chapter 1, the formation of nanosize particles is of considerable importance in heterogeneous catalysis. The large surface area available for reaction may increase the reactive sites/mass ratio and enhance the catalytic activity (for structure-insensitive reactions). As a consequence, many research groups have used various methods to synthesize dispersed particles of high specific surface area for catalysis applications (1-3). Recently a novel microemulsion-based synthesis method has attracted the attention of catalyst preparation scientists (3).

The synthesis of nanosize particles using inverse micelles has been reported for a wide variety of materials (3-26). In this Chapter the synthesis of molybdenum sulfide catalyst particles by acidification of ammonium tetrathiomolybdate in the microemulsion water cores is reported. In particular the effect of the water-to-surfactant molar ratio (R) on the molybdenum sulfide particle size is investigated.

The microemulsion system polyoxyethylene(5)nonylphenyl ether (NP-5)/cyclohexane/water was used in this study. In this system, the water molecules interact first with the hydrophilic polar groups of the surfactant molecules via hydrogen bonding to form the inverse micelles. The addition of more water molecules results in the formation of swollen inverse micelles, i.e., microemulsions. The water pools inside the inverse micelles vary in size (3-30 nm) (4,5), depending on the water-to-surfactant molar ratio (R). Due to the cage-like

nature of the water pools, particle growth is limited when particle precipitation is effected in them. However, the average number of reactant species per water core is vital in designing the optimal conditions needed to make particles of desired size (3). Advantage has been taken of these unique properties of metal-loaded inverse micelles to synthesize nanosize molybdenum sulfide particles in the size range 10-80 nm.

2.2 EXPERIMENTAL

2.2.1 Materials

The following chemicals were obtained from Aldrich: the nonionic surfactant polyoxyethylene(5)nonylphenyl ether (NP-5; molecular weight, 440.63), sodium polyphosphate (96%), ammonium tetrathiomolybdate (99.97%), and cyclohexane (99%). (The molecular weight calculations for sodium polyphosphate was based on the assumption that the polymeric species was made up of six monomers, i.e., hexametaphosphate.) Before use, cyclohexane was dried with molecular sieves.

2.2.2 Microemulsion Characterization

The phase diagram of the microemulsion system 0.15 M NP-5/cyclohexane/sulfuric acid was recorded as follows: The phase behavior of a number of samples containing a fixed surfactant-to-oil molar ratio and different water contents was observed as a function of temperature. The solubility and solubilization limits were found to be reproducible within ±0.5 °C for a given R

value. The density of the NP-5/cyclohexane/water system for each R value was measured with a digital densitometer (DMA 40, Paar Co.) at 25 °C. The partial molar volume of solubilized water at various R values was calculated as in Ref. 27.

2.2.3 Particle Synthesis

The w/o microemulsion NP-5/cyclohexane/sulfuric acid was prepared at room temperature by adding 12 mL of 1.1 M aqueous sulfuric acid to a 10 mL solution of 0.15 M NP-5/cyclohexane. The acid-solubilized microemulsion was deoxygenated by bubbling high-purity nitrogen gas through it. This procedure was followed by adding 12.8 μL of (2.5-5)x10^{-3} M ammonium tetrathiomolybdate to the 0.15 M NP-5/cyclohexane/sulfuric acid microemulsion. Nitrogen was further bubbled while the molybdenum sulfide was being precipitated according to Equation 2.1.

$$MoS_4^{2-} + 2H^+ = MoS_3 + H_2S \qquad [2.1]$$

The concentrations of the reactant species with respect to the total microemulsion were as follows: (3.2-6.4)x10^{-6} M ammonium tetrathiomolybdate and 1.3x10^{-3} M sulfuric acid.

For [MoS_4^{2-}] = 3.2x10^{-6} M, an attempt was made to reduce particle aggregation in the inverse micelles by adding sodium polyphosphate. The concentration of polyphosphate with respect to the total microemulsion was 3.2x10^{-6} M. The experiments were done for $R < 2$. Phase separation occurred at $R > 2$ due to the shift in the solubilization curve toward lower temperatures in the presence of the polyphosphate.

2.2.4 Particle Characterization

Molybdenum sulfide particles were extracted from the microemulsion by inducing phase separation at 60 °C (see Figure 2.1). Surfactant molecules adsorbed on the particles were repeatedly removed with 70% ethanol/water mixture; the particles were then dried in vacuum at 150 °C for 2 hours. Dried samples were sent to Galbraith Laboratories (Knoxville, Tennessee) for quantitative microanalysis. Ultraviolet/visible spectra were obtained with a Hewlett Packard 8451A diode array spectrophotometer. Differential thermal analysis measurements were done with a Dupont 2100 Differential Scanning Calorimeter; Al_2O_3 was used as a standard. For the gravimetric analysis measurements, a Dupont 910 thermogravimetric analyzer was used.

Samples for transmission electron microscopy were prepared by directly dropping a very small amount of molybdenum sulfide dispersion on carbon-coated copper grids and drying at room temperature. Prior to sample extraction, each sample bottle was sonicated for one minute. Particle size was determined with a Philips 420 transmission electron microscope operating at 120 kV with a resolution of about 0.6 nm. The diameters of at least 300 particles were measured for each sample to obtain an average particle diameter.

2.3 RESULTS AND DISCUSSION

2.3.1 Microemulsion and Particle Characterization

Phase Behavior. Figure 2.1 presents the solubilization diagram of the 0.15 M NP-5/cyclohexane/sulfuric acid microemulsion. The region between the solubilization

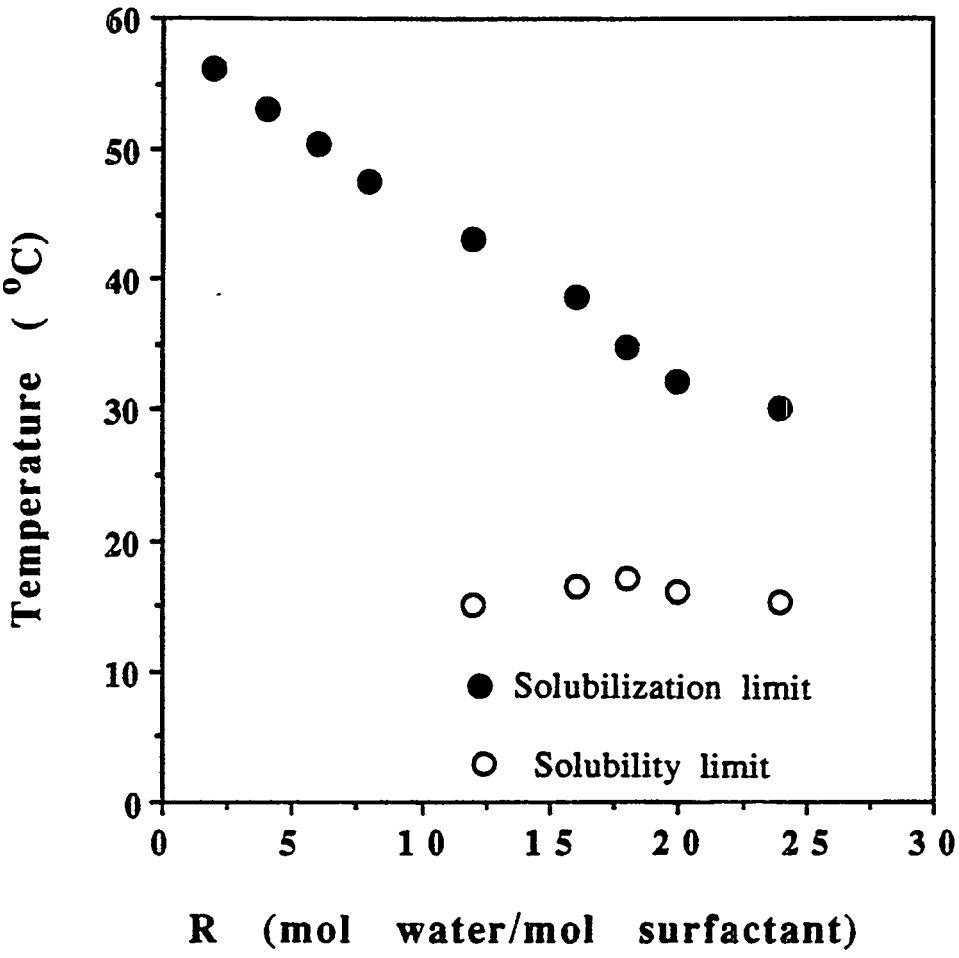

Figure 2.1

Solubilization diagram for aqueous sulfuric acid in the 0.15 M NP-5/cyclohexane system. ($[H_2SO_4] = 1.3 \times 10^{-3}$ M.)

and solubility curves (i.e., the upper and lower temperature boundaries) represents the one-phase microemulsion domain in which the nanosize molybdenum sulfide particles were synthesized. The trends in Figure 2.1 are consistent with previous solubilization studies performed with polyoxyethylene nonylphenyl ethers (5,28).

Partial Molar Volume. Figure 2.2 presents a plot of the partial molar volume of water (0.15 M NP-5/cyclohexane microemulsion) versus the water-to-surfactant molar ratio (R). The rate of change of partial molar volume with R is initially high and slows down at R ~ 2. At R > 2.5-4, the partial molar volume of water in the microemulsion approaches that of bulk water (18.069 at 25 °C) (29). This result suggests that at R < 2 the water molecules are relatively immobilized (they are bound to the hydrophilic portion of the amphiphile (NP-5) via hydrogen bonding), and that free or unbound water molecules exist in the hydrophilic core of the inverse micelles at R > 2. This finding is in agreement with previously reported studies on the state of water solubilized in inverse micellar systems (5,30) formulated with polyoxyethylene nonylphenyl ether.

Chemical analysis. A sample of molybdenum sulfide powder extracted from the NP-5/cyclohexane/water microemulsion was sent to Galbraith Laboratories for quantitative microanalysis. The results gave a sulfur-to-molybdenum molar ratio of 2.72. This is reasonable since both dithiomolybdate and tetrathiomolybdate species are converted to molybdenum oxysulfide in the presence of an acid, (see Equation 2.2, p. 36).

Absorption spectra. Ultraviolet/visible absorption spectra of the solubilized ammonium tetrathiomolybdate, taken before and after acidification, are shown in Figures 2.3a and 2.3b, respectively. For these two systems, the microemulsion

34

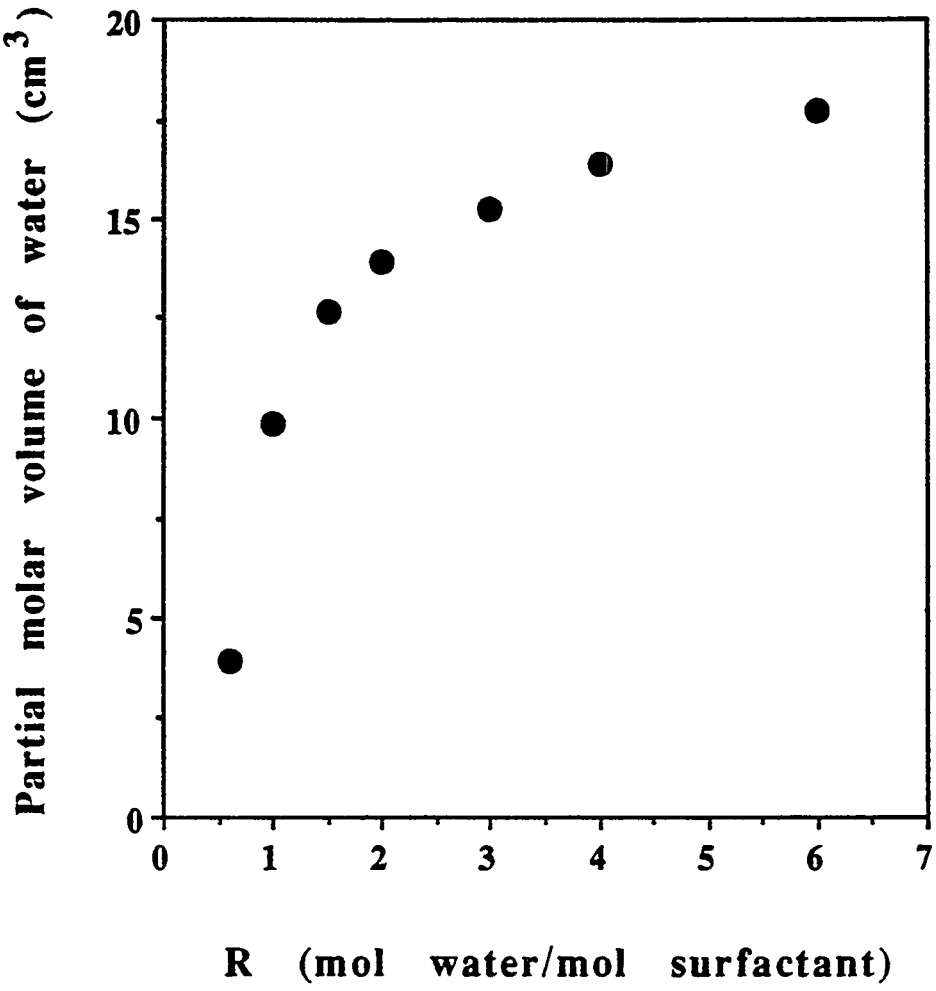

Figure 2.2

Effect of water-to-surfactant molar ratio (R) on the partial molar volume of water at 25 °C in the 0.15 M NP-5/cyclohexane microemulsion system.

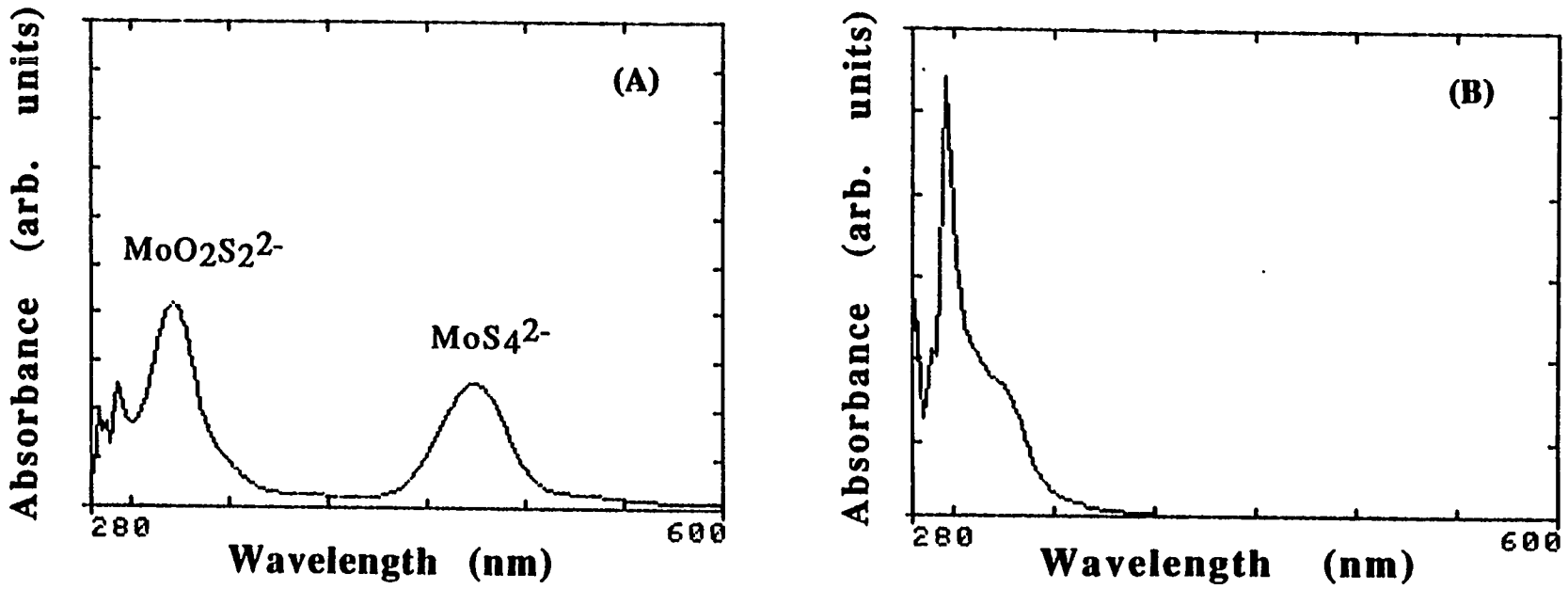

Figure 2.3

Absorption spectrum of thiomolybdate species and molybdenum sulfide particles in 0.15 M NP-5/cyclohexane microemulsion, R=4, $[MoS_4^{2-}] = 6.4 \times 10^{-6}$ M, $[H_2SO_4] = 1.3 \times 10^{-3}$ M:

(a) without sulfuric acid, (b) with sulfuric acid.

(The concentration of sulfuric acid and thiomolybdate species is with respect to the total microemulsion volume.)

contained equal amounts of $5.0x10^{-3}$ M ammonium tetrathiomolybdate, except that the microemulsion represented in Figure 2.3b contained sulfuric acid as well. These two figures are different, in that the absorption peaks for MoS_4^{2-} and $MoO_2S_2^{4-}$ (31) are absent in Figure 2.3b while a peak with an onset wavelength of about 350 nm appears. The disappearance of the peaks for the thiomolybdate species suggests that conversion (e.g., Equations 2.1 and 2.2) took place in the w/o microemulsion when thiomolybdate species found themselves in the same inverse micelle with protons:

$$MoO_xS_y^{2-} + 2H^+ = MoO_xS_{(y-1)} + H_2S \qquad [2.2]$$

TGA and DTA studies. Figures 2.4a and 2.4b present the gravimetric and differential thermograms of molybdenum sulfide particles extracted from the 0.15 M NP-5/cyclohexane microemulsion system. The gravimetric thermogram (Figure 2.4a) shows a loss in weight between temperatures of 200 and 400 °C. This corresponds to the removal of NP-5 (surfactant) from the particle surface. The broad peak on the differential thermogram (Figure 2.4b) at a temperature of 296 °C is assigned to the loss of NP-5, which occurs at about the same temperature as that on the gravimetric curve in Figure 2.4a. The sharp exothermic peak at 375 °C is due to the formation of hexagonal MoS_2 from MoS_3 (32). The exothermic peak at 500 °C is attributed to the reaction MoS_2 (hexagonal) -> MoS_2 (rhombohedral). Similar observations have been made by other research groups (32-34).

2.3.2 Effect of Water-to-Surfactant Molar Ratio (R) on Particle Size

Figure 2.5 presents plots of the average particle diameter versus R. The corresponding size histograms are shown in Figure 2.6. Figure 2.7 presents TEM

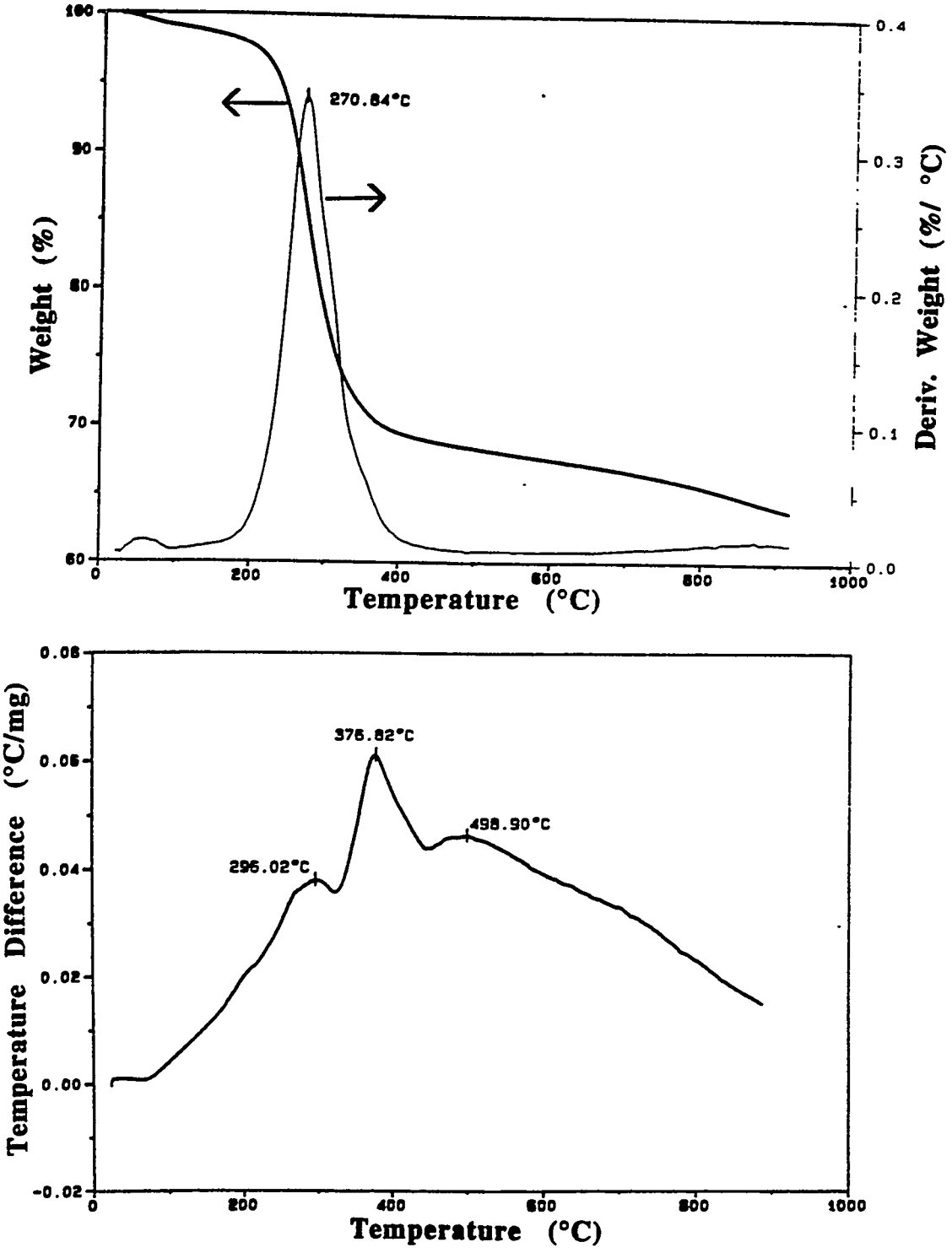

Figure 2.4

Thermal analysis of molybdenum sulfide particles extracted from the 0.15 M NP-5/cyclohexane microemulsion: (a) TGA; (b) DTA.

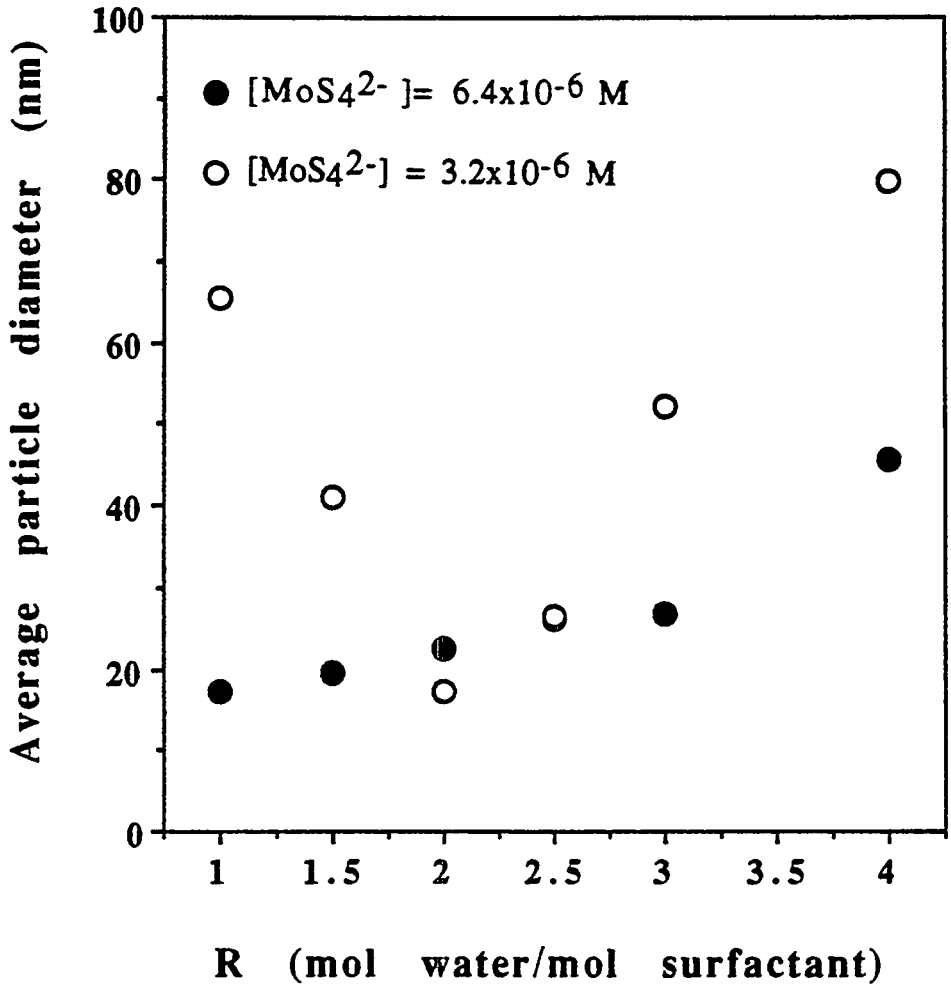

Figure 2.5

Effect of water-to-surfactant molar ratio (R) on the average molybdenum sulfide particle size for the 0.15 M NP-5/cyclohexane microemulsion. ($[H_2SO_4] = 1.3x10^{-3}$ M.)

Figure 2.6

Size histograms of molybdenum sulfide particles prepared in the 0.15 M NP-5/cyclohexane microemulsion system: Top, $[MoS_4^{2-}] = 3.2 \times 10^{-6}$ M; bottom, $[MoS_4^{2-}] = 6.4 \times 10^{-6}$ M.

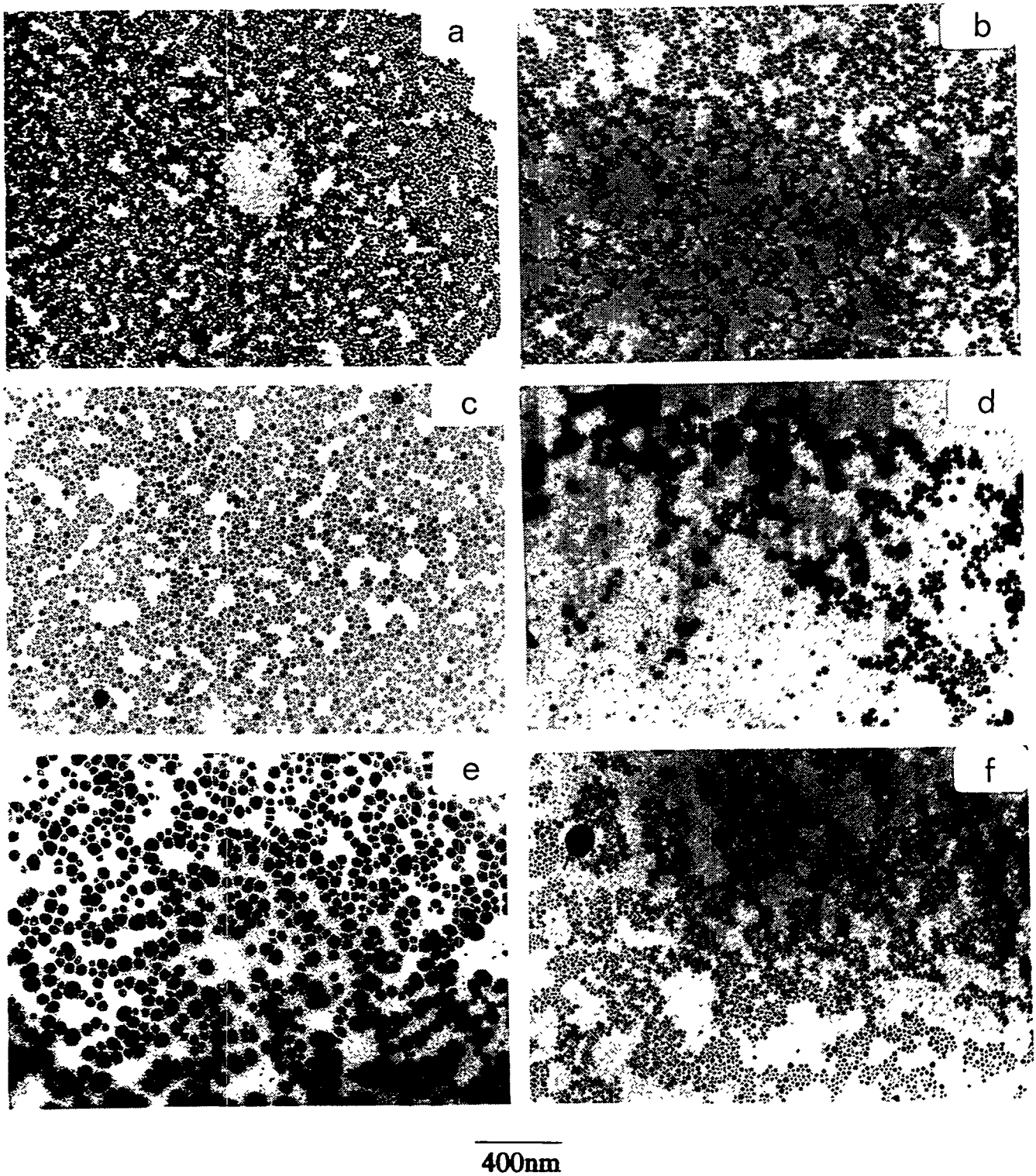

Figure 2.7
TEM micrographs of molybdenum sulfide particles prepared in 0.15 M NP-5/cyclohexane microemulsions:
$[MoS_4^{2-}] = 6.4 \times 10^{-6}$ M: (a) R=1; (b) R=2; (c) R=3;
$[MoS_4^{2-}] = 3.2 \times 10^{-6}$ M: (d) R=1; (e) R=2; (f) R=4.

micrographs of molybdenum sulfide particles produced with the 0.15 M NP-5/cyclohexane microemulsion system. For $[MoS_4^{2-}] = 3.2x10^{-6}$ M, the average particle diameter decreases with R up to a value of 2 and then increases with R. On the other hand, for $[MoS_4^{2-}] = 6.4x10^{-6}$ M, the average particle diameter increases monotonically with R.

These trends may be rationalized by considering the underlying nucleation and growth phenomena (3,12,35). The process of particle formation from dissolved ions can be represented in the following order: Ions -> Monomers -> Nuclei -> Particles (3,35). After a stable nucleus is formed, it can grow by the following processes: (a) incorporation of ions and monomers in solution into already formed nuclei (3), and (b) aggregation of primary particles or nuclei to form bigger particles (12,25,35,36). In order to form a stable nucleus, a cluster containing a critical number of monomers (N_c) must form (3,12,35). An important parameter in this connection is the ion occupancy number, i.e., the number of reactant species in an inverse micelle. A nucleus is formed if the ion occupancy number is greater than N_c. For a fixed oil-to-surfactant molar ratio, the surfactant aggregation number increases as R is increased (5,38). Consequently the number of inverse micelles in a fixed volume of microemulsion (micellar concentration) will decrease. This corresponds to an increase in the ion occupancy number since, for a given set of experiments, the concentrations of the reactant species (MoS_4^{2-} and H^+) with respect to the total microemulsion volume are maintained constant. Molybdenum sulfide will precipitate when protons and tetrathiomolybdate ions find themselves in the same inverse micelle. Here we assume that only one nucleus forms in a water pool. The probability of the reactant species meeting in one water pool increases as the ion occupancy number increases; hence, an increase in the number of nuclei in the microemulsion with increasing ion occupancy number is to be expected.

Summarized in Table 2.1 are data on the number of inverse micelles (N_m), the average molybdate occupancy number (N_{oc}, i.e., the ratio of the number of tetrathiomolybdate ions to the number of inverse micelles, $N_{oc} = N_{MoS_4^{2-}}/N_m$), the number of particles in 10 mL of microemulsion (N_p) and the ratio N_m/N_p for different R values. The calculation of the average molybdate occupancy number is based on the reasonable assumption that all solubilized ions are confined in the cores of the inverse micelles. An important point worth noting in Table 2.1 is that most of the inverse micelles are vacant, i.e., there is one MoS_4^{2-} ion for every 10^3 inverse micelles. This indicates that nucleation through inter-micellar interaction will predominate over that of intra-micellar interaction, i.e., the nucleation and initial growth of particles takes place through collision, fusion and splitting of inverse micelles.

As demonstrated by the data in Table 2.1, the surfactant aggregation number decreases, and the micellar concentration increases, as R is decreased (5,38). Thus, for a constant thiomolybdate reactant concentration (e.g., $[MoS_4^{2-}] = 3.2\times10^{-6}$ M) and low R values, relatively fewer water cores will contain the minimum number of ions required to form a nucleus. As a result, the nucleation rate should be low, and fewer nuclei are formed. The number of ions not utilized in the nucleation process is relatively large. These ions will be incorporated into the already formed nuclei via inter-micellar communication and will contribute to growth, leading to large particles, as demonstrated for R = 1 and $[MoS_4^{2-}] = 3.2\times10^{-6}$ M.

For $[MoS_4^{2-}] = 3.2\times10^{-6}$ M, the observed decrease in the particle size with an increase in R below R = 2 (Figure 2.5) can be attributed to the corresponding increase in average molybdate occupancy number. As R increases, the aggregation number increases, the micellar concentration decreases, and therefore the thiomolybdate occupancy number increases, as indicated in Table 2.1. The consequence of higher occupancy numbers is an increase in the probability that the inverse micelles will

Table 2.1

Selected Statistical Parameters for the Formation of Molybdenum Sulfide Particles in the 0.15 M NP-5/Cyclohexane Microemulsion

			N_{oc} x10^3		N_p x 10^{-11} (c)		(N_m/N_p) x 10^{-8}	
R	N (a)	N_m x 10^{-19} (b)	$[MoS_4^{2-}]$= $3.2x10^{-6}$	$[MoS_4^{2-}]$= $6.4x10^{-6}$	$[MoS_4^{2-}]$= $3.2x10^{-6}$	$[MoS_4^{2-}]$= $6.4x10^{-6}$	$[MoS_4^{2-}]$= $3.2x10^{-6}$	$[MoS_4^{2-}]$= $6.4x10^{-6}$
1	45	2.0	1.0	1.9	0.08	9.1	24	0.2
2	77	1.2	1.7	3.3	4.6	4.1	0.2	0.3
3	113	0.8	2.4	4.8	0.13	3.2	6.3	2.5
4	148	0.6	3.2	6.3	0.05	0.7	13	0.91

(a) N = surfactant aggregation number (obtained from Ref. 38).
(b) N_m = number of inverse micelles in 10 mL of microemulsion.
(c) N_p = number of particles in 10 mL of microemulsion.

contain the critical number of monomers needed to form a nucleus. This results in a high nucleation rate and thus small particles are made. However, primary particle aggregation may have occurred to a limited extent at $R < 2$ since the minimum particle size obtained is 17 nm. Furthermore, one may argue that, at $R = 2$, the nucleation rate is relatively high compared to $R < 2$. This implies that, in relative terms, the mechanism of ion addition becomes important as the average molybdate-to-micelle ratio decreases.

To check the possibility that the mechanisms of ion/monomer addition and primary particle aggregation are both operative at $R < 2$, the following growth experiments, the results of which are summarized in Figures 2.8 and 2.9, were conducted. Molybdenum sulfide was first prepared in the 0.15 M NP-5/cyclohexane microemulsion at $R = 1.75$ and $[MoS_4^{2-}] = 3.2 \times 10^{-6}$ M. Then 6.2 μL of 2.5×10^{-3} M ammonium tetrathiomolybdate were added. As indicated in Figure 2.8, molybdenum sulfide particles initially having an average size of 16 nm (Figure 2.8a) have grown to 60 nm (Figure 2.8b). In a second set of experiments, molybdenum sulfide particles were synthesized in the presence of sodium polyphosphate. This reagent has been reported to decrease particle aggregation (39). As shown in Figure 2.9a, few particles with an average diameter of about 10 nm were formed. This suggests that particle aggregation was decreased in the presence of the polyphosphate, but apparently only to a limited extent, as a greater number of larger particles (having an average diameter of 42 nm) was also found on many sections of the TEM grid (see Figure 2.9b).

For a constant R value of 1, the average molybdate occupancy number will increase with the number of tetrathiomolybdate ions in solution. Table 2.1 shows that, as the concentration of ammonium tetrathiomolybdate is doubled and $R = 1$ is maintained, the occupancy number increases. As can be seen from Figure 2.5, there is a corresponding decrease in particle size. Similar observations have been reported

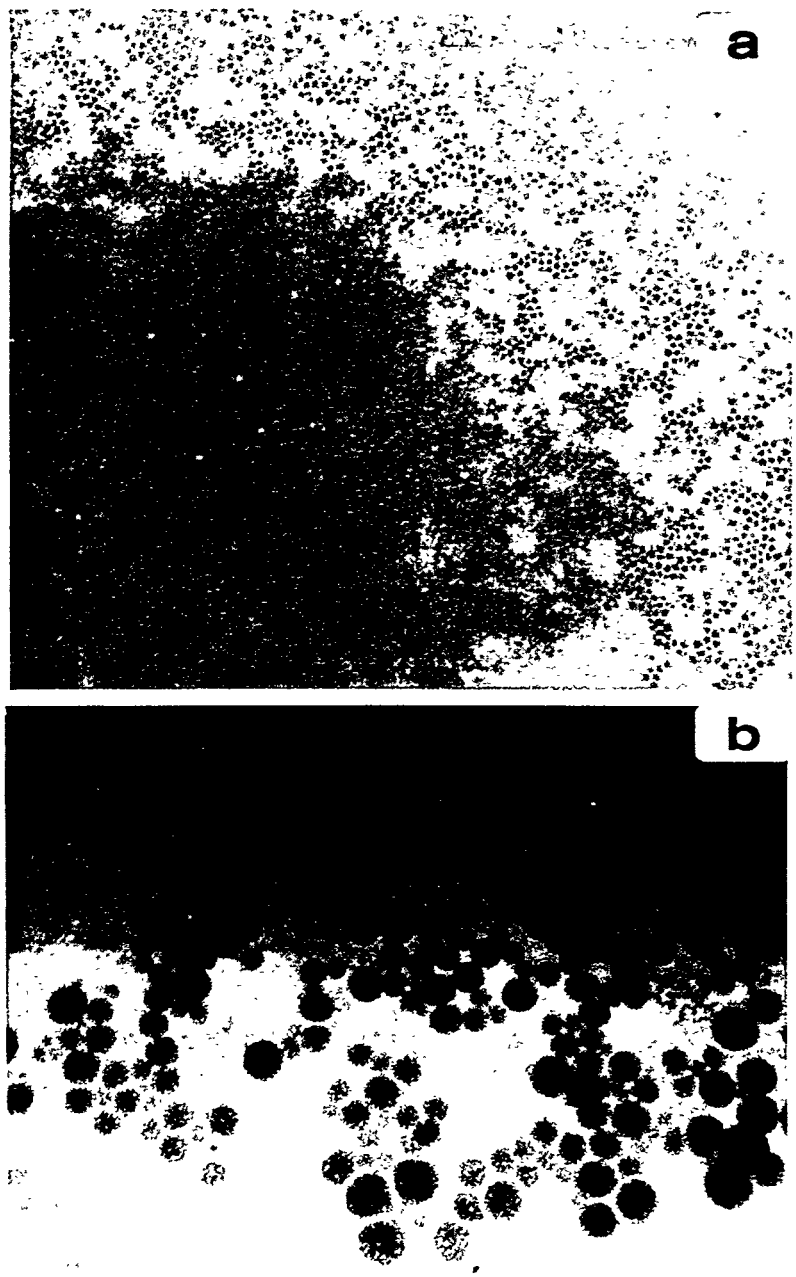

Figure 2.8
TEM micrographs of molybdenum sulfide particles prepared in 0.15 M NP-5/cyclohexane microemulsions:
(a) $[MoS_4^{2-}] = 3.2x10^{-6}$ M, R=1.75; (b) $[MoS_4^{2-}] = 3.2x10^{-6}$ M, R=2.

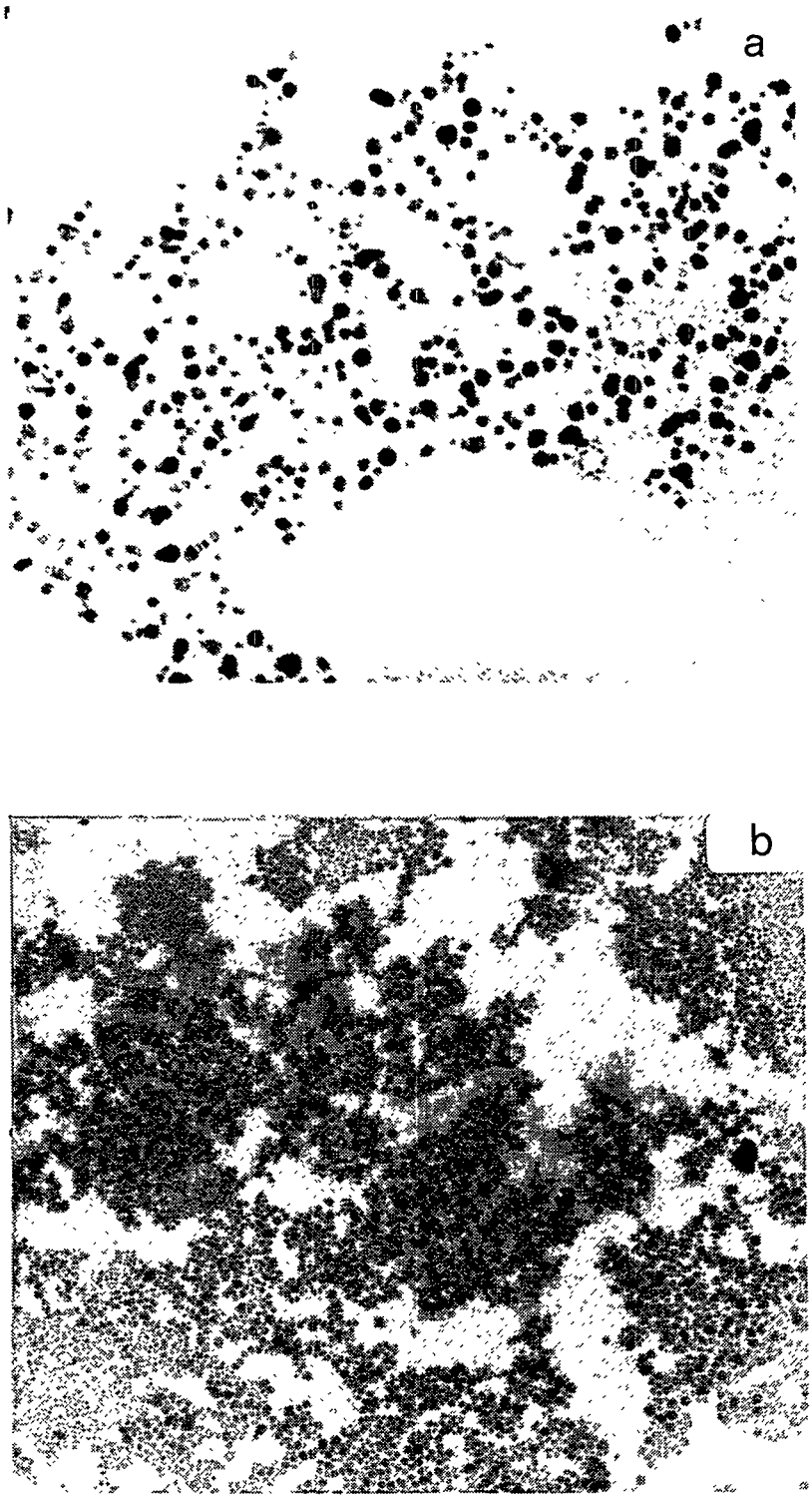

Figure 2.9
TEM micrographs of molybdenum sulfide particles prepared in 0.15 M NP-5/cyclohexane microemulsions in the presence of sodium polyphosphate. $[MoS_4^{2-}] = 3.2 \times 10^{-6}$ M; R=1.5.

by Lianos and Thomas (14) in the synthesis of CdS in the AOT/heptane/water microemulsion; at R = 32, smaller particles were formed at higher occupancy numbers. From nucleation theory (35), it is expected that as the number of nuclei in the microemulsion increases, the corresponding final particle size will decrease. This is because there will be relatively few ions left over after the nucleation process (i.e., almost all the ions are used up in the nucleation process).

For $[MoS_4^{2-}]$ =3.2x10^{-6} M and R > 2, the proportion of water in the microemulsion is relatively high; hence, the aggregation number is large, the concentration of swollen inverse micelles is reduced, and the occupancy number is significantly increased. Thus a greater number of nuclei and a correspondingly smaller particle size are expected. Contrary to expectation, however, large particle sizes were obtained. The trend observed at R > 2 may be rationalized by considering the micelle-to-particle ratio, N_m/N_p. As mentioned earlier (see Table 2.1), on average, one MoS_4^{2-} ion is solubilized per 10^3 inverse micelles. As a first approximation, if two molybdenum sulfide monomers form a particle, then the magnitude of N_m/N_p should be of the order of 10^3. However, from Table 1 N_m/N_p is of the order of 10^8. That is, one out of every 10^8 inverse micelles forms a particle. This suggests that initially many nuclei were formed and that the aggregation of nuclei and primary particles via inter-micellar interaction is the predominant mechanism of particle growth at R > 2.5. To test this hypothesis, particles were prepared at relatively high thiomolybdate occupancy numbers ($[MoS_4^{2-}]$ = 6.4x10^{-5} M, N_{oc} = 4x10^{-2}). As evidenced in Figure 2.10, aggregation of 5 nm particles, to form 50 to 90 nm secondary particles, takes place. Similar results have been reported by Robinson and coworkers (12) and by Kitahara and coworkers (36), respectively, for CdS and $CaCO_3$ particles synthesized in microemulsions.

In Figure 2.6, it is interesting to note that, for $[MoS_4^{2}]$ = 3.2x10^{-6} M, the polydispersity decreases with R up to a value of 2 (where monodispersity is virtually

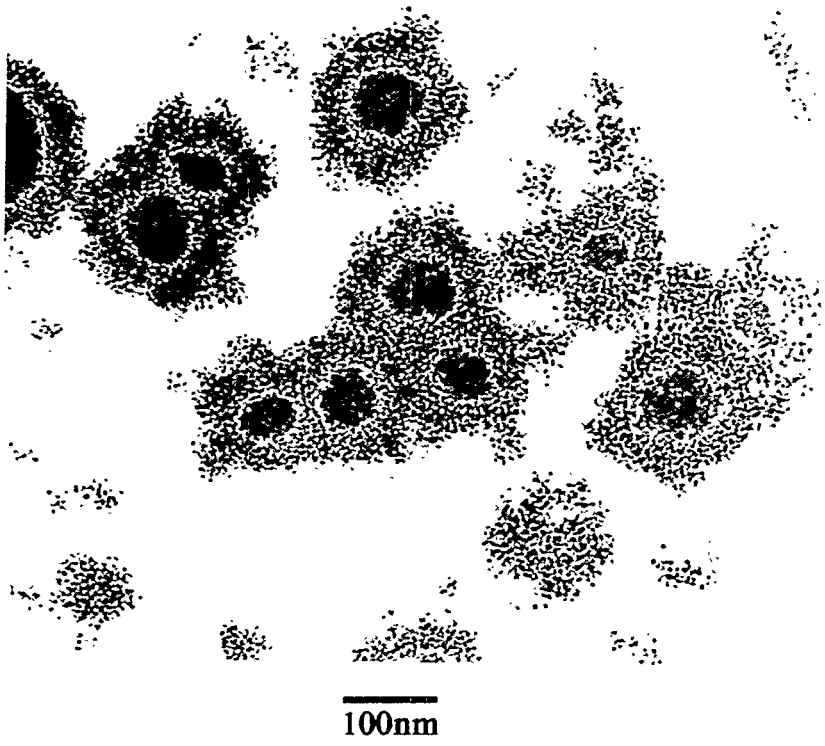

Figure 2.10

TEM micrograph of molybdenum sulfide particles prepared in the 0.15 M NP-5/cyclohexane microemulsion: R = 2.5, $[MoS_4^{2-}] = 6.4 \times 10^{-5}$ M, $[H_2SO_4] = 1.3 \times 10^{-3}$ M.

attained), and then increases. This may be due to the fact that, at R = 2, particle growth is relatively slow and hence monodispersed particles are obtained. This trend supports the argument that at R < 2 the decrease in particle size with increasing R is a consequence of an increase in the occupancy number, which results in increased nucleation, with a corresponding decrease in growth by monomer addition. The increase in polydispersity at R > 2 may be a result of the aggregative growth mechanism which enhances polydispersity (13).

At R = 1, both the particle size and polydispersity decrease when the concentration of ammonium tetrathiomolybdate is increased from 3.2×10^{-6} M to 6.4×10^{-6} M. The latter decrease implies that, at a relatively high occupancy number ($[MoS_4^{2-}] = 6.4 \times 10^{-6}$ M, R = 1), growth is inhibited as more nuclei are formed, which results in relatively small monodispersed particles.

For $[MoS_4^{2-}] = 6.4 \times 10^{-6}$ M and R < 3, the occupancy numbers are relatively high; hence monodispersed particles are obtained (Figure 2.6). However, at R = 4 the size distribution is broadened as a result of the aggregation of nuclei and/or primary particles, which produces polydispersed particles (13).

2.4 CONCLUSIONS

Nanosize molybdenum sulfide particles have been synthesized in 0.15 M NP-5/cyclohexane microemulsions. The results indicate that careful control of the water-to-surfactant molar ratio (R) and the ion occupancy number is vital in designing the optimal conditions needed to make particles of desired size. The mechanism of growth may be different for R values less than and greater than ~2.5. At R < 2.5, growth is probably due to both ion addition and primary particle aggregation, while at R > 2.5, growth is due to nuclei and/or particle aggregation.

2.5 REFERENCES

1. Haruta, M., Lamaitre, J., Delannay, F., and Delmon, B., *J. Colloid Interface Sci.* **101**, 59 (1984).
2. Andres, M., Charcosset, H., Chiche, P., Davignon, L., Djega-Mariadassou, G., Joly, J.P., and Pregermain, S., *Fuel* **62**, 69 (1983).
3. Nagy, J.B., *Colloids Surf.* **35**, 201 (1989).
4. Fendler, J.H., *Chem. Rev.* **87**, 877 (1987).
5. Osseo-Asare, K., and Arriagada, F.J., *Colloids Surf.* **50** 321 (1990).
6. Barnickel, P., Wokaun, A., *Mol. Phys.* **69**, 1 (1990).
7. Barnickel, P., Wokaun, A., Sager, W., and Eicke, H.F., *J. Colloid Interface Sci.* **148**, 80 (1992).
8. Boutonnet, M., Kizling, J., Stenius, P., and Maire, G., *Colloids Surf.* **5**, 209 (1982).
9. Claerbout, A., and Nagy, J.B., in "Preparation of Catalysts V" (G. Poncelet, P.A. Jacobs, P. Grange and B. Delmon, Eds.), Elsevier, 1991, p. 705.
10. Touroude, R., Girard, P., Maire, G., Kizling, J., Boutonnet, M., and Stenius, P., *Colloids Surf.* **67**, 19 (1992).
11. Kumar, P., Pillai, V., and Shah, D.O., *Appl. Phys. Lett.* **62**, 765 (1993).
12. Towey, T.F., Khan-Lodhi, A., and Robinson, B.H., *J. Chem. Soc. Faraday Trans.* **86**, 3757 (1990).
13. Modes, S. and Lianos, P., *J. Phys. Chem.* **93**, 5854 (1989).
14. Lianos, P. and Thomas, J.K., in "Materials Science Forum", Vol. 25-26 (G.E. Murch and F.H. Wohlbier, Eds.), 1988, p. 369.
15. Petit, C., and Pileni, M.P., *J. Phys. Chem.* **92**, 2282 (1988).
16. Motte, L., Petit, C., Boulanger, L., Lixon P., and Pileni, M.P., *Langmuir* **8**, 1049 (1992).

17. Pileni, M.P., Motte, L., and Petit, C., *Chem. Mater.* **4**, 338 (1992).

18. Robinson, B.H., Towey, T.F., Zourab, S., Visser A.J.W.G., and Hoek, A.V., *Colloids Surf.* **61**, 175 (1991).

19. Dannhausser, T., O'Neil, M., Johansson, K., Whitten, D., and McLendon, G., *J. Phys. Chem.* **90**, 6074 (1986).

20. Steigerwald, M.L., Alivisatos, A.P., Gibson, J.M., Harris, T.D., Kortan, R., Müller, A.J., Thayer, A.M., Duncan, T.D., Douglas D.C., and Brus, L.E., *J. Am. Chem. Soc.* **110**, 3046 (1988).

21. Arriagada, F.J. and Osseo-Asare, K., *Colloids Surf.* **69**, 105 (1992).

22. Yamauchi, H., Ichikawa, T., and Kondo, S., *Colloids Surf.* **37**, 71 (1989).

23. Yanagi, M., Asano, Y., Kandori, K., Kon-no, K., and Kitahara, K., 1986 Shikizai Technical Conference (Osaka, Japan), 1986, p. 86.

24. Dvolaitzky, M., Ober, R., Taupin, C., Anthore, R., Auvray, X., Petipas, C., and Williams, C., *J. Dispersion Sci. Technol.* **4**, 29 (1983).

25. Hou, M.J., and Shah, D.O., in" Interfacial Phenomena in Biotechnology and Materials Processing" (Y.A. Attia, B.M. Moudgil and S. Chander, Eds.), Elsevier, 1988, p. 443.

26. Vaidyanathan, N., Boakye, E., Osseo-Asare, K., and Radovic, L.R., *ACS Preprints (Division of Fuel Chemistry)* **37**, 480 (1992).

27. Christenson, H., Friberg, S.E., and Larsen, D.W., *J. Phys. Chem.* **84**, 3633 (1980).

28. Kon-no, K., and Kitahara, A., *J. Colloid Interf. Sci.* **34**, 221 (1970).

29. Handbook of Chemistry and Physics, 64th Ed. (R.C. Weast, M.J. Astle and W.H. Beyer, Eds.), CRC Press, 1983-84.

30. Fendler, J.H., *Acc. Chem. Res.* **9**, 153 (1976).

31. Aymonino, P.J., Ranade, A.C., Diemann, E., and Müller, A., *Z. Anorg. Allg. Chem.* **371**, 300 (1969).

32. Ratnasamy, P., Rodrique, L., and Leonard, A.J., *J. Phys Chem.* **77**, 2242 (1978).

33. Busetto, L., Iannibello, A., Pincolini, F., and Trifiro, F., *Bull. Soc. Chim. Belg.* **90,** 1233 (1981).

34. Ratnasamy, P. and Leonard, A.J., *J. Catal.* **26,** 352 (1972).

35. Nielson, A.E., "Kinetics of Precipitation", MacMillan, New York (1964).

36. Kandori, K., Kon-no, K., and Kitahara, A., *J. Colloid Interface Sci.* **122,** 78 (1988).

37. Bogush, G.H., and Zukoski IV, C.F., *J. Colloid Interface Sci.* **142,** 19 (1991).

38. Kitahara, A., *J. Phys. Chem.* **69,** 2788 (1965).

39. Henglein, A., *Chem. Rev.* **89,** 1861 (1989).

CHAPTER 3

SYNTHESIS OF NANOSIZE MOLYBDENUM SULFIDE IN MICROEMULSIONS: EFFECT OF THE SYNTHESIS PROTOCOL ON PARTICLE SIZE

3.1 INTRODUCTION

The synthesis of particles in water-in-oil (w/o) microemulsions is a technique that has prospects in a wide variety of fields, such as ceramics, photographic emulsion technology and catalysis (1-8). The synthesis protocols that have been used can be classified broadly as follows: (a) microemulsion plus a second reactant, (b) two microemulsions, and (c) microemulsion plus trigger (7).

For particles made in inverse micelles, the water-to-surfactant molar ratio (R), the reactant concentrations, and the dynamic behavior of the microemulsion droplets are among the key factors that determine particle size and size distribution. Recent publications (9-12) show that the synthesis method may predetermine the particle size, although some ambiguities exist. For example, Lianos and Thomas (9) reported that CdS particles synthesized in the AOT/heptane/water microemulsion system produced particles of different sizes when the microemulsion-plus-a-second-reactant and the two-microemulsions synthesis methods were used. The differences in particle size were attributed to the unequal solubilization rates of the ions in the microemulsion system, depending on the synthesis method. However, no investigation or demonstration of the differences in the solubilization rates was presented. On the other hand, Ward et al. (10) obtained particles of similar size and size distribution when the microemulsion-plus-a-second-reactant and the two-

microemulsions synthesis protocols were used to synthesize PbS particles in a nonionic microemulsion.

In Chapter 2, the effects of the water content of the microemulsion and the tetrathiomolybdate ion concentration on the molybdenum sulfide particle size was reported for two ammonium tetrathiomolybdate precursor reactant concentrations. This Chapter deals with the effect of the synthesis protocol on the molybdenum sulfide particle size and size distribution. In order to relate the particle size to the microemulsion properties, additional experiments were conducted involving measurements of the solubilization and solubility limits of aqueous acid and of ammonium tetrathiomolybdate solutions. The effects of the electrolytes on the microemulsion droplet size were also investigated. As in Chapter 2, the microemulsion system polyoxyethylene(5)nonylphenyl ether (NP-5)/cyclohexane/water was used. The overall chemistry of molybdenum sulfide formation from ammonium molybdate is summarized in Equations 3.1 and 3.2:

$$MoO_4^{2-} + 4HS^- = MoS_4^{2-} + 4OH^- \qquad [3.1]$$

$$MoS_4^{2-} + 2H^+ = MoS_3 + H_2S \qquad [3.2]$$

From Equation 3.2 it follows that molybdenum sulfide will form when the thiomolybdate species combine with protons in an inverse micelle.

3.2 EXPERIMENTAL

3.2.1 Materials

The following chemicals were obtained from Aldrich and were used as received: the nonionic surfactant polyoxyethylene(5)nonylphenyl ether (NP-5; molecular weight, 440.63), ammonium tetrathiomolybdate (99.97%), and cyclohexane (99%).

3.2.2 Phase Behavior

The methodology used to characterize the phase behavior of the microemulsion system 0.15 M NP-5/cyclohexane was as reported in Chapter 2. To check for the effect of the reactant species on the solubilization and solubility limits, the phase behavior of a number of samples containing 1.3×10^{-3} M sulfuric acid or 6.4×10^{-6} M ammonium tetrathiomolybdate and different water contents was observed as a function of temperature. (The concentrations are with respect to the total microemulsion volume.) The phase behavior of the microemulsion samples containing only water as the solubilizate was also recorded to analyze the effects of the electrolytes on the solubilization and solubility limits. The measurements of solubility and solubilization limits were reproducible to within ±0.5 °C for a given R value. In preparing the ammonium tetrathiomolybdate impregnating solution, sodium hydroxide was added to enhance the dissolution of the molybdenum salt in water. Thus in making the 6.4×10^{-6} M ammonium tetrathiomolybdate microemulsion solution, aqueous sodium hydroxide was co-solubilized. In all cases, the concentration of sodium hydroxide with respect to the total microemulsion volume was 1.4×10^{-5} M. This procedure was followed in the

preparation of all the tetrathiomolybdate-containing microemulsions used in the present investigation.

3.2.3 Micellar Size Measurement

Photon correlation spectroscopy (PCS) was used to measure the microemulsion droplet size (13-16). The light source was a coherent Innova 70-2 argon ion laser operating at 488 nm. The scattered light was collected at an angle of 90 degrees by a goniometer and focused on a photomultiplier tube (Malvern Instruments Inc.) The correlation function was recorded with a Malvern 7032-8 correlator with 256 channels. The hydrodynamic size was calculated using a particle size distribution software provided by Malvern. Before carrying out the micellar size measurements, the sample was centrifuged to remove particles that may exist in the microemulsion. The refractive index of cyclohexane was measured with an Abbe-3L refractometer (Milton Roy Company). The viscosity was determined with an Ubbelohde viscometer immersed in a thermostatted bath.

In the PCS technique, the fluctuations in scattered intensity of the inverse micelles due to their Brownian motion are measured over small time intervals. The magnitudes of the intensity and its delayed version are compared. The result is represented by the intensity autocorrelation function $G(\tau)$. The measured intensity autocorrelation function is related to the autocorrelation function $g(\tau)$ by Equation 3.3.

$$G(\tau) = A(1 + B|\, g(\tau)\,|^2) \qquad [3.3]$$

In Equation 3.3, A and B are instrumental constants. For monodispersed colloidal particles, the autocorrelation function $g(\tau)$ is represented by the equation,

$$g(\tau) = \exp(-\Gamma\tau) \qquad [3.4]$$

where G (the decay constant) is related to the diffusion coefficient of the particle (D) as in Equation 3.5.

$$\Gamma = Dq^2 \qquad [3.5]$$

The scattering vector q is given by

$$q = [4\pi n/\lambda] \sin(\Theta/2) \qquad [3.6]$$

where n is the refractive index of the solvent, λ is the wavelength of the incident light and Θ is the scattering angle.

A least squares fit permits the determination of B and Γ, from which the diffusion coefficient is obtained. Finally, the diffusion coefficient is related to the micellar radius (R) via the Stokes-Einstein relation (Equation 3.7), which assumes that the inverse micelles are spherical in shape:

$$D = k_B T/6R\pi\eta \qquad [3.7]$$

In Equation 3.7, η is the viscosity of the solvent, T is the absolute temperature and k_B is the Boltzmann constant. For polydispersed systems $g(\tau)$ deviates from a single exponential (i.e., one particle size representation). Hence the method of moments (or cumulants) (17) was used to analyze the data.

3.2.4 Particle Synthesis

Three synthesis protocols were used in this study. Considering the reaction in Equation 3.2, we describe the synthesis methods as: (a) acid-solubilized microemulsion plus tetrathiomolybdate (ASMPT), (b) tetrathiomolybdate-solubilized microemulsion plus acid (TSMPA), and (c) microemulsion plus microemulsion (MPM), i.e., acid-solubilized microemulsion plus tetrathiomolybdate-solubilized microemulsion. Figure 3.1 is a schematic illustration of how each of the methods was implemented. In the ASMPT method (a), 12 μL of 1.1 M aqueous sulfuric acid was first solubilized in 10 mL of NP-5/cyclohexane solution while bubbling high purity nitrogen gas. This was followed by adding 12.8 μL of $5x10^{-3}$ M ammonium tetrathiomolybdate. Nitrogen was further bubbled while molybdenum sulfide formed. On the other hand, for the TSMPA method (b), 12.8 μL of ammonium tetrathiomolybdate was first solubilized, followed by the addition of 12 μL of 1.1 M dilute sulfuric acid. The final concentrations of sulfuric acid and ammonium tetrathiomolybdate were, respectively, $1.3x10^{-3}$ and $6.4x10^{-6}$ M with respect to the total microemulsion volume (10 mL). The synthesis was done at a temperature of 50 °C. For the MPM synthesis method (Figure 3.1c), 5 mL each of two microemulsion solutions, containing $2.6x10^{-3}$ M sulfuric acid and $1.28x10^{-5}$ M ammonium tetrathiomolybdate, were mixed at 50 °C while bubbling nitrogen gas. Before mixing the microemulsion solutions, they were brought to a temperature of 50 °C while bubbling high purity nitrogen gas. As noted above, all the tetrathiomolybdate-containing microemulsions also contained NaOH ($1.4x10^{-5}$ M).

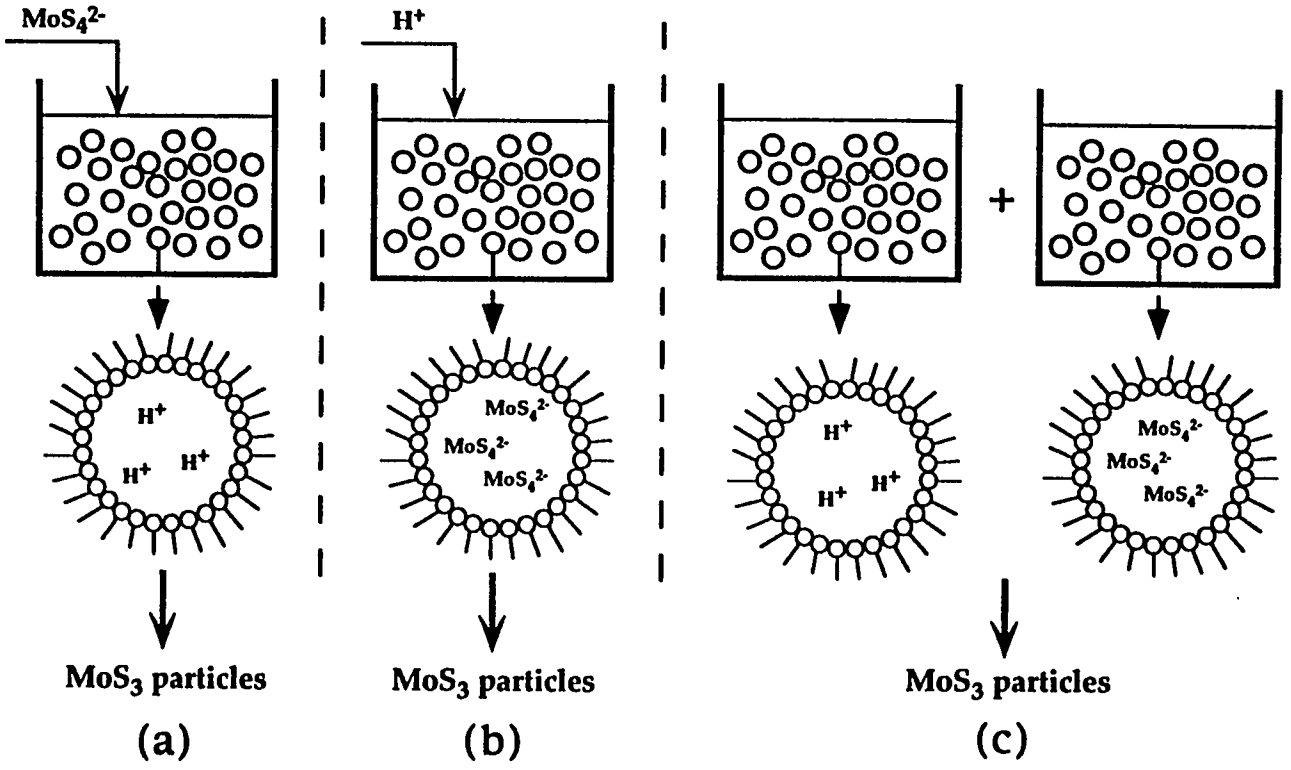

Figure 3.1

Particle synthesis methods in water-in-oil (w/o) microemulsions:
(a) Acid-solubilized microemulsion plus tetrathiomolybdate (ASMPT); (b) tetrathiomolybdate-solubilized microemulsion plus acid (TSMPA); (c) acid-solubilized microemulsion plus tetrathiomolybdate-solubilized microemulsion (MPM).

3.3 RESULTS AND DISCUSSION

3.3.1 Phase Behavior

Figure 3.2a shows the effect of temperature on the solubilization of water and dilute sulfuric acid in the solvent system NP-5/cyclohexane. The region between the solubilization and solubility limits represents the one-phase microemulsion domain where the surfactant-stabilized microdroplets of water are dispersed in oil (cyclohexane). The water-in-oil microemulsion exists with excess water above the solubilization limit, whereas the surfactant phase containing dissolved water is separated from the oil below the solubility limit. The trend in Figure 3.2a is consistent with the previously reported solubilization studies performed with nonionic surfactants as amphiphilic agents (18-25). The solubilization diagrams for water and acid are superimposed for comparison. No distinct differences are observed.

Figure 3.2b summarizes the combined solubility and solubilization diagrams for the solvent system 0.15 M NP-5/cyclohexane with water or a mixture of sodium hydroxide and ammonium tetrathiomolybdate solution as the aqueous domain. It is obvious that for the microemulsion system 0.15 M NP-5/cyclohexane/ammonium tetrathiomolybdate/sodium hydroxide, the one-phase microemulsion region is shifted to lower temperatures when compared to that of water as the solubilizate.

The small differences in the solubility curves obtained with ammonium tetrathiomolybdate/sodium hydroxide and dilute sulfuric acid as solubilizates may be due to the following factors: (a) the ether oxygen atom may be regarded as a weak Lewis base (this is due to its possession of two lone pairs of electrons) and the water

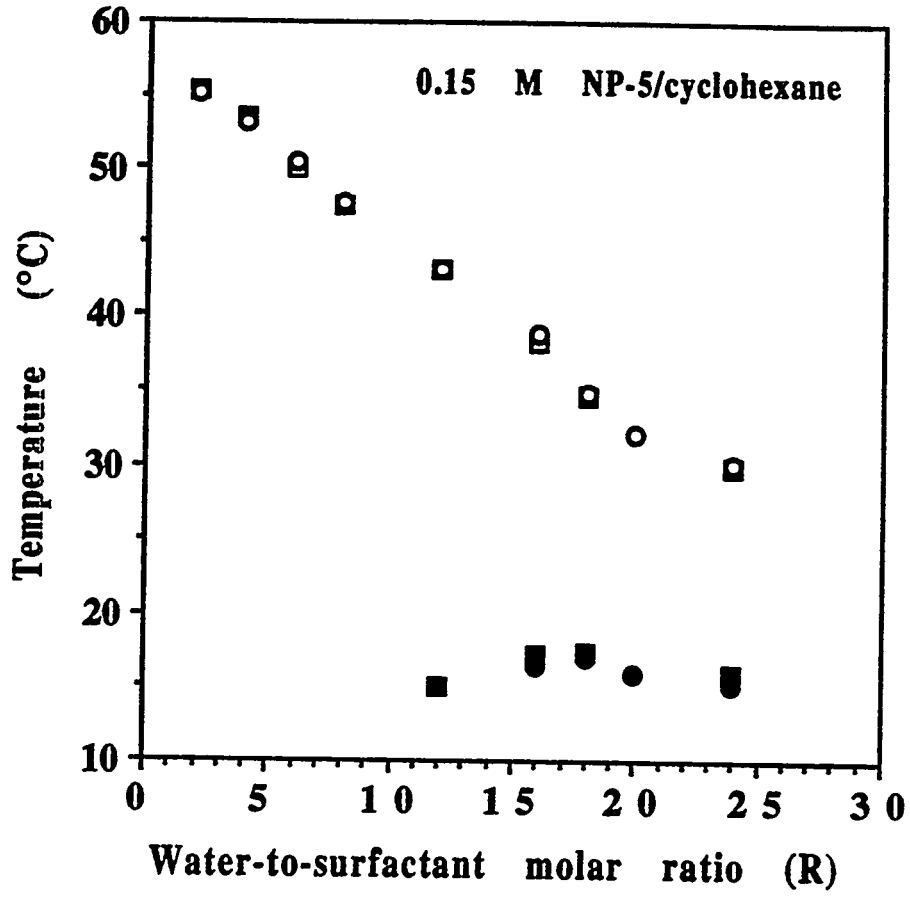

Figure 3.2a

Solubilization diagrams of water and of dilute sulfuric acid in the 0.15 M NP-5/cyclohexane microemulsion; $[H_2SO_4] = 1.3 \times 10^{-3}$ M.

●, solubility limit, H_2O; ○, solubilization limit, H_2O;

■, solubilty limit, H_2SO_4; □, solubilization limit, H_2SO_4.

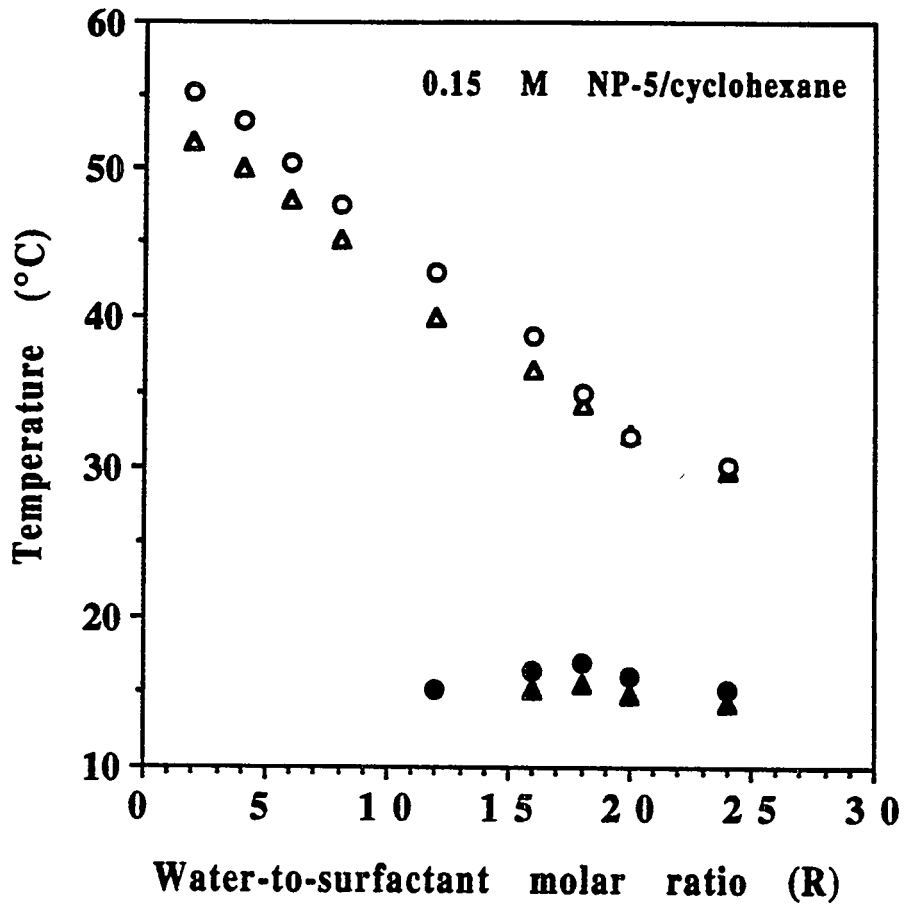

Figure 3.2b

Solubilization diagrams of water and of aqueous ammonium tetrathiomolybdate/sodium hydroxide in the 0.15 M NP-5/cyclohexane microemulsion; $[MoS_4^{2-}] = 6.4 \times 10^{-6}$ M, $[NaOH] = 1.4 \times 10^{-5}$ M.

◐, solubility limit, H_2O; O, solubilization limit, H_2O;

▲, solubility limit, $(NH_4)_2MoS_4$; Δ, solubilization limit, $(NH_4)_2MoS_4$.

solubilized by the amphiphile as a weak Lewis acid; (b) the surfactant molecules may be salted out in the presence of electrolytes.

To separate the effects of aqueous ammonium tetrathiomolybdate and sodium hydroxide on the solubilization limits, the following experiments were conducted. The phase behavior of a number of microemulsion samples containing $1.4x10^{-5}$ M NaOH and different water contents was observed as a function of temperature. The results showed that, for all water-to-surfactant molar ratios, the solubilization limit is reduced by about the same extent for the following combinations of solubilizates: (a) ammonium tetrathiomolybdate plus sodium hydroxide and (b) sodium hydroxide. From the above observations, it is concluded that the lowering of the solubilization diagram in the ammonium-tetrathiomolybdate-plus-sodium-hydroxide system may be attributed to the presence of aqueous sodium hydroxide.

A base such as OH^- (with three lone pairs of electrons) will compete for water molecules with the oxygen atoms of the surfactant oxyethylene groups. As a result, the extent of hydrogen bonding between the ether oxygen and water, which is the driving force for the solubilization of water molecules in the microemulsion (26,27), will decrease. Consequently the solubility of the electrolyte in the microemulsion will decrease.

Other investigators have offered a complementary explanation (23,24,28,29) for this behavior in terms of the 'salting-out' effect. This mechanism refers to the effective removal of water molecules from the ether oxygen group as a result of the preferential hydration of the solubilizates (30). In support of this view, Kon-no and Kitahara (23) found that the solubilization and solubility limits of the microemulsion system NP-8/tetrachloroethylene/water depended on the nature of the anion solubilized. The order of decrease in the solubilization diagram was reported as $F^- > Cl^- > NO_3^- > I^- > SCN^-$. These results were rationalized by the

argument that the more basic anion dehydrates the ether oxygen group to a greater extent, thus lowering the solubilization diagram to a greater degree. Firman et al. (28) have summarized the salting-out mechanism using the principle of hard and soft acids and bases (HSAB) which states that hard acids prefer hard bases while soft acids prefer soft bases (31). In this view, bases such as F^- and OH^-, which are regarded as hard, will interact preferentially with H_2O (Lewis acid) and are therefore selectively hydrated. In other words, the ether oxygen group is dehydrated and this results in a decrease in the solubility of water in the nonionic surfactant.

3.3.2 Effect of Salinity on Micellar Size

Presented in Figure 3.3 are the results of the micellar size measurements for the solvent system 0.15 M NP-5/cyclohexane with water, ammonium tetrathiomolybdate and aqueous sulfuric acid as solubilizates. For each solubilizate, the micellar diameter increases with the water-to-surfactant molar ratio (R). Furthermore, for each R value, the microemulsion droplet size decreases on solubilizing ammonium tetrathiomolybdate or aqueous sulfuric acid.

3.3.3 Particle synthesis

Effects of R and synthesis protocol on particle size. Figure 3.4 summarizes the effects of the synthesis method on the average particle diameter for various R values. Figures 3.5, 3.6 and 3.7 present the corresponding TEM micrographs of the molybdenum sulfide particles. Generally, for all the synthesis schemes, the average particle diameter increases with R. Also within the limits of the standard deviation of the average particle size, the diameter is relatively insensitive to the method of preparation for R = 1 - 2.5. However at R > 2.5, the particle size and the size

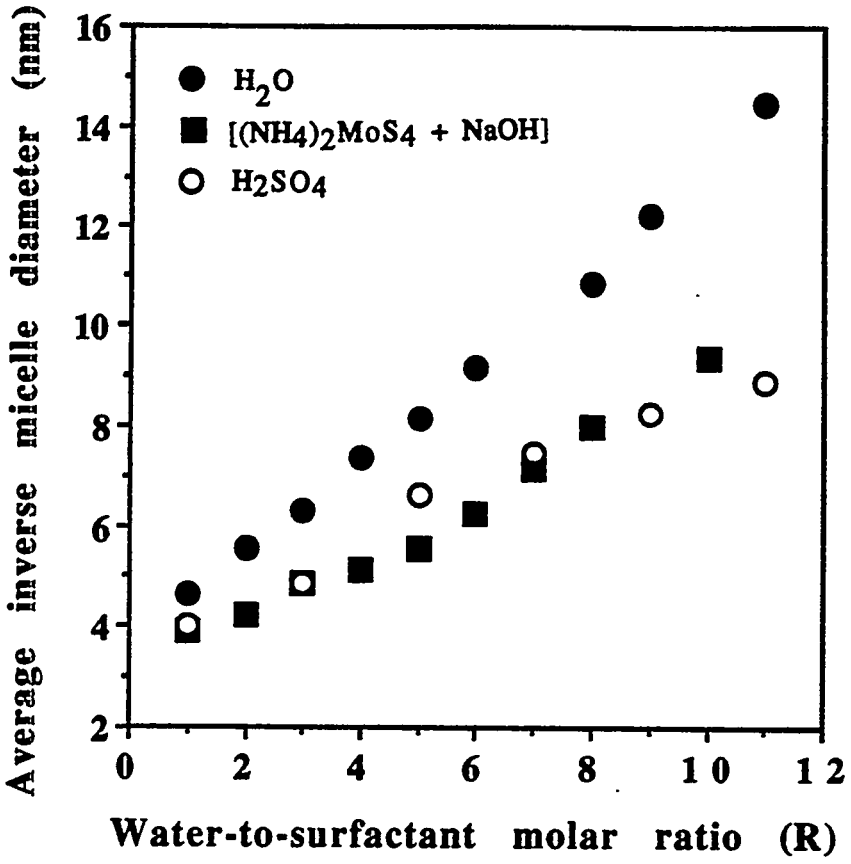

Figure 3.3

Effect of the water-to-surfactant molar ratio (R) on the hydrodynamic diameter of the inverse micelles in the microemulsion system 0.15 M NP-5/cyclohexane at 30 °C. $[H_2SO_4] = 1.3 \times 10^{-3}$ M, $[MoS_4^{2-}] = 6.4 \times 10^{-6}$ M, $[NaOH] = 1.4 \times 10^{-5}$ M.

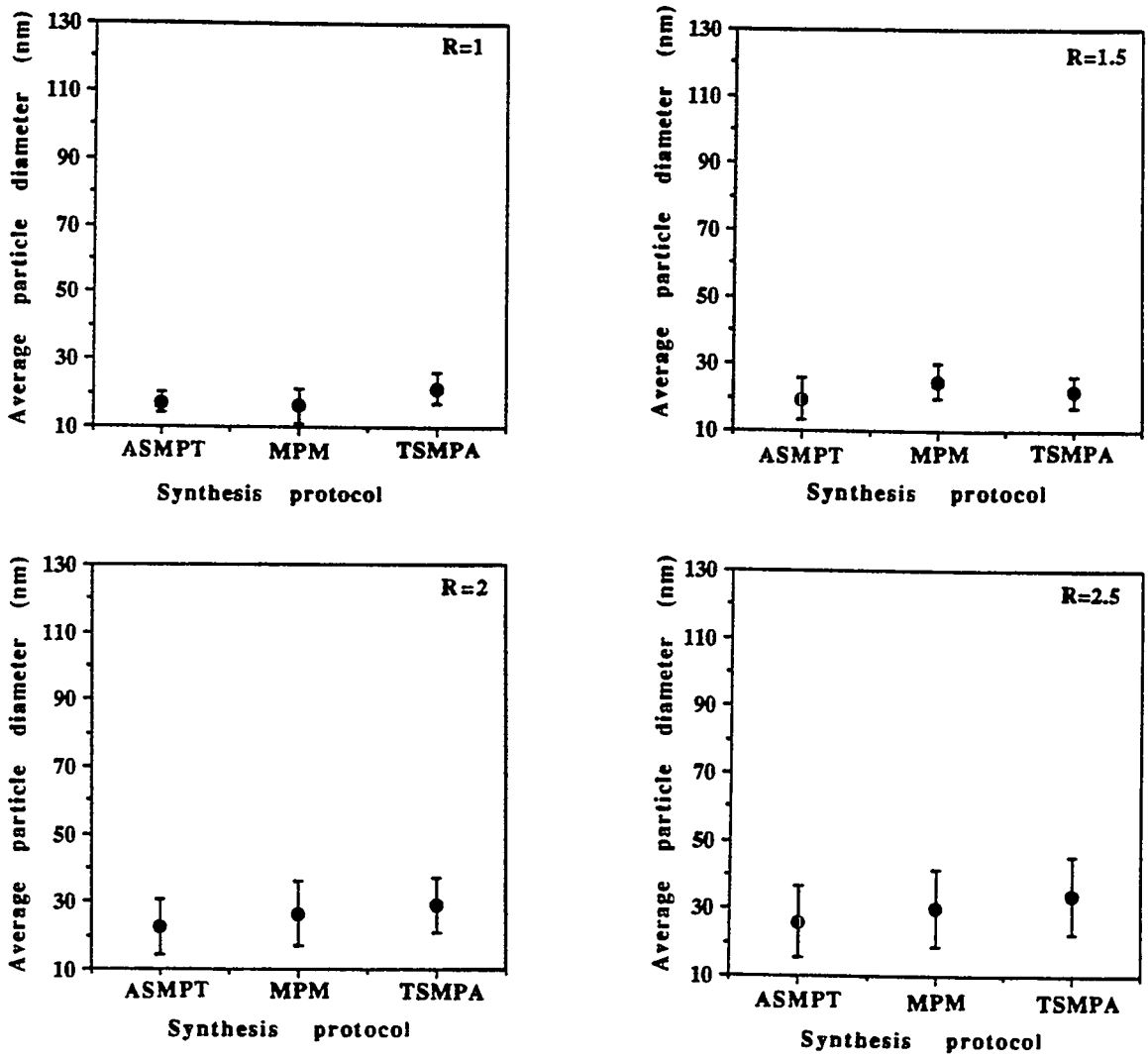

Figure 3.4

Effect of the water-to-surfactant molar ratio (R) on the average molybdenum sulfide particle size for the 0.15 M NP-5/cyclohexane microemulsion system using different synthesis protocols.

$[H_2SO_4] = 1.3 \times 10^{-3}$ M, $[MoS_4^{2-}] = 6.4 \times 10^{-6}$ M, $[NaOH] = 1.4 \times 10^{-5}$ M.

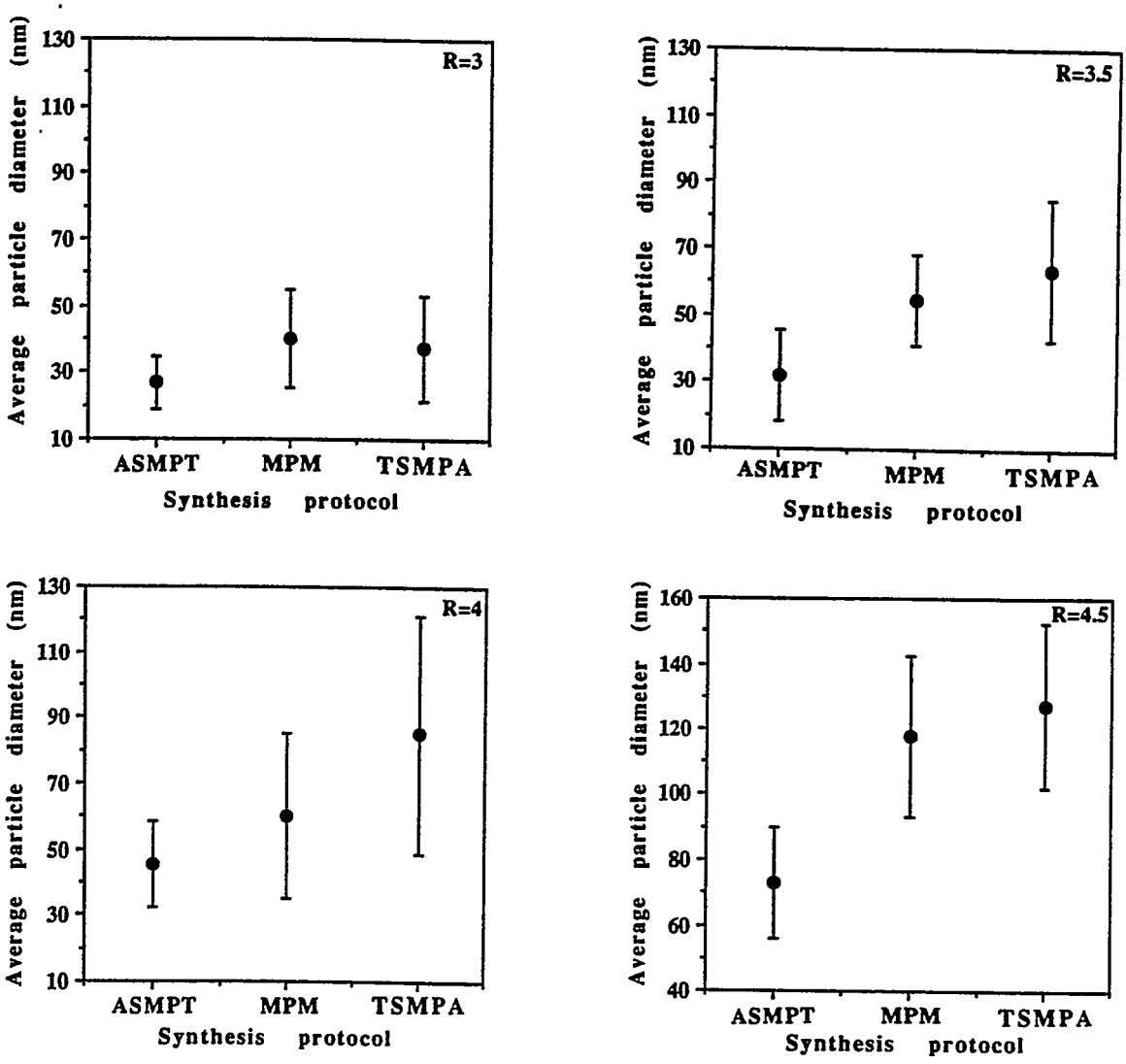

Figure 3.4
(Continued)

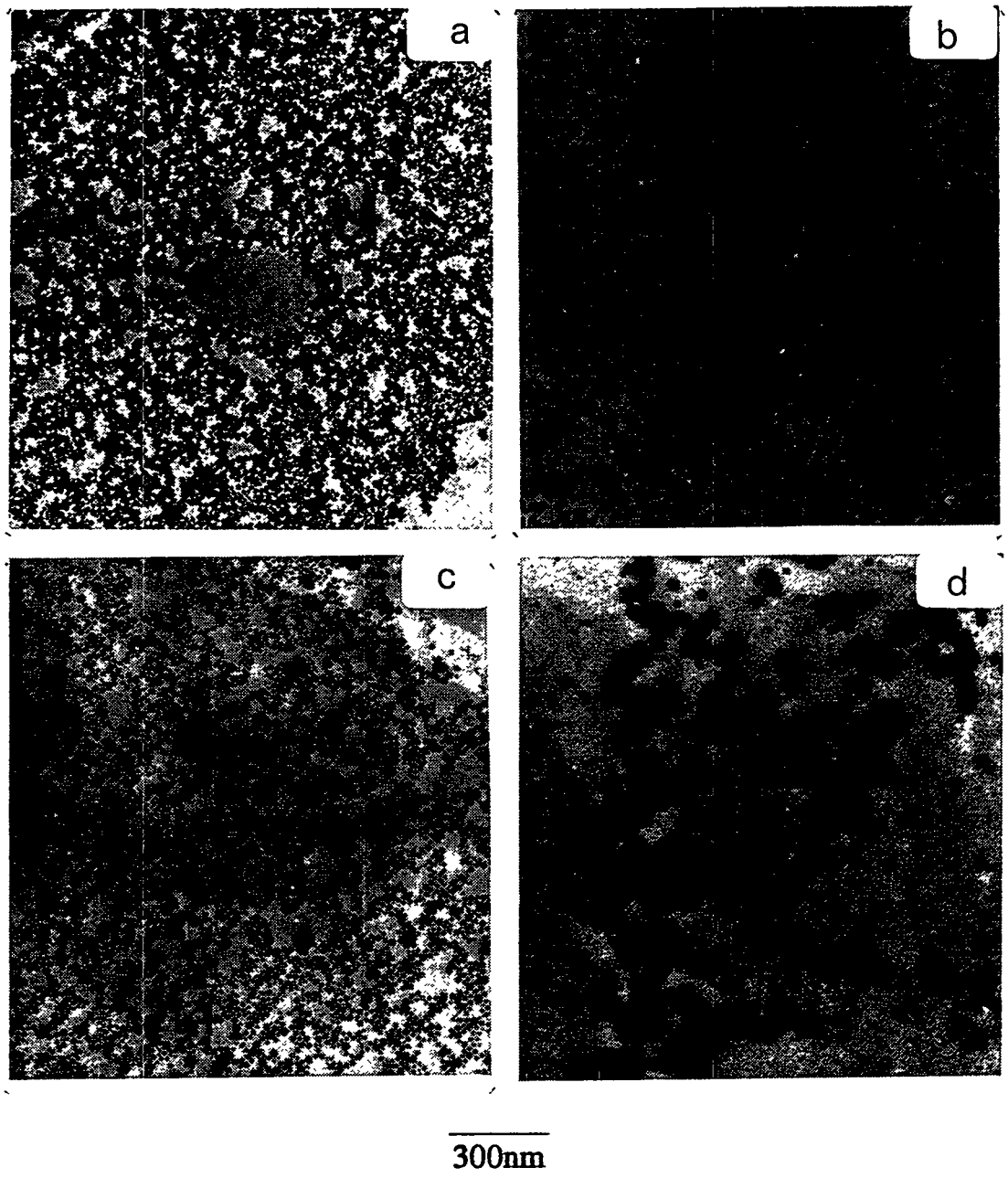

Figure 3.5

TEM micrographs of molybdenum sulfide particles prepared in the 0.15 M NP-5/cyclohexane microemulsion system, using the acid-solubilized microemulsion plus tetrathiomolybdate (ASMPT) protocol; $[H_2SO_4] = 1.3 \times 10^{-3}$ M; $[MoS_4^{2-}] = 6.4 \times 10^{-6}$ M; $[NaOH] = 1.4 \times 10^{-5}$ M. (a) R=1; (b) R=2; (c) R=3; (d) R=4.

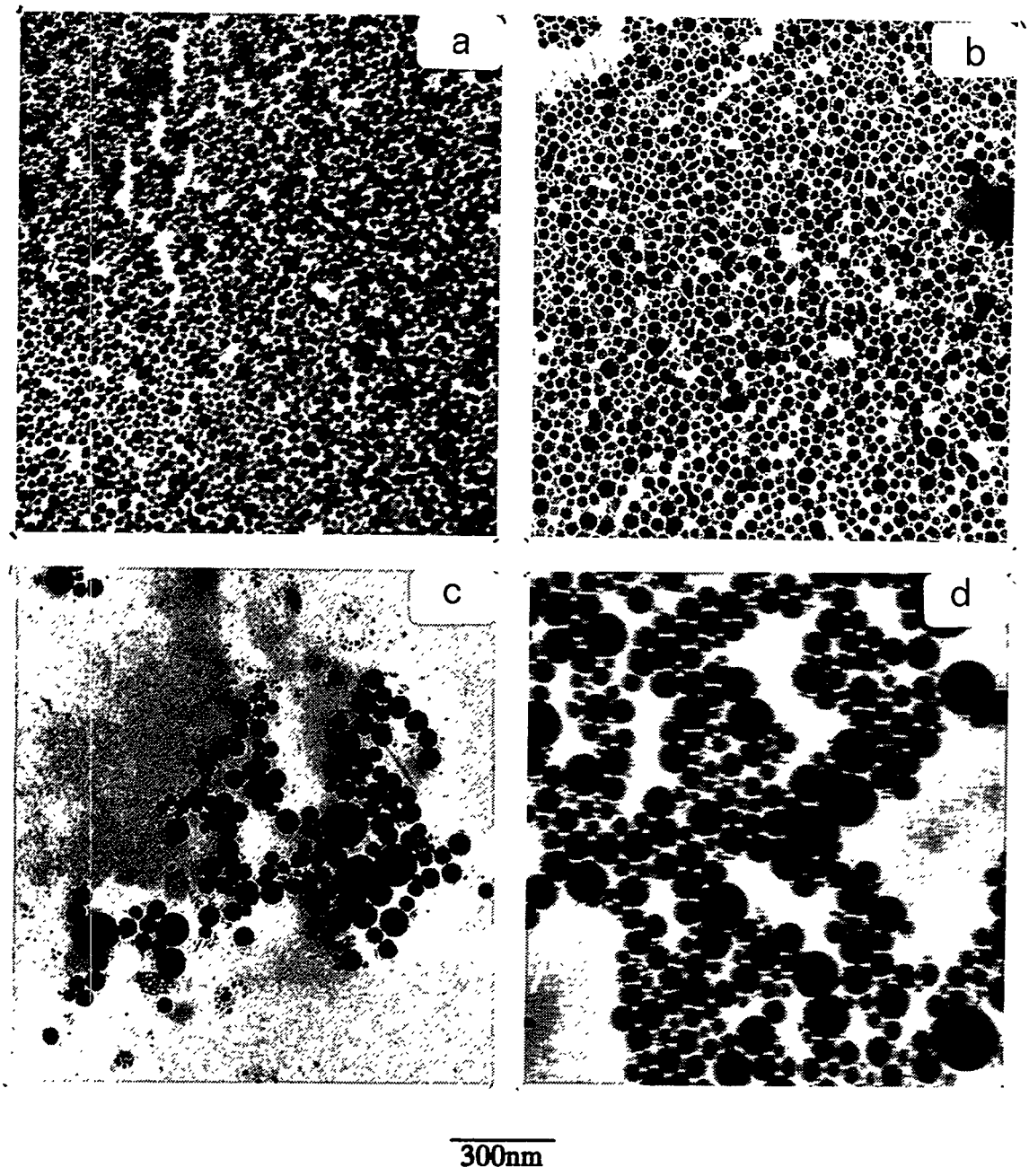

Figure 3.6

TEM micrographs of molybdenum sulfide particles prepared in the 0.15 M NP-5/cyclohexane microemulsion system, using the acid-solubilized microemulsion plus tetrathiomolybdate-solubilized microemulsion (MPM) protocol; $[H_2SO_4] = 1.3 \times 10^{-3}$ M; $[MoS_4^{2-}] = 6.4 \times 10^{-6}$ M; $[NaOH] = 1.4 \times 10^{-5}$ M. (a) R=2; (b) R=2.5; (c) R=3; (d) R=4.

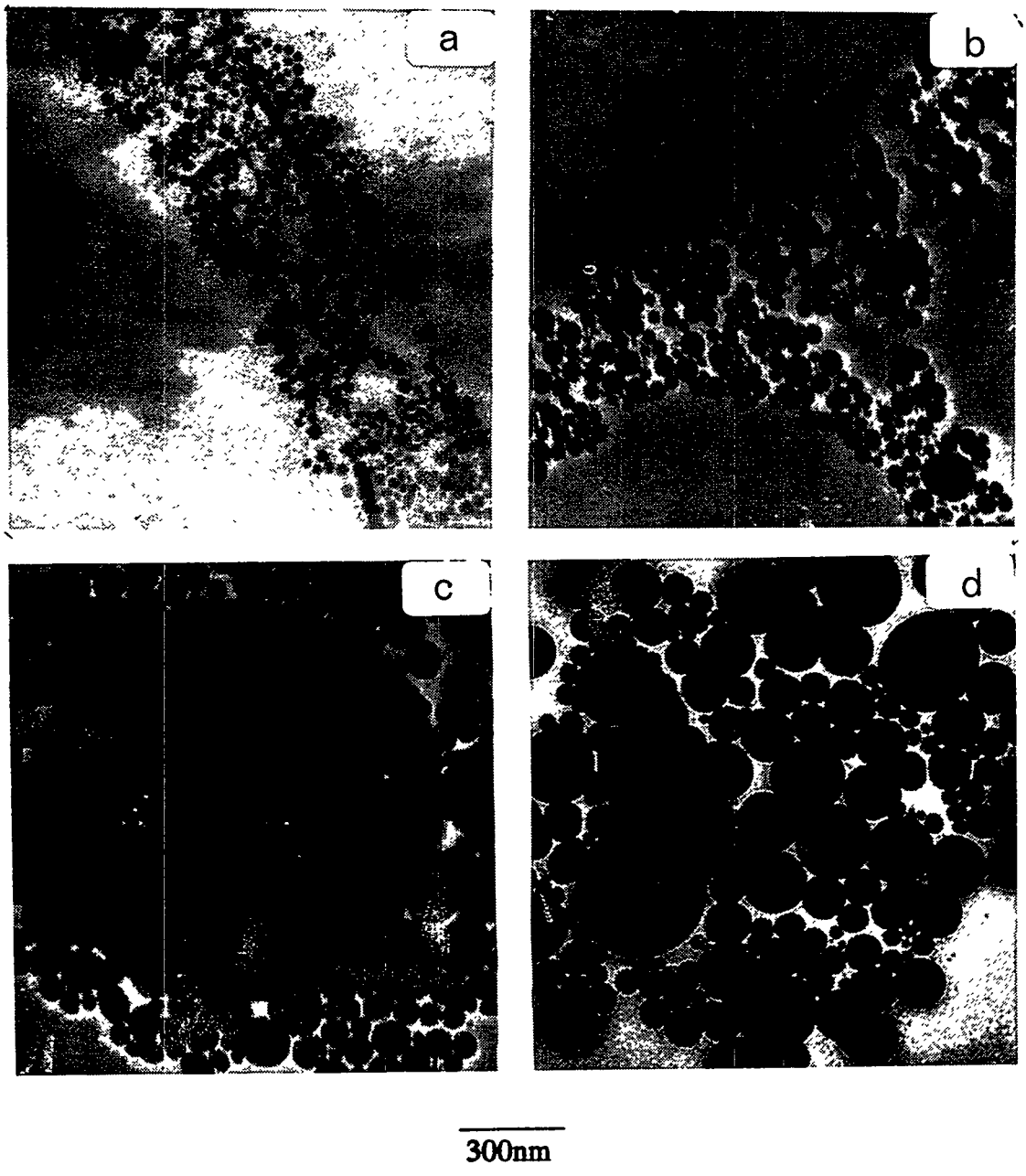

Figure 3.7

TEM micrographs of molybdenum sulfide particles prepared in the 0.15 M NP-5/cyclohexane microemulsion system, using the tetrathiomolybdate-solubilized microemulsion plus acid (TSMPA) protocol;

$[H_2SO_4] = 1.3 \times 10^{-3}$ M; $[MoS_4^{2-}] = 6.4 \times 10^{-6}$ M; $[NaOH] = 1.4 \times 10^{-5}$ M.

(a) R=2; (b) R=3; (c) R=3; (d) R=4.

distribution depend on the synthesis method. At R=3, the dependence of the particle size on the synthesis protocol is as follows: acid-solubilized microemulsion plus aqueous tetrathiomolybdate (ASMPT) < microemulsion plus microemulsion (MPM) ~ tetrathiomolybdate-solubilized microemulsion plus acid (TSMPA). At R= 3.5 - 4.5 the particle size strongly depends on the synthesis protocol and is in the order ASMPT < MPM < TSMPA.

Particle morphology. For R values in the range 1-4, sphere-like particles were obtained for all the synthesis methods. On the other hand for R= 4.5 - 5, depending on the synthesis method, particles with sphere-like or irregular morphology were produced. Figures 3.8 and 3.9 present the TEM micrographs of the molybdenum sulfide particles synthesized in the NP-5/cyclohexane/water microemulsion system at R = 4.5 and R = 5, respectively, using the various synthesis schemes. For the ASMPT protocol, the particles are spherical in shape (Figures 3.8a and 3.9a). However, as demonstrated in Figures 3.8b, 3.8c, 3.9c and 3.9d, particles with irregular morphology are obtained for the MPM and TSMPA synthesis methods at R = 4.5 - 5.

Particle formation scheme. To rationalize the results presented in Figure 3.5, the following particle formation scheme in the w/o microemulsions is considered: (a) Tetrathiomolybdate ions and protons react in the water cores of the inverse micelles to form molybdenum sulfide monomers, (b) a critical number of molybdenum sulfide monomers combine in an inverse micelle to form a nucleus; the nuclei grow either by adding on monomers or by aggregating (2,32,33,34).

Monomer addition growth. Particle growth and polydispersity due to monomer addition can be controlled by increasing the rate of nucleation of the particles in the microemulsion system. The nucleation rate in the microemulsion fluid phase is controlled by the ion occupancy number, N_{oc} (18,20,34,35), which represents the number of reactant species in an inverse micelle. As N_{oc} is

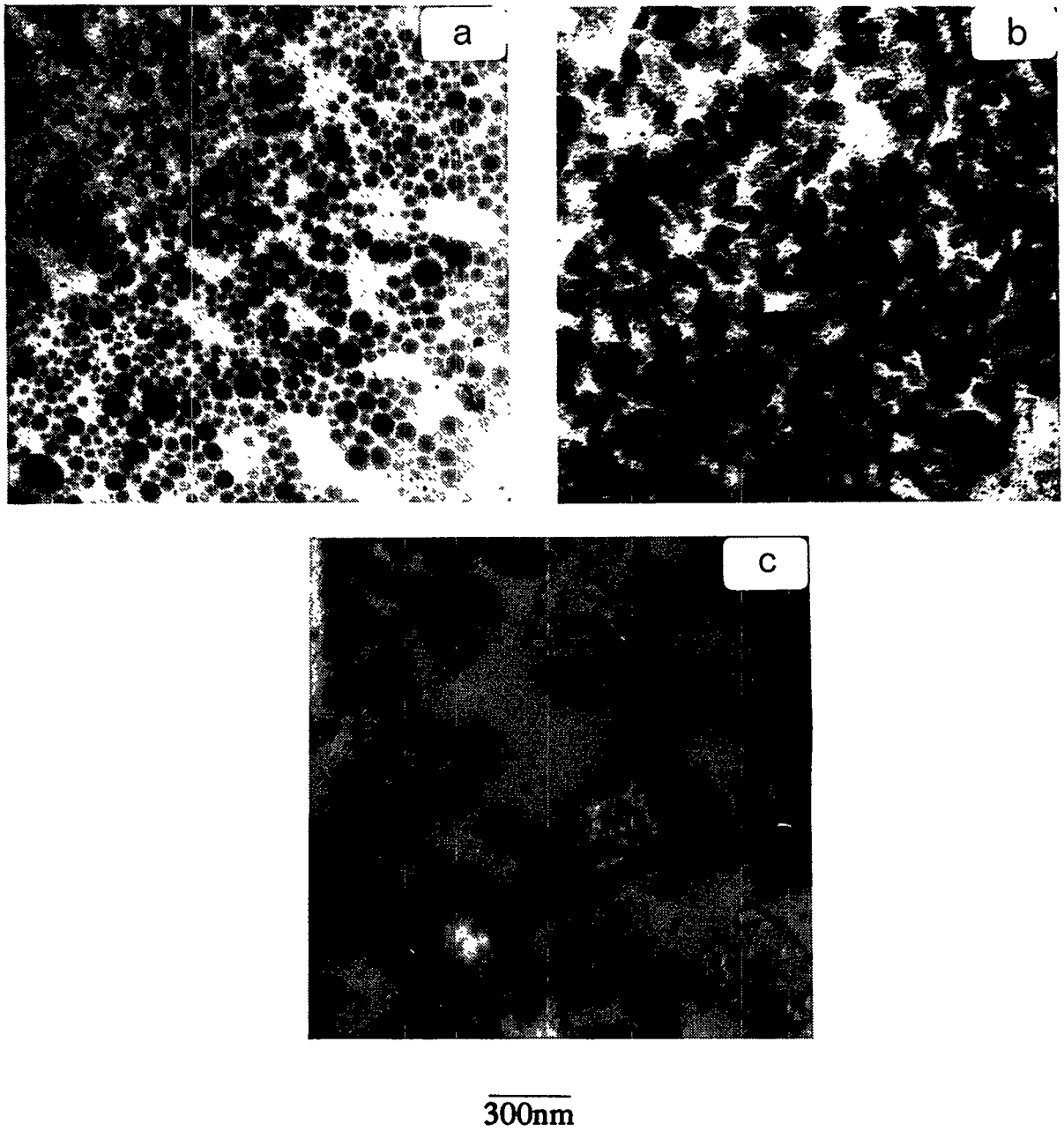

Figure 3.8

TEM micrographs of molybdenum sulfide particles prepared in the 0.15 M NP-5/cyclohexane microemulsion system at R=4.5 using different protocols:
(a) acid-solubilized microemulsion plus tetrathiomolybdate (ASMPT);
(b) acid-solubilized microemulsion plus tetrathiomolybdate-solubilized microemulsion (MPM), and
(c) tetrathiomolybdate-solubilized microemulsion plus acid (TSMPA).
$[H_2SO_4] = 1.3 \times 10^{-3}$ M; $[MoS_4^{2-}] = 6.4 \times 10^{-6}$ M; $[NaOH] = 1.4 \times 10^{-5}$ M.

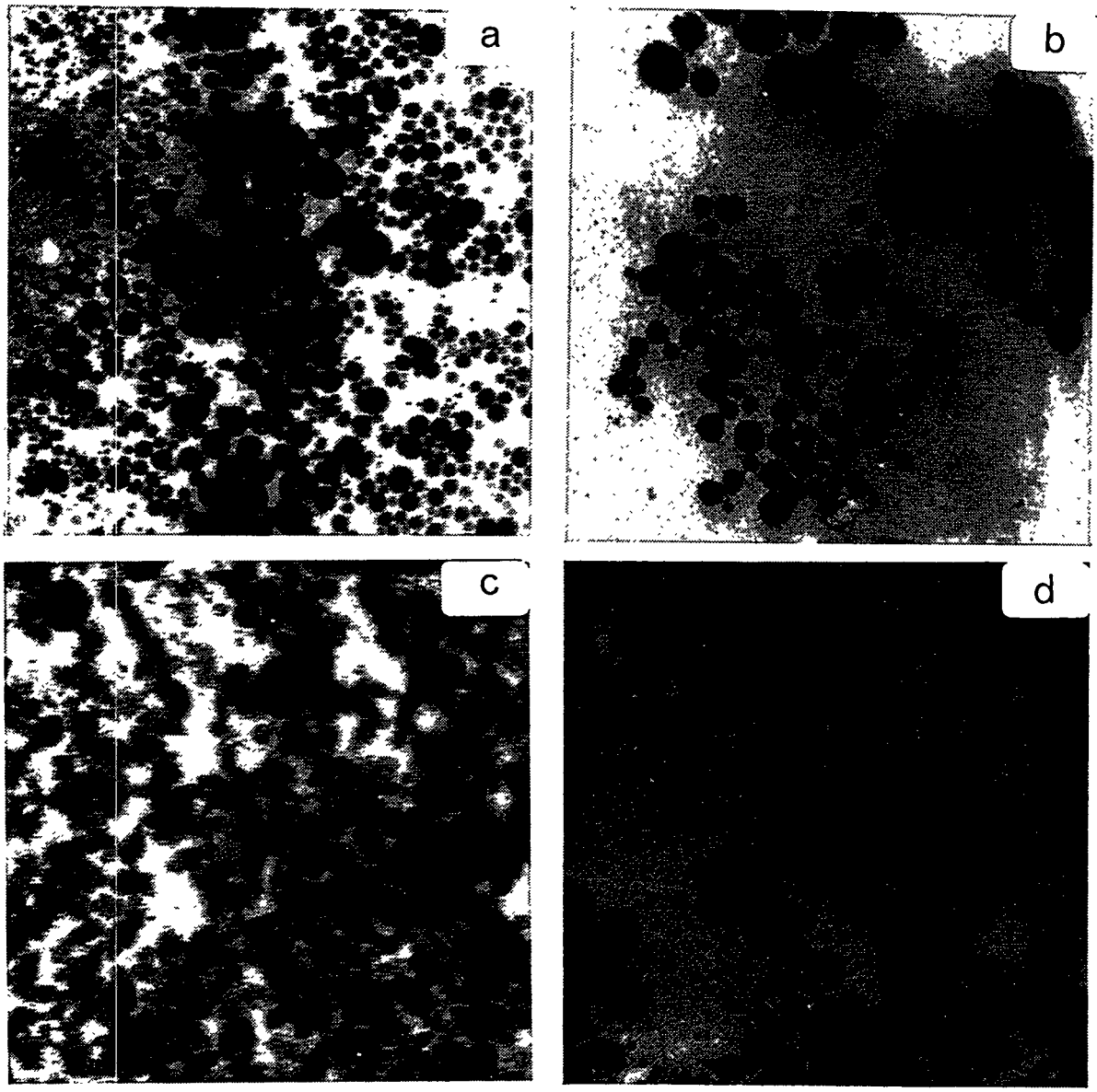

Figure 3.9

TEM micrographs of molybdenum sulfide particles prepared in the 0.15 M NP-5/cyclohexane microemulsion system at R=5 using different protocols:
(a) acid-solubilized microemulsion plus tetrathiomolybdate (ASMPT);
(b,c) acid-solubilized microemulsion plus tetrathiomolybdate-solubilized microemulsion (MPM), and
(d) tetrathiomolybdate-solubilized microemulsion plus acid (TSMPA);
$[H_2SO_4] = 1.3 \times 10^{-3}$ M; $[MoS_4^{2-}] = 6.4 \times 10^{-6}$ M; $[NaOH] = 1.4 \times 10^{-5}$ M.

increased, the supersaturation ratio ($S=C/C_{eq}$, where C_{eq} and C are the solute concentrations in the equilibrium and supersaturated solutions, respectively) increases and consequently the nucleation rate increases (34,36).

Summarized in Table 3.1 are data on the surfactant aggregation number (N), the number of inverse micelles (N_m), and the average molybdate occupancy number (N_{oc}). From the moles of the surfactant (NP-5) in the microemulsion (N_s), the average micellar diameter (D_m), and the volume of the dispersed (aqueous plus surfactant) phase (V_a), the number of inverse micelles (N_m) and the aggregation number (N) were calculated according to Equations 3.8 and 3.9:

$$N_m = V_a/(4/3)\pi(D_m/2)^3 \qquad [3.8]$$

$$N = 6.022\text{x}10^{23} \text{ x } N_s/N_m \qquad [3.9]$$

Here it is assumed that the solubility of water in the oil (cyclohexane) is negligible. The volume of surfactant associated with the dispersed phase in the microemulsion was found from the mass and density of NP-5 (0.997 g cm^{-3}). The average molybdate occupancy number (N_{oc}), i.e., the number of ammonium tetrathiomolybdate molecules per inverse micelle, is given by Equation 3.10:

$$N_{oc} = N_{mo} \text{ x } 6.022\text{x}10^{23}/N_m \qquad [3.10]$$

where N_{mo} represents the moles of MoS_4^{2-} in the microemulsion. The calculation of the average occupancy number is based on the assumption that the reactant species are confined to the cores of the inverse micelles. This assumption is reasonable in that the reactant species are ionic and therefore incompatible with the nonpolar oil phase. Since the micellar aggregation numbers were affected by the

Table 3.1

Selected Statistical Parameters for the Formation of Molybdenum Sulfide Particles in the 0.15 M/NP-5/Cyclohexane Microemulsion

	Particle diameter (nm)[a]			N^b			$N_m x10^{-19}$ c			$N_{oc} x10^3$ d		
R	ASMPT	MPM	TSMPA	ASMPT	MPM	TSMPA	ASMPT	MPM	TSMPA	ASMPT	MPM	TSMPA
1.0	17.3	16.3	21.5	44	43	42	4.1	4.3	4.5	0.94	0.90	0.87
1.5	19.5	24.9	21.8	54	50	45	3.6	3.8	4.0	1.07	1.01	0.95
2.0	22.4	26.6	29.0	65	57	50	3.1	3.4	3.6	1.24	1.15	1.07
2.5	26.1	30.2	34.0	69	65	61	2.8	2.9	3.1	1.39	1.32	1.26
3.0	26.7	40.0	37.2	73	73	73	2.5	2.5	2.5	1.57	1.56	1.55
3.5	31.8	54.8	64.1	100	89	78	2.0	2.2	2.3	1.90	1.77	1.65
4.0	48.7	60.3	85.0	127	105	82	1.6	1.9	2.2	2.42	2.04	1.76
4.5	72.9	118	127	149	120	92	1.3	1.7	2.0	2.90	2.33	1.95
5.0	-	-	-	170	155	139	1.1	1.4	1.8	3.62	2.73	2.18

[a] Average molybdenum sulfide particle diameter obtained via TEM measurements.

[b] N is the surfactant aggregation number (Equation 3.9).

[c] N_m is the number of inverse micelles in 10 ml of microemulsion (Equation 3.8).

[d] N_{oc} is the average molybdate occupancy number (Equation 3.10).

presence of the reactant species, the number of inverse micelles in Table 3.1 was calculated using the measured diameter of the inverse micelle for the particular solubilized electrolyte.

As shown in Table 3.1, for a fixed volume of microemulsion containing a constant number of reactant species, the micellar size (as reflected by the aggregation number N) increases as R is increased. Consequently, the number of inverse micelles decreases and the average occupancy number increases. This increase in N_{oc} is expected to cause a corresponding increase in the nucleation rate. As a result of the relatively high nucleation rate achieved at high R, more nuclei are produced and relatively few monomers (which can partake in the subsequent growth process) remain after the nucleation event and thus smaller particle sizes are to be expected (34). The above qualitative analysis, based on the occupancy number concept and the monomer addition growth process, indicates that smaller particles should be made at high R values (i.e., high occupancy numbers), while larger particles are to be expected at low R values (low occupancy numbers). However, in contrast to such an expectation, the reverse result was obtained, as seen from the particle diameter data in Table 3.1.

Figure 3.10 presents a plot of the occupancy number versus R for the various synthesis methods. An interesting observation in Figure 3.10 is that, for R = 1-3, the occupancy numbers are about the same for all the synthesis protocols. It therefore follows that, based on the principles of particle growth outlined above, the particle diameter should be the same for all the synthesis methods, provided that R is in the range 1-3. Experimentally this was found to be true. For a given R value in the range 1-3, the average diameter is relatively insensitive to the synthesis method, as shown in Figure 3.4. For R = 3.5-5 (Figure 3.10), N_{oc} decreases according to the synthesis protocol in the order ASMPT > MPM > TSMPA. Thus, the number of nuclei formed is expected to increase in the order ASMPT > MPM > TSMPA. The

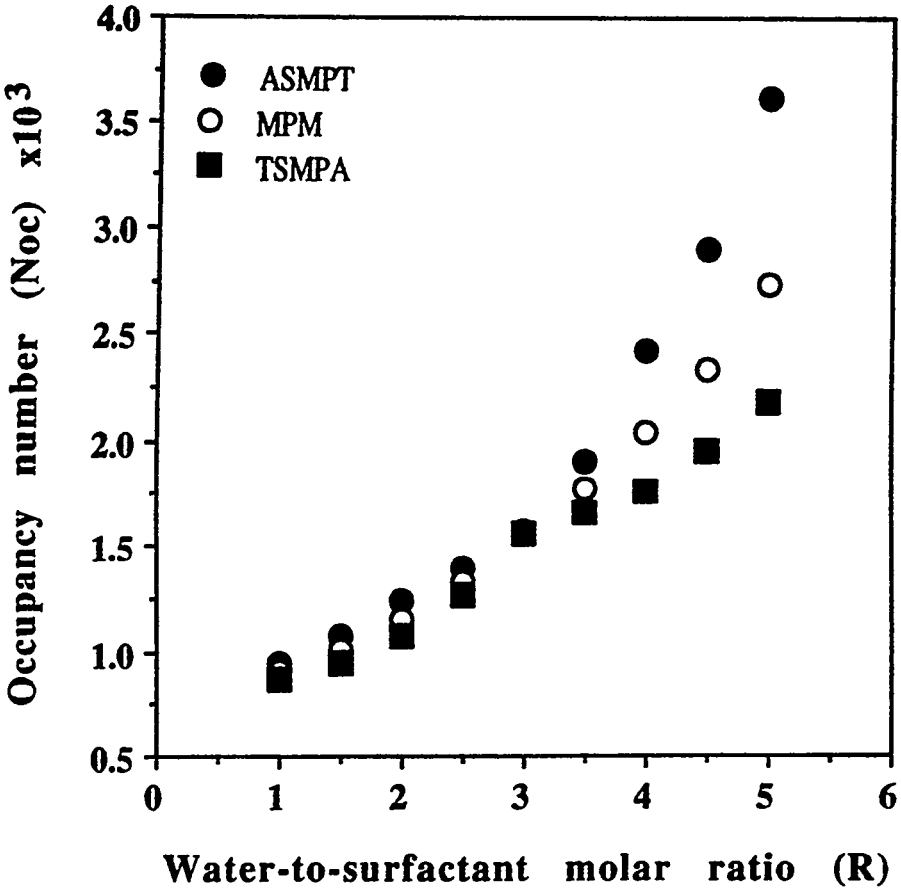

Figure 3.10

Effect of the water-to-surfactant molar ratio (R) on the average molybdate occupancy number;

$[MoS_4^{2-}] = 6.4 \times 10^{-6}$ M; $[NaOH] = 1.4 \times 10^{-5}$ M.

number of excess monomers (which are unutilized in nuclei formation) should then decrease in the order TSMPA > MPM > ASMPT. Therefore, for R = 3.5-4.5, the particle size should increase in the order ASMPT <MPM < TSMPA. This is indeed found to be true for R values in the range 3.5-4.5 (see Figure 3.4).

From the analysis of the results presented so far, it can be concluded that the monomer addition model of growth consistently explains why the particle size increases in the order ASMPT < MPM < TSMPA. However, as already noted above, it fails to rationalize why, for all the synthesis protocols, the particle size increases with R. This suggests that there may be another growth mechanism in operation, e.g., molybdenum sulfide particle aggregation.

3.3.4 Reactant Distribution and Particle Formation

To elucidate the growth mechanism in the microemulsion fluid phase, it is useful to determine the number of nuclei expected to be produced by each synthesis method for various R values. As a first approximation, the distribution of ammonium tetrathiomolybdate ions in the micellar aggregates is considered to follow the Poisson statistical distribution law (34,35,37). This distribution gives the probability (P_k) of having k ammonium tetrathiomolybdate ions per inverse micelle as:

$$P_k = N_{oc}^{k}(e^{-N_{oc}}/k!) \qquad [3.11]$$

In Equation 3.11, N_{oc} is the molybdate occupancy number. If at least two ammonium tetrathiomolybdate ions are needed to form a critical nucleus, and if it is assumed that only one nucleus can be produced in a given water pool, then the number of molybdenum sulfide nuclei produced in the w/o microemulsion should

be equivalent to the number of micellar aggregates that contain two or more tetrathiomolybdate ions. That is, the number of nuclei (N_n) formed in the microemulsion can be written as follows:

$$N_n = N_m \sum_{k=i_c}^{\infty} P_k \qquad [3.12]$$

where P_k is the probability that an inverse micellar water pool contains i_c or more MoS_3 monomers.

Figure 3.11 presents plots of the number of nuclei (determined using Equation 3.12, with i_c=2) versus R for all the synthesis methods. From Figure 3.11, the following observations can be made: (a) For each synthesis protocol, the number of nuclei increases with R, (b) for R = 1-3, the number of nuclei is independent of the synthesis protocol; however, for R = 3.5-4.5, the number of nuclei depends on the synthesis protocol in the order ASMPT >MPM > TSMPA.

Monomer addition versus particle aggregation growth. The number of particles (N_p) in the microemulsion fluid phase may be determined as in Equation 3.13:

$$N_p = M_{MoS_3(t)} / M_p \qquad [3.13]$$

where $M_{MoS_3(t)}$ corresponds to the total mass of MoS_3 in the microemulsion, and M_p is the mass of one MoS_3 particle (obtained from the product of the volume and the density of one MoS_3 particle). In the post-nucleation period, if growth occurred only by monomer addition, then the (experimentally determined) number of particles calculated with Equation 3.13 should be equal to the expected (theoretical) number of nuclei produced initially (i.e., N_n, given by Equation 3.12). This implies

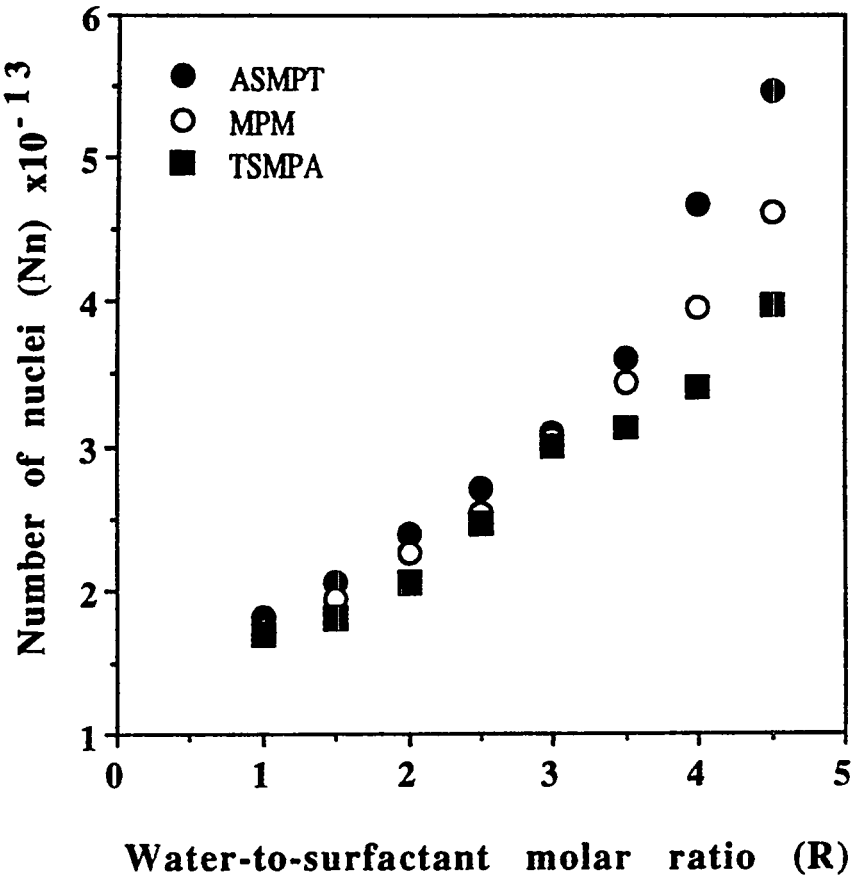

Figure 3.11

Effect of the water-to-surfactant molar ratio (R) on the number of nuclei formed in the NP-5/cyclohexane/water microemulsion;
$[H_2SO_4]=1.3\times10^{-3}$ M; $[MoS_4^{2-}] = 6.4\times10^{-6}$ M; $[NaOH] = 1.4\times10^{-5}$ M.

that, as with the number of nuclei (Figure 3.11), the number of particles determined from Equation 3.13, should increase with R. However, in contrast to expectation, and as shown in Figure 3.12, the experimentally determined number of particles (N_p, Equation 3.13) decreases with increasing R. This indicates that initially many nuclei were produced in the microemulsion fluid phase and that these nuclei subsequently aggregated.

The ratio of the theoretical number of nuclei (N_n, Equation 3.12) to the number of particles (N_p, Equation 3.13) was determined. The results are summarized in Table 3.2. It can be seen that, for each synthesis protocol, $N_n > N_p$, i.e., $N_n/N_p > 1$ for any given R. This trend suggests that post-nucleation events, such as aggregation of nuclei and/or primary particles, are important. From Table 3.2, the following additional observations can be made: (a) for all three synthesis protocols, the ratio N_n/N_p increases with R; (b) comparing the different synthesis protocols, there is no major difference in the N_n/N_p values for R = 1-2.5; and (c) for R = 3.5-4.5, the ratio N_n/N_p increases dramatically in the order ASMPT < MPM < TSMPA. If the ratio N_n/N_p is used as a measure of aggregation, then the following conclusions, corresponding to observations (a) to (c), can be reached: (a) particle aggregation should increase with R; (b) the degree of aggregation should be independent of R for R = 1-2.5; (c) for R = 3.5-4.5, the degree of particle aggregation should decrease in the order TSMPA > MPM > ASMPT. It is well known that as R increases, the rate of exchange (K_{ex}) of material between the microemulsion droplets increases (38-40); this should enhance the aggregation of particles and/or nuclei. The work of Shah and coworkers (32,33) on silver halides in w/o microemulsions demonstrates that both the size and the polydispersity of AgCl and AgBr particles increase when the chain length of oil increases, the amount of cosurfactant increases and the chain length of the cosurfactant decreases. These trends correlate very well with the increase in K_{ex} as the microemulsion components are varied (32,33).

Table 3.2

Selected Statistical Parameters for the Formation of Molybdenum Sulfide Particles in the NP-5/Cyclohexane/Water Microemulsion

	N_n/N_p			$(N_m/N_p)x10^{-8}$		
R	ASMPT	MPM	TSMPA	ASMPT	MPM	TSMPA
1.0	13	10	23	0.29	0.25	0.59
1.5	21	41	25	0.37	0.81	0.54
2.0	37	58	69	0.49	0.86	1.2
2.5	65	95	130	0.68	1.1	1.6
3.0	80	260	240	0.65	2.1	2.0
3.5	150	760	1100	0.89	4.9	8.4
4.0	430	1100	2700	1.5	5.5	18
4.5	2900	10000	11200	7.0	38	56

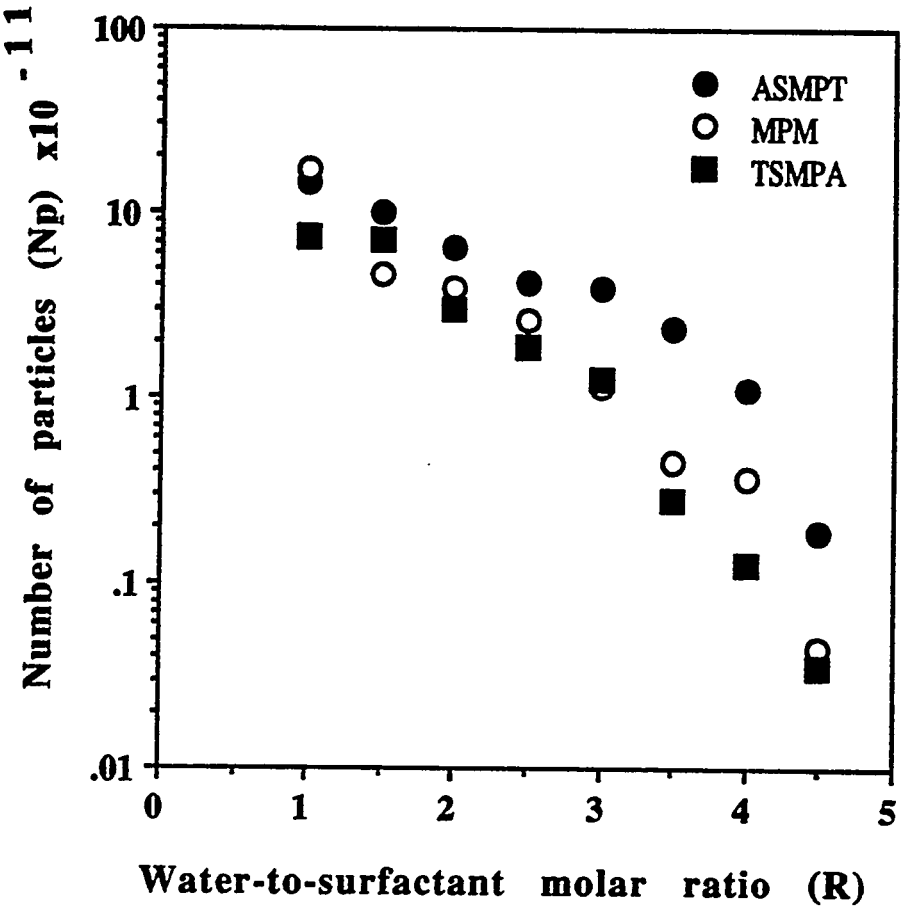

Figure 3.12

Effect of the water-to-surfactant molar ratio (R) on the number of molybdenum sulfide particles formed in the NP-5/cyclohexane/water microemulsion; $[H_2SO_4] = 1.3 \times 10^{-3}$ M; $[MoS_4^{2-}] = 6.4 \times 10^{-6}$ M; $[NaOH] = 1.4 \times 10^{-5}$ M.

From the N_{oc} data in Table 3.1, it is seen that for every 10^3 inverse micelles there is approximately one thiomolybdate ion. If two molybdenum sulfide monomers are needed to form a critical nucleus (as previously assumed) and if aggregation of nuclei and/or primary particles does not occur (so that $N_n=N_p$), then the magnitude of the ratio N_m/N_p should be of the order of 10^3. Based on the N_p values determined from Equation 3.13, the N_m/N_p ratios were determined. The results are included in Table 3.2. It is seen that out of every 10^8 inverse micelles only one particle forms. This is in contrast to the expected $10^3/1$ ratio noted above. This in turn supports the conclusion that particle aggregation occurs in the w/o microemulsion via micellar fusion. In addition, due to the aggregation phenomena, the number of particles (N_p) in the microemulsion fluid phase decreases as R is increased while the ratio N_m/N_p increases. This is a result of the increase in the rate of exchange of material between inverse micelles as the water-to-surfactant molar ratio (R) increases (38-40). Furthermore, for R values in the range 1-4.5, the particle diameter (17-127 nm) is far larger than the micellar diameter (4-10 nm), which demonstrates that particles grow when inverse micelles coalesce and that the dynamic nature of the inverse micelles is a factor that should be considered in predicting particle growth in w/o microemulsions.

3.3.5 Microemulsion Destabilization and Particle Aggregation

It is interesting to note that for R = 3.5-4.5, the extent of particle aggregation (as determined by the ratios N_n/N_p and N_m/N_p) strongly depends on the synthesis method. These ratios decrease in the order TSMPA > MPM > ASMPT (Table 3.2). This trend may be explained by referring to Figures 3.2a and 3.2b. As concluded in Section 3.3.1, the phase stability diagram is lowered by about 4 °C, especially at relatively low R values (R < 10), when aqueous tetrathiomolybdate (containing

NaOH) is used as the solubilizate, compared to the case where dilute sulfuric acid is used. At R = 4 the solubilization limit is 50 ± 0.5 °C, while it is below 50 ± 0.5 °C at R > 4. Thus, solubilization of aqueous ammonium thiomolybdate in the microemulsion at 50 °C (before the addition of acid) induced phase separation. Observations made during the experiments showed some cloudiness.

Therefore, when the TSMPA protocol is used (i.e., solubilizing aqueous ammonium tetrathiomolybdate-containing sodium hydroxide before the addition of aqueous sulfuric acid), the solvent system 0.15 M NP-5/cyclohexane/thiomolybdate will be composed of excess aqueous ammonium thiomolybdate solution and dispersed droplets of aqueous thiomolybdate solution stabilized by surfactant films in cyclohexane. The phase separation will induce polydispersity in the synthesis product since some particles will form in the one-phase microemulsion system whereas others will not (but are formed in the conjugate bulk aqueous phase). In addition, the particles made outside the one-phase microemulsion domain have a greater tendency to aggregate since they are produced outside the microemulsion cages and are not protected by surfactant films. A typical example of aggregation is presented in Figure 3.7c: the TEM micrograph shows particles of 70 nm (average size) clustering around a central particle of ~1200 nm.

For the MPM synthesis protocol, ammonium tetrathiomolybdate and the acid are solubilized in separate microemulsions at 50 °C before mixing. Although the microemulsion containing the thiomolybdate ions will phase-separate at 50 °C (Figure 3.2b), that of the acid will not (Figure 3.2a). The degree of phase separation when the tetrathiomolybdate-solubilized microemulsion is added to the acid-solubilized microemulsion may be relatively smaller compared to the TSMPA method. Thus, it is reasonable to expect that at R = 4 particle aggregation occurs to a lesser extent when the MPM method is used compared to the TSMPA method.

On solubilizing aqueous sulfuric acid before the addition of aqueous ammonium tetrathiomolybdate at 50 °C, there is no phase separation at R = 1-4.5. Thus the degree of phase-separation-related particle aggregation is expected to be relatively small. Consequently, the particle size is expected to be small when the ASMPT synthesis protocol is used compared to the MPM and TSMPA methods.

Aggregation, induced by the destabilization of the microemulsion water cores, becomes less prominent as R is decreased, and more pronounced as R increases. As R decreases the solubilization limit (the temperature limit above which the two-phase microemulsion region is reached) increases. Thus at high R values (e.g., 3.5-5) the instability of the microemulsion droplets may be the reason why the extent of particle aggregation strongly depends on the synthesis protocol. However, at R = 1-2.5, the thiomolybdate microemulsion is stable at the synthesis conditions; hence, there is no significant dependence of the particle size on the synthesis protocol. Similar observations have been reported recently by Wilcoxon et al. (41) and Barnikel et al. (42), respectively, in the synthesis of gold and silver particles in microemulsions. Polydispersed aggregates of gold and silver particles were formed outside the one-phase microemulsion region.

At R values of 4.5 and 5 (Figures 3.8 and 3.9) particles of irregular morphology are made when the TSMPA and the MPM synthesis methods are used. On the other hand, sphere-like particles are obtained when the ASMPT protocol is used (Figures 3.8a and 3.9a). Examples of particles of irregular morphology are presented in Figures 3.8b, 3.8c, 3.9c and 3.9d. These particles were made outside the one-phase microemulsion region (outside the micellar cages). That is, they were synthesized in the absence of protective surfactant cages. In this case extensive aggregation of the primary particle may lead to larger particles with non-spherical shape. This effect appears to be more significant for the TSMPA method (Figure 3.9d), where the destabilization of the microemulsion droplets is expected to be

greatest (Figure 3.2b). For the MPM method (Figure 3.9b), some sections of the TEM grid also contained spherical particles with rough surfaces, indicating particle aggregation.

Kitahara and coworkers (43,44) have shown that the particle size and the size distribution of calcium and barium carbonate particles made in the NP-6/cyclohexane/water microemulsion system depend on the microemulsion phase region where the particles are made. Monodispersed spherical calcium carbonate particles were made in the colorless one-phase microemulsion region whereas in the blue translucent region, polydispersed particles were obtained (43). In the case of the barium carbonate system (44), depending on the microemulsion region, particles of different morphology were produced. Rod-like and ellipsoidal particles were made in the colorless and blue translucent regions, respectively. The above observations and the results of this study show that, depending on the microemulsion region, particles of different morphology could be made in the microemulsion system.

3.4 CONCLUSIONS

This work dealing with the effect of the synthesis protocol on the particle size shows that at water-to-surfactant molar ratios (R) in the range 1-2.5 the particle size is insensitive to the synthesis protocol. On the other hand, at R = 3.5-4.5 the average particle size increases according to the synthesis method in the following order: acid-solubilized microemulsion plus aqueous tetrathiomolybdate (ASMPT) < acid-solubilized microemulsion plus tetrathiomolybdate-solubilized microemulsion (MPM) < tetrathiomolybdate-solubilized microemulsion plus aqueous sulfuric acid (TSMPA). At R = 3.5-4.5 the dependence of particle size on the synthesis method is

due to the destabilization of the microemulsion droplets, which is caused by first solubilizing the ammonium tetrathiomolybdate precursor solution containing aqueous sodium hydroxide at 50 °C. For the MPM and TSMPA synthesis protocols, particles of irregular morphology were obtained at R = 4.5 and R = 5, which is also due to extensive aggregation of primary particles outside the one-phase microemulsion domain. By considering the distribution of ammonium tetrathiomolybdate ions in the microemulsion fluid phase, a quantitative growth model shows that particle growth occurs by aggregation. For each synthesis protocol, the extent of aggregation increases with R, which is attributed to the increasing rate of fusion and fission of water pools as R is increased.

3.5 REFERENCES

1. Haruta, M., and Delmon, B., *J. Chim. Phys.* **83**, 859 (1986).
2. Dvolaitzky, M., Ober, R., Taupin, C., Anthore, R., Auvray, X., Petipas, C., and Williams, C., *J. Dispersion Sci. Technol.* **4**, 29 (1983).
3. Boutonnet, M., Kizling, J., Mintsa-Eya, V., Choplin, A., Touroude R., Maire, G., and Stenius P., *J. Catal.* **103**, 95 (1987).
4. Boutonnet, M., Kizling, J., Touroude, R., Maire, G., and Stenius, P., *Appl. Catal.* **20**, 163 (1986).
5. Touroude R., Girard, P., Maire, G., Kizling, J., Boutonnet-Kizling, M., and Stenius, P., *Colloids Surf.* **67**, 9 (1992).
6. Fendler, J.H., *Chem. Rev.* **87**, 877 (1987).
7. Osseo-Asare, K., and Arriagada, F.J., in "Ceramic Powder Science III", (G.L. Messing, S. Hirano and H. Hausner, Eds.) American Ceramic Society, Westerville, OH, 1990, p. 3.

8. Ward, A.J.I., and Friberg, S.E., *Mater. Res. Bull.* **14,** 41 (1989).

9. Lianos, P., and Thomas, J.K., *J. Colloid Interface Sci.* **117,** 505 (1987).

10. Ward, A.J.I., O'Sullivan, E.C., Rang, J.C., Nedeljkovic, J., and Patel R.C. *J. Colloid Interface Sci.* **161,** 316 (1993).

11. Pileni, M.P., Motte, L., and Petit, C., *Chem. Mater.* 4, 338 (1992).

12. Petit, C., Lixon, P., and Pileni, M.P., *J. Phys. Chem.* **94,** 1598 (1990).

13. Midmore, B.R., *J. Chem. Soc. Faraday Trans.* **86,** 3763 (1990).

14. Virden, J.W., and Berg, J.C., *J. Colloid Interface Sci.* **149,** 528 (1992).

15. Dunn, C.M., Robinson, B.R., and Leng, F.J., *Spectrochimica Acta.* **46A,** 1017 (1990).

16. Zulauf, M., and Eicke, H.-F., *J. Phys. Chem.* **83,** 480 (1979).

17. Koppel, D.E., *J. Chem. Phys.* **57,** 4814 (1972).

18. Boakye, E., Radovic L.R., and Osseo-Asare, K., *J. Colloid Interface Sci.* **163,** 120 (1994).

19. Arriagada, F.J., and Osseo-Asare, K., *Colloids Surf.* **69,** 105 (1992).

20. Osseo-Asare, K., and Arriagada, F.J., *Colloids Surf.* **50,** 321 (1990).

21. Shinoda, K., and Saito, H., *J. Colloid Interface Sci.* **26,** 70 (1968).

22. Kahlweit, M., Lessner, E., and Strey, R., *J. Phys. Chem.* **88,** 1937 (1984).

23. Kon-no, K., and Kitahara, A., *J. Colloid Interface Sci.* **34,** 221 (1970).

24. Kitahara, A., and Kon-no, K., *J. Phys. Chem.* **70,** 3394 (1966).

25. Kizling, J., and Stenius P., *J. Colloid Interface Sci.* **118,** 482 (1987).

26. Schick, M.J., *J. Colloid Sci.* **17,** 801 (1962).

27. Becher P., *J. Colloid Sci.* **17,** 325 (1962).

28. Firman, P., Haase, D., Jen, J., Kahlweit, M. and Strey, R., *Langmuir* **1,** 718 (1985).

29. Wiencek, J.M., and Qutubuddin, S., *Colloids Surf.* **54,** 1 (1991).

30. Mukerjee, P., *J. Phys. Chem.* **69,** 4038 (1965).

31. Pearson, R.G., *Surv. Prog. Chem.* **5,** (1969).

32. Hou, M.J., and Shah, D.O., in "Interfacial Phenomena in Biotechnology and Materials Processing" (Y.A. Attia, B.M. Moudgil and S. Chander, Eds.), Elsevier, Amsterdam/New York, 1988, p. 443.

33. Chew, C.H., Gan, L.M., and Shah, D.O., *J. Dispersion Sci. Technol.* **11,** 593 (1990).

34. Nagy, J.B., *Colloids Surf.* **35,** 201 (1989).

35. Arriagada, F.J., Osseo-Asare, K., in "The Colloid Chemistry of Silica" (H.E. Bergna, Ed.), Advances in Chemistry Series, Vol. 234, 1994, p. 113.

36. Nielsen, A.E., "Kinetics of Precipitation," Macmillan, New York, 1964, p. 12.

37. Atik, S.S., and Thomas, J.K., *J. Am. Chem. Soc.* **103,** 7403 (1981).

38. Clark, S., Fletcher, P.D.I., and Ye, X., *Langmuir* **6,** 1301 (1990).

39. Almgren, M., Stam, J.V., Swarup, S., and Lofroth, J.-E., *Langmuir* **2,** 432 (1986).

40. Bommarius, A.S., Holzwarth, J.F., Wang, D.I.C. and Hatton, T.A., *J. Phys. Chem.* **94,** 7232 (1990).

41. Wilcoxon, J.P., Williamson, R.L., and Baughman, R., *J. Chem.Phys.* **98,** 9932 (1993).

42. Barnickel, P., Wokaun, A., Sager, W., and Eicke, H.-F., *J. Colloid Interface Sci.* **148,** 80 (1992).

43. Kandori, K., Shizuka, N., Kon-no, K., and Kitahara, A., *J. Dispersion Sci. Technol.* **8,** 477 (1987).

44. Kon-no, K, Koide, M., and Kitahara, A., *Nippon Kagaku Kaishi* **6,** 815 (1984).

CHAPTER 4

SYNTHESIS OF NANOSIZE MOLYBDENUM SULFIDE PARTICLES IN NONIONIC MICROEMULSIONS: EFFECTS OF AMMONIUM TETRATHIOMOLYBDATE AND ACID CONCENTRATIONS ON PARTICLE SIZE

4.1 INTRODUCTION

As discussed in previous chapters, the compartmentalization provided by water-in-oil (w/o) microemulsions can be exploited in the preparation of nanosize materials (1-24). A major advantage of microemulsion-based techniques in the production of fine particles is the ability to limit particle aggregation. This is due to the isolation of the nucleation sites (water pools) from each other by the adsorbed films of surfactant molecules present at the microscopic organic/aqueous interfaces.

In order to generate small and monodispersed particles, it is important to control the nucleation and growth processes in the microemulsion fluid phase. In Chapter 2 it was shown that the size of molybdenum sulfide particles in the polyoxyethylene(5)nonylphenyl ether (NP-5)/cyclohexane/water microemulsion could be controlled by varying the average molybdate occupancy number (i.e., the number of thiomolybdate ions per inverse micelle). The experiments were conducted with two constant thiomolybdate concentrations of 3.2×10^{-6} M and 6.4×10^{-6} M, and the thiomolybdate occupancy number was varied by increasing the water-to-surfactant molar ratio (R) from R = 1 to R = 4. For a microemulsion of constant R, the thiomolybdate occupancy number can also be varied by increasing the thiomolybdate concentration. In Chapter 2 it was also found that doubling the thiomolybdate concentration from 3.2×10^{-6} M to 6.4×10^{-6} M resulted in a decrease in

particle size. In the present Chapter, the effects of the reactant concentration are further examined by using a wider range of thiomolybdate concentrations (3.2-11.2x10^{-6} M). Also considered here is the effect of variations in acid concentration on molybdenum sulfide particle size.

4.2 EXPERIMENTAL

4.2.1 Materials

The following chemicals were obtained from Aldrich and were used as received: the nonionic surfactant polyoxyethylene(5)nonylphenyl ether (NP-5; molecular weight 440.63), ammonium tetrathiomolybdate (99.97%), and cyclohexane (99%).

4.2.2 Microemulsion Characterization

Micellar size measurements. Photon correlation spectroscopy (PCS) was used to measure the microemulsion droplet size (25-29). The PCS instrumentation and methodology was as reported in Chapter 3. Two major experiments, comprising the effects of thiomolybdate and acid concentration on the hydrodynamic micellar diameter, were conducted. For the experiment concerning the thiomolybdate concentration, the water-to-surfactant molar ratio was kept constant (R = 1) while ammonium tetrathiomolybdate concentration was varied in the range 3.2-11.2x10^{-6} M. The effect of acid concentration on micellar size was investigated by determining the micellar size of microemulsions with various water contents and with acid concentration in the range 0.65-2.6x10^{-3} M. In preparing the ammonium

tetrathiomolybdate impregnating solution, sodium hydroxide was added to enhance the dissolution of the molybdenum salt in water. In all, for each thiomolybdate-solubilized microemulsion (i.e., microemulsions containing $3.2x10^{-6}$-$11.2x10^{-6}$ M thiomolybdate ions), the concentration of sodium hydroxide was $1.4x10^{-5}$ M. Before solubilizing the impregnating solutions, they were filtered with a 2-mm filter obtained from Aldrich.

Phase behavior. In Chapter 3 it was shown that molybdenum sulfide particles synthesized in the NP-5/cyclohexane/water microemulsion aggregate at temperatures close to the solubilization limit, especially when ammonium tetrathiomolybdate containing sodium hydroxide is first solubilized before adding sulfuric acid. Hence the phase behavior of the 0.15 M NP-5/cyclohexane microemulsion was investigated. The methodology used to characterize the phase behavior of the microemulsion system 0.15 M NP-5/cyclohexane was as reported in Chapter 3. The phase behavior of a number of microemulsion samples with R = 1 and various ammonium tetrathiomolybdate concentrations (3.2-$11.2x10^{-6}$ M) was observed as a function of temperature. Each of the ammonium tetrathiomolybdate solutions contained $1.4x10^{-5}$ M NaOH. Also the phase behavior of three microemulsion samples with acid concentrations of 0.65-$2.6x10^{-3}$ M and various water contents (R = 1-4) was observed as a function of temperature.

4.2.3 Particle Synthesis

The microemulsion-plus-a-second-reactant method (7,30) was used in this work. To study the effect of ammonium tetrathiomolybdate concentration on the average molybdenum sulfide particle size, 12 μL of aqueous sulfuric acid was added to 10 mL of 0.15 M NP-5/cyclohexane solution. The acid-solubilized microemulsion was deoxygenated by bubbling high purity nitrogen gas through it. This procedure

was followed by adding 13 μL of 2.5-8.62x10^{-3} M ammonium tetrathiomolybdate to form molybdenum sulfide particles according to Equation 4.1.

$$MoS_4^{2-} + 2H^+ = MoS_3 + H_2S \qquad [4.1]$$

The water-to-surfactant molar ratio (R) was kept constant (R = 1). The concentrations of the reactant species with respect to the total microemulsion volume were as follows: ammonium tetrathiomolybdate, 3.2-11.2x10^{-6} M; and sulfuric acid, 1.3x10^{-3} M .

The experiments on the effect of dilute sulfuric acid concentration on the average particle size were conducted similarly as above. Twelve μL of 0.53-2.3 M aqueous sulfuric acid was added to 10 mL of NP-5/cyclohexane solution followed by deoxygenation with nitrogen. Thirteen μL of 5x10^{-3} M ammonium tetrathiomolybdate was added to produce molybdenum sulfide particles. The concentrations of sulfuric acid and ammonium tetrathiomolybdate with respect to the total microemulsion volume were 0.65-2.6x10^{-3} and 6.4x10^{-6} M, respectively.

4.2.4 Particle Characterization

Molybdenum sulfide particle dispersions were characterized with a Philips 420 transmission electron microscope as reported in Chapter 3. The diameters of at least 250 particles were measured for each sample to obtain an average particle diameter and standard deviation.

4.3 RESULTS AND DISCUSSION

4.3.1 Microemulsion Characterization

Effect of salinity on micellar size. For the purpose of determining the thiomolybdate occupancy number and its relationships with the nucleation rate and the resulting particle size, the average inverse micelle diameter of the NP-5/cyclohexane/water microemulsion with thiomolybdate and sulfuric acid as solubilizates was measured. Figure 4.1 presents a plot of the average inverse micelle diameter of the 0.15 M NP-5/cyclohexane solution versus the thiomolybdate concentration (each of the tetrathiomolybdate solutions contained 1.4×10^{-5} M NaOH). Figure 4.2 shows a plot of the micellar diameter versus R for various sulfuric acid concentrations. At R = 1, the average micellar size decreases as the thiomolybdate concentration is increased (Figure 4.1). Also for the same R value the average micellar size decreases as the acid concentration is increased (Figure 4.2). In addition, for each sulfuric acid concentration, the micellar size increases as the water-to-surfactant molar ratio (R) is increased.

Phase behavior. In Chapter 3 it was reported that the synthesis of molybdenum sulfide particles above the solubilization limit induces particle aggregation. This tendency is especially prevalent when the thiomolybdate-sololubilized-microemulsion-plus-acid protocol (7) is used (i.e., first solubilizing the thiomolybdate solution before the addition of sulfuric acid). Above the solubilization limit, water-in-oil microemulsions co-exist with excess water. The phase separation induces particle aggregation and polydispersity in the synthesis product since some particles are formed in the w/o microemulsions whereas others are formed in the conjugate aqueous phase. Therefore in the experiments of the present Chapter, to avoid phase-separation-induced particle aggregation, the

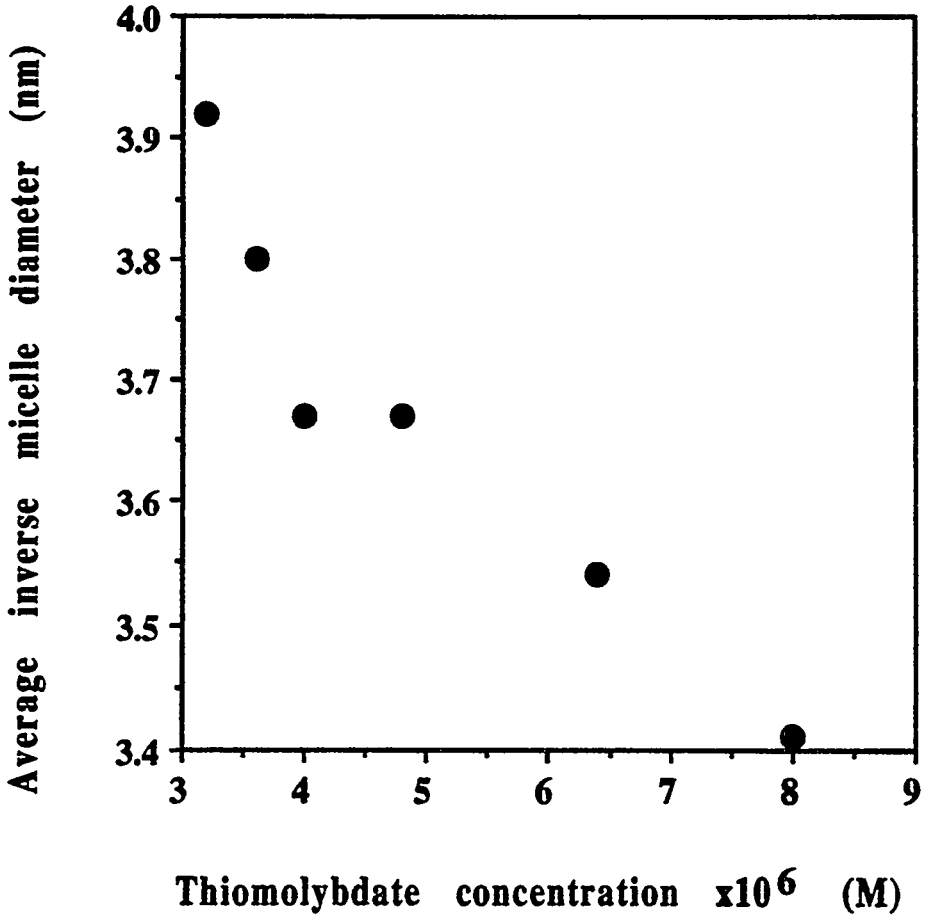

Figure 4.1

Effect of ammonium tetrathiomolybdate concentration on the hydrodynamic diameter of the inverse micelles in the microemulsion system 0.15 M NP-5/cyclohexane at 25 °C;

$[MoS_4^{2-}]=(3.2\text{-}11.2)\times10^{-6}$ M, $[NaOH]=1.4\times10^{-5}$ M, R=1.

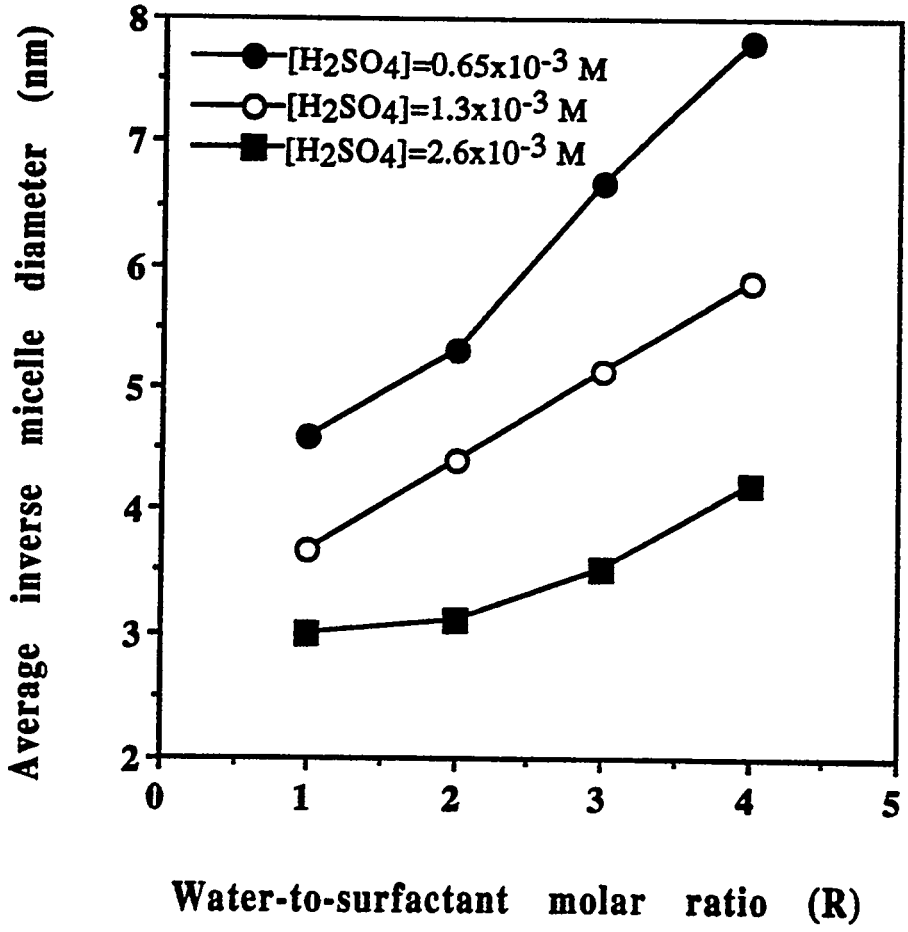

Figure 4.2
Effect of sulfuric acid concentration and water-to-surfactant molar ratio (R) on the hydrodynamic diameter of the inverse micelles in the microemulsion system 0.15 M NP-5/cyclohexane at 25 °C.

solubilization limits were investigated for the 0.15 M NP-5/cyclohexane microemulsion with ammonium tetrathiomolybdate and sulfuric acid as solubilizates. Tables 4.1a, and 4.1b, respectively, summarize the pertinent solubilization data for ammonium tetrathiomolybdate and sulfuric acid as solubilizates. From Table 4.1a it is seen that the solubilization limit is independent of the thiomolybdate concentration. A similar conclusion was reached in Chapter 3. However, the solubilization limit does depend on the microemulsion water content (Table 4.1b). In addition, for R values in the range 1-4, the solubilization limit is above 50 °C which is the synthesis temperature of this study. As a reminder, it must be noted that in this work the acid-solubilized-microemulsion-plus-thiomolybdate protocol was used (i.e., sulfuric acid was first solubilized, before adding the thiomolybdate solution). Thus particle aggregation caused by the presence of the conjugate aqueous phase is not expected.

4.3.2 Effect of Molybdate Concentration on Particle Size

Figures 4.3 and 4.4, respectively, present the TEM micrographs of the molybdenum sulfide particles synthesized in the NP-5/cyclohexane/water microemulsion and a plot of the average particle diameter versus the thiomolybdate concentration. Both the particle size and standard deviation decrease with an increase in the thiomolybdate concentration to $[MoS_4^{2-}] = 4.8 \times 10^{-6}$ M and then increase with further increase in thiomolybdate concentration. A similar observation was reported by Nagy (18) for cobalt boride particles synthesized in the CTAB/hexanol/water microemulsion. It is of interest to note that the average molybdenum sulfide particle diameters (10-90 nm) reported in this study (i.e., using the microemulsion-based method) are much smaller than those of colloidal MoS_3 particles (100-700 nm) made in aqueous solution by Haruta and coworkers (31).

Table 4.1a

Effect of Ammonium Tetrathiomolybdate Concentration on the Solubilization Limit of the 0.15 M NP-5/Cyclohexane Microemulsion (R=1, [NaOH] = 1.4×10^{-5} M).

Thiomolybdate concentration $\times 10^6$ M	Solubilization limit (°C)
3.2	52.2
4.0	51.7
4.8	52.4
6.4	52.5
8.0	51.6
9.6	51.9
11.2	51.8

Table 4.1b

Effects of Sulfuric Acid Concentration and Microemulsion Water Content on the Solubilization Limit of the 0.15 M NP-5/Cyclohexane Microemulsion

	Solubilization limit (°C)		
R	$[H_2SO_4]=0.65 \times 10^{-3}$ M	$[H_2SO_4]=1.3 \times 10^{-3}$ M	$[H_2SO_4]=2.6 \times 10^{-3}$ M
1	57.5	57.5	58.0
2	55.1	55.2	55.6
4	53.1	53.6	53.3

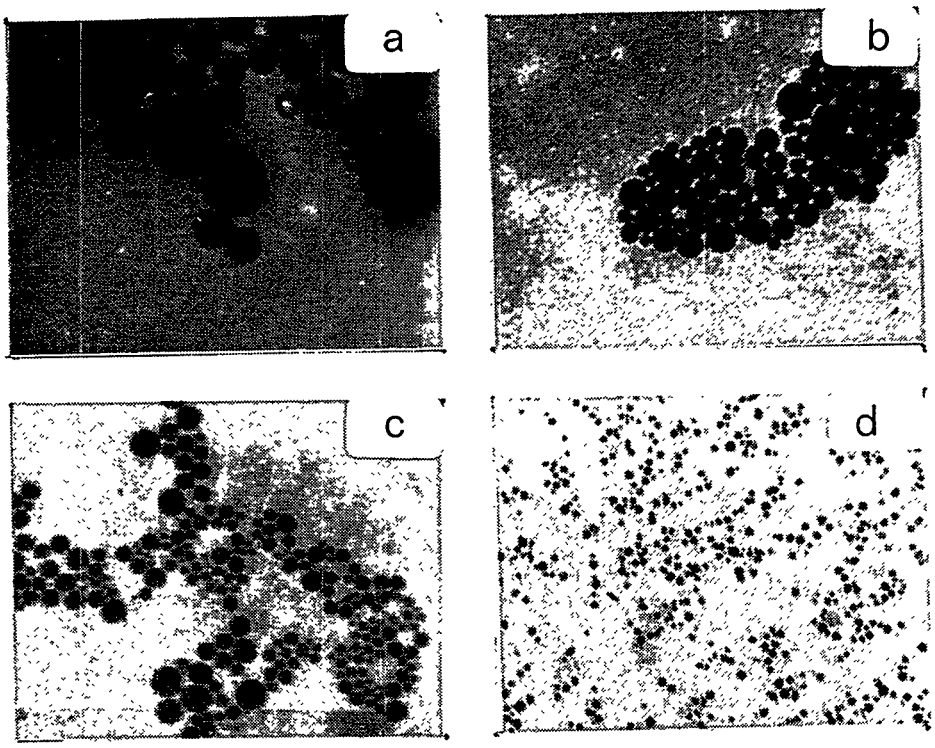

Figure 4.3

TEM micrographs of molybdenum sulfide particles made in the 0.15 M NP-5/cyclohexane microemulsion (R=1, $[H_2SO_4] = 1.3x10^{-3}$ M).

Ammonium tetrathiomolybdate concentrations:

(a) $3.2x10^{-6}$ M; (b) $3.6x10^{-6}$ M; (c) $4.0x10^{-6}$ M; (d) $4.8x10^{-6}$ M; (e) $6.4x10^{-6}$ M; (f) $8.0x10^{-6}$ M; (g) $9.6x10^{-6}$ M; (h) $11.2x10^{-6}$ M.

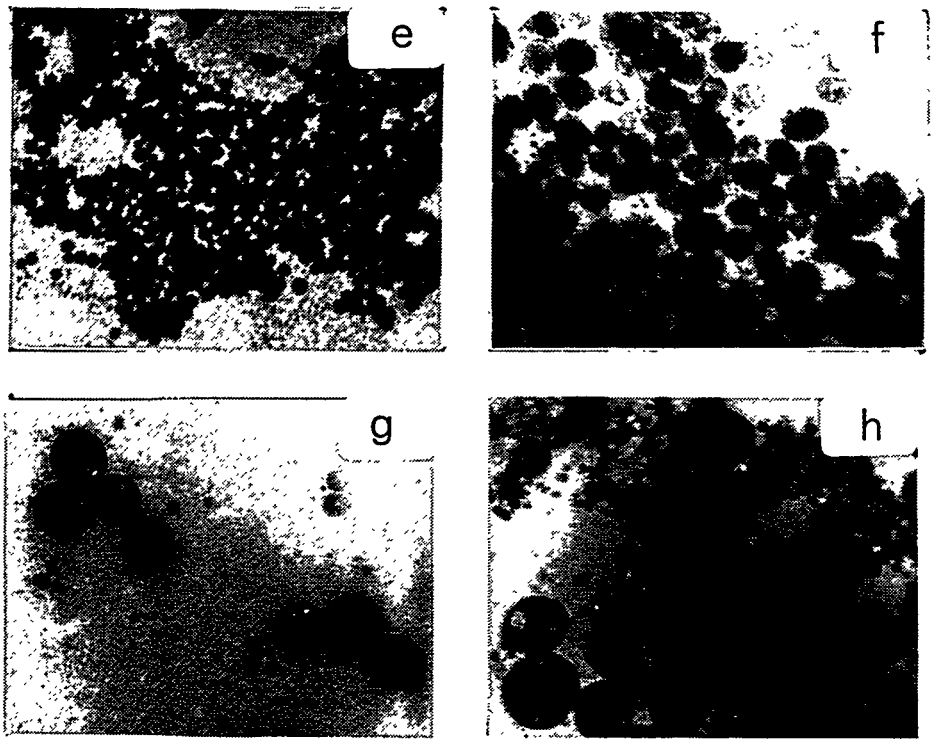

Figure 4.3
(Continued)

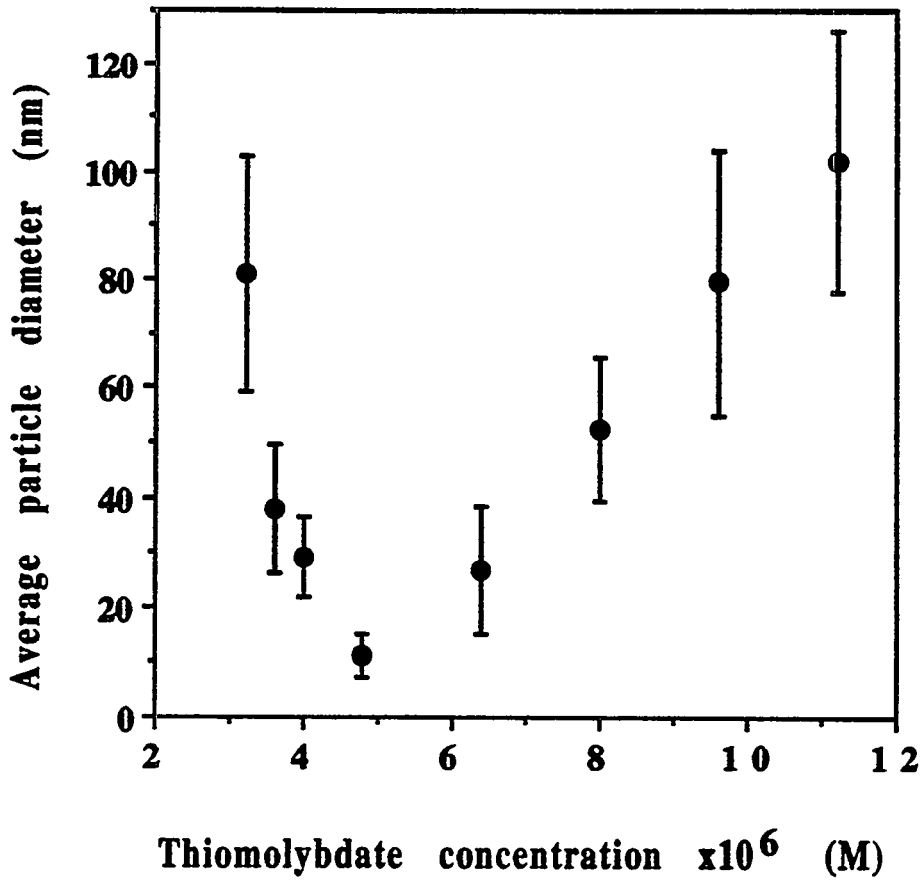

Figure 4.4

Effect of ammonium tetrathiomolybdate concentration on the average molybdenum sulfide particle size for the 0.15 M NP-5/cyclohexane microemulsion; $[H_2SO_4]=1.3x10^{-3}$ M, R=1.

Particle formation scheme. To analyze the data presented in Figures 4.1 to 4.4, the particle formation scheme as discussed in Chapter 3 (Section 3.3.3) will be considered.

Molybdate occupancy number and particle size. The occupancy number (i.e., the number of ammonium tetrathiomolybdate ions per surfactant aggregate), is a key parameter that controls the nucleation rate in the microemulsion fluid phase (6,18,32). Summarized in Table 4.2 are data on the thiomolybdate occupancy number (N_{oc}), the theoretical number of nuclei (N_n) and the number of particles (N_p) in 10 mL of microemulsion. Due to the difficulties in determining the inverse micelle diameter at $[MoS_4^{2-}]>8x10^{-6}$ M, the values at $[MoS_4^{2-}] > 8x10^{-6}$ M were assumed to be equal to that of $[MoS_4^{2-}]=8x10^{-6}$ M (i.e., D_m=3.4 nm). The occupancy numbers at $[MoS_4^{2-}]>8x10^{-6}$ M are based on this assumption. The molybdate occupancy number was obtained using Equation 4.2.

$$N_{oc} = N_{mo} \times 6.022x10^{23}/N_m \qquad [4.2]$$

where N_m is the number of micellar aggregates in 10 mL of microemulsion (Equation 4.3) and N_{mo} represents the moles of MoS_4^{2-} in the microemulsion.

$$N_m = V_a/[(4/3)\pi(D_m/2)^3] \qquad [4.3]$$

In Equation 4.3, V_a is the volume of the dispersed (aqueous plus surfactant) phase and D_m is the average micellar diameter.

As shown in Table 4.2, N_{oc} increases as the tetrathiomolybdate ion concentration is increased. The greater the occupancy number, the higher the likelihood that a critical number of molybdenum sulfide monomers will encounter each other in a particular inverse micelle to form a nucleus (18,32). Accordingly, for

Table 4.2

Selected Statistical Parameters for the Formation of Molybdenum Sulfide Particles in the 0.15 M NP-5/Cyclohexane Microemulsion ($[H_2SO_4] = 1.3 \times 10^{-3}$ M, $i_c = 2.5$).

$[MoS_4^{2-}] \times 10^6$ M	D_m (nm)	$N_{oc} \times 10^3$	$N_n \times 10^{-11}$	$N_p \times 10^{-11}$
3.2	3.9	0.44	0.35	0.07
3.6	3.8	0.45	0.60	0.77
4.0	3.7	0.47	1.0	1.84
4.8	3.7	0.54	1.5	39.3
6.4	3.5	0.65	3.0	3.92
8.0	3.4	0.73	4.0	0.64
9.6	-	0.87	5.0	0.22
11.2	-	1.01	6.0	0.12

high tetrathiomolybdate ion concentrations, a greater number of nuclei should be formed in the w/o microemulsions. This implies that for high tetrathiomolybdate ion concentrations the number of monomers left over after the nucleation process (i.e., the number of monomers not utilized in the nucleation step) should be very small. In the post-nucleation period, if growth occurs by monomer addition only, then at high occupancy numbers (high initial thiomolybdate concentration) relatively few monomers will be available to partake in the growth process. Consequently, it is reasonable to conclude that for the case where the nucleation rate is high (i.e., high N_{oc}) smaller particles should be made.

It can be seen from Figure 4.4 that the preceding discussion on the expected relationship between the thiomolybdate occupancy number and molybdenum sulfide particle size is consistent with the experimental data for $[MoS_4^{2-}] < 4.8 \times 10^{-6}$ M. However for $[MoS_4^{2-}] > 4.8 \times 10^{-6}$ M, although the occupancy number increases with thiomolybdate concentration, the average molybdenum sulfide particle diameter also increases with thiomolybdate concentration. To rationalize this increase in particle diameter with thiomolybdate concentration at $[MoS_4^{2-}] > 4.8 \times 10^{-6}$ M, a simulation of the theoretical particle size (which is based on the monomer addition mechanism) for the various thiomolybdate concentrations is considered next.

Particle size simulation. To probe the growth mechanism of the molybdenum sulfide particles in the microemulsion fluid phase, the monomer addition growth model is used to calculate the expected (theoretical) particle size. Subsequently, the theoretical particle size is compared with the average particle size determined from TEM measurements.

If molybdenum sulfide particle growth occurs by monomer addition only, then the theoretical number of nuclei should equal the experimental number of particles, i.e., $N_n = N_p$. In order to determine N_n, it is first necessary to determine the

distribution of thiomolybdate ions among the available water pools. The probability to have k ammonium tetrathiomolybdate ions per inverse micelle (P_k) can be described by the Poisson statistical distribution law (32-34):

$$P_k = N_{oc}{}^k(e^{-Noc}/k!) \qquad [4.4]$$

where N_{oc} is the average molybdate occupancy number (the number of tetrathiomolybdate ions per inverse micelle). Assuming that the minimum number of ammonium tetrathiomolybdate ions that is needed to form a nucleus is i_c, and that only one molybdenum sulfide nucleus forms in a water pool, then the number of molybdenum sulfide nuclei produced in the w/o microemulsion should be equivalent to the number of micellar aggregates that contain tetrathiomolybdate ions equal to or greater than i_c. That is, the number of nuclei can be written as:

$$N_n = N_m \sum_{k=i_c}^{\infty} P_k \qquad [4.5]$$

The experimentally determined number of particles observed in the microemulsion fluid phase (N_p) is calculated as:

$$Np = M_{MoS_3(t)}/M_p \qquad [4.6]$$

where $M_{MoS_3(t)}$ is the total mass of molybdenum sulfide particles made in 10 mL of microemulsion, and M_p is the mass of a single molybdenum trisulfide particle. For a molybdenum sulfide particle with a diameter D_p (obtained from TEM measurement), the mass (M_p) is given by Equation 4.7:

$$M_p = (4/3)\rho\pi(D_p/2)^3 \qquad [4.7]$$

where $\rho = 3.2$ g cm^{-3} is the density of molybdenum trisulfide (36).
Combining Equations 4.5-4.7, Equation 4.8 is obtained, which gives the theoretical particle diameter (D_{theor}):

$$D_{theor} = 2[M_{MoS_3}/N_n(4/3)\pi\rho]^{1/3} \qquad [4.8]$$

Presented in Figure 4.5 is a plot of the theoretical particle diameter versus the thiomolybdate concentration for i_c values of 2 and 3, i.e., N_n in Equation 4.5 was obtained with i_c=2,3. Also presented in Figure 4.5 is a plot of the theoretical particle diameter of molybdenum sulfide particles versus the thiomolybdate concentration for i_c=2.5 (i.e., considering a combination of i_c values of 2 and 3 in the ratio 1:1). The experimental particle size is superimposed for comparison purposes. The following observations can be made from Figure 4.5: (a) For any i_c value, the theoretical particle diameter decreases as the thiomolybdate concentration is increased; (b) for $[MoS_4^{2-}] < 4.8\text{x}10^{-6}$ M both the theoretical and experimental particle diameters decrease with increasing thiomolybdate concentration. In addition, for i_c= 2.5 (i_c= 2-3) and $[MoS_4^{2-}] < 4.8\text{x}10^{-6}$ M the theoretical particle diameter coincides quite well with the corresponding experimental particle diameter, which implies that 2-3 monomers may combine to form a molybdenum sulfide particle. In agreement with the assumption made in the derivation of Equation 4.8, the latter observation suggests that for $[MoS_4^{2-}] = 3.2\text{-}4.8\text{x}10^{-6}$ M, particle growth is by monomer addition. However, for i_c=2.5, and $[MoS_4^{2-}] > 4.8\text{x}10^{-6}$ M, although the rate of change of the theoretical particle diameter with thiomolybdate concentration can be considered to remain constant, the experimental particle diameter is seen to increase with

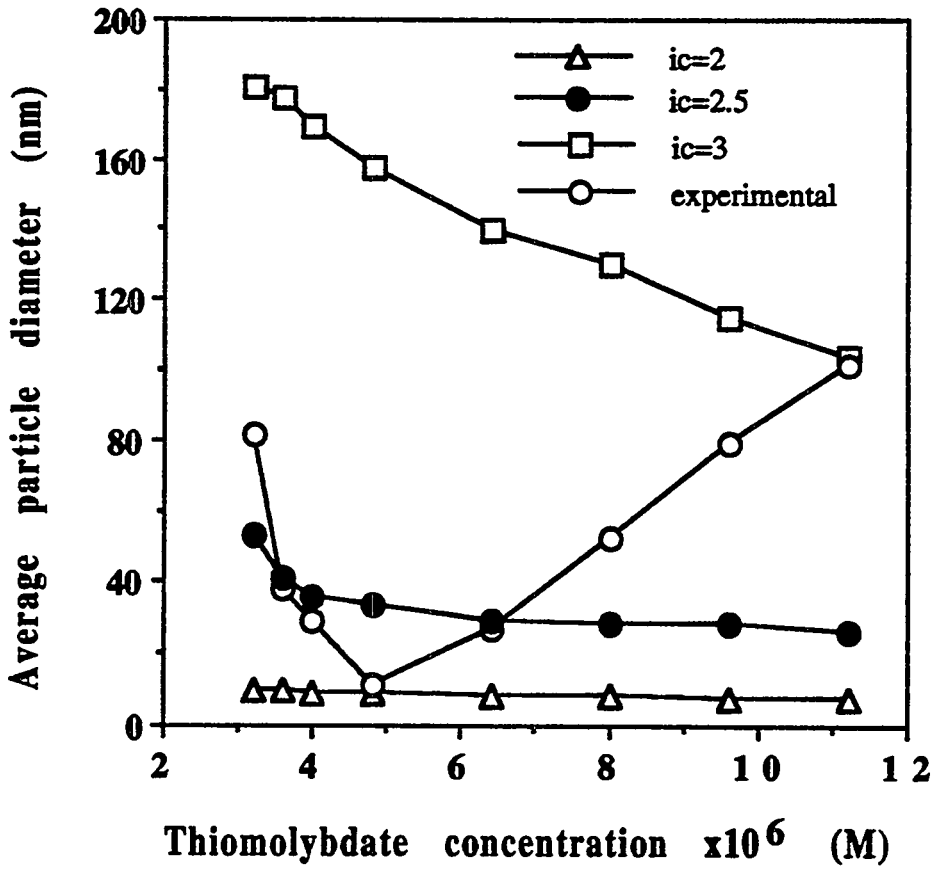

Figure 4.5

Effect of thiomolybdate concentration on theoretical and experimental molybdenum sulfide particle diameter. The microemulsion system 0.15 M NP-5/cyclohexane was used as the reaction medium

(R=1; i_c=2-3; $[MoS_4^{2-}]$=(3.2-11.2)x10^{-6} M; $[H_2SO_4]$=1.3x10^{-3} M).

the thiomolybdate concentration. The rationalization of this difference is considered next.

Growth mechanisms for $[MoS_4^{2-}]>4.8x10^{-6}$ M. To resolve the growth mechanism in the microemulsion fluid phase, it is useful to compare the number of nuclei (N_n, Equation 4.5) expected to be produced for the various thiomolybdate occupancy numbers. Figure 4.6 presents a plot of the theoretical number of nuclei (N_n, Equation 4.10) versus the thiomolybdate concentration. Also presented in Figure 4.6 is the average thiomolybdate occupancy number (N_{oc}, Equation 4.2) versus the thiomolybdate concentration. The calculation of the theoretical number of nuclei is based on the assumption that a minimum of 2-3 molybdenum sulfide monomers are needed to form a nucleus, e.g., i_c=2.5. The theoretical number of nuclei initially increases sharply with thiomolybdate concentration to $[MoS_4^{2-}] = 4.8x10^{-6}$ M; at $[MoS_4^{2-}]>4.8x10^{-6}$ M its rate of increase begins to slow down. This implies that at $[MoS_4^{2-}]>4.8x10^{-6}$ M the rate of increase of the number of nuclei with the thiomolybdate concentration is "quasi constant". On the other hand, the molybdate occupancy number monotonically increases with thiomolybdate concentration; thus at $[MoS_4^{2-}]> 4.8x10^{-6}$ M the number of excess thiomolybdate ions not utilized in nuclei formation will also increase. The excess unutilized ions will subsequently add onto an approximately constant number of nucleated primary particles and hence, for $[MoS_4^{2-}]>4.8x10^{-6}$ M, the particle size increases as the thiomolybdate concentration increases. A similar explanation was offered by Nagy (18) for the formation of cobalt boride in the CTAB microemulsions.

It is noteworthy that on the TEM micrographs (Figures 4.4f and 4.4h) a bimodal distribution is observed for $[MoS_4^{2-}] = 8x10^{-6}$ and $11.2x10^{-6}$ M, especially at $[MoS_4^{2-}] = 11.2x10^{-6}$ M. This evidence suggests, however, that at relatively high thiomolybdate concentration, i.e., $[MoS_4^{2-}] > 8x10^{-6}$ M, the molybdenum sulfide

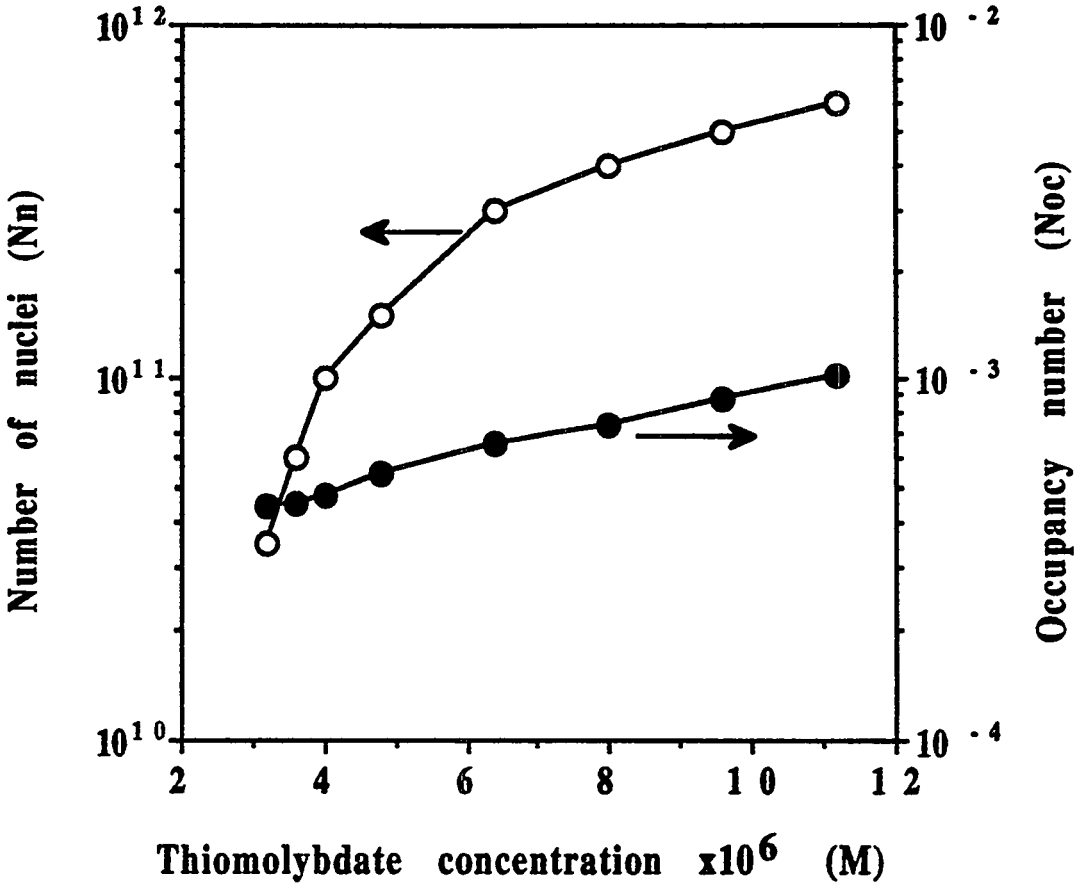

Figure 4.6

Effect of ammonium tetrathiomolybdate concentration on the thiomolybdate occupancy number and the number of molybdenum sulfide nuclei (R=1; i_C=2.5; [MoS_4^{2-}]=(3.2-11.2) x10^{-6} M; [H_2SO_4]=1.3x10^{-3} M).

particles may also grow by aggregation. Similar observations of aggregative growth have been reported by Zukoski and coworkers (36-39). In the synthesis of silica particles in ethanol, (36-39) they used TEM to show that small and large silica particles were present throughout the growth period. In addition to the TEM results, ionic strength and seeded growth experiments (36,39) showed that particle growth was not by monomer addition. Growth of silica particles was reported to occur via aggregation of small particles (<10 nm) on larger ones.

The results of the present study indicate that the monomer addition and aggregation growth mechanisms may take place concurrently. The occurrence of both growth mechanisms for silica particles has been reported by Vrij and coworkers (40,41). In this connection, these authors (40,41) showed that silica particles prepared by hydrolysis of tetraethoxysilane (TEOS) grow by both monomer addition and aggregation processes. They proposed that at the early stage of silica particle growth, aggregation is important and that the particle size depends on the ionic strength (varied by adding $LiNO_3$) of the synthesis solvent (water, lower alcohols and ammonia). However, in the latter stage of the growth process, where monomer addition is dominant, the particle size is insensitive to ionic strength.

To further explore the possibility of aggregative growth mechanism at $[MoS_4^{2-}] > 4.8 \times 10^{-6}$ M, a superimposed plot of the number of nuclei (i_c=2.5) and number of particles versus the thiomolybdate concentration is presented in Figure 4.7. In the post-nucleation period, if the molybdenum sulfide nuclei grow by the addition of monomers only, then the number of nuclei (N_n, Equation 4.5) should be equal to the observed number of particles (N_p, Equation 4.6). This implies that a plot of the observed number of molybdenum sulfide particles versus thiomolybdate concentration should exhibit an increase similar to that of the theoretical number of nuclei (N_n, Equation 4.5). This is indeed found to be the case for $[MoS_4^{2-}] < 4.8 \times 10^{-6}$ M. The latter implies in turn that, for $[MoS_4^{2-}] < 4.8 \times 10^{-6}$ M, the growth of

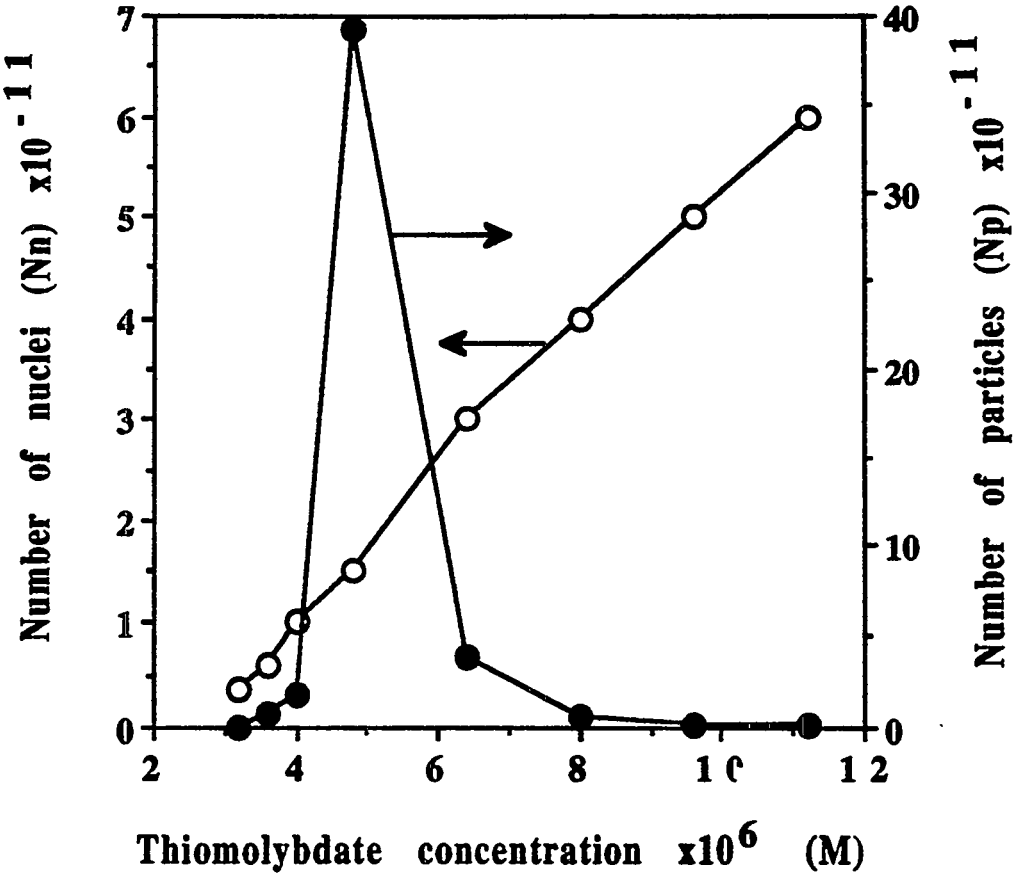

Figure 4.7

Effect of ammonium tetrathiomolybdate concentration on the number of molybdenum sulfide nuclei and particles formed in the 0.15 M NP-5/cyclohexane microemulsion

(R=1; i_C=2.5; [MoS_4^{2-}]=(3.2-11.2) x10^{-6} M; [H_2SO_4]=1.3x10^{-3} M).

molybdenum sulfide particle occurs by monomer addition. On the other hand, for $[MoS_4^{2-}] > 4.8x10^{-6}$ M, while the theoretical number of nuclei increases with thiomolybdate concentration, the observed number of particles decreases. This observation leads to the conclusion that, in addition to the monomer addition mechanism, molybdenum sulfide particles in the microemulsion fluid phase may grow by aggregation at $[MoS_4^{2-}] > 4.8x10^{-6}$ M.

4.3.3 Effect of Sulfuric Acid Concentration and R on Particle Size

Figure 4.8 and Table 4.3 summarize the effects of sulfuric acid concentration and the microemulsion water content on the molybdenum sulfide particle diameter. Selected TEM micrographs are presented in Figure 4.9. The following observations can be made from Figure 4.8: (a) For all R values, the average particle diameter is larger for an acid concentration of $2.6x10^{-3}$ M compared to the concentrations of $0.65x10^{-3}$ and $1.30x10^{-3}$ M; (b) for all acid concentrations, and within the limits of the standard deviation, the molybdenum sulfide particle diameter increases with R. Unlike typical TEM micrographs of aggregated molybdenum sulfide particles that have rough surfaces (34), the surfaces of the particles in Figure 4.9 are smooth.

Figure 4.10 presents a plot of the expected number of nuclei (N_n, Equation 4.5) versus sulfuric acid concentration for various R values. The calculation of the number of nuclei is based on the distribution of molybdate species in the microemulsion. For each R value the number of nuclei decreases with increasing acid concentration. If the growth mechanism of molybdenum sulfide particles in the microemulsion is by monomer addition only, then for each R value more monomers should be available to partake in the growth process at high acid concentrations and hence larger particles are expected to be produced at high sulfuric

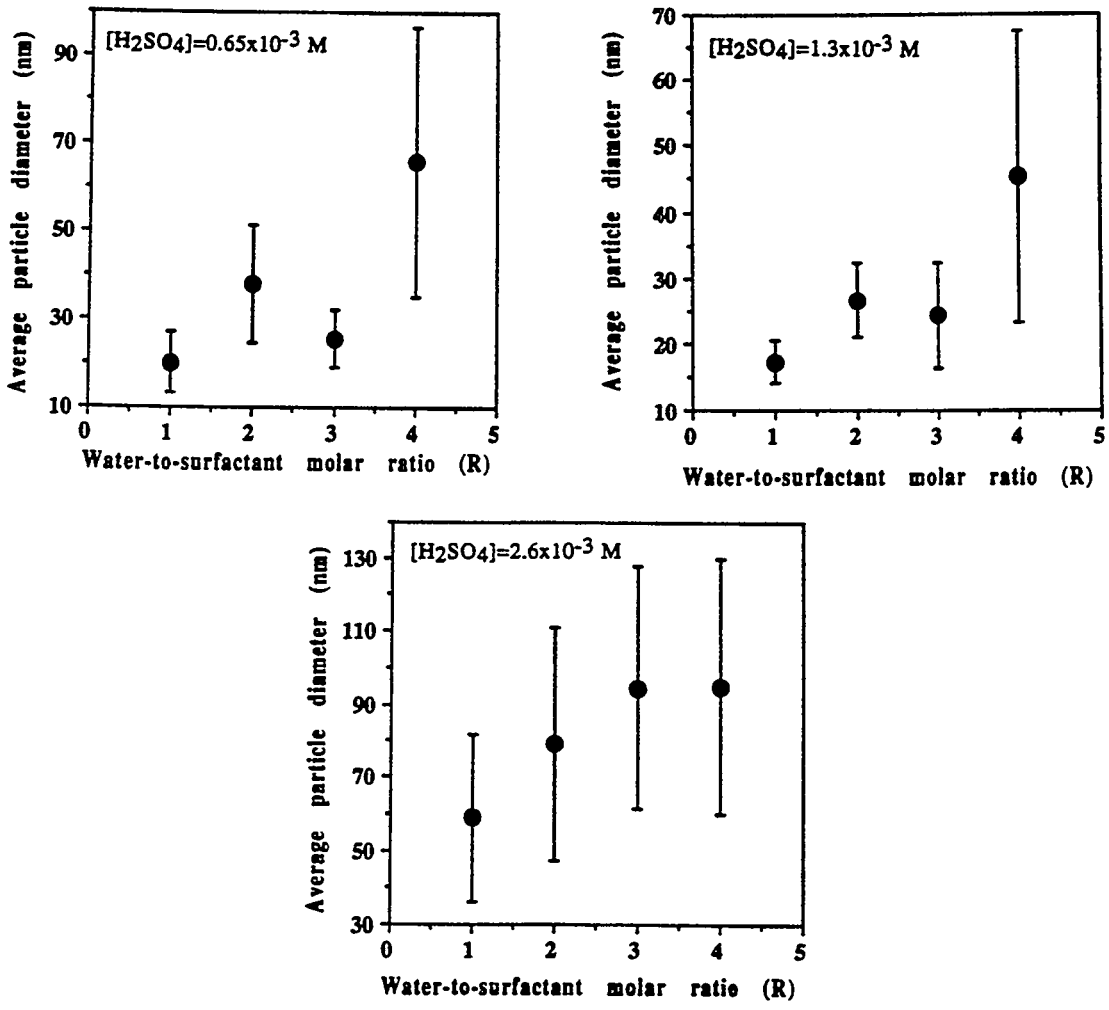

Figure 4.8

Effects of acid concentration and water-to-surfactant molar ratio (R) on the diameter of molybdenum sulfide particles synthesized in the 0.15 M NP-5/cyclohexane microemulsion ($[MoS_4^{2-}]$=6.4 x10^{-6} M).

Table 4.3

Effects of Sulfuric Acid Concentration and Microemulsion Water Content on the Size of Molybdenum Sulfide Particles Synthesized in the 0.15 M NP-5/Cyclohexane Microemulsion ($[MoS_4^{2-}] = 6.4 \times 10^{-6}$ M).

	Average particle diameter (nm)			Standard deviation (nm)		
R	$[H_2SO_4]=$ 0.65×10^{-3} M	$[H_2SO_4]=$ 1.3×10^{-3} M	$[H_2SO_4]=$ 2.6×10^{-3} M	$[H_2SO_4]=$ 0.65×10^{-3} M	$[H_2SO_4]=$ 1.3×10^{-3} M	$[H_2SO_4]=$ 2.6×10^{-3} M
1	20.2	17.3	58.9	6.9	3.2	22.9
2	37.9	26.7	79.0	13.2	5.6	31.9
3	25.5	24.4	94.5	6.4	8.1	33.1
4	65.9	45.4	95.0	30.7	22.1	35.1

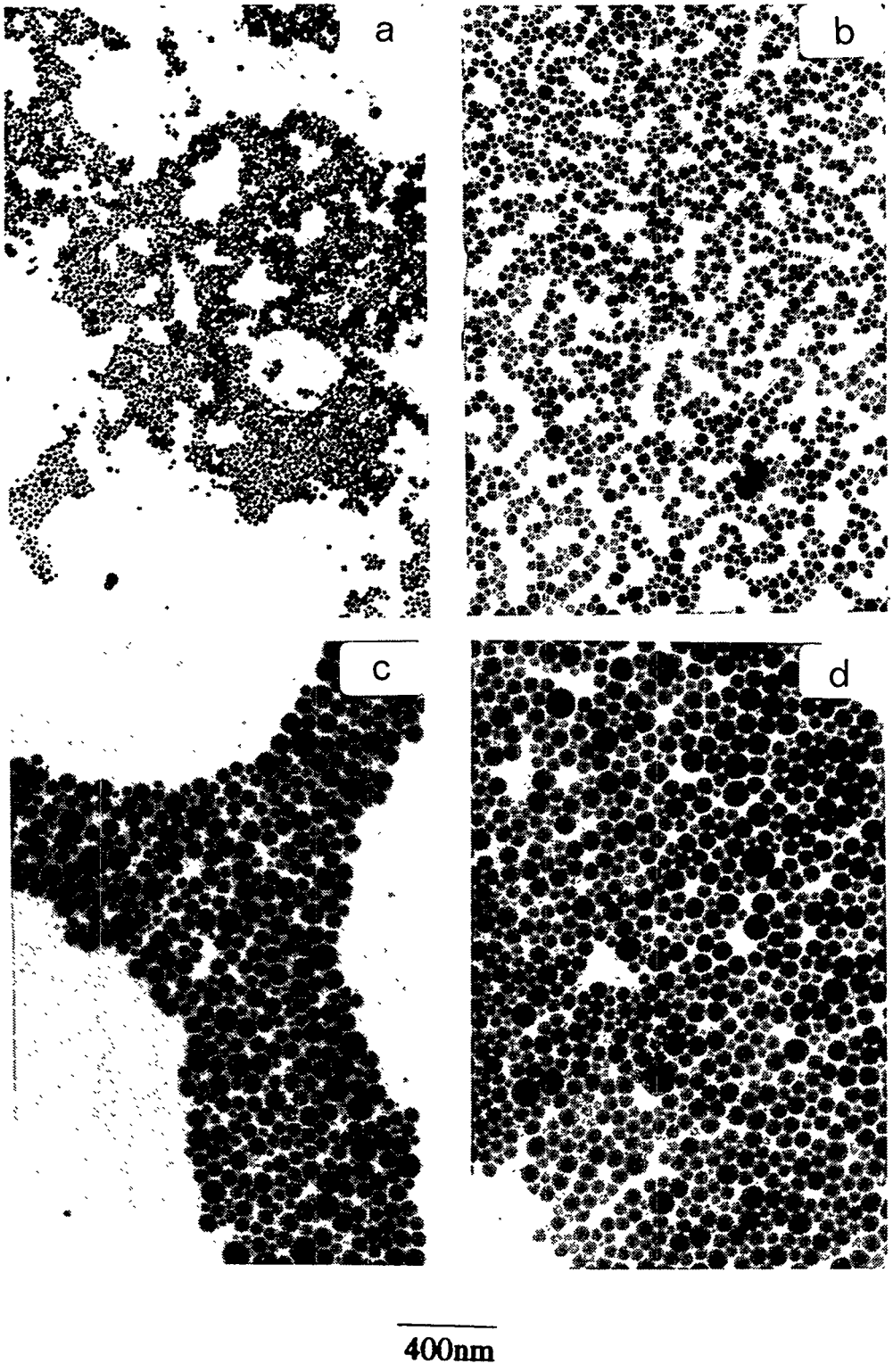

Figure 4.9
TEM micrographs of molybdenum sulfide particles prepared in the 0.15 M NP-5/cyclohexane microemulsion ($[MoS_4^{2-}]=6.4\times10^{-6}$ M).
(a) R=1, $[H_2SO_4]=1.30\times10^{-3}$ M; (b) R=2, $[H_2SO_4]=0.65\times10^{-3}$ M;
(c) R=3, $[H_2SO_4]=2.6\times10^{-3}$ M; (d) R=4, $[H_2SO_4]=2.6\times10^{-3}$ M.

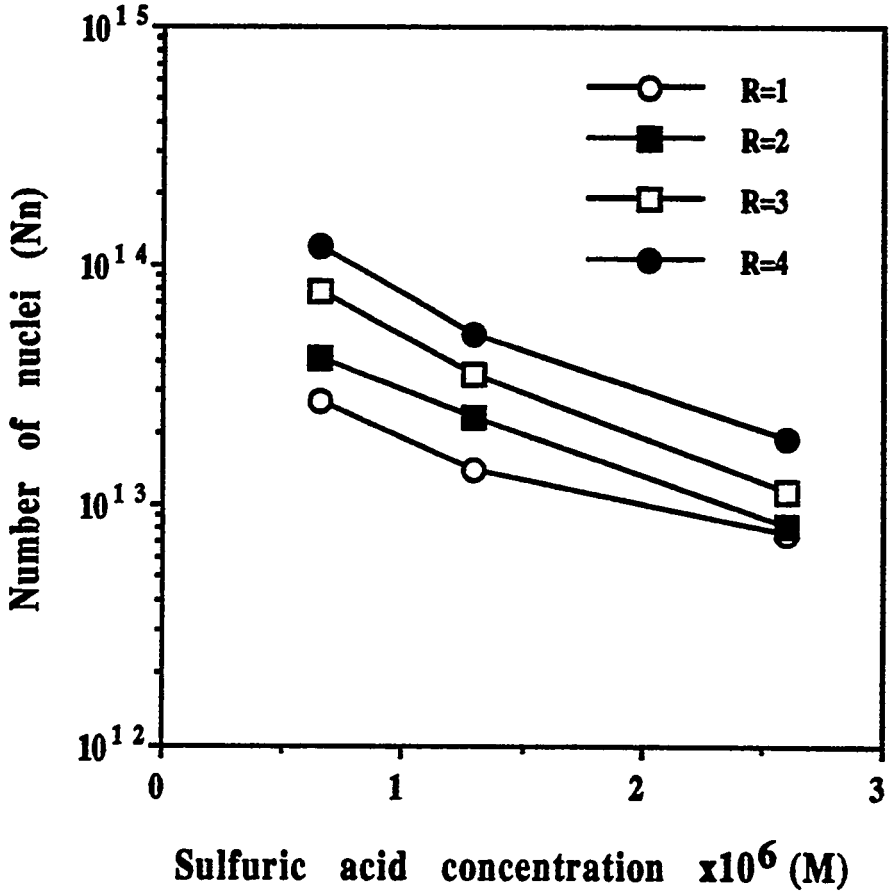

Figure 4.10

Effect of acid concentration and water-to-surfactant molar ratio on the number of nuclei formed in the 0.15 M NP-5/cyclohexane microemulsion (i_C=2, [MoS_4^{2-}]=6.4 x10^{-6} M).

acid concentrations. This rationalization is consistent with the results shown in Figure 4.8 (i.e., larger particles are produced at high acid concentrations). However, for each acid concentration, the number of nuclei increases with R; but the average particle diameter also increases with R, which is unexpected if growth occurs only by monomer addition. This apparent contradiction is discussed next.

Figure 4.11 presents plots of number of nuclei and particles versus R. It can be seen that, for each acid concentration, the number of nuclei increases with R and the number of particles decreases with R. As discussed previously, if the molybdenum sulfide particles grow only by monomer addition in the post-nucleation period then the theoretical number of nuclei should equal the number of particles. This implies that as in the case of the theoretical number of nuclei (Figure 4.10), a plot of the experimental number of particles (N_p, Equation 4.6) should increase with R. The opposing trends observed in Figure 4.11 suggest that particle aggregation also occurs in the microemulsion fluid phase. However, the TEM micrographs (Figure 4.9) show that the particle surfaces are smooth, which apparently contradicts the proposed particle aggregative growth. These observations can be reconciled by the fact that the occurrence of both aggregation and monomer addition growth (i.e, aggregation followed by monomer addition) has been shown (39,40) to result in the formation of particles that have smooth surfaces. The effect of molybdenum sulfide surface charge on particle growth is considered next.

To investigate the effect of pH on the surface charge of the molybdenum sulfide particles, the reactions as carried out in the water cores were simulated in bulk aqueous solutions. Here it is assumed that the concentrations of the impregnating acid and thiomolybdate solutions are equal to those in the microemulsion water cores. Five mL of 0.53-2.3 M sulfuric acid was added to 5 mL of $5x10^{-3}$ M ammonium tetrathiomolybdate. The pH was measured after the reaction. The measurements gave pH values that are less than 0.5 for all acid

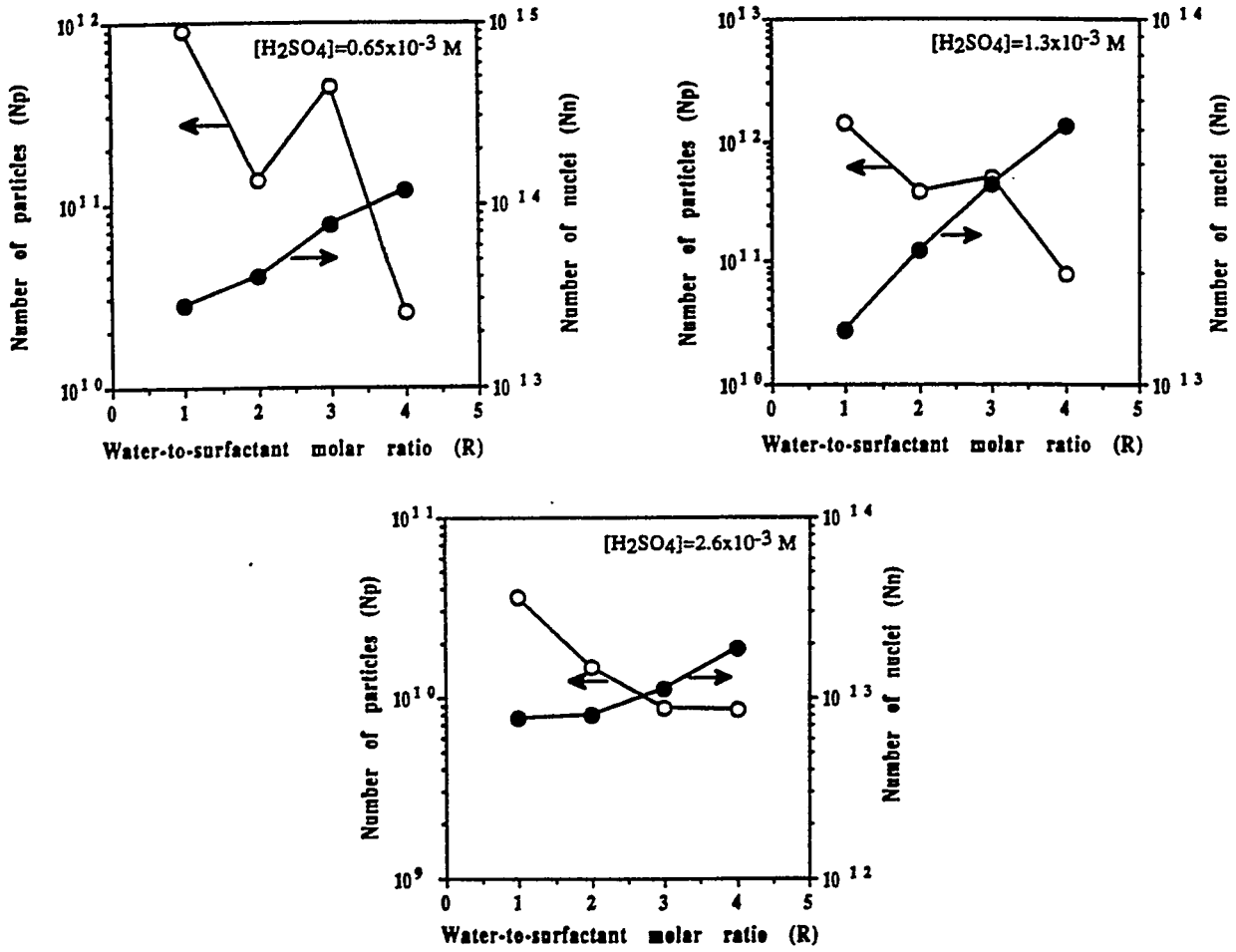

Figure 4.11

Effect of acid concentration and the water-to-surfactant molar ratio on number of molybdenum sulfide particles and nuclei formed in the 0.15 M NP-5/cyclohexane microemulsion (i_C=2, [MoS_4^{2-}]=6.4 x10^{-6} M).

concentrations. The isoelectric point of molybdenum trisulfide is 1.9 (31). Thus at pH < 0.5 the particle surface is positively charged and hence the resulting inter-particle repulsion should discourage growth by aggregation. On the other hand, at pH < 0.5, the addition of MoS_4^{2-} will be favored since the protons adsorbed at the particle surface will attract the anionic tetrathiomolybdate species, resulting in deposition of molybdenum sulfide monomers on the particle surface.

From Equation 4.1, the solubility of ammonium tetrathiomolybdate can be written as:

$$[MoS_4^{2-}] = [H_2S]/[H^+]^2 K_S \qquad [4.9]$$

where K_S is the solubility product. It is seen from Equation 4.9 that at high acid concentrations (at low pH values), the solubility of tetrathiomolybdate species is small, which implies that more MoS_3 nuclei should be formed and smaller particles made. However, the reverse result was obtained in this study, which indicates that material addition is not the only mechanism of particle growth and that aggregation is also important. Further studies of the factors controlling the aggregation process are needed.

4.4 CONCLUSIONS

The results presented in this study show the possibility of making nanosize molybdenum sulfide particles with variable average diameter and size distribution by changing the concentration of the precursor reactant molecules. The effect of ammonium tetrathiomolybdate concentration on molybdenum sulfide particle size shows that an optimum concentration exists which minimizes both the average

particle size and the polydispersity. A quantitative growth model, which is based on the monomer addition growth mechanism, has been used to predict the theoretical particle size. At $[MoS_4^{2-}] < 4.8x10^{-6}$ M the decrease in particle size with increasing thiomolybdate concentration is due to an increase in the nucleation rate. At $[MoS_4^{2-}] > 4.8x10^{-6}$ M the increase in particle size is attributed to both monomer addition and aggregative growth processes. A study of the effect of sulfuric acid concentration on the average molybdenum sulfide particle size shows that at low concentrations ($6.5x10^{4}$, $1.3x10^{-3}$ M) the particle size does not change but it increases at higher concentration ($2.6x10^{-3}$ M). This observation is attributed to the decreasing thiomolybdate occupancy number as the sulfuric acid concentration is increased. A simulation of the pH values in the microemulsion water cores suggests that the particle surfaces are positively charged (i.e., the isoelectric point of molybdenum trisulfide is 1.9). Thus inter-particle repulsion is predicted to discourage particle aggregation. On the other hand, the positive nature of the particle surface will encourage material addition through the attraction of the anionic tetrathiomolybdate species.

4.5 REFERENCES

1. Wilcoxon, J.P., Williamson, R.L., and Baughman, R., *J. Chem. Phys.* **98,** 9933 (1993).
2. Ward, A.J.I., O'Sullivan, E.C., Rang, J.C., Nedeljkovic, J., and Patel, R.C., *J. Colloid Interface Sci.* **161,** 316 (1993).
3. Lianos, P., and Thomas, J.K., in "Materials Science Forum", Vol. 25-26 (G.E. Murch and F.H. Wohlbier, Eds.), 1988, p. 369.

4. Motte, L., Petit, C., Boulanger, L., Lixon, P., Pileni M.P., *Langmuir* **8,** 1049 (1992).

5. Pileni, M.P., Motte, L., Petit, C., *Chem. Mater.* **4,** 338 (1992).

6. Boakye, E., Radovic, L.R., and Osseo-Asare, K., *J. Colloid Inteface Sci.* **163,** 120 (1994).

7. Boakye, E., Radovic, L.R., and Osseo-Asare, K., submitted to *J. Colloid Interface Sci.* (1994).

8. Arriagada, F.J., and Osseo-Asare, K., *Colloids Surf.* **50,** 321 (1990).

9. Arriagada, F.J., and Osseo-Asare, K., *Colloids Surf.* **69,** 105 (1992).

10. Pileni, M.P., *J. Phys. Chem.* **97,** 6961 (1993).

11. Petit, C., Lixon, P., and Pileni, M.P., *J. Phys. Chem.* **97,** 12974 (1993).

12. Boutonnet, M., Kizling, J., Stenius, P., and Maire, G., *Colloids Surf.* **5,** 209 (1982).

13. Petit, C., and Pileni, M.P., *J. Phys. Chem.* **92,** 2282 (1988).

14. Petit, C., Lixon, P., and Pileni, M.P., *J. Phys. Chem.* **94,** 1598 (1990).

15. Steigerwald, M.L., Alivisatos, A.P., Gibson, J.M., Harris, T.D., Kortan, R., Muller, A.J., Thayer, A.M., Duncan, T.M., Douglas, D.C., and Brus, L.E., *J. Am. Chem. Soc.* **110,** 3046 (1988).

16. Pileni, M.P., and Lisieki, I., *Colloids Surf.* **80,** 63 (1993).

17. Lianos, P., and Thomas, J.K., *Chem Phys. Lett.* **125,** 299 (1986).

18. Nagy, J.B., *Colloids Surf.* **35,** 201 (1989).

19. Hou, M.J., and Shah, D.O., in "Interfacial Phenomena in Biotechnology and Materials Processing." (Y.A. Attia, B.M. Moudgil, and S. Chander, Eds.), Elsevier, Amsterdam/New York, 1988, p. 443.

20. Chew, C.H., Gan, L .M., and Shah, D.O., *J. Dispersion Sci. Technol.* **11,** 593 (1990).

21. Dvolaitzky, M., Ober, R., Taupin, C., Anthore, R, Auvray, X., Petipas, C., and Williams, C., *J. Dispersion Sci. Technol.* **4,** 29 (1983).

22. Robinson, B.H., Towey, T.F., Zourab, S., Visser, A.J.W.G., and Hoek, A.V., *Colloids Surf.* **61,** 175 (1991).

23. Lianos, P., and Thomas, J.K., *J. Colloid Interface Sci.* **117,** 505 (1987).

24. Kumar, P., Pillai, V., and Shah, D.O., *Appl. Phys. Lett.* **62,** 765 (1993).

25. Midmore, B.R., *J. Chem. Soc. Faraday Trans.* **86,** 3763 (1990).

26. Virden, J.W., and Berg, J.C., *J. Colloid Interface Sci.* **149,** 528 (1992).

27. Dunn, C.M., Robinson, B.R., and Leng, F.J., *Spectrochimica Acta.* **46A,** 1017 (1990).

28. Zulauf, M., and Eicke, H.-F., *J. Phys. Chem.* **83,** 480 (1979).

29. Koppel, D.E., *J. Chem. Phys.* **57,** 4814 (1972).

30. Osseo-Asare, K., and Arriagada, F.J., in "Ceramic Powder Science III", (G.L. Messing, S. Hirano and H. Hausner, Eds.) American Ceramic Society, Westerville, OH, 1990, p. 3.

31. Haruta, M., Lamaitre, J., Delannay F., and Delmon, B., *J. Colloid Interface Sci.* **101,** 59 (1984).

32. Ravet, I., Nagy, J.B., and Derouane, E.G., in "Preparation of Catalysts IV", (B. Delmon, P. Grange, P.A. Jacobs and G. Poncelet, Eds.), Elsevier, 1987, p. 505.

33. Arriagada, F.J., and Osseo-Asare, K., in "Colloid Chemistry of Silica" (H.E. Bergna, Ed.), Advances in Chemistry Series, Vol. 234, 1994, p. 113.

34. Boakye, E., Radovic, L.R., and Osseo-Asare, K., to be submitted.

35. Atik, S.S., and Thomas, J.K., *J. Am. Chem. Soc.* **103,** 3543 (1981).

36. Schleich, D.M., Chang, H.S., Barberio, Y.L., and Hanson, K.J., *J. Elecrochem. Soc.* **136,** 3274 (1989).

37. Bogush, G.H., Tracy, M.A., and Zukoski IV, C.F., *J. Non-Cryst. Solids* **104,** 95 (1988).

38. Look, J.-L., Bogush, G.H., and Zukoski IV, C.F., *Faraday Discuss. Chem. Soc.* **90,** 345 (1990).

39. Bogush, G.H., ad Zukoski IV, C.F., *J. Colloid Interface Sci.* **142,** 1 (1991).

40. Bogush, G.H., and Zukoski IV, C.F., *J. Colloid Interface Sci.* **142,** 19 (1991).

41. Van Blaaderen, A.V. and Vrij, A., in "Colloid Chemistry of Silica" (H.E. Bergna, Ed.), Advances in Chemistry Series, Vol. 234, 1994, p. 82.

42. Blaaderen, A., Van Geest, J., and Vrij, A., *J. Colloid Interface Sci.* **154,** 481 (1992).

CHAPTER 5

MICROEMULSION-MEDIATED PARTICLE SYNTHESIS: AGREGATIVE GROWTH OF MOLYBDENUM SULFIDE PARTICLES IN NONIONIC INVERSE MICROEMULSIONS

5.1 INTRODUCTION

Nanosize particles are attracting increasing attention in the fields of materials science and catalysis, a development which is partly due to the extremely large specific surface areas characteristic of materials of this high degree of subdivision, and the ability of these nanoparticles to exhibit certain electronic and optical properties that differ from those characteristic of the corresponding bulk materials (1-15). The compartmentalization provided by the surfactant-stabilized microdroplets offers the opportunity to synthesize nanoparticles in water-in-oil (w/o) microemulsions (15- 27).

Nanosize molybdenum sulfide is of interest as a potential coal liquefaction catalyst (28). In Chapters 2-4, a relatively low precursor reactant loading was used, i.e., $[MoS_4^{2-}] = 3.2\text{-}11.2 \times 10^{-6}$ M. In this Chapter, the formation of molybdenum sulfide nanoparticles at a higher precursor reactant loading ($[MoS_4^{2-}] = 1.25 \times 10^{-3}$ M) is presented. In addition, a unique method for the extractive dissolution of the powder form of ammonium tetrathiomolybdate into the water cores of the inverse micelles is described. This method increases the reactant loading in the w/o microemulsion water pools. A similar method was recently reported by Wilcoxon and co-workers in connection with their work on gold particle synthesis (11).

Increasing the volume fraction of the molybdenum sulfide product is advantageous for an industrial process, such as coal liquefaction, where a relatively high catalyst loading is usually required (~1% molybdenum by weight). Furthermore, particle size uniformity is desirable for establishing an unambiguous relationship between particle size and catalytic efficiency. In previous chapters it has been shown that the particle size can be controlled by varying the water-to-surfactant molar ratio (R) of a microemulsion (13-18,20,23,24). In this Chapter an attempt is made to uncover the window where monodispersed molybdenum sulfide nanoparticles are synthesized at high ammonium tetrathiomolybdate loading. We present a study of the effect of R on particle size at different sampling times. In addition, the effect of the size of the surfactant polar headgroups on molybdenum sulfide particle characteristics was investigated. Two nonionic surfactants, with 4 and 9.5 oxyethylene units (polar headgroups) per surfactant molecule, respectively, were used: (a) polyoxyethylene(5)nonylphenyl ether (NP-5), and (b) polyoxyethylene tert-octylphenyl ether (Triton X-100).

A study of the published reports on the formation of CdS particles in AOT microemulsions (13,27,29,30) shows that, for $R > 10$, large and polydispersed particles are made, while for $R < 10$ small monodispersed particles are obtained. Although these reports have linked the water-to-surfactant molar ratio to particle size, they have not identified any relationships between R_c (where R_c represents the minimum R value above which "free water" molecules exist in the w/o microemulsion) and the onset of extensive particle growth. In this Chapter, the onset of extensive particle growth (aggregation) is linked with R_c. As a background to the results and discussion that follow, a brief review of the state of solubilized water molecules is presented. The issue is whether water molecules are free or bound to the surfactant headgroups in microemulsions formulated with an anionic

surfactant such as di(2-ethylhexyl) sodium sulfosuccinate (Aerosol OT, AOT) as well as with nonionic surfactants such as alkylphenol ethoxylates.

5.1.1 Background

State of solubilized water molecules in AOT microemulsions. Among the amphiphiles that form inverse micelles, AOT has received by far the greatest attention, as a result of its ability to solubilize large amounts of water in various nonpolar organic solvents. From the results in the literature, two types of water exist in AOT/oil/water microemulsions (31-40): (a) "bound" water molecules that represent the water of hydration of the surfactant headgroup (i.e., SO_3^-) and the counter ion (Na^+); and (b) "bulk" or "free" water molecules that are located in the core of the inverse micelles. Free water molecules become available at a certain R value (R_c) after the surfactant headgroups and the counterions have become sufficiently hydrated. Table 5.1 presents a collection of R_c values taken from the literature (31-40) and determined by spectroscopic and calorimetric methods. The proportions of bound and free water molecules depend on the water-to-surfactant molar ratio (R). Thomas and coworkers (34) have assigned the first six water molecules to the hydration of the sodium counter ions. The water of hydration is strongly bound, to the extent that its crystallization is prevented. This makes the bound water molecules unfreezable (31,40). At $10 > R > 6$, the excess water molecules that are unutilized in hydrating the sodium counter ion are still bound to the sulfonate headgroup through ion-dipole interactions and hydrogen bonding. At $R > 10\text{-}12$, free or unbound water molecules exist in AOT microemulsions.

State of solubilized water molecules in nonionic microemulsions. For nonionic surfactants, e.g., the alkylphenol ethoxylates, the first few water molecules solubilized in the inverse micelles interact with the oxyethylene units (EO) of the

Table 5.1
R_C Values for AOT Microemulsions

System	Method/Probe	R_C	Reference
AOT/Isooctane/water	ESR NMR DSC	10 6 6	31
AOT/heptane/water	Fluorescence polarization studies 3,4,9,10-perylenetetra carboxylate	10	32
AOT/decane/water	Fluorescence polarization studies 3,4,9,10-perylenetetra carboxylate	10	33
AOT/heptane/water	Fluorescence probing ANS	8	34
AOT/dodecane/water	Fluorescence probing ANS	8	34
AOT/isooctane/water	Hydrated electron studies	12-15	35
AOT/isooctane/water	Microwave conductivity	10	36
AOT/heptane/water	Proton transfer	12	37
AOT/cyclohexane/water AOT/heptane/water AOT/isooctane/water AOT/dodecane/water	Light scattering Fluorescence Near IR NMR	4.9-12 4.7-11.9 4.8-12.1 4.7-11.8	38
AOT/heptane/water	FT-IR	6.7	39
AOT/dodecane/water AOT/isooctane/water	DSC DSC	6.5 4.5	40

amphiphile via hydrogen bonding and dipole-dipole interactions (41-46). At very low water contents, the water molecules are immobilized, i.e., they are strongly bound to the EO units of the surfactant headgroups. As the water content increases above a certain critical value (R_c), free water molecules become available in the cores of the inverse micelles (16,18). Table 5.2 presents R_c values for selected microemulsions formulated with nonionic surfactants (16,18,44,45). Depending on the type of microemulsion, the R_c values vary from 1.2 to 5.8.

5.1.2 Free Water Molecules and Particle Aggregation

Recent reports in the literature dealing with the synthesis of CdS in AOT microemulsions clearly show that relatively small and monodispersed particles are made at $R < 10$ (13,27,29,30). On the other hand, relatively large and polydispersed particles are obtained at $R > 10$. As discussed in the previous section, for the AOT microemulsions, free water molecules become available in the inverse micelles at $R > 10$-12. In this connection, therefore, an important issue that needs to be addressed is the following: Is it merely an accident that the onset of extensive growth and polydispersity coincides with R_c?

Steigerwald et al. (47) reported that CdSe particles prepared at $R = 4$ in AOT/heptane/water microemulsions aggregated extensively when excess water molecules were added. The work of Wilcoxon et al. (11) also shows that the stability of gold colloids in AOT microemulsions depends on R. Gold colloids prepared at $R > 10$ were found to be unstable and exhibited aggregation; however, when the reactant species were extracted directly into the inverse micelles, without any water addition, (i.e., water-free inverse micelles), stable particles were obtained.

In the synthesis of copper particles in AOT microemulsions by reacting copper ions and hydrazine, Pileni and Lisiecki (48) reported that the particle size increased

Table 5.2
R_c Values for Nonionic Microemulsions

System	method/probe	R_c	Reference
NP-5/cyclohexane/water	Partial molar volume	2	16
NP-5/cyclohexane/water	Fluorescence probing Ru(Byp)3	1.25	18
$C_{12}EO_7$/hexanol/decane/water	Fluorescence probing Ru(Byp)3	1.4	44
Triton X-100/hexanol/cyclohexane/water	Fluorescence probing ANS	5.8	45
NP-5/cyclohexane/water	Fluorescence probing ANS	1.75	This work
Triton X-100/cyclohexane/water	Fluorescence probing ANS	4.0	This work

with the water content. This result was rationalized as follows. At low water contents, copper ions are not totally hydrated. Furthermore, the relative number of hydrated copper ions available for reaction increases with R. This implies that smaller particles should be made at high R values, since relatively more copper ions are available for nucleation. That is, as a consequence of the relatively high supersaturation ratio ($S= C/C_{eq}$, where C_{eq} and C are the solute concentrations in the equilibrium and supersaturated solutions, respectively), a greater number of nuclei would be produced at high R values and smaller particles would be expected. However, the authors reported that larger particles were formed at high R values (R = 10). It is herein proposed that the increase in particle size at R = 10 may be a result of water-induced particle aggregation.

Kitahara and coworkers (49) have shown that the average diameters and standard deviations of $CaCO_3$ particles synthesized in AOT/cyclohexane/water microemulsions differed below and above R = 10. At R < 10 the average particle sizes were in the range 48-63 nm, whereas at R > 10 (R = 10-30) the average particle diameters were large, converging to 110-120 nm. Although the authors stated that at R > 10 extensive particle aggregation and growth was caused by the formation of w/o microemulsions (R > 10), no explanation of the role of the w/o microemulsion in particle aggregation was offered.

We recently reported on the influence of R and the thiomolybdate occupancy number on the size of molybdenum sulfide particles synthesized in the nonionic microemulsion system NP-5/cyclohexane/water (16). For $[MoS_4^{2-}] = 3.2x10^{-6}$ M, the average particle size decreased with R up to R = 2, and then increased. For R < 2, the decrease in particle size was attributed to the increase in the average thiomolybdate occupancy number, and the subsequent increase in the nucleation rate. For R > 2, the increase in particle size was rationalized in terms of particle aggregation growth. It is noteworthy that, as in the case of CdS particles (13,27,29,30), the onset of the

postulated particle aggregation coincided with R_c; for the 0.15 M NP-5/cyclohexane microemulsion, R_c was found to be at R=2 (16).

From the examples given so far, it is evident that the free water molecules play an active role in the chemistry of particle formation, growth, and stabilization in inverse micelles. Therefore in this Chapter an attempt is made to link the aggregation of primary particles with the presence of free water molecules in microemulsions formulated with nonionic surfactants (Triton X-100, NP-5) and their mixtures.

5.2 EXPERIMENTAL

5.2.1 Materials

The following chemicals, obtained from Aldrich, were used as received: the nonionic surfactants polyoxyethylene(5)nonylphenyl ether (NP-5; molecular weight, 440.63); polyoxyethylene tert-octylphenyl ether (Triton X-100; molecular weight, 680); ammonium tetrathiomolybdate (99.97%) and cyclohexane (99%). The fluorescence probe 8-anilino-1-naphthalene-sulfonic acid (99%) was obtained from Kodak; before use, it was recrystallized to the magnesium salt form.

5.2.2 Microemulsion Formulation

Two types of microemulsions, designated as Microemulsion 1 and Microemulsion 2, were prepared. For Microemulsion 1, 200 mL of 0.15 M Triton X-100/cyclohexane solution was first prepared. Next, 40-80 μL of water and 20 μL of 40% ammonium hydroxide solution were added to 0.130 g of ammonium

tetrathiomolybdate. This was followed by adding roughly 10 mL of freshly prepared Triton X-100/cyclohexane solution and shaking. Ammonium tetrathiomolybdate ions were extracted into the micellar water core. The top layer, a transparent red solution, was decanted into a volumetric flask. More Triton X-100/cyclohexane solution was added to the residue and the extraction procedure was repeated. In all, for 0.130 g of ammonium tetrathiomolybdate, 20-25 batch extractions were done and 200 mL of 0.15 M Triton X-100/cyclohexane was used. To 10 mL of Microemulsion 1, the necessary amount of water was added to obtain a particular R value. For Microemulsion 2, 454 μL of 25% sulfuric acid was added to 200 mL of 0.3 M NP-5/cyclohexane solution. Water was then added to obtain different R values. Table 5.3 summarizes the water contents of the two microemulsions and the mixtures obtained after they were added together.

5.2.3 Micellar Size Measurement

The micellar size of microemulsions formulated with the nonionic surfactants (NP-5, TX-100) and their mixtures was determined using photon correlation spectroscopy (PCS). The experimental method and instrumentation employed were as reported in Chapter 3.

5.2.4 Fluorescence Spectroscopy

Fluorescence measurements were undertaken with a Shimadzu RF-5000 spectrophotometer. Samples with R values in the range 0.24-12 were prepared by the addition of water and aqueous magnesium aniline naphthalene sulfonate (ANS). The concentration of the probe (ANS) with respect to a fixed volume of microemulsion was kept constant at 8×10^{-6} M. The excitation wavelength was 360

Table 5.3
Microemulsion Parameters for the Synthesis of Molybdenum Sulfide in the NP-5/Triton X-100/Cyclohexane/Water System

	Water-to-surfactant molar ratio (R)					
Microemulsion 1	1.88	2.86	3.87	4.82	5.79	6.77
Microemulsion 2	0.42	0.90	1.38	1.87	2.35	2.83
Microemulsion 1 plus Microemulsion 2	1.15	1.88	2.63	3.34	4.07	4.80

nm. The ratio Q of the quantum yield of ANS in the microemulsion sample to that in water, $Q = Q_{sample}/Q_{water}$ was determined as in reference 34.

5.2.5 Particle Synthesis

The solubilization of reactant molecules and their subsequent reaction to form products are illustrated in Figure 5.1. To 10 mL of Microemulsion 1 (containing 2.5×10^{-3} M ammonium tetrathiomolybdate) was added 10 mL of Microemulsion 2, containing 6.8×10^{-3} M sulfuric acid (Figure 5.1a). Both microemulsions were preequilibrated at 50 °C and the reaction proceeded at this temperature. Nitrogen was bubbled both before mixing and during reaction. Due to the frequent collision, fusion, and fission of the microemulsion droplets (Figure 5.1b), the reactant species, namely H^+ and MoS_4^{2-}, can meet in an inverse micelle to form a molybdenum sulfide monomer, according to Equation 5.1:

$$MoS_4^{2-} + 2H^+ = MoS_3 + H_2S \qquad [5.1]$$

The water pools act as nanosize reactors for the precipitation reaction, with a monolayer of surfactant molecules covering the primary particles and hence hindering particle coagulation (Figure 5.1c).

Particle characterization. Molybdenum sulfide particle dispersions were extracted at different times and characterized with a Philips 420 transmission electron microscope, as reported in Chapters 2-4. At least 250 particles were analyzed for each sample to obtain an average particle diameter.

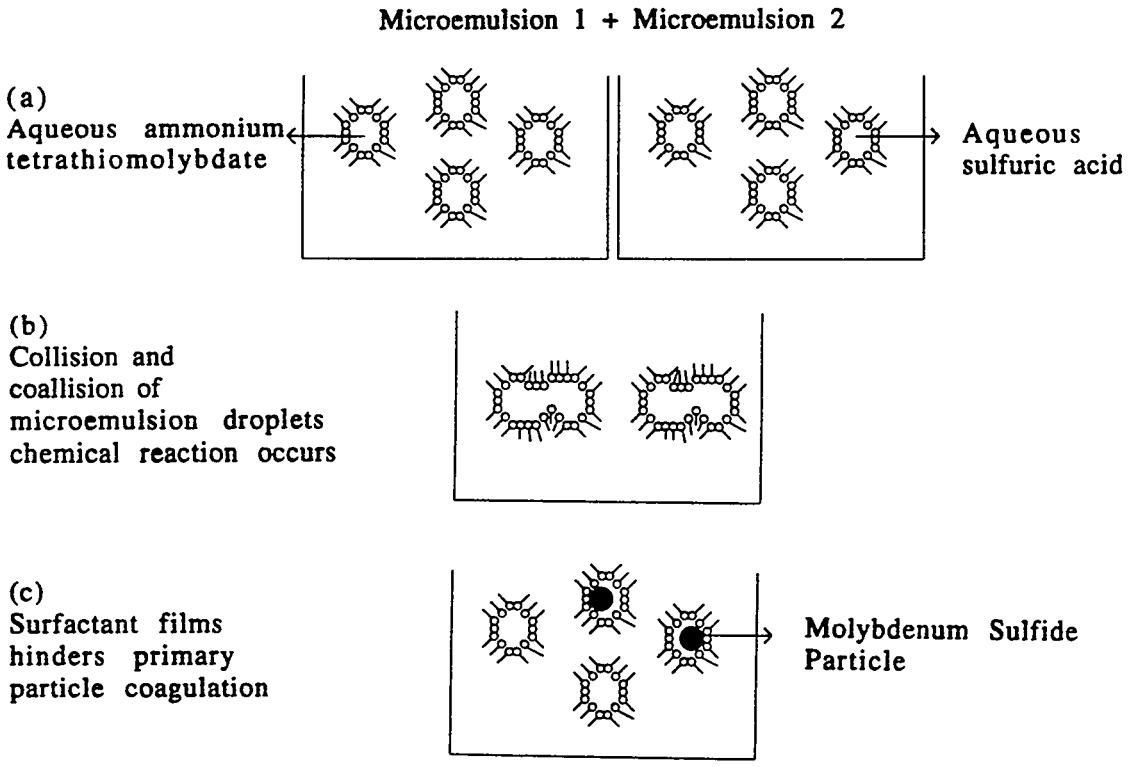

Figure 5.1
Schematic representation of molybdenum sulfide formation in the nonionic microemulsion NP-5/TX-100/cyclohexane/water.

5.3 RESULTS AND DISCUSSION

5.3.1 Micellar Size

For a particular nonionic surfactant or a combination of surfactants, the apparent hydrodynamic diameter (D_m) of the inverse micelles is a function of R, as shown in Figure 5.2. For the Triton X-100/cyclohexane/water microemulsion, the D_m versus R curve can be partitioned into three regions: (A) $0 < R < 1.5$, characterized by a linear increase of D_m with R, (B) $1.5 < R < 3.25$, characterized by a monotonic decrease of D_m with increasing R, and (C) $3.25 < R < 4.5$, characterized by an increase of D_m with R. Furthermore, for region B, when NP-5 is used as the additional surfactant and its fraction increases, there is a reduction in the decline in D_m as R increases. When the ratio NP-5/Triton X-100 is 2/1, region B disappears. Similar results have been reported by Schelly and coworkers (50) for Triton X-100/benzene/heptane/water microemulsions and by Shah and coworkers (51) for CTAB/butanol/octane/water microemulsions. Also, it can be seen in Figure 5.2 that, for the same R value, D_m decreases as the NP-5/Triton X-100 ratio increases.

5.3.2 State of Solubilized Water Molecules

It is well known that the quantum yield and fluorescence maximum of ANS depend on solvent polarity (52,53). The more polar the solvent, the lower the fluorescence quantum yield and the more red-shifted the emission maximum of the fluorescence probe. The first water molecules added to the NP-5/cyclohexane/water microemulsion interact with the oxyethylene (EO) units of the nonionic surfactant. Free water molecules become available in the core of the surfactant aggregates at $R = R_c = 1\text{-}2$ (16,18). Therefore, it is reasonable to suppose that the polarity of the

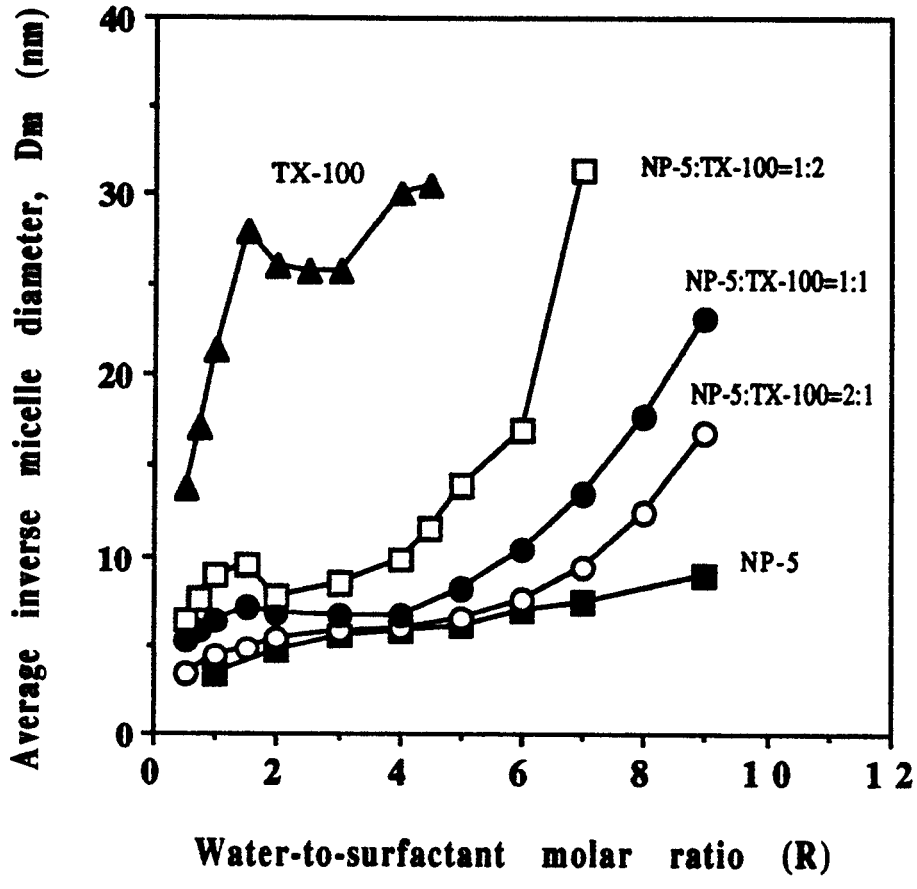

Figure 5.2
Effect of the water-to-surfactant molar ratio (R) and the polar headgroup on the average hydrodynamic diameter for the microemulsion system NP-5/TX-100/cyclohexane/water.

nonionic microemulsions increases with increasing water content. Furthermore, at $R > R_c$ a drastic increase in polarity is expected as free water molecules become available in the microemulsion fluid phase.

Consistent with the above expectation, the fluorescence quantum yield of ANS (Figures 5.3a and 5.3b) decreases with increasing R, and the emission maximum of the fluorescence peak is red-shifted as the water content of the microemulsion fluid phase is increased. Figures 5.4a and 5.4b present plots of the ratio of the quantum yield of ANS dissolved in the microemulsion to that in water (i.e., Q_{sample}/Q_{water}) versus R. For the NP-5 microemulsion, the experiment was performed for surfactant concentrations of 0.15 and 0.4 M. As shown in Figure 5.4a, the ratio is independent of the surfactant concentration. That is, for equal water-to-surfactant molar ratios, the quantum yield ratio, (Q_{sample}/Q_{water}) is the same for experiments done with either surfactant concentration. However, it depends strongly on the water-to-surfactant molar ratio. The variation of the quantum yield ratio with R is initially large and becomes smaller at R = 1.75; at R = 6, it begins to level off. This implies that at R > 1.75, the polarity of the aqueous domain of the microemulsion begins to change drastically. That is, at R = 0-1.75 the water molecules are immobilized (they are bound to the oxyethylene units); free water molecules become available in the micellar aggregates at R> 1.75. This finding is consistent with the trends reported earlier for the same solvent system using fluorescence probe studies (18) and partial molar volume measurements (16).

For the microemulsion system Triton X-100/cyclohexane/water (Figure 5.4b), the variation of the quantum yield ratio with R is as follows: it decreases with increasing R up to R = 1.25 and remains constant until R = 2. The ratio further decreases with R from R = 2, and reaches a plateau at R = 4. It is believed that the first plateau is related to a morphological change (51), and that free water molecules become available in the microemulsion at $R = R_c = 4$.

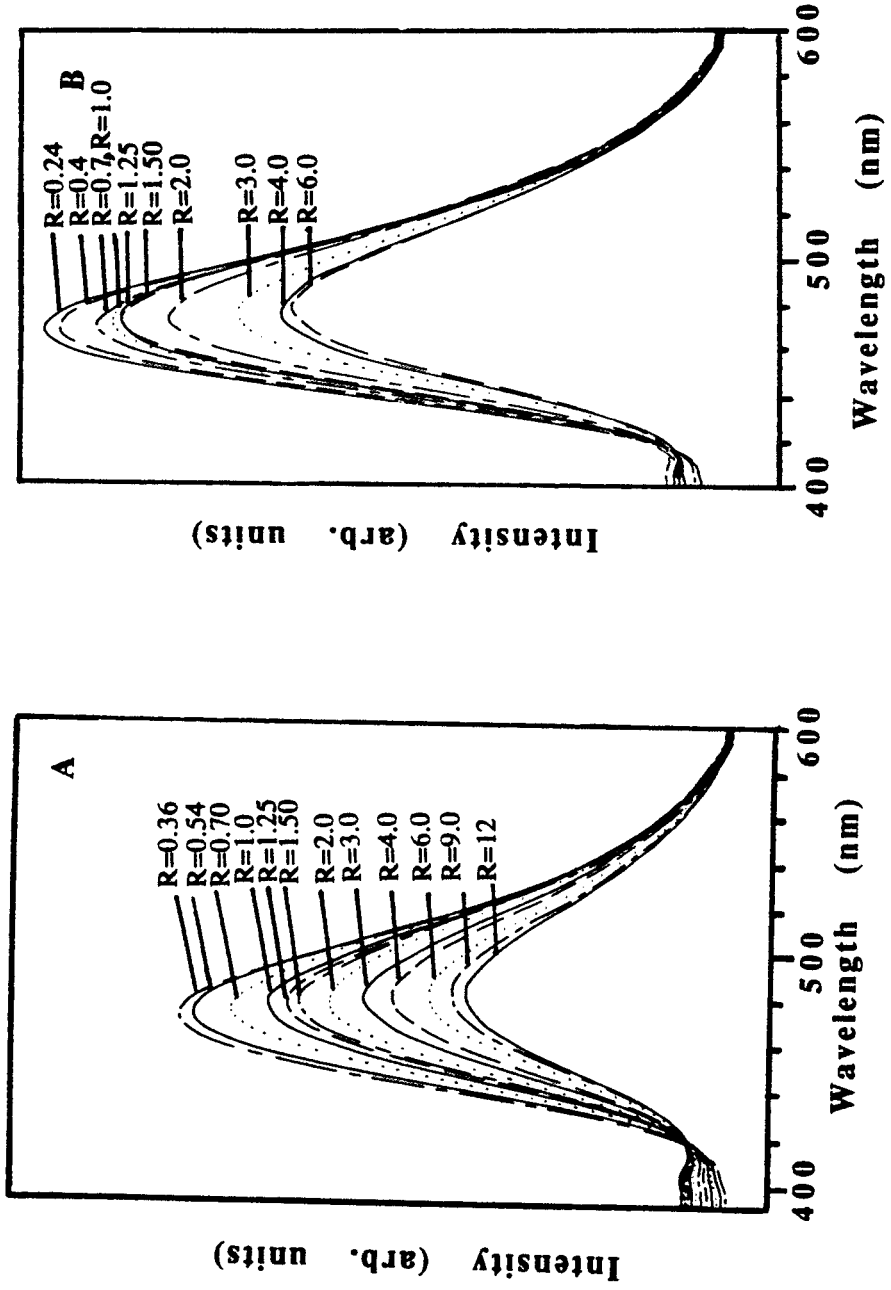

Figure 5.3

Effect of water-to-surfactant molar ratio on the fluorescence spectrum of ANS. (A) NP-5/cyclohexane/water; (B) TX-100/cyclohexane/water.

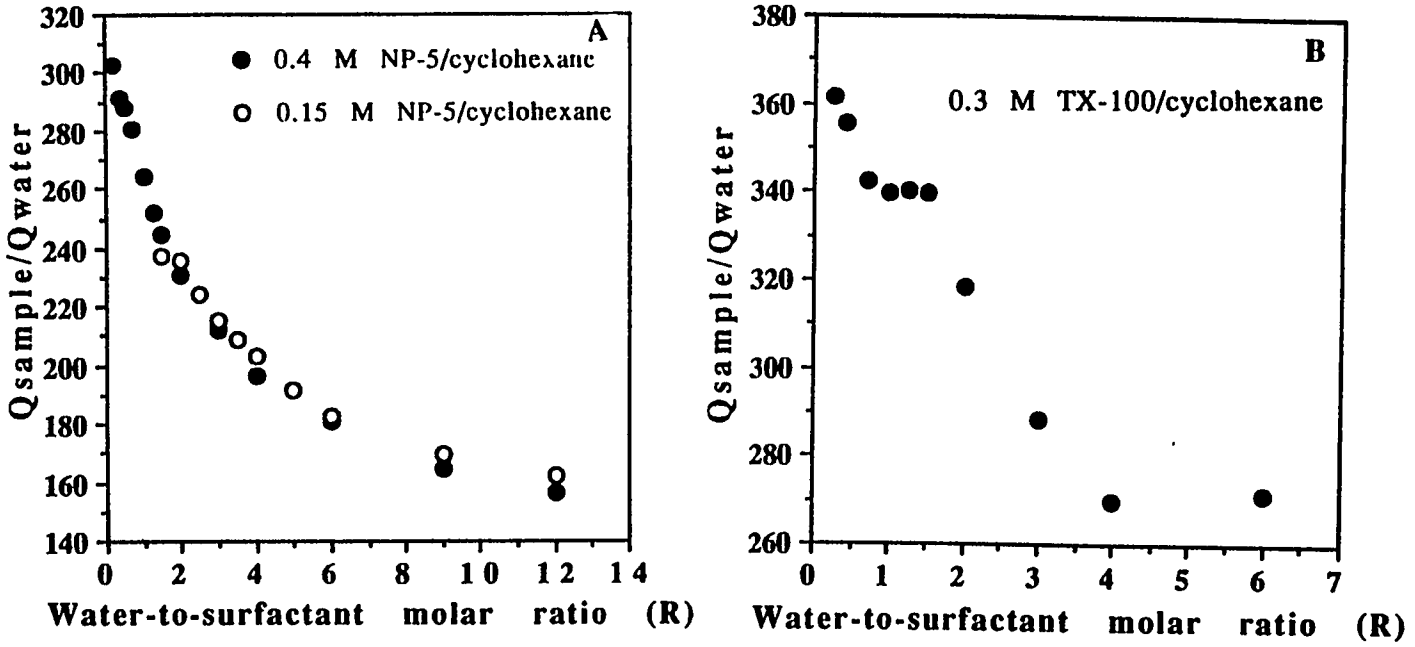

Figure 5.4

Effect of water-to-surfactant molar ratio on the ratio of quantum yield of ANS in microemulsion to that in water.

(A) NP-5/cyclohexane/water; (B) TX-100/cyclohexane/water.

The choice of R_c=4 for the Triton X-100 system is supported by the fact that for the same R value, the magnitude of the quantum yield ratio of the Triton X-100 microemulsion is higher than the corresponding value for the microemulsion formulated with NP-5. For example, at R = 1 this ratio is 340 for the Triton X-100 microemulsion while it is 260 for the NP-5 microemulsion. This suggests that at the same R value, the solvent system Triton X-100/cyclohexane/water is less polar compared to the NP-5/cyclohexane/water microemulsion. Furthermore, since Triton X-100 and NP-5 have 9.5 and 4 ethylene oxide groups per surfactant molecule, respectively, more water will be needed to hydrate the EO groups of Triton X-100. Indeed, if 1.75 water molecules are needed to hydrate 4 EO groups, then 4.16 water molecules will be needed to hydrate 9.5 EO groups. This calculation is consistent with the R_c value of 4 assigned to the Triton X-100/cyclohexane/water microemulsion system.

5.3.3 Particle Synthesis

Particle characteristics. Figures 5.5-5.8, respectively, present the TEM micrographs and the particle size distributions of the molybdenum sulfide particles sampled at the following times: 3, 40, 360 and 900 minutes; for these experiments the microemulsion was formulated with the mixture of surfactants NP-5/TX-100 = 2/1. The corresponding particle sizes are presented in Table 5.4 and plotted in Figure 5.9. The following observations can be made. (a) For a sampling time of 3 minutes, the particle size initially increases only slightly with R from R = 1.2 to R = 1.9, followed by a monotonic increase with R to R = 4.1 and then a plateau at R = 4.1-4.8. (b) For sampling times of 40-900 minutes, the particle size is independent of R (within the limits of standard deviation) for R values of 1.2-2.6. (c) For R > 2.6 the particle size increases with R. However, it should be noted that for a sampling time

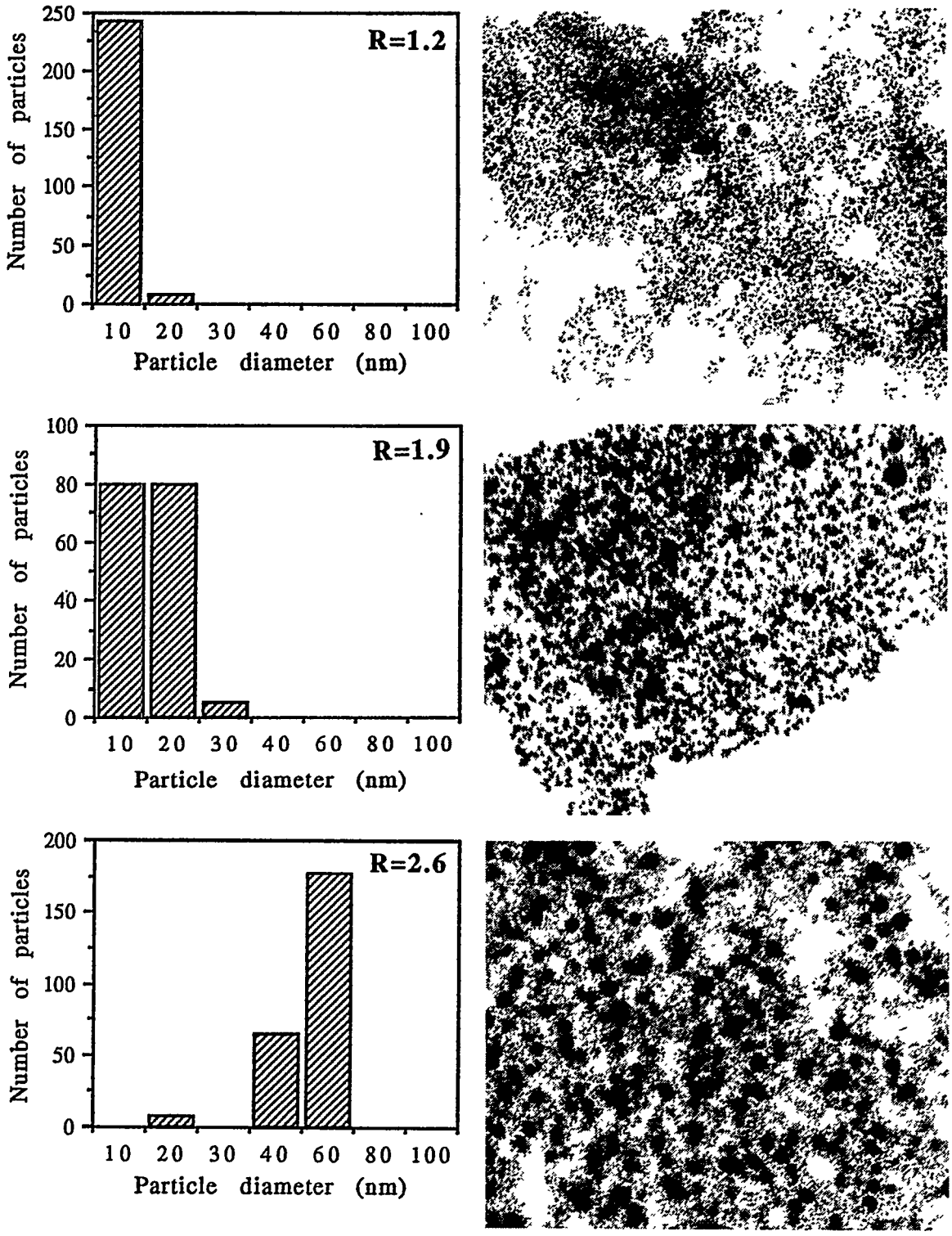

Figure 5.5
TEM micrographs and size histograms of molybdenum sulfide particles synthesized in the NP-5/TX-100/cyclohexane/water microemulsion (Sampling time, 3 minutes; NP-5/TX-100=2/1; $[MoS_4^{2-}] = 1.25 \times 10^{-3}$ M; $[H_2SO_4] = 3.42 \times 10^{-3}$ M).

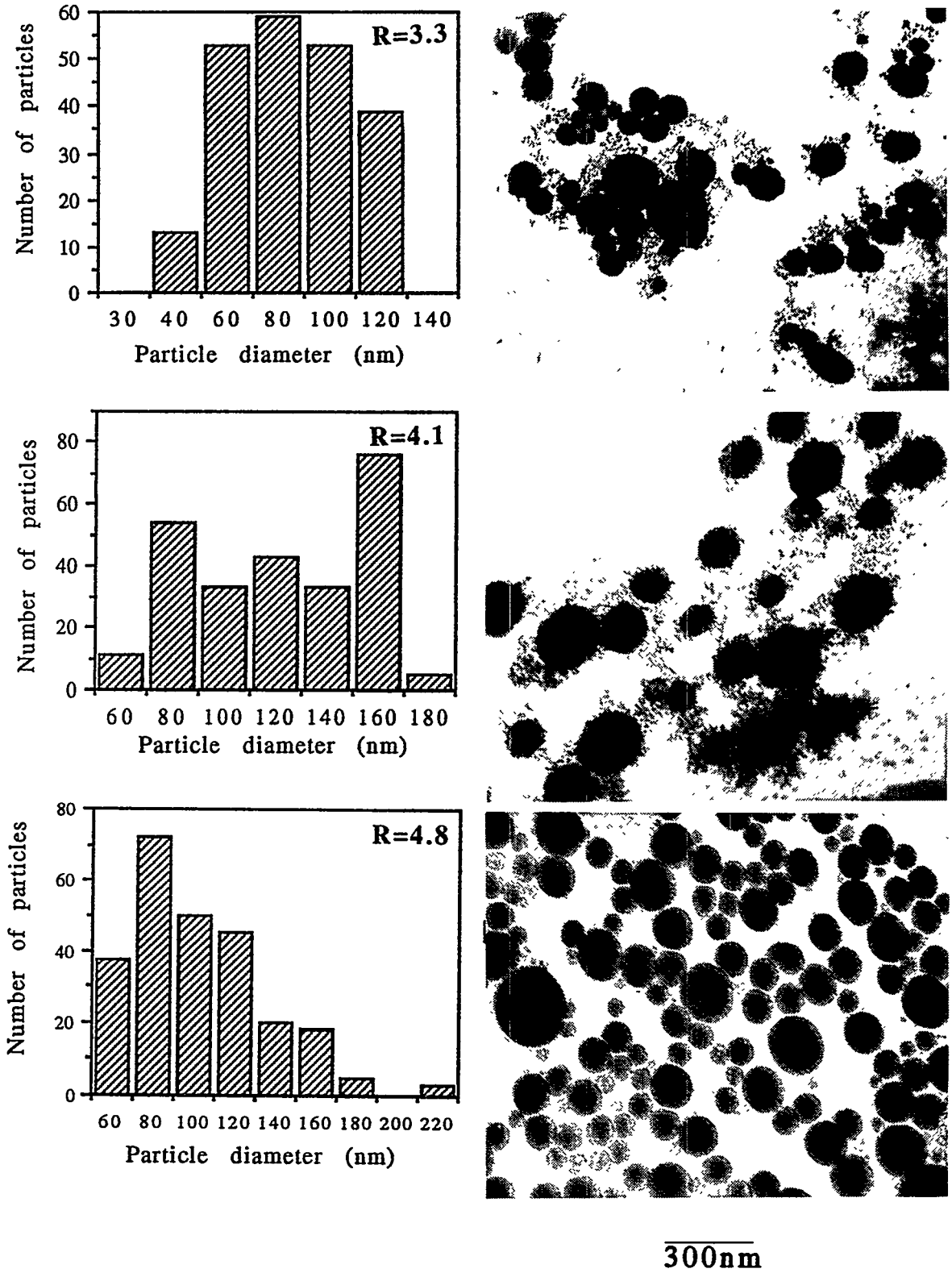

Figure 5.5
(Continued)

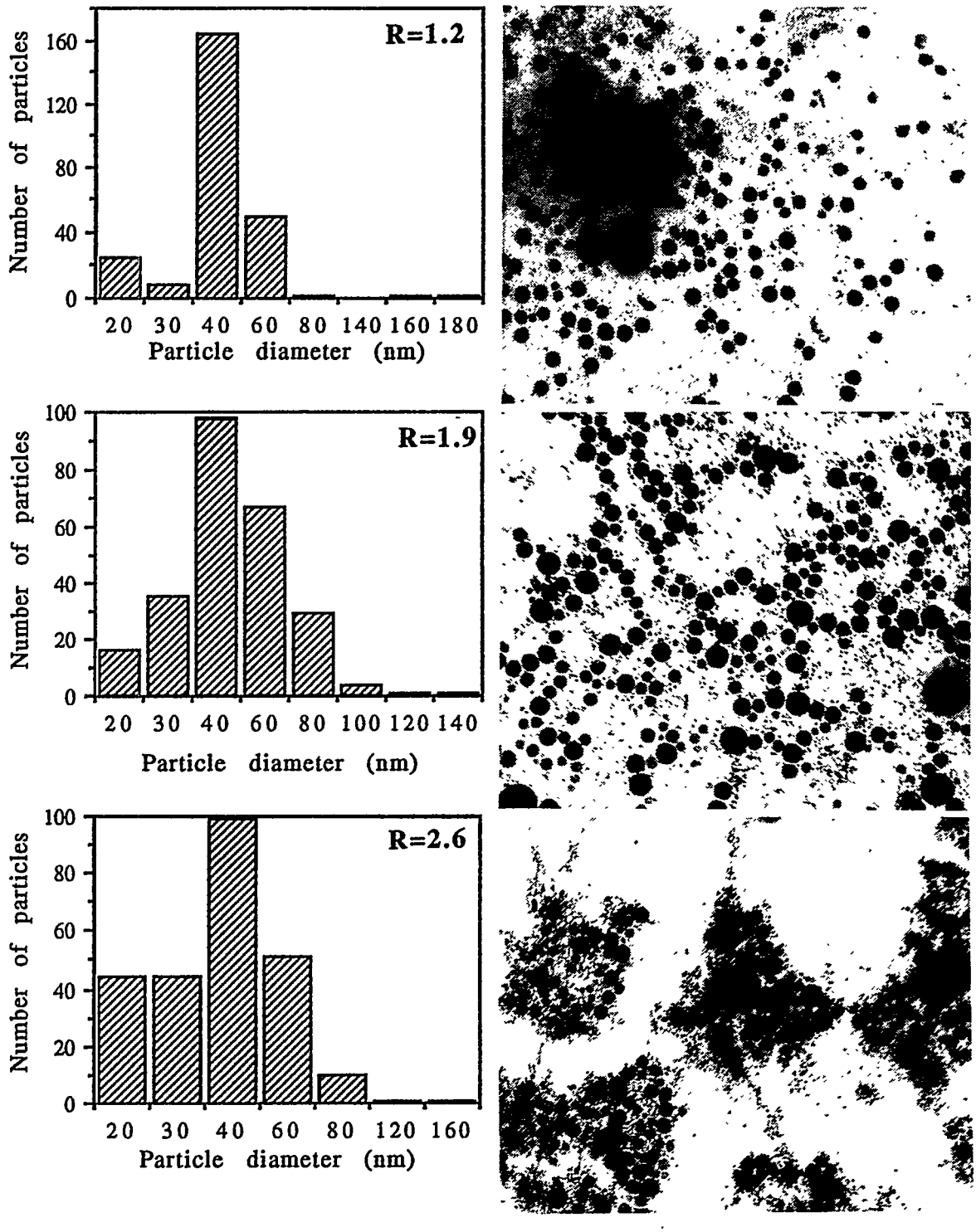

Figure 5.6
TEM micrographs and size histograms of molybdenum sulfide particles synthesized in the NP-5/TX-100/cyclohexane/water microemulsion (Sampling time, 40 minutes; NP-5/TX-100=2/1; $[MoS_4^{2-}] = 1.25 \times 10^{-3}$ M; $[H_2SO_4] = 3.42 \times 10^{-3}$ M).

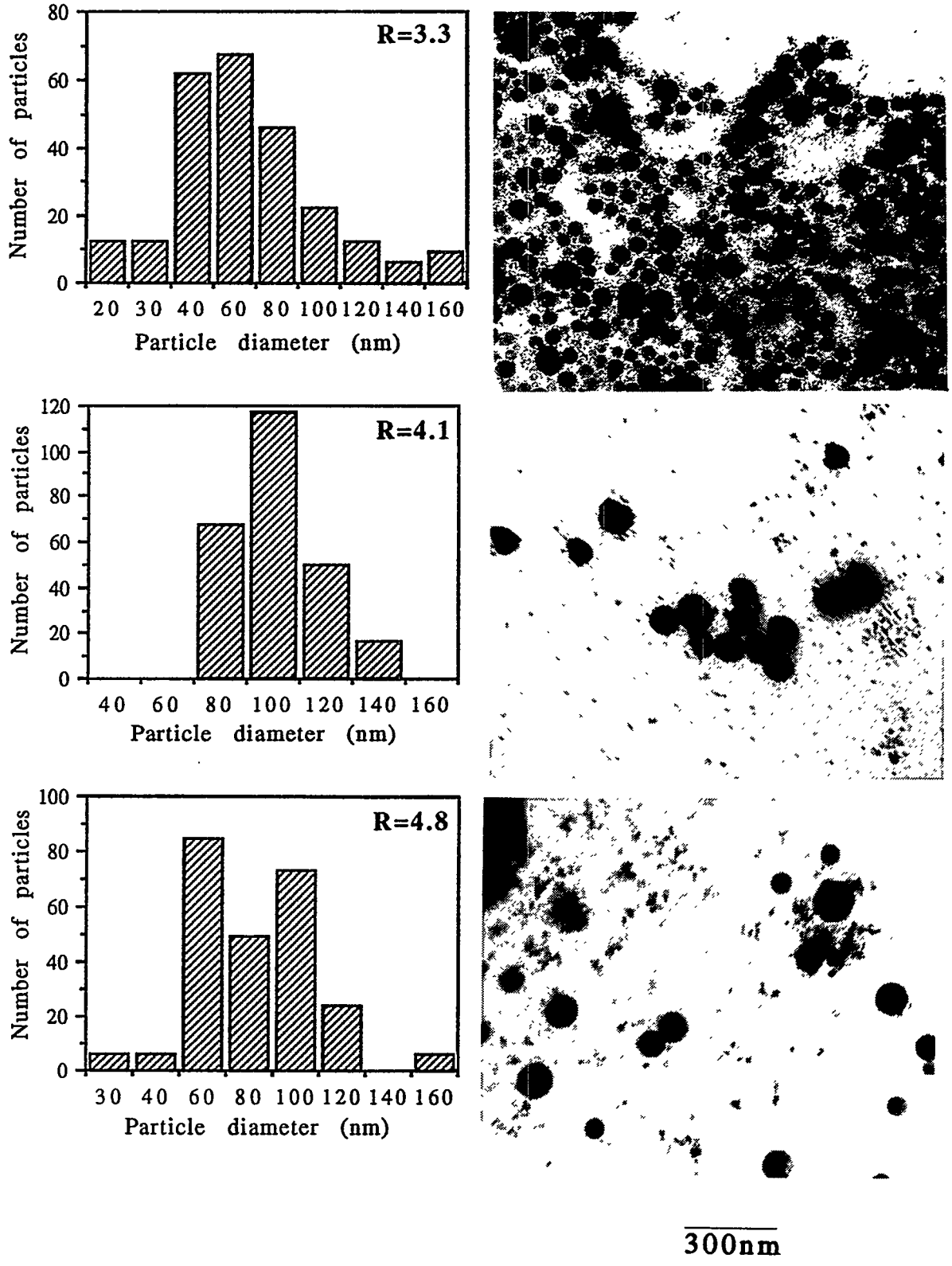

Figure 5.6
(Continued)

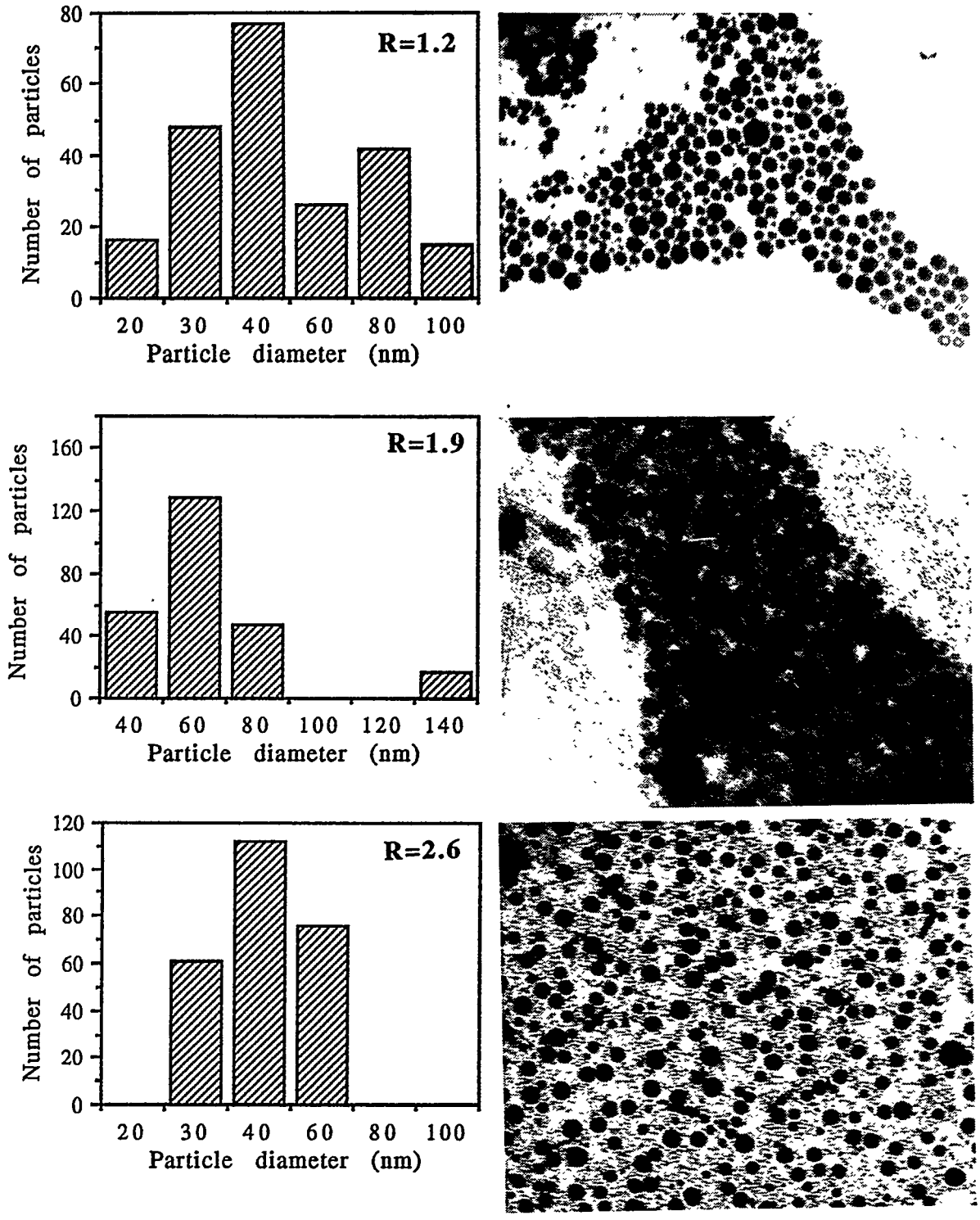

Figure 5.7
TEM micrographs and size histograms of molybdenum sulfide particles synthesized in the NP-5/TX-100/cyclohexane/water microemulsion (Sampling time, 360 minutes; NP-5/TX-100=2/1; $[MoS_4^{2-}] = 1.25 \times 10^{-3}$ M; $[H_2SO_4] = 3.42 \times 10^{-3}$ M).

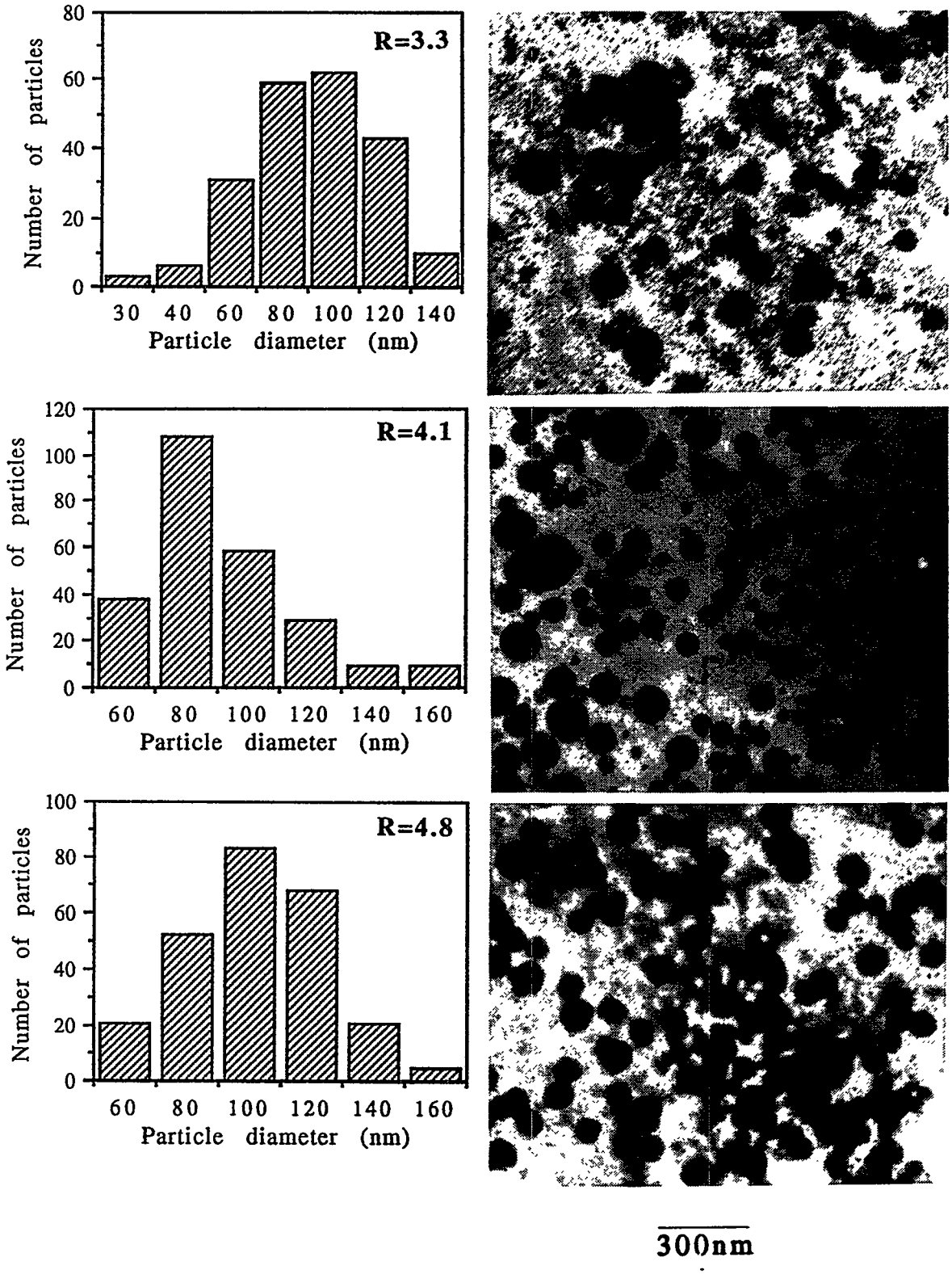

Figure 5.7
(Continued)

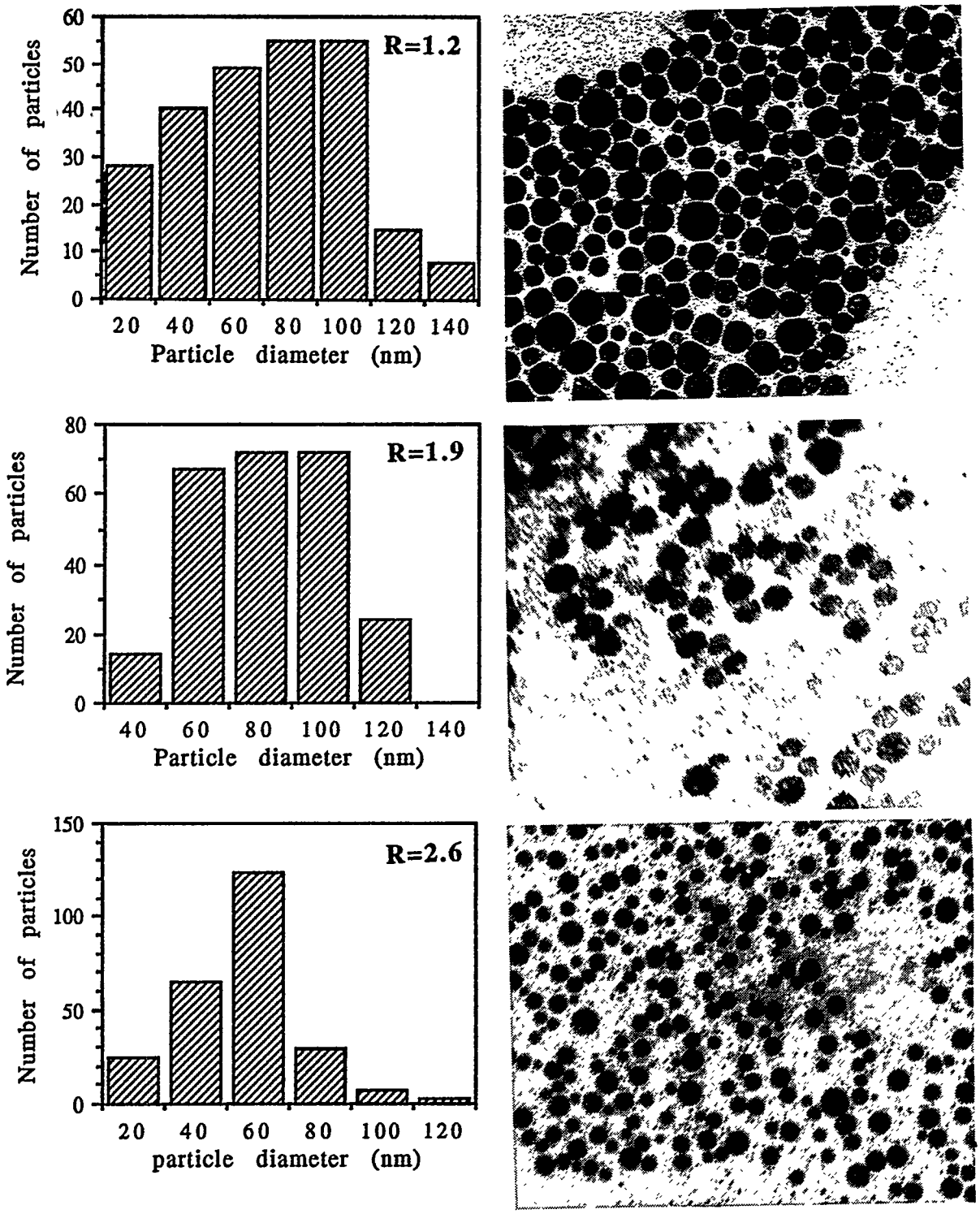

Figure 5.8
TEM micrographs and size histograms of molybdenum sulfide particles synthesized in the NP-5/TX- 100/cyclohexane/water microemulsion (Sampling time, 900 minutes; NP-5/TX-100=2/1; $[MoS_4^{2-}] = 1.25 \times 10^{-3}$ M; $[H_2SO_4] = 3.42 \times 10^{-3}$ M).

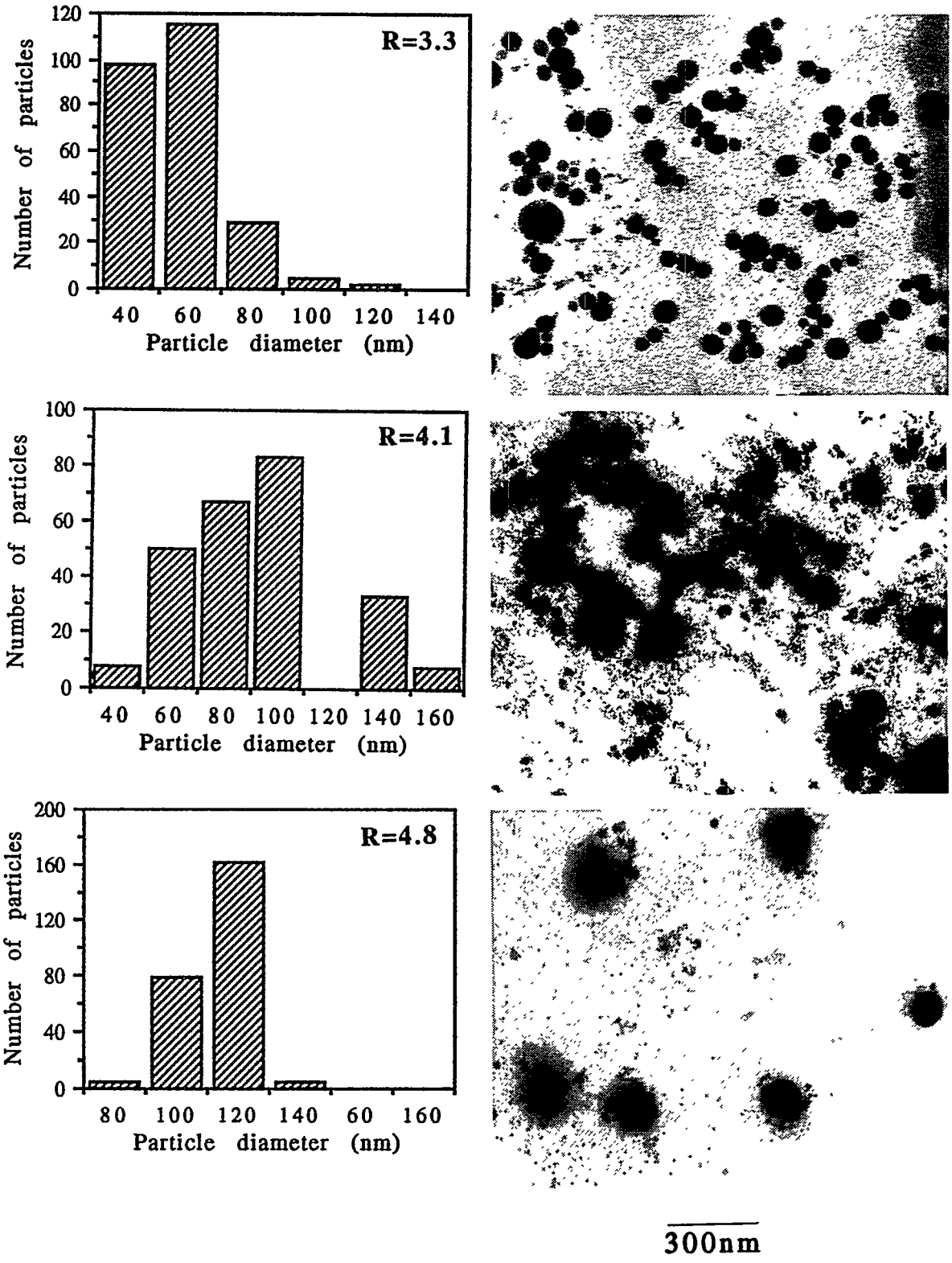

Figure 5.8
(Continued)

Table 5.4

Effect of Water-to-Surfactant Molar Ratio (R) on the Molybdenum Sulfide Particle Size at Different Sampling Times. (The microemulsion system NP-5/TX-100 (2/1)/cyclohexane/water was used as reaction medium.)

	Average particle diameter (nm)			
R	t = 3 min	t = 40 min	t = 360 min	t = 900 min
1.15	12.6	44.6	51.3	73.0
1.88	17.1	56.8	65.9	63.9
2.63	55.8	41.2	44.6	55.9
3.34	91.3	68.0	83.1	57.2
4.07	124	103	93.0	96.0
4.80	113	98.6	91.4	115

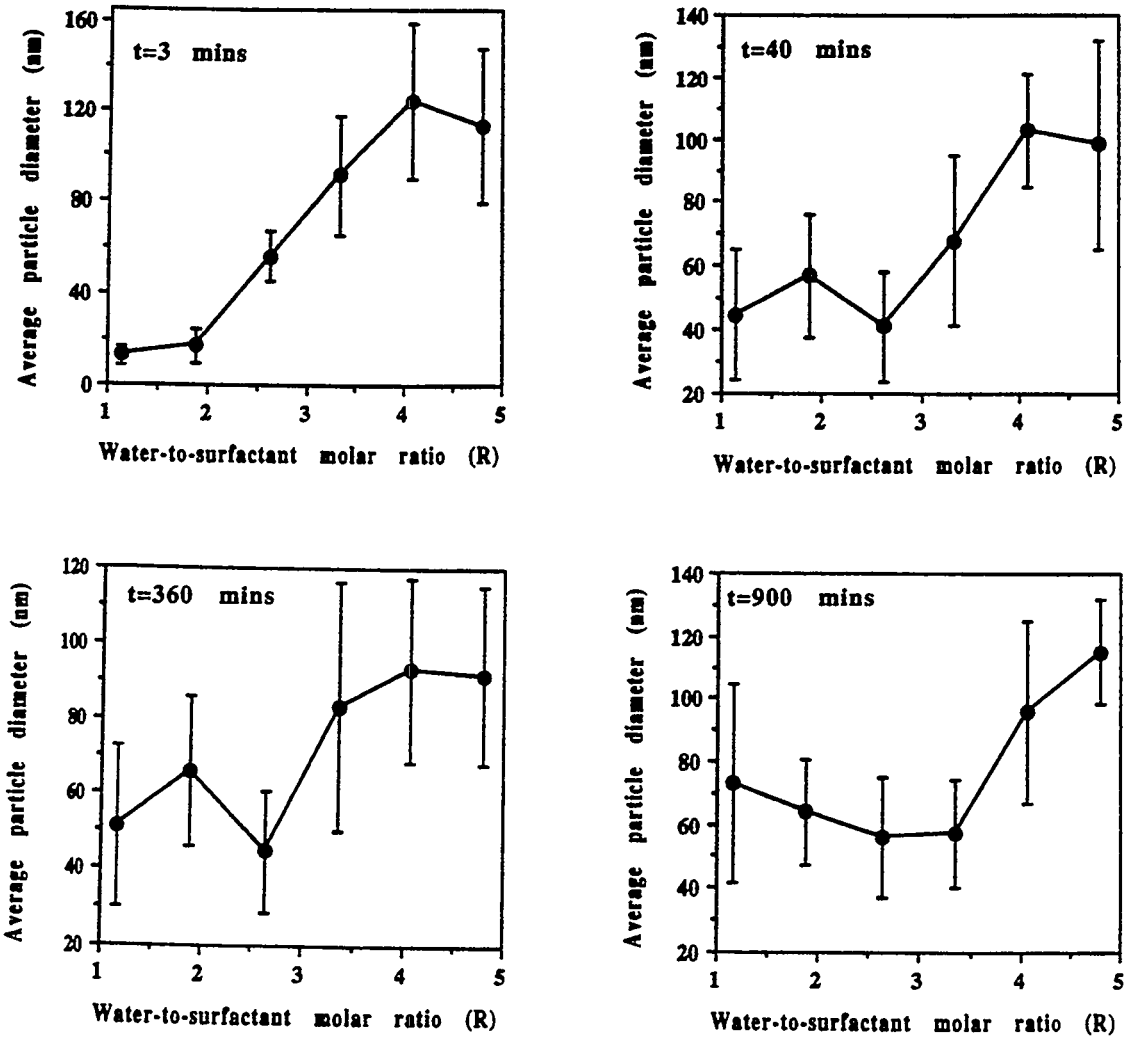

Figure 5.9

Effect of water-to-surfactant molar ratio on the average molybdenum sulfide particle size for the NP-5/TX-100/cyclohexane/water microemulsion at different sampling times ($[MoS_4^{2-}] = 1.25 \times 10^{-3}$ M, $[H_2SO_4] = 3.42 \times 10^{-3}$ M).

of 900 minutes, the average particle size decreases slightly with R to R = 2.63 and then increases sharply as R is further increased. For sampling times of 40-900 minutes, the average particle diameters are in the range of 55±11 nm, for R = 1.2-2.6 and 90±18 nm for R = 3.3-4.8.

Particle formation scheme. To further analyze the data presented in Figures 5.5-5.9 and in Table 5.4, the particle formation scheme, previously discussed in Chapter 3 (Section 3.3.3) is considered: (a) ammonium tetrathiomolybdate ions and protons react in an inverse micelle to form a molybdenum sulfide monomer; (b) a nucleus is formed if a critical number of molybdenum sulfide monomers combine in an inverse micelle (54,55); (c) due to the exchange of reactant species between the inverse micelles, a monomer may add onto a nucleus (54,55) in step (b) or two nuclei may aggregate to form a larger particle (27,56,57-59). It is believed that the above experimental data strongly suggest an important role of particle aggregation in the growth of nanosize molybdenum sulfide particles. To support this view, the relationship between the concentration of inverse micelles and molybdenum sulfide supersaturation is considered first. Subsequently, a qualitative discussion is presented of the correlation between the particle size and the R value where free water molecules become available in the inverse micelles. Finally, the statistical distribution of tetrathiomolybdate reactant in the water pools will be considered, in order to assess whether or not the resulting occupancy numbers are compatible with particle growth by monomer addition.

Average molybdate occupancy number and particle size. The occupancy number (N_{oc}) is a key parameter that controls the nucleation of particles in w/o microemulsions (13,16,18,24,55). If $N_{MoS_4^{2-}}$ is the number of tetrathiomolybdate ions in a fixed volume of microemulsion, and N_m is the number of inverse micelles, then the average molybdate occupancy number may be defined as follows:

$$N_{oc} = N_{MoS_4^{2-}}/N_m \qquad [5.2]$$

From the average micellar diameter (D_m) and the total volume (V_a) of the dispersed (aqueous plus surfactant) phase, the number of inverse micelles in a fixed volume of microemulsion may be calculated as follows:

$$N_m = V_a/(4/3)\pi(D_m/2)^3 \qquad [5.3]$$

Here it is assumed that the solubility of water in oil (cyclohexane) is negligible. The surfactant volume associated with the dispersed phase was found from the mass fractions of NP-5, Triton X-100 and their corresponding densities of 0.997 and 1.07 g cm^{-3} (60).

Figure 5.10 presents a plot of the number of micellar aggregates (N_m) and the molybdate occupancy number versus R. It can be seen that the number of inverse micelles decreases with R; this is due to the increase in the aggregation number of the surfactant molecules as the microemulsion water content is increased. In addition, Figure 5.10 shows that the thiomolybdate occupancy number increases with R. This is expected because, for a constant concentration of tetrathiomolybdate species, the ratio $N_{MoS_4^{2-}}/N_m$ should increase with R if N_m decreases with R.

As the occupancy number increases, the supersaturation ratio in the water pools concomitantly increases, and therefore the nucleation rate is expected to increase. Accordingly, as a consequence of the production of a larger number of nuclei at high occupancy numbers (55,61), smaller particle sizes are expected at high R values (13,55) if growth occurs only by monomer addition. This is because a smaller number of monomers remain after the nucleation process, to contribute to growth. However, the trends expected from the above considerations do not

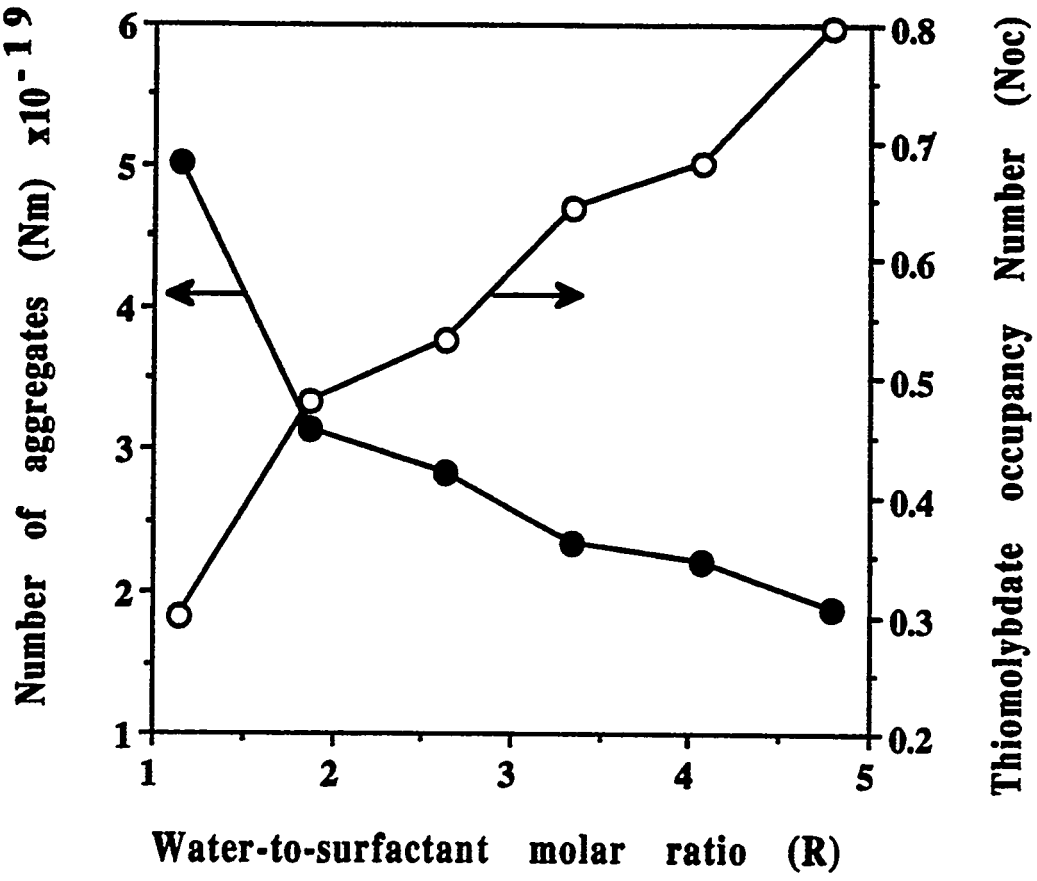

Figure 5.10

Effect of water-to-surfactant molar ratio on the number of inverse micelles and the average molybdate occupancy number ($[MoS_4^{2-}] = 1.25 \times 10^{-3}$ M).

conform to the experimental results summarized in Table 5.4 and Figure 5.9; larger particle sizes are seen to be produced at high occupancy numbers (high R), while at low molybdate occupancy (low R) smaller particles are obtained. Therefore, it appears that monomer addition is not controlling the growth of molybdenum sulfide particles. An alternative growth process via particle aggregation is considered below.

5.3.4 R_c and Particle Aggregation

The distinct boundary in particle size for R values of 1.2-2.6 and 3.3-4.8 (Table 5.4 and Figure 5.9) can be rationalized by considering the availability of free water molecules in the inverse micelles. It must be recalled at this point that the data in Table 5.4 and Figure 5.9 are based on experiments conducted with microemulsions formulated with NP-5/TX-100 = 2/1. In Section 5.3.2 it was concluded that for the NP-5 and Triton X-100 microemulsions, free water molecules become available in the inverse micelles at R values of 1.75 and 4, respectively. It is therefore reasonable to assume that, if 1.75 molecules of water interact with 4 EO groups, then 2.5 molecules of water will hydrate 6 EO groups. That is, for the microemulsion formulated with a mixture of NP-5 and Triton X-100 in the ratio of 2/1 (EO = 6), free water molecules will be available in the microemulsion fluid phase at $R > 2.5$.

Steigerwald et al. (47) have proposed a mechanism that explains flocculation of particles in w/o microemulsions. They have drawn an analogy between the surfactant-coated particle and an organometallic molecule; the particle is taken to be the central metal atom, while the surfactant molecules are the ligands. In addition, the surfactant coating is regarded as a semipermeable membrane that allows the ions (such as MoS_4^{2-} in our case) access to the particle surface, but prevents the particles from aggregating. As discussed above for the 2/1 NP-5/Triton X-100

microemulsion system, free water molecules are available in the microemulsion fluid phase at R > 2.5. Under these conditions the free or unbound water molecules may strip some of the surfactant molecules from the particle surface (47,56). That is, there is a competition between the solid particles and water droplets for the surfactant molecules, as illustrated in Figure 5.11. The removal of surfactant molecules opens empty coordination sites (48,55), and this enhances particle aggregation. Since free water molecules are present at R > 2.5, the above mechanism of water-induced aggregation is expected to become important at R > 2.5. If the aggregation process is promoted by the free water molecules, then it should be expected that the extent of aggregation will increase dramatically at $R = R_c$, where free water molecules first become available in the inverse micelles. This explains why for R > 2.6 the general trend in Figure 5.9 is an increase in particle size with R.

To test the above hypothesis of water-induced aggregation, molybdenum sulfide particles were synthesized in the Triton X-100/cyclohexane/water microemulsion using the same synthesis parameters and protocol as exploited for the microemulsion formulated with the mixture of surfactants, NP-5 and Triton X-100. The molybdenum sulfide particles were sampled after 40 minutes. Presented in Figure 5.12 are the corresponding TEM micrographs. Figures 5.13a and 5.13b, respectively, present plots of average particle size versus R for the 2/1 NP-5/TX-100 and TX-100 microemulsions. Comparing Figures 5.13a and 5.13b, it can be seen that, for the particles synthesized in the NP-5/TX-100/cyclohexane/water microemulsion, the particle size is independent of R for R = 1.2-2.6, but it increases with R above R = 2.6. In contrast, for particles made in the TX-100/cyclohexane/water microemulsion, the average particle size is essentially independent of R; for the range investigated (R = 1.2-4.8), the average particle diameter is 54±17 nm.

Among the key differences in properties of the two microemulsions are: (a) the sizes of the inverse micelles, and (b) the R_c values. It is of interest to examine

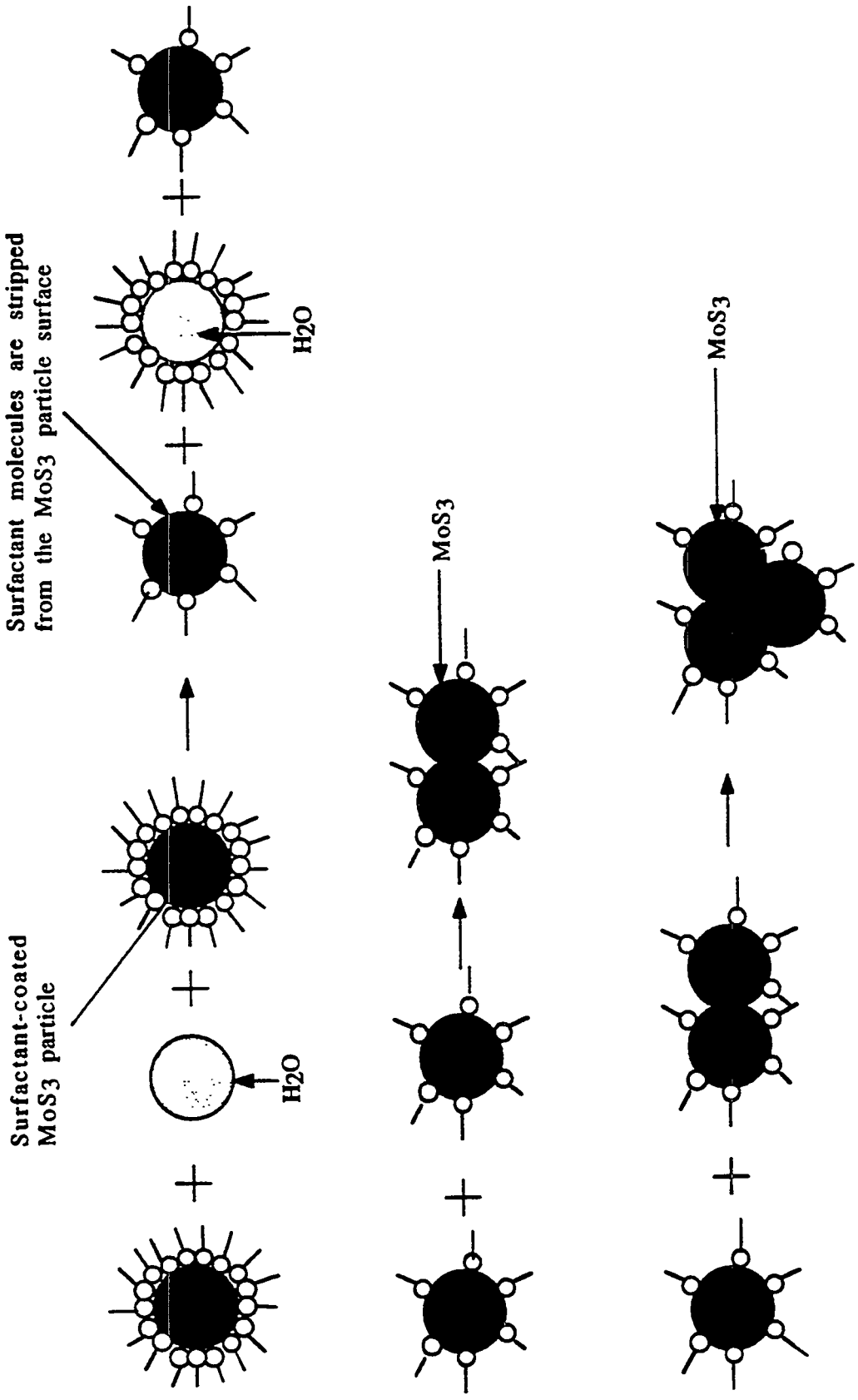

Figure 5.11
Schematic representation of water-induced aggregation of molybdenum sulfide particles in nonionic microemulsions.

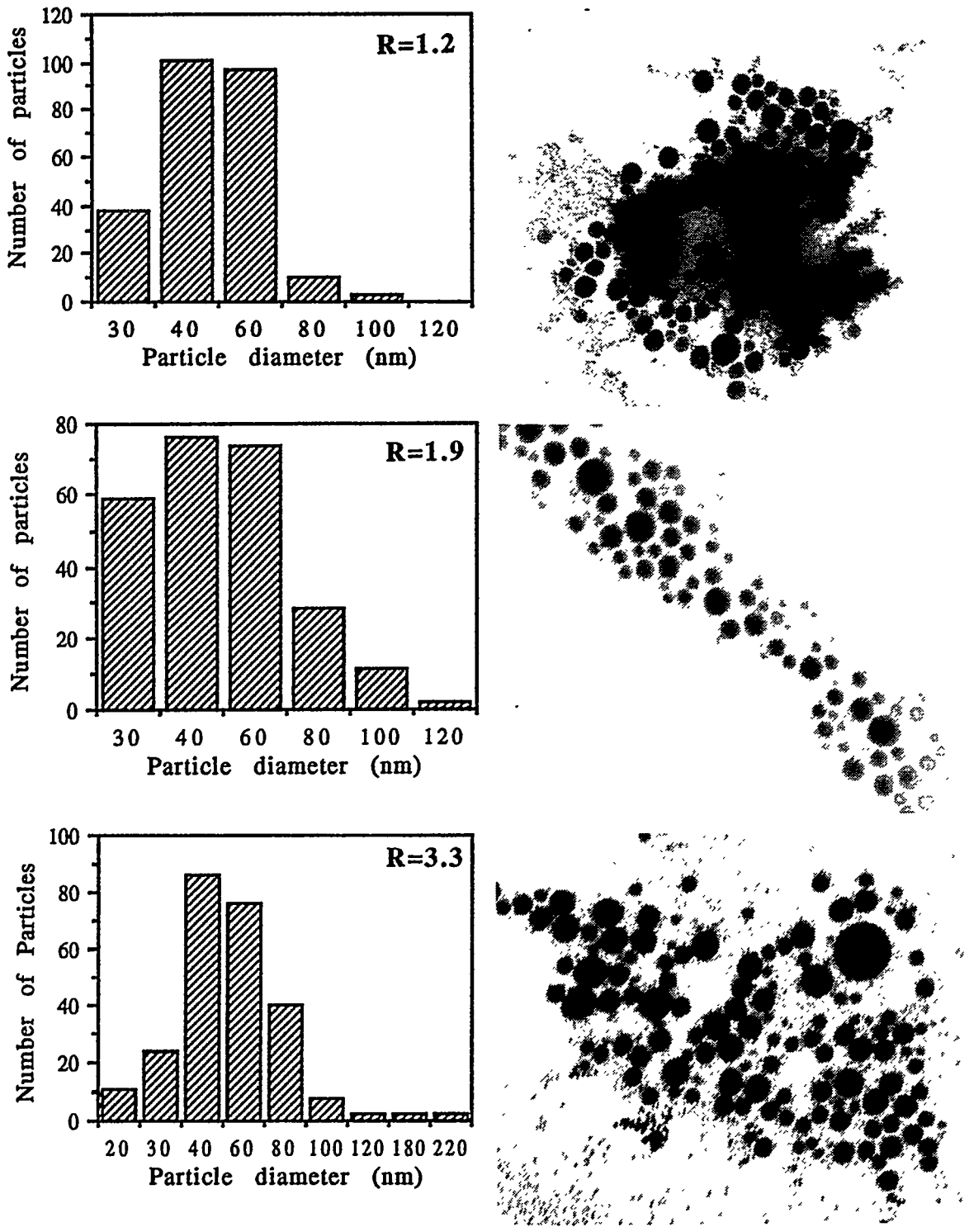

Figure 5.12
TEM micrographs and size histograms of molybdenum sulfide particles synthesized in the TX-100/cyclohexane/water microemulsion
(sampling time, 40 minutes; $[MoS_4^{2-}] = 1.25 \times 10^{-3}$ M; $[H_2SO_4] = 3.42 \times 10^{-3}$ M).

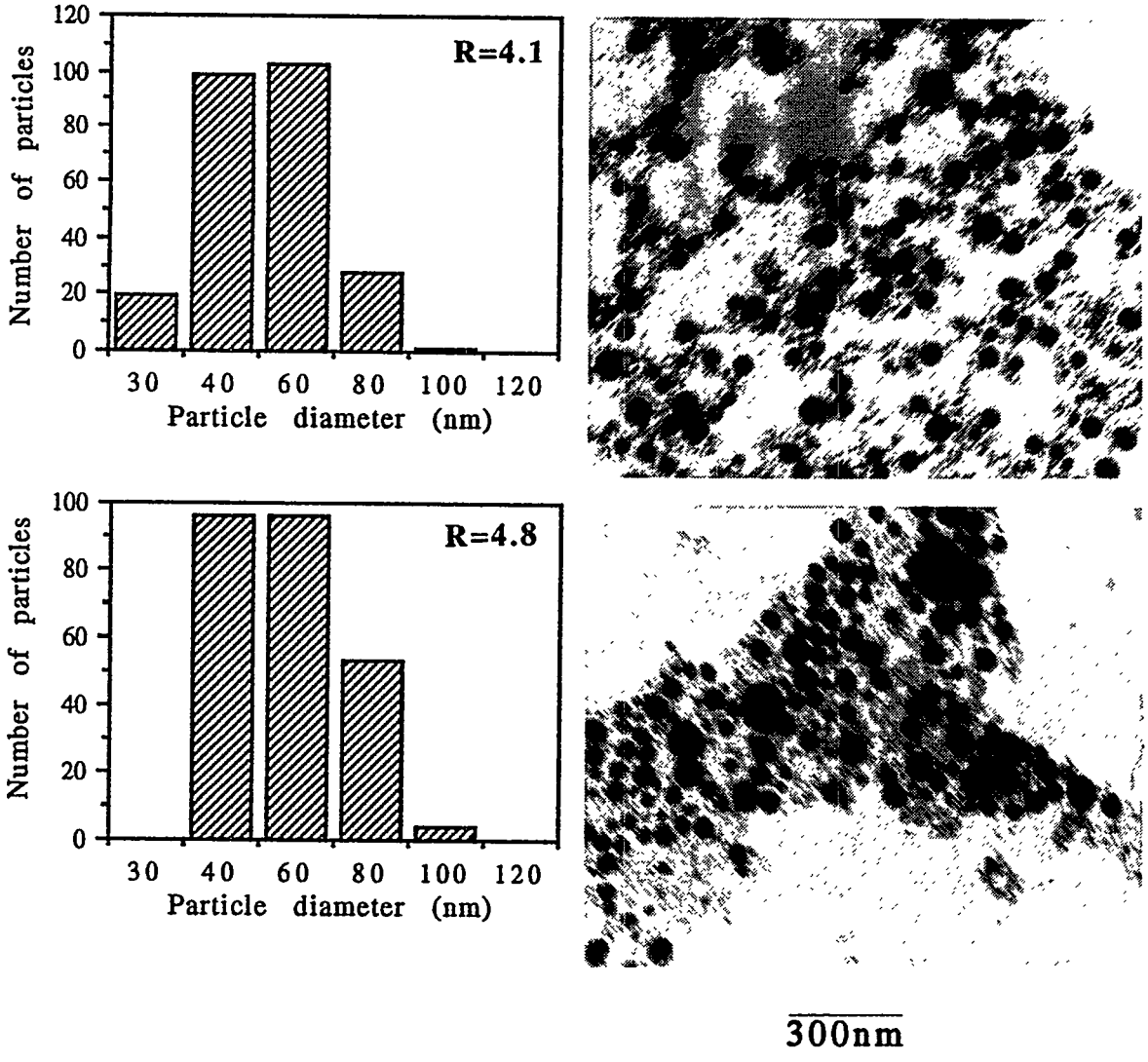

Figure 5.12
(Continued)

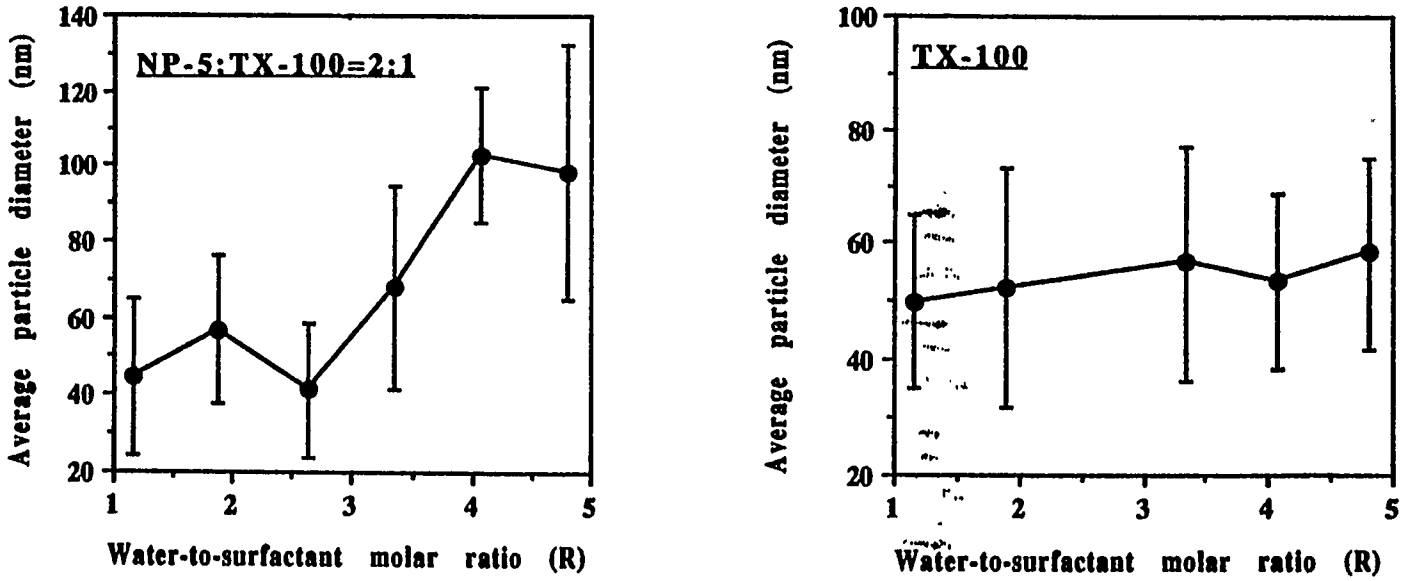

Figure 5.13
Effect of water-to-surfactant molar ratio (R) on the average molybdenum sulfide particle size (sampling time, 40 minutes; $[MoS_4^{2-}] = 1.25 \times 10^{-3}$ M; $[H_2SO_4] = 3.42 \times 10^{-3}$ M):
(a) NP-5/TX-100/cyclohexane/water; (b) TX-100/cyclohexane/water.

whether these property differences can account for the particle size versus R trends noted above. As shown in Figure 5.2, for the same R value, the inverse micelles are larger for the Triton X-100 microemulsion. For a given R value, the TX-100 microemulsion will thus contain a lower concentration of inverse micelles compared with the NP-5/TX-100 system. Consequently, one may argue that, for a constant concentration of ammonium tetrathiomolybdate ions, the occupancy number will be lower for the microemulsion system NP-5/TX-100/cyclohexane/water compared to the TX-100/cyclohexane/water system. However, although for the Triton X-100 microemulsion the occupancy number is expected to increase with R, the particle size is essentially independent of R (Figure 5.13). As discussed in Chapters 2 and 3, as R increases, the occupancy number increases. Consequently, the nucleation rate increases. Hence, as a result of the expected high nucleation rate at high R values, smaller and larger particles should be made at high and low R values, respectively. This trend is not observed in Figure 5.13b. This implies that for the same R value, although the occupancy number of the TX-100 microemulsion is smaller than that of the NP-5/TX-100 microemulsion (NP-5/TX-100=1/2), the occupancy number does not control the particle size. In addition, for R = 3.3-4.8, the molybdenum sulfide particles produced in the TX-100 microemulsion have smaller diameters compared to those of the NP-5/TX-100 microemulsion (NP-5/TX-100=2/1). This trend is the opposite of that expected, given the higher occupancy number of the TX-100 microemulsion.

In view of the apparent lack of a correlation between occupancy number and particle size, it is proposed here that the noted differences in R_c values can help explain the different trends in particle size versus R for the two microemulsion systems. As discussed earlier, the R_c values for the microemulsions formulated with Triton X-100 and 2/1 NP-5/Triton X-100 are 4 and 2.5, respectively. Thus, for the NP-5/TX-100 microemulsion system, the water-induced particle aggregation

should begin at R > 2.5, whereas in the case of the TX-100 microemulsion particle aggregation is expected to become significant at R > 4. Referring to Figure 5.9, it is seen that, indeed, for the NP-5/TX-100 microemulsion it is at R~2.5 that the increase in particle size (attributed to water-induced aggregation) is observed. For the molybdenum sulfide particles synthesized in the TX-100 microemulsion, R values in the range R = 1.2-4.8 were utilized. As a reminder, for the TX-100 microemulsion $R_c = 4$. Thus, the fact that for R > 2.5 the particle size is virtually unchanged from the value observed at R < 2.5 suggests that water-induced particle aggregation may not be taking place, because there are no free water molecules in the microemulsion.

Previous work in this laboratory on silica (24) and molybdenum sulfide particles (16) supports these proposals. Summarized in Figure 5.14 is a plot of the average particle diameter of silica and molybdenum sulfide synthesized in the NP-5/cyclohexane/water microemulsion (which has an R_c value of 1.75). For both particulate materials, the particle size is seen to decrease with R to R = 1.75-2 and then to increase. As R is increased, the initial decrease in particle size is due to an increase in the precursor reactant occupancy numbers (16,24). At R > 2, although the occupancy numbers are large, the particle size increases with R, which is contradictory to the monomer addition mechanism of growth (16,17). It is thus herein suggested that the increase in particle size at R > 1.75 is related to water-induced aggregation.

Further supportive evidence for water-induced particle aggregation in microemulsions is provided by the work of Steigerwald et al. (47). They found that CdSe particles prepared in AOT/heptane/water microemulsions at R = 4 aggregated extensively when excess water molecules were added. In addition, the flocculated particles could not be redispersed in organic solvents. However, evaporation of the surfactant-stabilized colloids prepared at R = 4 to dryness allowed subsequent

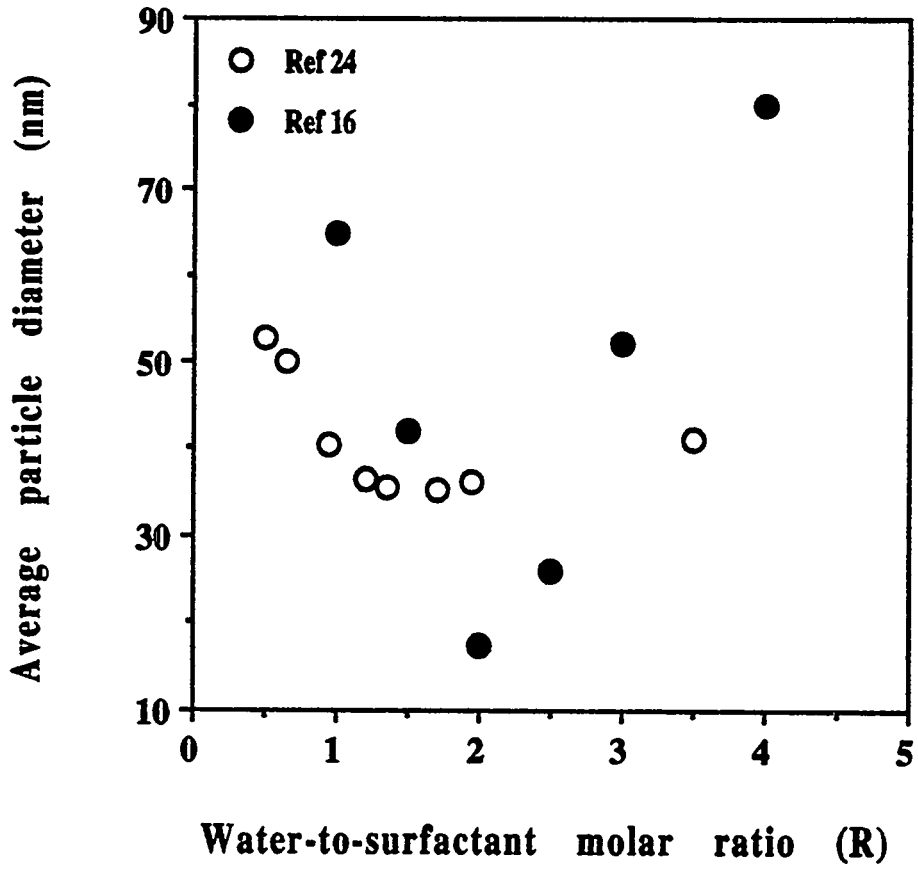

Figure 5.14
Effect of water-to-surfactant molar ratio on the average size of silica and molybdenum sulfide particles synthesized in the NP-5/cyclohexane/water microemulsion (from Refs. 16 and 24).

dispersion of the particles in an organic medium. Furthermore, after drying and dispersing in organic solvents, the resulting colloids were stable for 8-10 months.

This proposal of water induced-particle aggregation is also supported by the early work of Damerell and coworkers (62,63) and by Kitahara and coworkers (64-66). The former group found that the degree of dispersion of di(2-ethylhexyl) sodium sulfosuccinate (AOT)-stabilized silica and carbon black particles in xylene depended on the water content. The rate of coagulation of the solid particles was reported to increase with increasing water content.

In addition, the work of Kitahara and coworkers (64-66) showed that the rate of flocculation of carbon black particles in the microemulsion systems NP-8/cyclohexane/water and AOT/cyclohexane/water increased with increasing water content. For the AOT microemulsion, the increase in flocculation rate with the water content was attributed to a decrease in the zeta potential (64,65), which resulted from the diffusion of the sodium counter ions of AOT to the carbon particle surface and thereby neutralizing the surface charge. However, no explanation was given for the decrease in dispersibility of the carbon black particles in the NP-8/cyclohexane/water microemulsion as the water content was increased, although the zeta potential of carbon black in the nonionic microemulsion (NP-4/cyclohexane/water) was reported to be independent of the water content (66). It is herein suggested that, at high water contents, the stripping of surfactant molecules from the particle surface removes the barrier that prevents aggregation (Figure 5.11).

5.3.5 Reactant Distribution and Particle Formation

To gain further insight into the particle growth process in the microemulsion fluid phase, the effect of R on the number of inverse micelles and the distribution of ammonium tetrathiomolybdate in the micellar aggregates are considered next. The

distribution of ions in w/o microemulsions follows the Poisson statistical distribution law (24,67,68). Invoking this law, the probability to have k thiomolybdate ions per inverse micelle can be expressed as follows:

$$P_k = N_{oc}^k(e^{-Noc}/k!) \qquad [5.4]$$

If the minimum number of thiomolybdate ions needed to form a nucleus is i_c, then the number of molybdenum sulfide nuclei (N_n) produced in the w/o microemulsion is equal to the number of micellar aggregates that contain i_c or more thiomolybdate ions, i.e.,.

$$N_n = N_m \sum_{k=i_c}^{\infty} P_k \qquad [5.5]$$

Figure 5.15 presents a plot of the expected number of nuclei, N_n (Equation 5.5) versus R for different i_c values. Two distinct trends are seen: (a) for any i_c value, the number of expected nuclei in the microemulsion increases as R is increased; (b) as i_c increases, the number of nuclei decreases. Concerning particle growth, an inference that can be made about observation (a) is that, as the number of nuclei increases, relatively few monomers unutilized in nuclei or primary particle formation will remain. Fewer ions or monomers will thus add onto nucleated primary particles at high R values. This implies that smaller and larger particles will be produced at high and low R values, respectively. However, this trend is not observed experimentally (Table 5.4 and Figure 5.9).

As shown in column 1 of Table 5.4, the particle size increases with R. Furthermore, for all sampling times, particles in the range 49 ± 18 nm are obtained at low R values (R = 1.2-2.6). At high R values (3.3-4.8) the particle size is large,

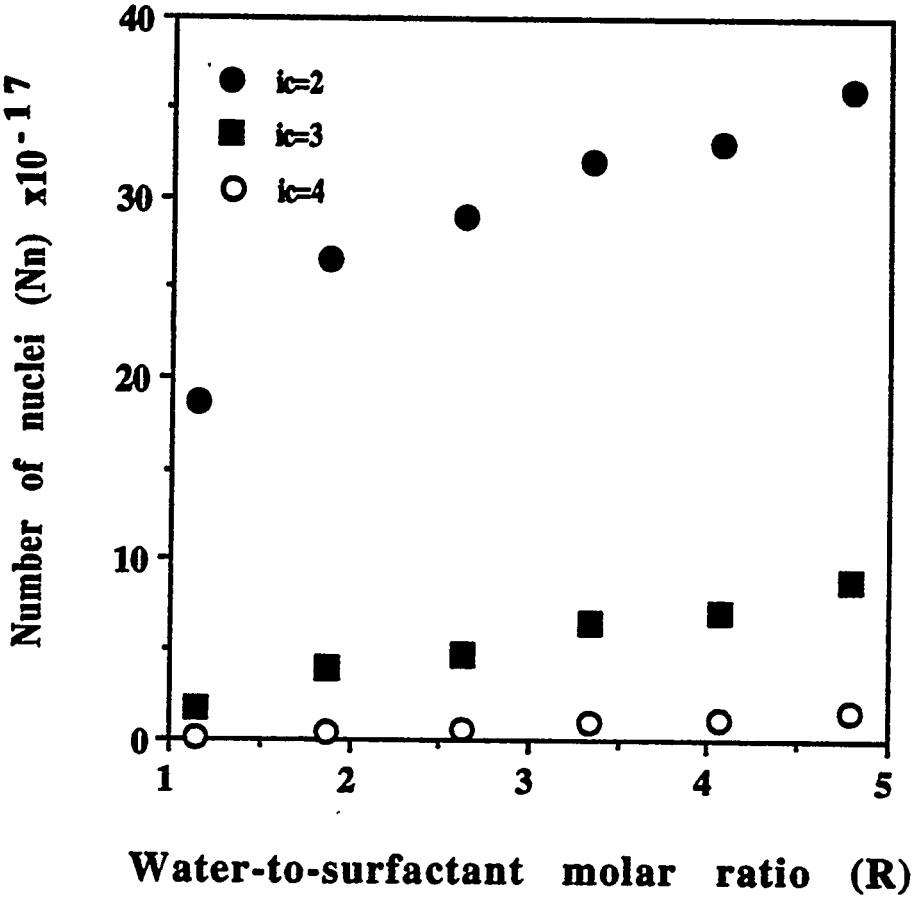

Figure 5.15
Effect of water-to-surfactant molar ratio on the number of nuclei formed in the NP-5/TX-100/cyclohexane/water microemulsion ($[MoS_4^{2-}] = 1.25x10^{-3}$ M).

in the range of 94±18 nm. The apparent discrepancy between these expected and experimental particle size versus R trends can be resolved by admitting the possibility of extensive particle aggregation at high R values, as discussed next.

Aggregative growth. The number of particles in the microemulsion fluid phase is obtained as in Equation 5.6:

$$N_p = M_{MoS_3(t)}/M_p \qquad [5.6]$$

where $M_{MoS_3(t)}$ is the total mass of MoS_3 in the microemulsion, and M_p is the mass of one MoS_3 particle given by:

$$M_p = (4/3)\pi\rho(D_p/2)^3 \qquad [5.7]$$

In Equation 5.7, ρ (3.2 g cm^{-3}) is the density of molybdenum trisulfide (69), and D_p is the average diameter of a single molybdenum sulfide particle (t=3 minutes).

If the nuclei initially produced in the microemulsion grow only by monomer addition, then the number of particles produced in the microemulsion (Equation 5.6) should be equal to the number of expected nuclei, (Equation 5.5). That is,

$$N_n = N_m \sum_{k=i_c}^{\infty} P_k = M_{MoS_3(t)}/M_p \qquad [5.8]$$

Combination of Equations 5.5, 5.7 and 5.8, followed by rearrangement, gives Equation 5.9, which is the theoretical or expected particle size (D_{theor}):

$$D_{theor} = 2[M_{MoS_3(t)}/N_n(4/3)\pi\rho]^{1/3} \qquad [5.9]$$

As can be seen from Equation 5.1, the number of moles of ammonium tetrathiomolybdate is equivalent to the number of moles of molybdenum trisulfide. Thus, the total weight $M_{MoS_3(t)}$ was calculated by multiplying the moles of ammonium tetrathiomolybdate by the molecular weight of molybdenum trisulfide. The calculation of the number of nuclei (Equation 5.5) was based on the assumption that a minimum of 2 ammonium tetrathiomolybdate ions is needed to form a nucleus (i.e., $i_c=2$).

Figure 5.16 presents a plot of the observed particle diameter (D_{obs}, obtained from TEM measurements) as a function of R. Also shown in Figure 5.16 is a plot of R dependence of the expected particle diameter calculated from Equation 5.9 (D_{theor}). The observed particle size increases with R. In contrast, the theoretical particle size (Equation 5.9) decreases with R. As a reminder, the derivation of Equation 5.9 is based on the monomer addition concept of growth. Therefore, the opposing trends obtained for the observed and theoretical particle sizes suggest that the mechanism of growth is not by monomer addition and that growth occurs by particle aggregation.

Further evidence in support of aggregative growth is provided in the TEM micrographs presented in Figures 5.5-5.8. It can be seen that the small particles, with an average diameter of 6 nm, aggregate around larger particles (50-120 nm). Also, the particle sizes are relatively large compared with the sizes of the corresponding inverse micelles (3-30 nm; Figure 5.2). This suggests that initially many nuclei were produced and that the primary particles aggregated when the microemulsion droplets fused together. Furthermore, it can be seen in the micrographs that the particle surfaces are not smooth, which is consistent with aggregative growth.

It must be noted, however, that conclusions based solely on the roughness of the particle surfaces and the porosity of particles may be ambiguous in distinguishing between monomer addition and particle aggregation growth

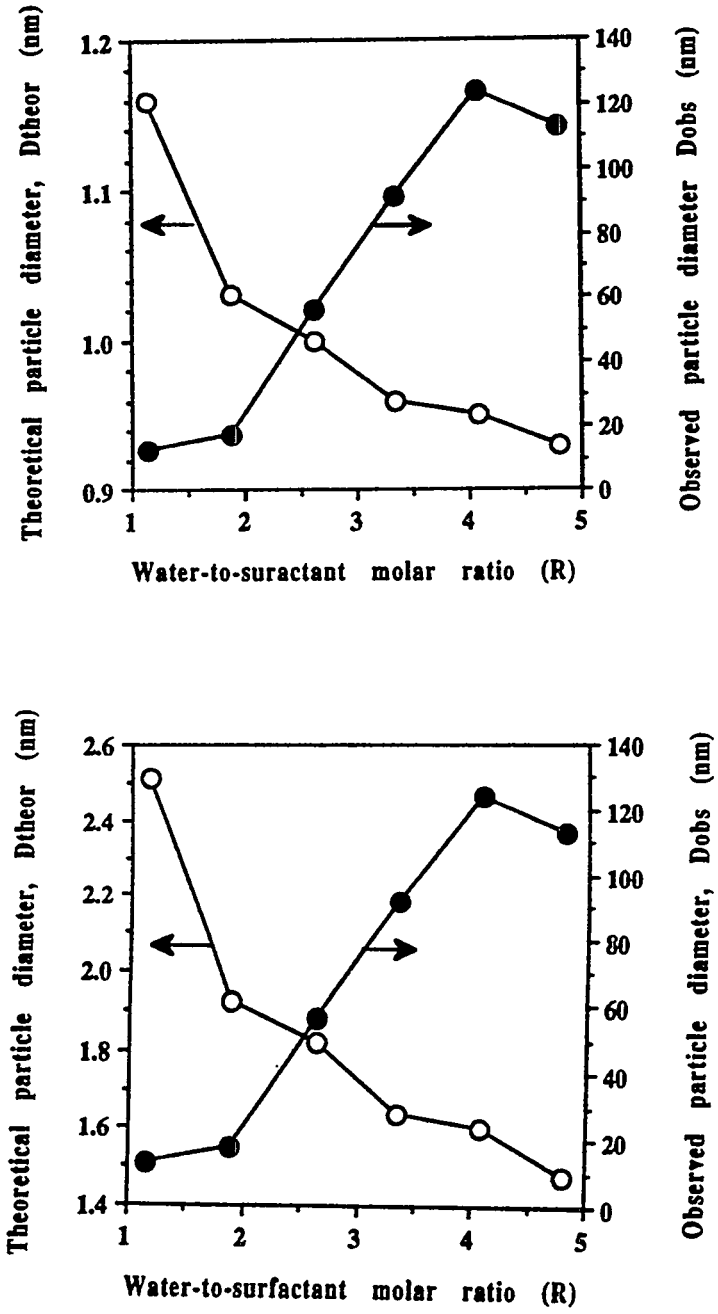

Figure 5.16

Effect of water-to-surfactant molar ratio on the experimental and theoretical molybdenum sulfide particle diameter

(MoS_4^{2-}] = 1.25x10^{-3} M, [H_2SO_4] = 3.42x10^{-3} M).

(A) i_c=2; (B) i_c=3.

mechanisms. Sugimoto and co-workers (70-72) have recently shown that, although polycrystalline hematite particles obtained by phase transformation of FeOOH are rough and porous, the mechanism of growth is by dissolution of the precursor solute FeOOH (73,74) and subsequent addition of the dissolved solute to the hematite nuclei. They further argued that the porosity and roughness of the particles are due to the two-dimensional epitaxial growth of the hematite nuclei and the restriction of lateral growth and fusion that is due to adsorption of chloride ion and/or ferric chloro-complexes at the crystal surfaces. It is believed, however, that the growth mechanism of Sugimoto et al., as outlined above, is inapplicable to the present results since the material under study, molybdenum trisulfide, is known to be amorphous (75-78).

Aggregative growth has been invoked in some recent investigations involving silica synthesis by the alkoxide process (79-82,83,84). Zukoski and coworkers (79-82) have used TEM to monitor the growth of silica particles made in ethanol. Their results show that small silica particles are produced at the early stage of the nucleation process and that these particles are present throughout the growth stage. In addition to the TEM results (79,82), ionic strength and seeded growth experiments (80,81) showed that the mechanism of particle growth is not by monomer addition. Growth of silica particles was attributed to aggregation of small particles (<10 nm) on larger particles.

Vrij and coworkers (83,84) propose that silica particles prepared by hydrolysis of tetraethoxysilane (TEOS) grow by both monomer addition and aggregative growth processes. They showed that in the early stage of silica particle growth, where aggregation is important, the particle size depends on the ionic strength (varied by adding $LiNO_3$) of the synthesis solvent (water, lower alcohols and ammonia). However, in the later stage of the growth process, where monomer addition is operative, particle size was found to be insensitive to ionic strength. Furthermore,

and contrary to the work of Zukoski and coworkers (79-82), Vrij and coworkers (83,84) showed some TEM micrographs of smooth silica particles, thus suggesting the importance of monomer addition growth.

From our TEM micrographs (Figures 5.5-5.8) and the results presented so far, particle aggregation is envisioned to take place in a manner similar to that proposed by Zukoski and coworkers (79-82) and by Vrij and coworkers (83,84). As can be seen in Figures 5.5-5.8, many small particles (~6 nm) are found surrounding the larger particles. Furthermore, these small particles are present during the entire growth period, i.e., 3-900 minutes. Finally, the particle surfaces are rough, e.g., Figure 5.5 (R = 1.2-4.8), Figure 5.6 (R = 3.3-4.8), Figure 5.7 (R = 3.3 and 4.8) and Figure 5.8 (R = 1.9, 4.07 and 4.80). In connection with the roughness of the particle surface, particles in the size range of 3.3-4.8 are generally found to be rougher, which indicates a greater rate of aggregation at R = 3.3-4.8 (i.e., aggregation is induced by free water molecules). We postulate therefore that many nuclei were produced initially and that these grew to a certain size (~6 nm);. further growth then occurred by radial aggregation of the primary particles (6 nm) on bigger particles.

Quantification of aggregation. Presented in Table 5.5 are the occupancy numbers and the N_m/N_p ratios for a sampling time of 3 minutes. It is seen that, roughly, for every two inverse micelles there is one ammonium thiomolybdate ion. Thus, assuming an i_c value of 2, one should expect the ratio N_m/N_p to be unity; instead, the observed ratio has values of the order of 10^4 - 10^6 (Table 5.5). This suggests that particles aggregate when microemulsion droplets fuse together.

To compare the degree of particle aggregation for the various R values, it is of interest to estimate the average number of molybdenum sulfide monomers in a single molybdenum sulfide particle for each R value. Let V_o and D_o be the

Table 5.5

Selected Statistical Parameters for the Synthesis of Molybdenum Sulfide in the 2/1 NP-5/Triton X-100/Water Microemulsion (t=3 min).

R	N_{oc}	N_m x10^{-19}	N_p x10^{-14}	(N_m/N_p)x10^{-6}
1.15	0.3	5.01	14.5	0.03
1.88	0.48	3.14	5.77	0.05
2.63	0.53	2.84	0.17	1.72
3.34	0.64	2.34	0.04	6.21
4.07	0.68	2.21	0.02	14.7
4.80	0.80	1.89	0.02	9.49

molecular volume and diameter of the MoS_3 monomer, respectively; then the molar volume can be expressed as follows:

$$V_o = N_{Avog}(4\pi/3)(D_o/2)^3 = M/\rho \qquad [5.10]$$

where N_{Avog} is the Avogadro number, M is the molar mass of MoS_3 (192.12) and ρ is the density of MoS_3. Equation 5.10 gives D_o as 0.575 nm for a nonporous molybdenum trisulfide particle with a density of 3.2 g cm^{-3}. Next the average number (n) of molybdenum trisulfide monomers in a single particle was found as:

$$n = V_p/V_o = (D_{obs}/D_o)^3 \qquad [5.11]$$

where V_p is the average volume of a molybdenum trisulfide particle, and D_{obs} is the experimentally determined particle size in Table 5.4. In calculating n the porosity of the material was neglected. However, errors associated with this approximation are expected to be minimal since the porosity effect cancels out in the ratio V_p/V_o. In addition, the approximate n values are good enough for comparing the degree of aggregation for various water-to-surfactant molar ratios. A similar assumption (using the same particle density for various R values) was adopted by Arriagada and Osseo-Asare (18) and by Kondori et al. (50). Figure 5.17 presents a plot of the number of monomers versus R. The number of monomers initially increases slightly with R from R = 1.2 to R = 1.9. However, from R = 1.9 to R = 2.6, the rate of change of n with R drastically increases. This observation implies that at R~2.6, particle aggregation is enhanced. At R = 2.6-4.1, n monotonically increases with R and levels off at R = 4.0-4.8.

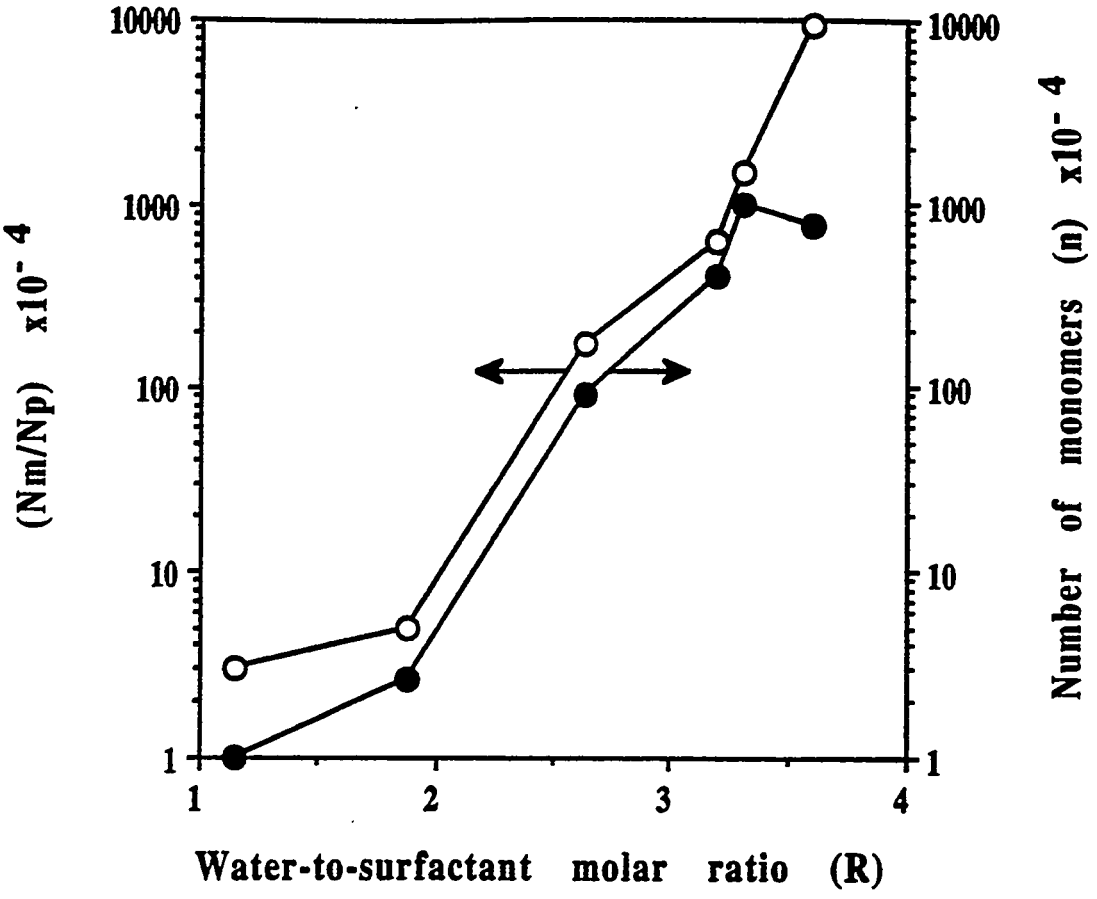

Figure 5.17

Effect of water-to-surfactant molar ratio on the number of molybdenum sulfide monomers and N_m/N_p

(t=3 minutes; i_c=2; $[MoS_4^{2-}] = 1.25x10^{-3}$ M; $[H_2SO_4] = 3.42x10^{-3}$ M).

It is noteworthy that, as concluded in Section 5.3.4, at R > 2.6 the presence of free water molecules causes extensive aggregation. Thus, this explains why at R = 2.6 the number of monomers in a molybdenum trisulfide particle dramatically increases with R; aggregation is enhanced by the presence of free water molecules at R = 3.3-4.8. Furthermore, if the ratio N_m/N_p is used as a criterion of aggregation (as evident in Table 5.5, due to particle aggregation, N_p decreases as R is increased, and the ratio N_m/N_p increases), then the degree of aggregation as represented by N_m/N_p will dramatically increase at $R > R_c$. This explains why, at t=3 minutes, a sudden increase in N_m/N_p occurs at R = 2.6.

5.4 CONCLUSIONS

Nanosize molybdenum sulfide particles have been synthesized in the microemulsions NP-5/Triton X-100/cyclohexane/water and Triton X-100/cyclohexane/water at high thiomolybdate ion loading. Direct extraction of ammonium tetrathiomolybdate ions into the water cores allowed the attainment of high reactant loading. For R = 1.2-2.6, the average particle diameter was found to be independent of R. However for R = 2.6-4.8 the particle size increased with R. For R > 2.63, particle aggregation is induced by the presence of free water molecules in the microemulsion. The onset of extensive aggregation coincides with the R value where free water molecules become available in the microemulsion fluid phase. A quantitative growth model, which is based on the monomer addition mechanism of growth, shows (by its lack of agreement with the experimental MoS_3 particle size versus R trends) that the molybdenum sulfide particle growth occurs via aggregation.

5.5 REFERENCES

1. Henglein, A., *Progr. Colloid Polymer Sci.* **73,** 1 (1987).
2. Fojtik, A., Weller, H., Koch, U., and Henglein, A., *Ber. Bunsenges. Phys. Chem.* **88,** 969 (1984).
3. Henglein, A., *J Chim. Phys.* **84,** 1043 (1987).
4. Koch, U., Fojtik, A., Weller, H., and Henglein, A., *Chem. Phys. Lett.* **122,** 507 (1985).
5. Wang, Y., Herron, N., *J. Phys. Chem.* **95,** 525 (1991).
6. Dannhauser, T., O'Neil, M., Johansson, K., Whitten, D., and McLendon, G., *J. Phys. Chem.* **90,** 3393 (1986).
7. Peterson, M.W., Nenadovic, M.T., Rajh, T., Herale, R., Micic, O.I., Goral, J.P., and Nozik, A.J., *J. Phys. Chem.* **92,** 1400 (1988).
8. Chestnoy, N., Harris, T.D., Hull, R., and Brus, L.E., *J. Phys. Chem.* **90,** 3393 (1986).
9. Rossetti, R., Hull, R., Gibson, J.M., and Brus, L.E., *J. Chem. Phys.* **83,** 1406 (1985).
10. Rossetti, R., Ellison, J.L., Gibson, J.M., and Brus, L.E., *J. Chem. Phys.* **80,** 4464 (1984).
11. Wilcoxon, J.P., Williamson, R.L., and Baughman, R. *J. Chem. Phys.* **98,** 9933 (1993).
12. Ward, A.J.I., O'Sullivan, E.C., Rang, J.-C., Nedeljkovic, J., and Patel, R.C., *J. Colloid Interface Sci.* **161,** 316 (1993).
13. Lianos, P., and Thomas, J.K., in "Materials Science Forum" (G.E. Murch and F.H. Wohlbier, Eds.), Vol. 25-26, 1988, p. 369.
14. Motte, L., Petit, C., Boulanger, L., Lixon, P., and Pileni M.P., *Langmuir* **8,** 1049 (1992).

15. Pileni, M.P., Motte, L., and Petit, C., *Chem. Mater.* **4,** 338 (1992).

16 Boakye, E., Radovic, L.R., and Osseo-Asare, K., *J. Colloid Interface Sci.* **163,** 120 (1994).

17. Boakye, E., Radovic, L.R., and Osseo-Asare, K., submitted to *J. Colloid Interface Sci.* (1994).

18. Osseo-Asare, K., Arriagada, F.J., *Colloids Surf.* **50,** 321 (1990).

19. Arriagada, F.J., and Osseo-Asare, K., *Colloids Surf.* **69,** 105 (1992).

20. Pileni. M.P., *J. Phys. Chem.* **97,** 6961 (1993).

21. Petit, C., Lixon, P., and Pileni, M.P., *J. Phys. Chem.* **97,** 12974 (1993).

22. Osseo-Asare, K., and Arriagada, F.J., in "Ceramic Powder Science III", (G.L. Messing, S. Hirano and H. Hausner, Eds.) American Ceramic Society, Westerville, OH, 1990, p. 3.

23. Arriagada, F.J., and Osseo-Asare, K., *J. Colloid Interface Sci.,* in press (1995).

24. Arriagada, F.J., and Osseo-Asare, K., in "The Colloid Chemistry of Silica" (H.E. Bergna, Ed.), Advances in Chemistry Series, Vol. 234, 1994, p. 113.

25. Ward, A.J.I., Friberg, S.E., *Mater. Res. Bull.* **14,** 41 (1989).

26. Arriagada, F.J., and Osseo-Asare, K., *J. Dispersion Sci. Technol.* **15,** 59 (1994).

27. Petit, C., and Pileni, M.P., *J. Phys. Chem.* **92,** 2282 (1988).

28. Vittal, M., Osseo-Asare, K., and Radovic, L.R., *Fuel,* submitted (1995).

29. Petit, C., Lixon, P., and Pileni, M.P., *J. Phys. Chem.* **94,** 1598 (1990).

30. Lianos, P., and Thomas, J.K., *Chem. Phys. Lett.* **125,** 299 (1986).

31. Hauser, H., Haering, G., Pande, A., and Luisi, P.L., *J. Phys. Chem.* **93,** 7869 (1989).

32. Valeur, B., and Keh, E., *J. Phys. Chem.* **83,** 3305 (1979).

33. Keh, E., and Valeur, B., *J. Colloid Interface Sci.* **79,** 465 (1981).

34. Wong, M., Thomas, J.K., and Gratzel, M., *J. Am. Chem. Soc.* **98,** 2391 (1976).

35. Pileni, M.P., Hickel, B., Ferradini, C., and Pucheault, J., *Chem. Phys. Lett.* **92,** 308 (1982).

36. Bakale, G., and Warman, J.M., *J. Phys. Chem.* **88,** 2927 (1984).

37. Bardez, E., Goguillon, B.-T., Keh, E., and Valeur, B., *J. Phys. Chem.* **88,** 1909 (1984).

38. Kawai, T., Hamada, K., Shindo, N., and Kon-no, K., *Bull. Chem. Soc. Jpn.* **65,** 2715 (1992).

39. Giammona, G., Goffredi, F., Turco Liveri, V., and Vassallo, G., *J. Colloid Interface Sci.* **154,** 411 (1992).

40. Boned, C., Peyrelasse, J., and Moha-Ouchane, M., *J. Phys. Chem.* **90,** 634 (1986).

41. Schick, M.J., *J. Colloid Sci.* **17,** 801 (1962).

42. Becher P., *J. Colloid Sci.* **17,** 325 (1962).

43. Ruckenstein, E., and Nagarajan, R., *J. Phys. Chem.* **84,** 1349 (1980).

44. Ravey, J.C., and Buzier, M., *J. Colloid Inteface Sci.* **116,** 30 (1987).

45. Handa, T., Sakai, M., and Nakagaki, M., *J. Phys. Chem.* **90,** 3377 (1986).

46. Kumar, C., and Balasubramanian, D., *J. Colloid Interface Sci.* **74,** 64 (1980).

47. Steigerwald, M.L., Alivisatos, A.P., Gibson, J.M., Harris, T.D., Kortan, R., Muller, A.J., Thayer, A.M., Duncan T.M., Douglas, D.C., and Brus. L.E., *J. Am. Chem. Soc.* **110,** 3046 (1988).

48. Pileni, M.P., and Lisiecki, I., *Colloids Surf.* **80,** 63 (1993).

49. Kandori, K., Kon-no, K., and Kitahara, A., *J. Colloid Interface Sci.* **122,** 78 (1988).

50. Zhu, D.-M., Wu, X., and Schelly, Z.A., *Langmuir* **8,** 1538 (1992).

51. Ayyub, P., Maitra, A., and Shah, D.O., *J. Chem. Soc. Faraday Trans.* **89,** 3585 (1993).

52. Kosower, E.M., Dodiuk, H., Tanizawa, K., Ottolenghi, M., and Orbach, N., *J. Am. Chem. Soc.* **97,** 2167 (1975).

53. Parker, C.A. and Rees, W.T., *Analyst* **85,** 587 (1960).

54. Nielsen, A.E., "Kinetics of Precipitation" MacMillan, New York, 1964, p. 12.

55. Nagy, J.B., *Colloids Surf.* **35,** 201 (1989).

56. Robinson, B.H. Towey, T.F., Zourab, S., Visser, A.J.W.G., and Van Hoek, A., *Colloids Surf.* **61,** 175 (1991).

57. Hou, M.J., and Shah, D.O., in "Interfacial Phenomena in Biotechnology and Materials Processing" (Y.A. Attia, B.M. Moudgil, and S. Chander, Eds.), Elsevier, Amsterdam/New York, 1988, p. 443.

58. Chew, C.H., Gan, L.M., and Shah, D.O., *J. Dispersion Sci. Technol.* **11,** 593 (1990).

59. Dvolaitzky, M., Ober, R., Taupin, C., Anthore, R., Auvray, X., Petipas, C., and Williams, C., *J. Dispersion Sci. Technol.* **4,** 29 (1983).

60. Catalog Handbook of Fine Chemicals, Aldrich, 1992-93: (a) p. 720; (b) p. 1267.

61. Lianos, P., and Thomas, J.K., *J Colloid Interface Sci.* **117,** 505 (1987).

62. Damerell, V.R., and Urbanic, A., *J. Phys. Chem.* **48,** 125 (1944).

63. Damerell, V.R., Gayer, K., and Laudenslager, H., *J. Phys. Chem.* **49,** 436 (1945).

64. Kitahara, A., Tamura, T., and Kon-no, K, *Separation Sci. Technol.* **15,** 249 (1980).

65. Kitahara, A., Tamura, T., and Matsumura, S., *Chem. Lett.* **9,** 1127 (1979).

66. Kitahara, A., Karasawa, S., and Yamada, H. *J. Colloid Interface Sci.* **25,** 490 (1967).

67. Ravet, I., Nagy, J.B., and Derouane, E.G., in "Preparation of Catalysts IV" (B. Delmon, P. Grange, P.A. Jacobs and G. Poncelet, Eds.), Elsevier, 1987, p. 505.

68. Atik, S.S., and Thomas, J.K., *J Am. Chem. Soc.* **103,** 3543 (1981).

69. Schleich, D.M., Chang, S., Barberio, Y.L., and Hanson, K.J., *J. Electrochem. Soc.* **136,** 3274 (1989).

70. Sugimoto, T., Khan, M.M., Muramatsu, A., and Itoh, H., *Colloids Surf.* **79,** 233 (1993).

71. Sugimoto, T., Sakata, K., and Muramatsu, A., *J. Colloid Interface Sci.* **159,** 372 (1993).

72. Sugimoto, T., Muramatsu, A., Sakata, K., and Shindo, D., *J. Colloid Interface Sci.* **158,** 420 (1993).

73. Morales, M.P., Gonzalez-Carreno, T., and Serna, C.J., *J. Mater. Res.* **7,** 2538 (1992).

74. Blesa, M.A., and Matijevic, E., *Adv. Colloid Interface Sci.* **29,** 173 (1989).

75. Jacobson, A.J. Chianelli, R.R., Rich, S.M., and Whittingham, M.S., *Mat. Res. Bull.* **14,** 1437 (1979).

76. Liang, K.S., de Neufville, J.P., Jacobson, A.J., and Chianelli, R.R., *J. Non-Cryst. Solids.* **35,** 1249 (1980).

77. Ratnasamy, P., and Leonard, A.J., *J. Catal.* **26,** 352 (1972).

78. Ratnasamy, P., Rodrique, L., and Leonard, A.J. *J. Phys. Chem.* **77,** 2242 (1973).

79. Bogush, G.H., Tracy, M.A., and Zukoski IV, C.F., *J. Non-Cryst. Solids* **104,** 95 (1988).

80. Look, J.-L., Bogush, G.H., and Zukoski IV, C.F., *Faraday Discuss. Chem. Soc.* **90,** 345 (1990).

81. Bogush, G.H., ad Zukoski IV, C.F., *J. Colloid Interface Sci.* **142,** 1 (1991).

82. Bogush, G.H., and Zukoski IV, C.F., *J. Colloid Interface Sci.* **142,** 19 (1991).

83. Van Blaaderen, A., and Vrij, A., in "Colloid Chemistry of Silica" (H.E. Bergna, Ed.), Advances in Chemistry Series, Vol. 234, 1994, p. 82.

84. Van Blaaderen, A., Van Geest, J., and Vrij, A., *J. Colloid Interface Sci.* **154,** 481 (1992).

CHAPTER 6

IN SITU TESTING OF MOLYBDENUM SULFIDE CATALYST PARTICLES SYNTHESIZED IN MICROEMULSIONS

6.1 INTRODUCTION

Certain highly dispersed catalysts have been found to be very active for the direct liquefaction of coal. In 1951, Weller and Pelipetz (1) demonstrated that a large increase in liquefaction efficiency could be achieved by impregnating the catalyst onto the coal. Since then, a number of studies on the importance of catalyst dispersion in coal liquefaction have appeared in the literature (2).

Dispersed-phase, i.e., unsupported, catalysts are usually introduced via impregnation techniques (1,3), as water-soluble (4,5) and oil-soluble salts (6,7), and as finely divided powders (1,8). The level of dispersion achieved is inferred – in most cases – from kinetic data. However, this method does not identify the factors that influence the distribution of catalyst over the coal, or its evolution during reaction. This inadequacy has spurred the use of other, hopefully more direct, techniques to study the dispersion of coal liquefaction catalysts.

Nowadays, a number of different techniques for characterizing catalytic materials are available. They have been reviewed recently by Haber (9). In coal liquefaction catalysis, the techniques of Mössbauer spectroscopy, magnetometry, electron microscopy, x-ray line-broadening, and BET surface area measurements are used to estimate the size of the solid catalyst precursor, and, in some cases, of the catalytically active phase after reaction. These techniques have also been evaluated recently (10).

It is of interest to study the effect of initial catalyst dispersion on coal liquefaction quantitatively. Using the above listed methods of introducing dispersed-phase catalysts, close control over the solid catalyst precursor particle size is generally not possible. A possible exception to this rule is when the catalyst precursor is introduced as finely divided powders, in which case the initial (average) particle size can be determined unambiguously. However, to study the effect of catalyst particle size on coal liquefaction, it would be of great interest to have the catalyst in the form of colloidal particles with uniform size, shape, and charge. A number of different methods are available for the preparation of such particles and they have been reviewed recently (11,12).

Liquid-phase synthesis methods are believed to be superior to others, insofar as achieving close control over the particle size distribution is concerned (11). Microemulsion-mediated synthesis is an example of a liquid-phase method for producing ultrafine, monodispersed solids. The method exploits the cage-like effect produced by surfactant-stabilized, metal-bearing microdrops to limit particle nucleation, growth and agglomeration. In recent years, a number of workers have reported the preparation of ultrafine, monodispersed inorganic solids via chemical reactions in microemulsions. Pileni (13) has recently reviewed the state of the art in this rapidly growing field.

In the present work (Chapters 2-5), molybdenum sulfide catalyst particles were synthesized in various microemulsions. Furthermore, an attempt was made to study the effect of molybdenum sulfide catalyst dispersion on the liquefaction of a subbituminous and a bituminous coal.

6.2 EXPERIMENTAL

6.2.1 Coal Selection and Preparation

The coals that were chosen for this study are a Wyodak subbituminous coal (PSOC 1401) and Blind Canyon bituminous coal (DECS-6). Both coals have a sufficiently extensive liquefaction database to permit a meaningful evaluation of the microemulsion-based catalysts used here. Table 6.1 gives a summary of the proximate and ultimate analyses provided by the Penn State Coal Data Base. The coal was ground to -60 mesh and dried in vacuum at 100 °C to <1% moisture before use.

6.2.2 Catalyst Particle Synthesis and Characterization

Nanometer-scale molybdenum sulfide particles were synthesized following the protocol outlined in Ref. 14. Additional relevant experiments are described in detail in Appendix V.

The composition of the micellar solution used for the preparation of particles is shown in Table 6.2. Tetralin (1,2,3,4-tetrahydronaphthalene) was used as the nonpolar phase because it is a popular model coal liquefaction solvent (16,17). Benzyl alcohol served as a cosurfactant. The synthesis experiments were conducted at 50 °C. First, a solution of 0.4 M polyoxyethylene nonylphenyl ether (NP-5)/tetralin/benzyl alcohol was prepared at room temperature. In a 10 mL portion of this solution in a vial, 36.2 μL of 1.1 M sulfuric acid were solubilized. The acid-solubilized microemulsion was immersed in a water bath thermostatted at 50 °C and deoxygenated by bubbling high-purity nitrogen gas through it. Next, 36.2 μL of

Table 6.1
Data for Coal Samples

Penn State Sample Bank No.	PSOC-1401	DECS-6
Seam	Canyon-Top	Blind Canyon
State	Wyoming	Utah
Country	USA	USA
ASTM Rank	Subbit. B	HVA bit.
Moisture (as received, wt%)	16.33	4.73
Mineral Matter (dry, wt%)	5.72	5.84
Elemental Composition		
Carbon	72.70	81.87
Hydrogen	4.62	6.29
Nitrogen	1.07	1.56
Sulfur (organic)	0.28	0.40
Oxygen (by difference)	21.38	10.10

Table 6.2
Composition of the Micellar Solution Used for the Preparation of Molybdenum Sulfide Catalyst Particles

COMPONENT	WT% IN SOLUTION
Tetralin	38.78
Benzyl Alcohol	43.73
NP-5	17.49

1.25×10^{-2} M ammonium tetrathiomolybdate (ATTM) were added, the vial manually shaken a few times, and returned to the water bath. Nitrogen was continuously bubbled through the solution while molybdenum sulfide was being precipitated according to Equation 6.1:

$$MoS_4^{2-} + 2H^+ = MoS_3 + H_2S \qquad [6.1]$$

The final concentrations of the reactant species (with respect to the total microemulsion) were as follows: sulfuric acid, 4×10^{-3} M; and ATTM, 4.5×10^{-5} M.

The average particle size of the molybdenum sulfide particles could be controlled by changing the amount of water solubilized in the microemulsion, characterized by the water-to-surfactant molar ratio (R). One example is shown in Figure 6.1 (see also Appendix V). The synthesis protocol described above corresponds to R = 2. For reasons that will become obvious later, this was the only formulation that was subsequently employed in microautoclave activity tests.

Particle characterization was accomplished using transmission electron microscopy (Philips 420T model), X-ray diffraction (Rigaku), and DTA/TGA (Perkin Elmer). The results have been presented elsewhere (14).

6.2.3 Preparation of ATTM-impregnated Coal Samples

For comparison purposes, a set of coal samples were impregnated with ATTM using a conventional method described in the literature (15). Briefly, ATTM was dissolved in sufficient distilled water in a flat-bottom flask to give an approximate water-to-coal ratio of 1/1 (v/w), and coal was added to this solution. After stirring for 30 min, the coal was dried in vacuum for 2 h at 110 °C and stored in tightly closed glass vials until further use. The final catalyst loading was 1 wt% Mo (daf).

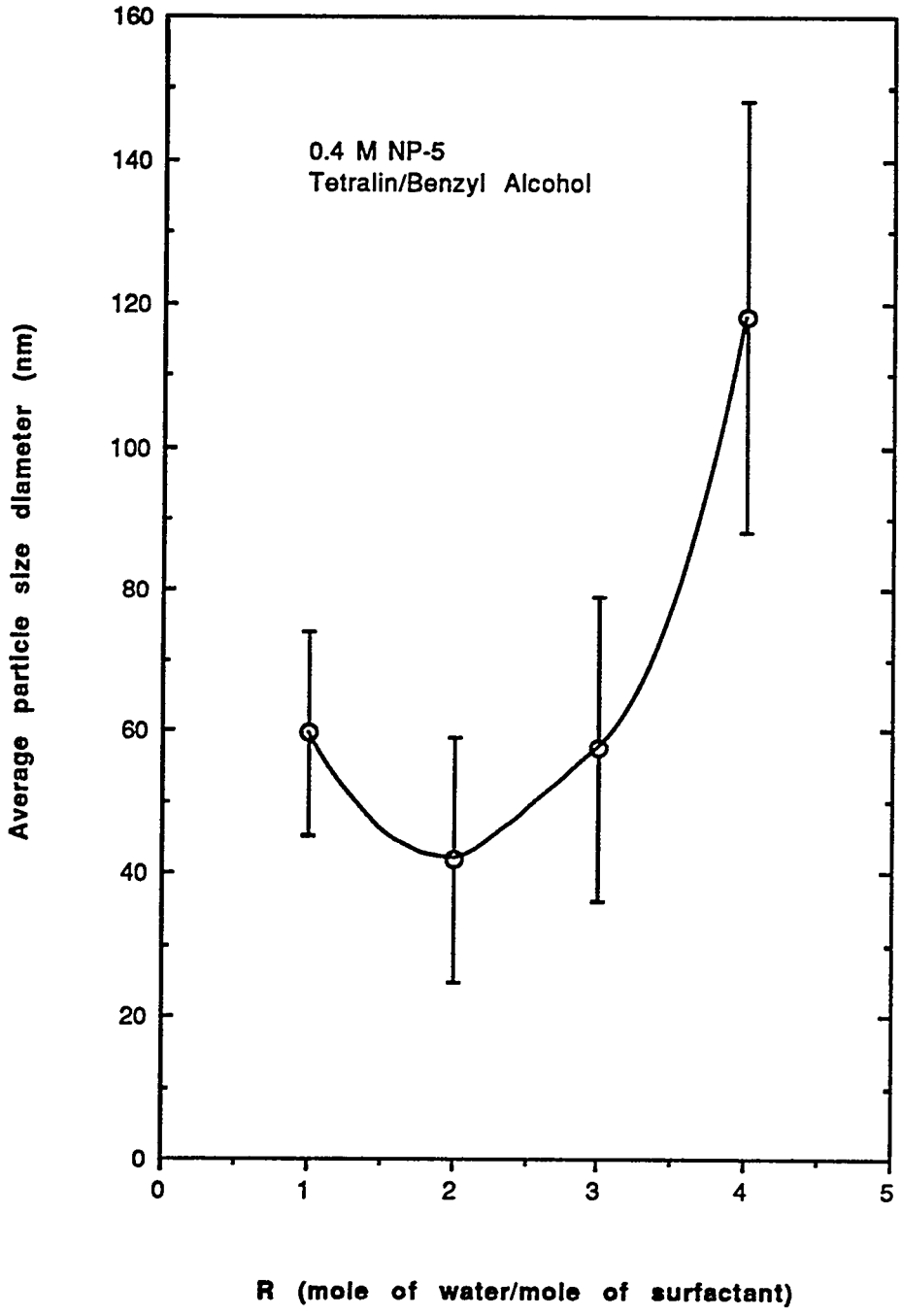

Figure 6.1
Plot of average particle diameter versus water-to-surfactant molar ratio (R).
(Note: Metal concentration increases as R increases for this particular case.)

6.2.4 Characterization of Coals and Their Insoluble Liquefaction Residues

The coal samples and their insoluble residues were qualitatively characterized using Fourier Transform Infrared Spectroscopy (FTIR). The spectra were obtained on a BIO-RAD 60 system by co-adding 256 scans at a resolution of 2 cm^{-1}. The samples were analyzed as KBr pellets. Approximately 2 mg of coal or residue was ground with 20 mg of KBr for 30 s in a Perkin-Elmer Wig-L-Bug. An additional 280 mg of KBr was added to the mixture and ground for 2 minutes to ensure intimate mixing. The mixture was then transferred to a mold and pressed into pellets.

6.2.5 Microautoclave Tests

The tests were conducted in 25 cc microautoclave reactors (tubing bombs) in a preheated fluidized sandbath. One gram of coal and 2 g of tetralin were charged into the reactor. Air was removed by repeatedly pressurizing the reactor to 6.9 MPa thrice with hydrogen. Subsequently, the reactor was pressurized to 6.9 MPa (cold) with hydrogen. It was then immersed in the sandbath and agitated at 200 cycles per minute. The reaction temperature of 350 °C was reached in all cases within three minutes of immersion. At the end of 30 minutes, the reactor was plunged into cold water to quench the reaction.

After depressurizing the reactor, its contents were rinsed with hexane into a dried soxhlet thimble and extracted overnight under nitrogen. The hexane was removed from the extract by rotary evaporation. The hexane-insoluble residue was then soxhlet-extracted with THF to separate asphaltenes from the residue. THF was removed from the extract by rotary evaporation.

Asphaltenes and residue were dried for 6 h and 2 h, respectively, in vacuum at 110 °C. Conversion was calculated by subtracting the weight of the residue from

the weight of the coal and dividing by the daf weight of the coal. Following convention, asphaltenes are THF-soluble, hexane-insoluble; oils are hexane-soluble.

6.2.6 Blank Runs

A special testing protocol had to be developed, owing to the unconventional form of the catalyst. It was sought to employ the catalyst particles in microautoclave activity tests in the as-prepared condition, i.e., while they were suspended in the microemulsion. Consequently, the microemulsion medium used to synthesize the particles also became the coal liquefaction solvent. As mentioned earlier, this fact prompted the choice of tetralin as one of the components of the microemulsion. Tetralin is a popular model coal liquefaction solvent and its behavior under liquefaction conditions is well documented (see, for examples, Refs. 16 and 17). However, as shown in Table 6.2, the microemulsion also has two other components present in significant amounts, viz., surfactant, NP-5, and co-surfactant, benzyl alcohol. Little or no information is available in the literature on either their behavior under liquefaction conditions, or their effect on coal liquefaction reactions. This is significant because it is well known that solvent composition can affect catalytic activity (2).

Therefore, a set of "blank runs" were performed to permit a distinction to be made between solvent and catalytic effects. Basically, a blank run consisted in liquefying coal (under the exact same conditions) in a catalyst-particle-free microemulsion. The rationale behind the blank run was that solvent effects – if any – could be subtracted out of the catalyzed run to obtain a result that would reflect solely the effect of the catalyst.

6.3 RESULTS

6.3.1 Reactions of Coals Impregnated with ATTM

Tables 6.3 and 6.4 show the conversion data from liquefaction of the subbituminous and bituminous coals, respectively. The reproducibility of the data was typically ± 2 %. For reaction without added ATTM, the presence of tetralin in the reactor doubled the total conversion of both coals. The increased conversion came solely through greater formation of asphaltenes for the subbituminous coal, while both asphaltene and oil yields were increased for the bituminous coal. Both findings are consistent with the well known observation that tetralin is an excellent hydrogen-donor solvent (18).

The use of ATTM without tetralin gave a higher total conversion than the use of tetralin without catalyst for the subbituminous coal. The increase came about via greater formation of oil. For the same coal, the use of both ATTM and tetralin resulted in a three-fold increase in the oil yield relative to the run with ATTM alone.

For the bituminous coal, the use of ATTM alone produced no significant changes relative to the uncatalyzed, solvent-free run. When both ATTM and tetralin were used, however, the yield of oil increased significantly, although the total conversion increased only slightly.

Therefore, the Mo catalyst produced a strong effect primarily on the dissolution of the subbituminous coal, while it mainly served to increase the oil yield from the bituminous coal. This is believed to be due to the fact that subbituminous coals contain a larger number of crosslinks and have a higher oxygen content (15).

Table 6.3
Liquefaction Conversion Data for Subbituminous Coal.
(T=350 °C, P=1000 psi H_2 (cold), t=30 min, tetralin solvent, 1 wt% Mo catalyst.)

Run	Solvent	Catalyst	Conversion (% d.a.f.)		
No.			Total	Asph.	Oils
74	None	None	12.3	12.3	0.0
75	None	ATTM	29.2	23.4	5.8
76	Tetralin	None	24.5	24.5	0.0
7	Tetralin	ATTM	24.9	6.1	18.8

Table 6.4
Liquefaction Conversion Data for Bituminous Coal.
(T=350 °C, P=1000 psi H_2 (cold), t=30 min, tetralin solvent, 1 wt% Mo catalyst.)

Run	Solvent	Catalyst	Conversion (% d.a.f.)		
No.			Total	Asph.	Oils
41	None	None	17.2	6.1	11.1
42	None	ATTM	21.3	8.9	12.4
46	Tetralin	None	40.2	24.8	15.4
39	Tetralin	ATTM	43.7	20.5	23.2

6.3.2 Activity of Catalyst Particles Suspended in Microemulsions

As noted earlier, the testing protocol for the molybdenum sulfide catalyst prepared in microemulsions was developed to distinguish between solvent and catalytic effects. According to this scheme, the experiment conducted in the catalyst-particle-free microemulsion became the "thermal", or uncatalyzed, run. To understand the effects of each of the microemulsion components on the liquefaction process, coal was also reacted in benzyl alcohol and NP-5 under identical conditions. The results of these tests are shown in Tables 6.5 and 6.6 for the subbituminous and bituminous coals, respectively.

For the subbituminous coal, no conversion data – either with catalyst-particle-free-, or catalyst-particle-bearing-microemulsion – are reported. This is because reliable and reproducible coal conversion figures could not be obtained in either case, owing to insurmountable problems with the removal of reaction products from the reactors. The products consisted of rock-like solids and black, viscous, tarry liquids – strong indications that severe retrogressive reactions had occurred. The insides of the reactor stems were also coated with some kind of gummy material. In view of their refractory nature, most of the products were simply worked out of the reactors with a steel spatula into ceramic thimbles using THF, and extracted under nitrogen. After the extract became nearly colorless (usually after a week or so), the THF-insoluble residue was dried and analyzed using FTIR spectroscopy.

From Table 6.5, it is evident that, for the subbituminous coal, both NP-5 and benzyl alcohol are very poor liquefaction media. In both runs, the yield of oils (hexane-solubles) was negative. This is attributed to the transformation of these solvents – both initially hexane-soluble – into hexane-insoluble materials under

Table 6.5

Conversion Data for Liquefaction of Subbituminous Coal in Blank and Catalyst-Particle-Bearing Microemulsions, Benzyl Alcohol and NP-5.
(T=350 °C, P=1000 psi H_2 (cold), t=30 min, 50 ppm Mo catalyst.)

Run No.	Liquefaction Medium	Conversion (% d.a.f.)		
		Total	Asph.	Oil
20	Blank Microemulsion[a]	N.D.*	N.D.	N.D.
17	Microemulsion w/Cat.[a]	N.D.	N.D.	N.D.
77	Benzyl Alcohol[b]	18.6	45.2	-26.2
62	NP-5[c]	13.3	17.8	-4.5

*N.D. = Not Determined

[a] microemulsion/coal=5.6; [b] benzyl alcohol/coal=2.0; [c] NP-5/coal=1.3.

Table 6.6

Conversion Data for Liquefaction of Bituminous Coal in Blank and Catalyst-Particle-Bearing Microemulsions, Benzyl Alcohol and NP-5.
(T=350 °C, P=1000 psi H_2 (cold), t=30 min, 50 ppm Mo catalyst.)

Run No.	Liquefaction Medium	Conversion (% d.a.f.)		
		Total	Asph.	Oil
28	Blank Microemulsion[a]	61.3	61.3	0.0
32	Microemulsion w/Cat.[a]	62.0	67.0	-5.0
36	Benzyl Alcohol[b]	69.4	67.2	2.2
64	NP-5[c]	19.9	58.8	-38.9

[a] microemulsion/coal=5.6; [b] benzyl alcohol/coal=2.0; [c] NP-5/coal=1.3

coal liquefaction conditions. The residues from these tests were also analyzed by FTIR spectroscopy.

Fourier Transform Infrared Spectroscopy (FTIR) has been used to investigate retrogressive reactions that occur during coal liquefaction (19). A detailed band assignment of the functional groups in coal was reported by Painter et al. (20). In the present study, FTIR spectra were obtained for qualitative comparison of the structural features of the THF-insoluble residues.

Figure 6.2 shows the FTIR spectra of pure benzyl alcohol and NP-5. The spectrum of the as-received subbituminous coal is shown in Figure 6.3a, and the spectra of the THF-insoluble residues from the subbituminous coal liquefied in tetralin, benzyl alcohol, NP-5 and microemulsion are shown in Figure 6.3b. It can be seen in Figure 6.3b that the spectrum of the benzyl alcohol residue is particularly different from the rest. First, its peaks are much sharper. Such sharp peaks are uncharacteristic of coals. Second, there are three finger-like peaks in the region 3100–3000 cm^{-1}. In the spectrum of pure benzyl alcohol (Figure 6.4a), very similar features may be seen in the same spectral region. These three closely-spaced peaks in the 3100–3000 cm^{-1} region are due to the aromatic C–H stretching vibrations in the benzyl alcohol molecule (21). Third, in the region 1500–500 cm^{-1}, several new peaks appear that are not found in the spectrum of the tetralin residue. Again, some of these new peaks are seen to coincide with those of pure benzyl alcohol. These observations seem to indicate that benzyl alcohol was incorporated into the coal and are consistent with those of Saini et al. (22). From a study of the liquefaction of a Wyodak subbituminous coal in various solvents, they found that benzyl alcohol can induce and participate in extensive retrogressive reactions involving itself and coal. In contrast, the NP-5 and tetralin residues show very similar spectra. The absence of solvent peaks in the NP-5 residue spectrum seems to indicate that it was not incorporated into the coal. Presumably, the negative oil yield that resulted when

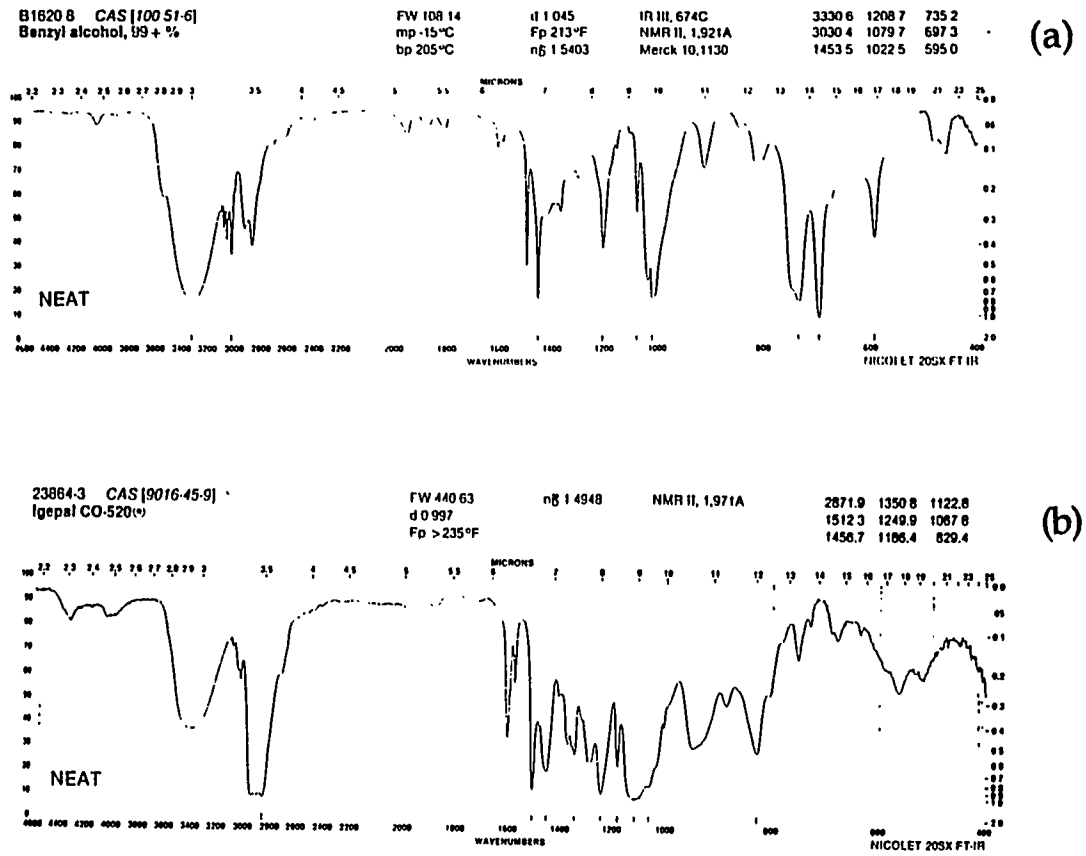

Figure 6.2
FTIR spectra of (a) benzyl alcohol and (b) NP-5.

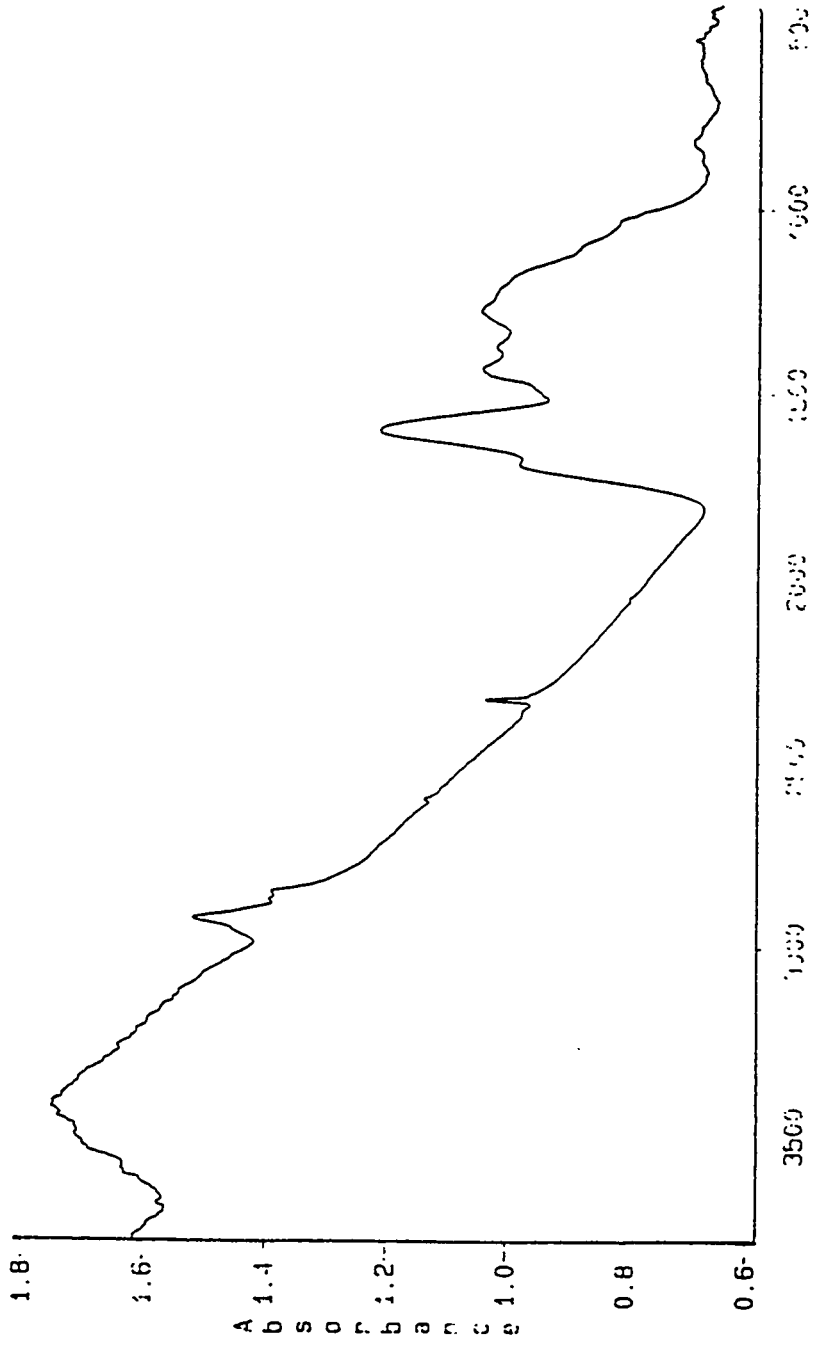

Figure 6.3a
FTIR spectrum of the subbituminous coal (PSOC 1401).

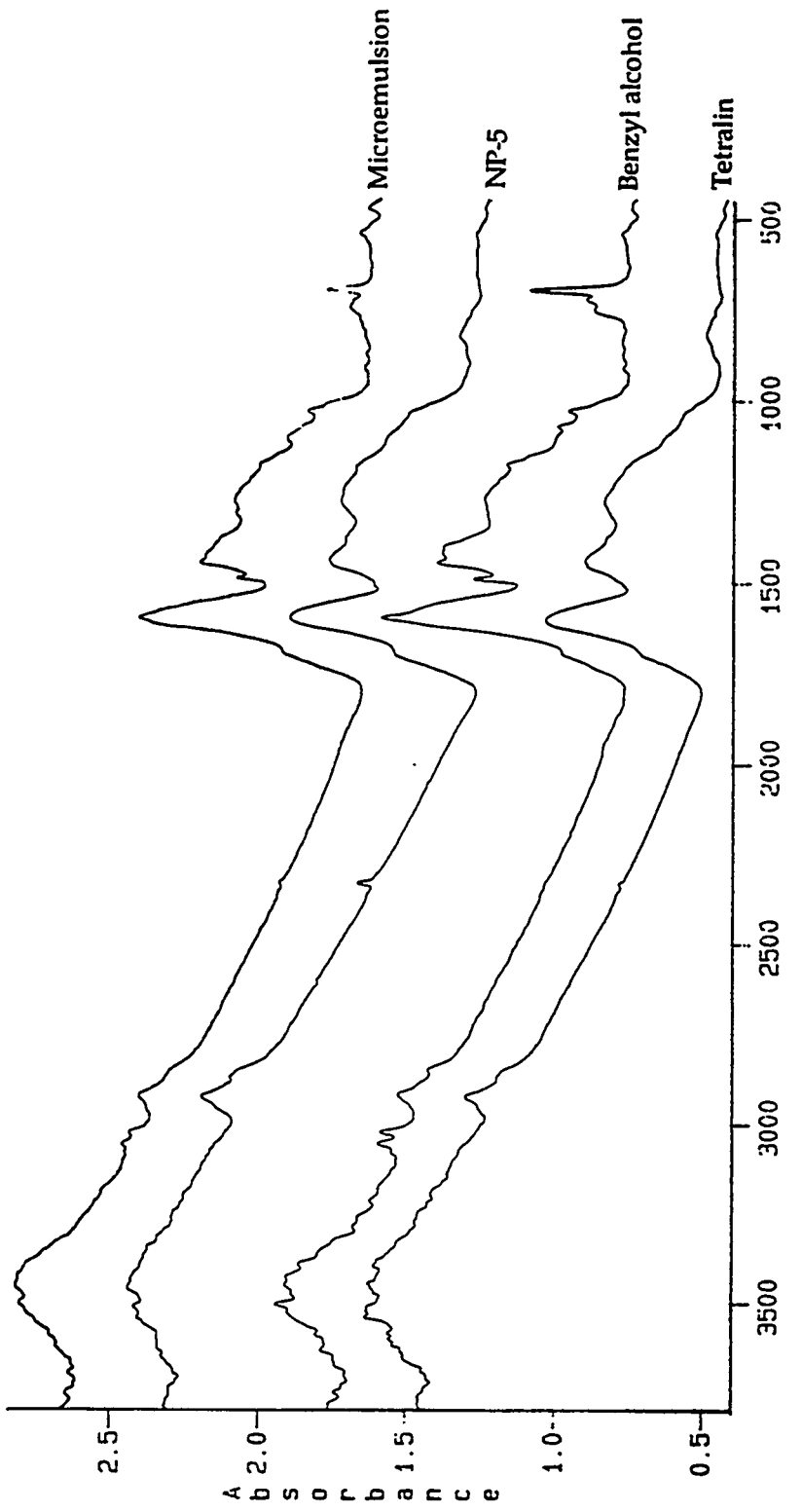

Figure 6.3b

FTIR spectra of the THF-insoluble residues from the subbituminous coal (PSOC 1401).

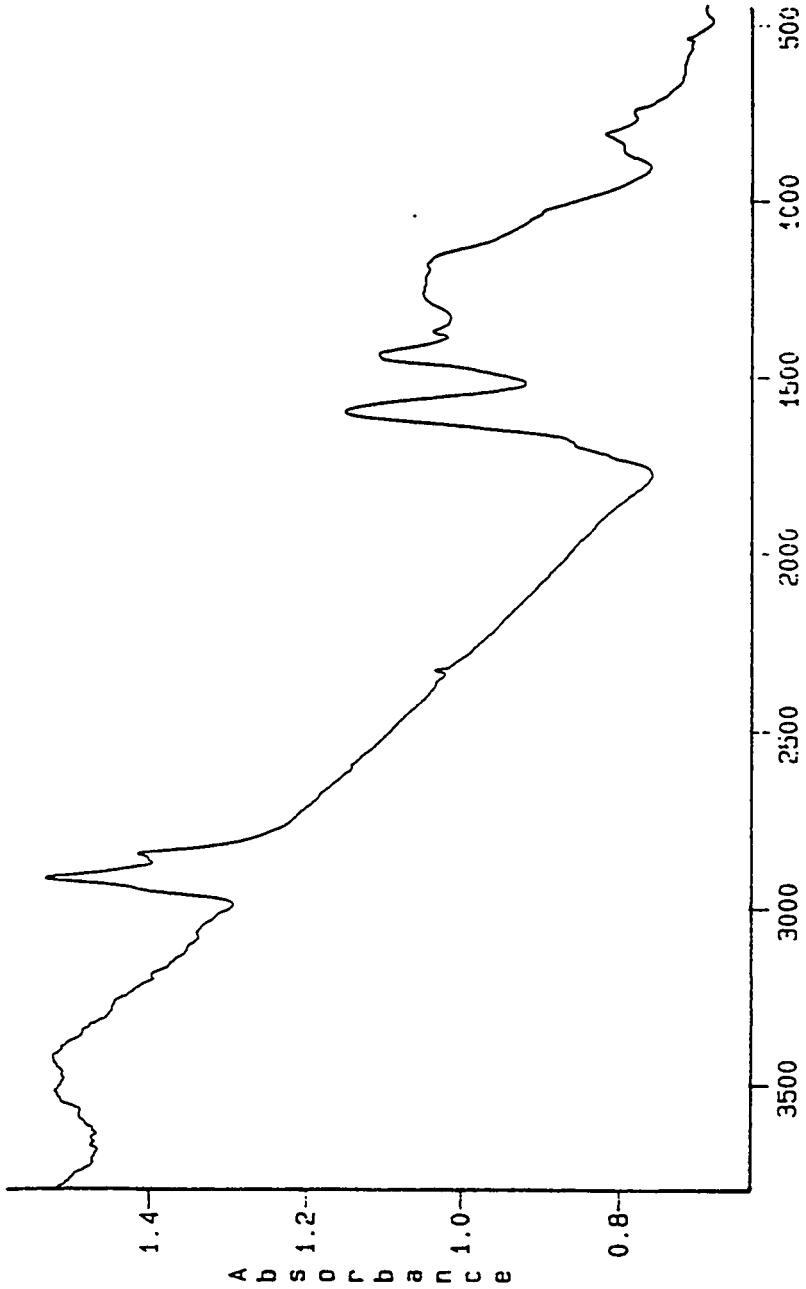

Figure 6.4a
FTIR spectrum of the bituminous coal (DECS-6).

NP-5 was used as the liquefaction medium was due to its own transformation into hexane-insoluble, THF-soluble material (asphaltene) under liquefaction conditions. Lastly, as would be expected from the composition of the microemulsion, the microemulsion residue is qualitatively similar to the benzyl alcohol residue. Even the presence of H-donor tetralin was unable to mitigate the retrogressive effects introduced by benzyl alcohol.

The bituminous coal behaved rather differently in the same set of experiments (Table 6.6). Relative to liquefaction in tetralin, when benzyl alcohol was used as the solvent, the total conversion to soluble products was greater by nearly 30%, while the hexane-soluble fraction decreased by about 15% [compare Run 28 to Run 46 (Table 6.4)]. This seems to indicate that, for the bituminous coal, benzyl alcohol is an excellent physical solvent for thermally derived coal fragments, but a poor hydrogen donor. It was also observed that the oil produced from the reaction in tetralin was free-flowing and light-colored, while that formed in benzyl alcohol was darker and more viscous. Furthermore, if Run 36 is compared to Run 41 (Table 6.4), it can be seen that not even the oil yield under non-catalytic, tetralin-free conditions was achieved when coal was liquefied in benzyl alcohol. It appears, therefore, that dissolution and dispersion of thermally derived coal fragments precludes their conversion to low-molecular-weight, hydrogen-rich products that are soluble in hexane. Such phenomena have also been observed during investigations into the beneficial effects of phenolic compounds on coal liquefaction (23).

The blank run for this coal (Run 28) appears to display a complex interplay between the effects of individual microemulsion components, viz., surfactant (NP-5), cosurfactant (benzyl alcohol) and non-polar phase (tetralin), on the liquefaction process. The total conversion was about 21% greater than when tetralin alone was used. This seems to be due to the superior ability of benzyl alcohol to dissolve and

disperse thermally derived coal fragments, as discussed earlier. The oil yield was observed to be 0%, indicating that the simultaneous presence of tetralin in the reactor had little or no effect on the hydrogenation process. Moreover, the total conversion was also about 8% less than that observed with benzyl alcohol alone as the solvent (Run 36). This suggested that the surfactant (NP-5) was also exerting a regressive influence on the overall process.

Figure 6.4b shows the FTIR spectra of the THF-insoluble residues from the bituminous coal liquefied in tetralin, benzyl alcohol, NP-5 and microemulsion. As with the subbituminous coal, the spectrum of the benzyl alcohol residue suggests that the alcohol has been incorporated into the coal. However, the spectra of the tetralin and NP-5 residues are not similar. The broad peak between 3750–3200 cm^{-1} is more intense for the latter. Coincidentally, there is a similar peak in the same region of the spectrum of pure NP-5 (Figure 6.2b). Possibly, NP-5 was also incorporated into the coal under liquefaction conditions.

6.4 DISCUSSION

It must be emphasized that it was impossible to observe purely catalytic effects in any of the experiments with the microemulsion-based catalyst. Several experiments were also conducted in which the catalyst loading was increased, but all of these were without profit. As pointed out earlier, in the presence of certain solvents, catalytic activity may be masked or suppressed altogether. This is evidently what happened.

A very recent report in the literature concerning the preparation of iron-based clusters in microemulsions and their use as catalysts in coal liquefaction reactions is of interest here (24). The results are reproduced in Table 2.7. The catalysts labeled

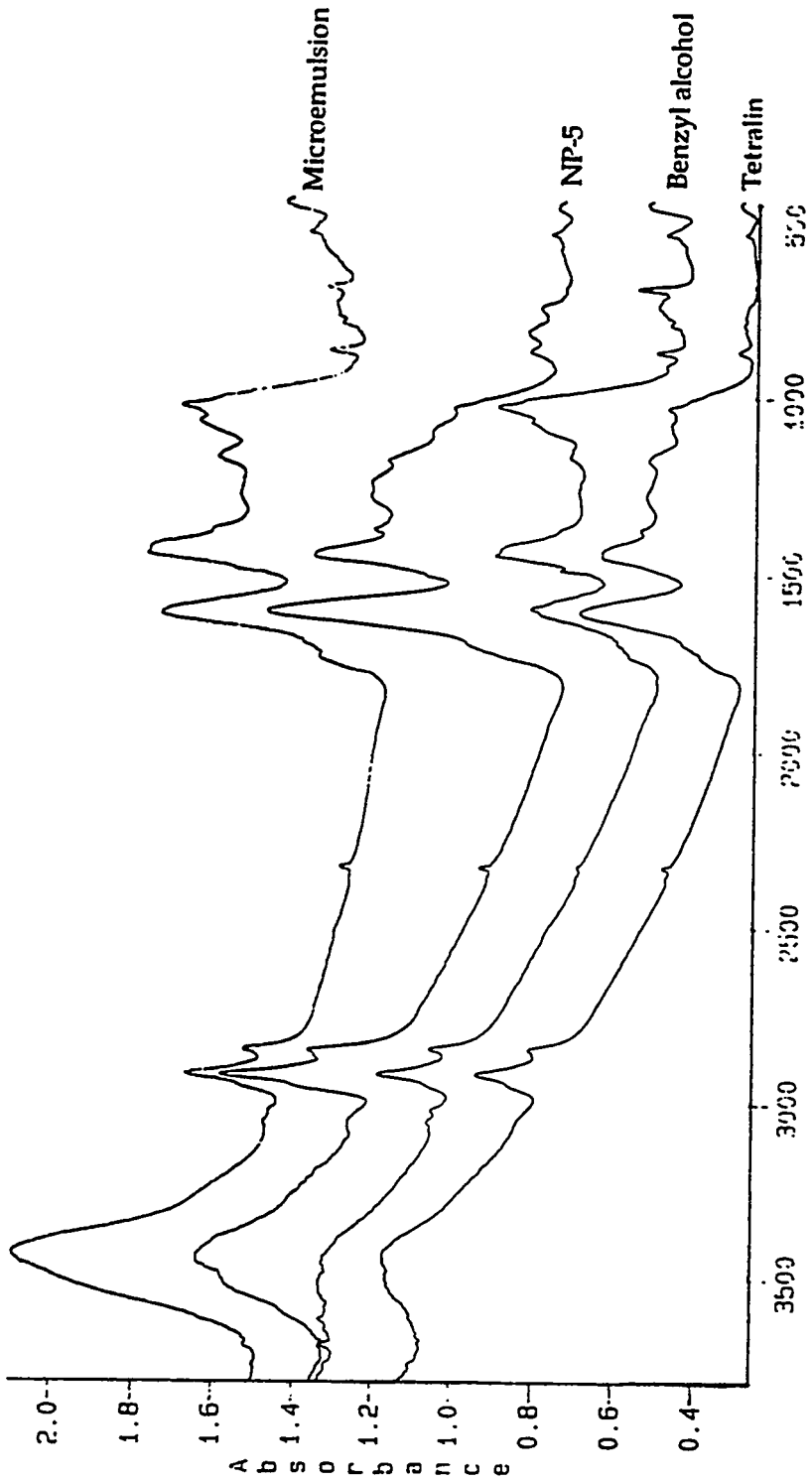

Figure 6.4b

FTIR spectra of the THF-insoluble residues from the bituminous coal.

Table 6.7
Micro-batch Liquefaction Results for the Blind Canyon, DECS-17 Coal.
(T=400°C, P=800 psi H_2 (cold), t=30 min, hexahydropyrene solvent,
2–5 wt% catalyst.) [Adapted from Reference 35.]

Catalyst	Conversion (% d.a.f.)		
	Total[a]	Asph.[b]	Oil[c]
None	90.1	58.0	30.1
Fe, *in situ*	**33.5**	**13.8**	**8.9**
Fe, powder	94.0	60.9	30.5
Fe, surfactant extracted liquid	50.0	27.3	22.7
FeS_2, *in situ*	**35.3**	**34.3**	**1.0**
FeS_2, powder	83.0	33.9	44.4
FeS_2, surfactant extracted liquid	90.2	57.3	28.7

[a] based on THF-insoluble residue; [b] asphaltene, THF-soluble/C7-insoluble;
[c] C7 solubles

"Fe, *in situ*" and "FeS_2, *in situ*" were those that were used in the as-prepared form to liquefy coal. In other words, the catalyst particles were employed while they were suspended in the microemulsion medium in which they were synthesized – as in the present study. Two significant conclusions may be drawn from the results. First, neither catalyst displayed any activity for the liquefaction reaction. Second, the yield of insoluble organic matter was inordinately high in both cases. The authors attributed this to "the wetting of coal by surfactant solutions, resulting in coal aggregation and poor mixing". Aggregated coal was believed to not participate in the reaction and wind up as insoluble organic material. In any case, their results for the *in situ* tests are qualitatively similar to those reported here.

Interestingly, surfactants have been found by other workers to *improve* coal liquefaction yields (25, 26). For example, Hickey and Sharma (25) found an increase in coal conversion yields upon addition of sodium lignosulfonate surfactant to coal during liquefaction batch autoclave tests. They postulated that the surfactant acts by dispersing the coal particles and facilitating the breakage of crosslinks in the coal matrix. However, the surfactant was added in concentrations of only 0.5 to 2.0 wt%. In our work, the surfactant concentration was about 17 wt% (Table 6.2). Besides, the increments in coal conversions observed by them in *batch autoclave tests* were not found in a *continuous flow test* conducted at HRI using their (HRI's) Continuous Two-Stage Liquefaction (CTSL) Process (26). They attributed this to surfactant deactivation of the catalyst used in the process. In the present study, a second surfactant – Aerosol OT (AOT) – which is quite similar to sodium lignosulfonate, was also used in autoclave tests with both coals. The results are shown in Table 6.8. The AOT appeared to be an even poorer liquefaction medium than NP-5 and was therefore not studied further.

Additional issues that have not been addressed here concern the tendency of surfactants to adsorb strongly at solid/liquid interfaces. Choi et al. (27) have found

Table 6.8
Effect of Surfactants NP-5 and AOT on Coal Conversions[a]

Run No.	Solvent	Conversion (% d.a.f.)		
		Total	Asph.	Oil
		Subbituminous Coal		
62	NP-5	13.3	17.7	-4.5
63	AOT	-9.1	29.9	-67.9
		Bituminous Coal		
64	NP-5	19.9	58.8	-38.9
65	AOT	-10.1	46.9	-57.0

[a] solvent/coal=1.3 (all other conditions same as in Table 6.3).

that coals adsorb surfactants until the available surface area is saturated. It is possible, therefore, that pore blockage by surfactant molecules may adversely affect the transport of reactants in and out of the coal matrix through the pore system. Finally, particles synthesized in microemulsion media are coated with surfactant, thereby lowering the accessibility of reactants to their surface. Catalyst poisoning by surfactant molecules has been observed by other investigators when metallic particles synthesized in microemulsions were tested *in situ* for activity.

6.5 CONCLUSIONS

Nanoscale molybdenum sulfide particles were prepared in microemulsions and tested *in situ* for catalytic activity in the direct liquefaction of a subbituminous and a bituminous coal. No effect of the catalyst on the liquefaction process could be perceived, owing to retrogressive reactions induced by certain components of the particle-synthesis medium, particularly benzyl alcohol. Spectroscopic analysis of the insoluble residues suggested that benzyl alcohol was chemically incorporated into the coal matrix. The results of these tests suggested that meaningful information on the relationship between catalyst dispersion and coal liquefaction yields can be obtained only if the particle synthesis and testing protocols are divorced completely from one another. This is discussed in Chapter 7.

6.6 REFERENCES

1. Weller, S. and Pellipetz, M.G. *Ind. Eng. Chem.* **43**, 1243, 1951.
2. Derbyshire, F.J. *Catalysis in Coal Liquefaction: New Directions for Research*; IEA Coal Research: London, 1988.
3. Derbyshire, F.J., Davis, A., Lin, R., Stansberry, P.G., Terrer, M.T. *Fuel Proc. Technol.* **12**, 127, 1986.
4. Moll, N.G. and Quarderer, G.J. *U.S. Patent 4, 090, 943* May 23, 1978.
5. Moll, N.G. and Quarderer, G.J. *Chem. Eng. Prog.* **75** (10), 46, 1979.
6. Anderson, R.R. and Bockrath, B.C. *Fuel* **64**, 329, 1984.
7. Song, C., Parfitt, D.S., and Schobert, H.H. *Catal. Lett.* **21**, 27, 1993
8. Proceedings of the ACS Div. Fuel Chemistry Symposium on Iron-Based Catalysts for Coal Liquefaction, *Energy & Fuels* **8**, 1994, pp. 2-123.
9. Haber, J. *Pure Appl. Chem.* **63** (9), 1227, 1991.
10. Rao, V.U.S. *Energy & Fuels* **8**, 44, 1994.
11. Sugimoto, T. *Adv. Colloid Interf. Sci.* **28**, 65, 1987.
12. Haruta, M. and Delmon, B. *J. Chim. Phys.* **83**, 1986.
13. Pileni, M.P. *J. Phys. Chem.* **97**, 6961, 1993.
14. Boakye, E., Radovic, L.R., and Osseo-Asare, K. *J. Colloid Interf. Sci.* **163**, 120, 1994.
15. Burgess, C.E., Artok, L., and Schobert, H.H. *Preprints, Amer. Chem. Soc., Div. Fuel Chem.* **36**, 462, 1991.
16. Hooper, R.J., Battaerd, H.A.J., and Evans, D.G. *Fuel* **58**, 134, 1979.
17. de Vlieger, J.J., Kieboom, A.P.G., and van Bekkum, H. *Fuel* **63**, 334, 1984.
18. Neavel, R.C. *Fuel* **55**, 237, 1976.
19. Painter, P.C., Yamada, Y., Jenkins, R.G., Coleman, M.M., and Walker, P.L., Jr. *Fuel* **58**, 293, 1979.

20. Painter, P.C., Starsinic, M., and Coleman, M.M. In *Fourier Transform Infrared Spectrometry*, Vol. 4 (J. Ferraro and L. Basile, Eds.), Academic Press, New York, 1985, p. 169.

21. Silverstein, R.M., Bassler, G.C., and Morrill, T.C. In *Spectrometric Identification of Organic Compounds*, 4th Ed., Wiley, 1963, p. 113.

22. Saini, A.K., Coleman, M.M., Song, C., and Schobert, H.H. *Energy & Fuels* **7**, 328, 1993.

23. Whitehurst, D.D., Mitchell, T.O., and Farcasiu, M. In *Coal Liquefaction - The Chemistry And Technology of Thermal Processes*, Academic Press, New York, 1980, p. 274.

24. Martino, A., Wilcoxon, J.P., Sylwester, A.P., and Kawola, J.S. *Preprints, Amer. Chem. Soc., Div. Fuel Chem.* **38** (1), 20, 1993.

25. Hickey, G.S. and Sharma, P.K. *Chemically Modified Surfaces Symposium* (Blue Bell, PA), Royal Society of Chemistry, Oxford, England, 1993.

26. Hickey, G.S. and Sharma, P.K. Proceedings of the 1993 Direct Liquefaction Contractors' Review Meeting, Department of Energy, Pittsburgh, PA, p. 631.

27. Choi, C.C., Bloomquist, A.A., and Dyrkacz, G.R. *Energy & Fuels* **3**, 38, 1989.

28. Boakye, E., Vaidyanathan, N., Radovic, L.R., and Osseo-Asare, K. *Preprints, Amer. Chem. Soc., Div. Fuel Chem.* **37** (1), 298, 1992.

CHAPTER 7

THE INFLUENCE OF IRON CATALYST PRECURSOR SURFACE AREA ON THE LIQUEFACTION OF A SUBBITUMINOUS COAL

7.1 BACKGROUND

Recently, there has been renewed interest in the use of iron-based catalysts for the direct liquefaction of coal. Provided sufficient sulfur is present, the catalyst precursors transform under liquefaction conditions to pyrrhotite, a non-stoichiometric iron sulfide believed to be the catalytically active phase (1).

However, compared to other coal liquefaction catalysts, e.g., molybdenum, iron is not extremely active. The low activity is believed to be due to poor initial dispersion of the catalyst precursor and a tendency for sintering of the pyrrhotite formed under reaction conditions (2). The introduction of iron catalyst precursors as finely subdivided, high-surface-area powders has been shown to be an effective method of increasing the dispersion (3,4). Additionally, treatment of certain iron catalyst precursors (notably, iron oxide and oxyhydroxide) with sulfate anions has been found to be a highly efficient method of sustaining their initial high dispersion (5,6). The presence of sulfate ions on the catalyst surface is believed to mitigate the loss of surface area that occurs through sintering (5).

7.2 INTRODUCTION

The effect of particle size on catalytic properties is of fundamental importance to understanding the role of catalysts in coal liquefaction. Usually, the extent of catalyst dispersion achieved is inferred from kinetic data. However, this method is inadequate as it does not identify the factors governing the distribution of the catalyst over the coal, or its evolution during reaction (7).

The root cause of this deficiency may be traced back to the catalyst synthesis stage itself. Usually, catalysts are prepared via precipitation and crystallization routes. In their conventional forms, such routes do not offer the potential for controlling the particle size of the solid catalyst precursor produced. However, in recent years, many developments have occurred in the field of inorganic synthesis, which now make it possible to control particle sizes and size distributions (8).

One such development is the use of chemical reactions in microemulsions. Catalyst particles synthesized by this route may be employed in a number of ways. It has already been demonstrated (Chapter 6) that it is important to divorce the catalyst synthesis and testing stages.

Therefore, in this study, iron oxyhydroxide particles were synthesized in microemulsions, separated from the fluid phase, cleaned to remove adsorbed species, dried, and calcined to obtain an iron oxide. The latter was used as a catalyst precursor in the hydroliquefaction of a subbituminous coal. Additional samples of iron oxide were also obtained from other sources. Thus, three particulate iron catalyst precursors of widely differing surface area were employed in liquefaction tests.

7.3 EXPERIMENTAL

7.3.1 Catalysts Used in This Study

The material designated Catalyst I is a powdered ferric oxide obtained from Fisher Scientific Co. Catalyst II was prepared in this laboratory using a microemulsion method as follows: The four-phase system chosen for the synthesis was: aqueous phase, water + $Fe(NO_3)_3$; non-polar phase, cyclohexane; surfactant, NP-5; co-surfactant, benzyl alcohol. $Fe(NO_3)_3$ was solubilized completely by a combination of ultrasonic agitation and manual shaking. Precipitation was achieved by adding NH_4OH. The precipitate was first washed with either tetrahydrofuran (THF) or acetone to remove adsorbed surfactant molecules, then with NH_4OH to remove adsorbed nitrate ions, and finally with distilled water. The precipitate was then dried at room temperature in vacuum and calcined at 450 °C for one hour to yield Fe_2O_3 (as determined by XRD). Catalyst III is a "Super Fine Iron Oxide" (SFIO) obtained from Mach I, Inc., King of Prussia, PA.

For comparison, an aqueous impregnation method (9) was also used to prepare ammonium heptamolybdate (AHM)- and $FeSO_4$-impregnated coal samples. Briefly, either $FeSO_4$ or AHM was dissolved in sufficient distilled water in a flat-bottom flask to give an approximate water-to-coal ratio of 1/1 (v/w), and coal was added to this solution. After stirring for 30 min, the coal was dried in vacuum for 2 h at 110 °C and stored in tightly stoppered glass vials in a desiccator until further use.

7.3.2 Catalyst Characterization

The catalysts were characterized by BET surface area analysis, x-ray diffraction and electron microscopy, as described below.

Surface Area Measurements. Volumetric N_2 (77 K) adsorption measurements were performed on an Autosorb apparatus (Quantachrome Corp.). Fully automatic control of the experimental parameters was utilized. Carefully weighed samples were placed into glass burettes which were then connected to an outgassing unit and dried at 150 °C for 3 hours. Following this, the temperature of the burette was lowered by immersing it in a level-controlled liquid nitrogen bath. After stabilization, its dead volume was determined using UHP helium. The helium was then evacuated and calibrated amounts of gaseous N_2 introduced in the system sequentially. Three points were collected in each case and the data fitted using the BET equation for calculation of the specific surface areas.

X-Ray Diffraction (XRD). X-ray diffraction spectra were collected on a Rigaku diffractometer (using CuKα radiation set at 40 kV and 20 mA) to determine composition information about the catalysts and THF-insoluble residues. Sample powders were pressed flat onto an all-glass holder. A scan rate of 4 degrees (2θ)/min and a step size of 0.010 were used.

Transmission Electron Microscopy (TEM). Sample preparation for TEM experiments consisted in preparing a 0.2 wt% slurry of the catalyst in methanol/ethanol using ultrasonic agitation (approx. 5 min). A very small amount of the dispersion was dropped onto carbon-coated copper grids and the liquid allowed to evaporate. Particle size was determined with a Philips 420 transmission electron microscope operating at 120 kV with a resolution of about 0.6 nm.

7.3.3 Liquefaction Tests

These were conducted in 25 cc microautoclave reactors (tubing bombs) in a preheated fluidized sandbath. A Wyodak subbituminous coal (PSOC 1401) was used in this study (see Table 6.1 for proximate and ultimate analysis). For each reaction, 2 g of coal, 4 g of either tetralin or naphthalene, 20 mg of catalyst, and 40 mg of elemental sulfur were charged into the reactor. Air was removed by repeatedly pressurizing the reactor to 6.9 MPa thrice with hydrogen. Subsequently, the reactor was pressurized to 6.9 MPa (cold) with hydrogen. It was then immersed in the sandbath and agitated at 200 cycles per minute. The reaction temperature of 400 °C was reached in all cases within four minutes of immersion. At the end of 60 min, the reactor was plunged into cold water to quench the reaction.

For tests performed using tetralin as the solvent, after depressurizing the reactor, its contents were rinsed with hexane into a dried soxhlet thimble and extracted overnight under nitrogen. The hexane was removed from the extract by rotary evaporation. The hexane-insoluble residue was then soxhlet-extracted with THF to separate asphaltene from the residue. The THF was removed from the extract by rotary evaporation. Asphaltene and residue were dried for 6 h in vacuum at 100 °C. Conversion was calculated by subtracting the weight of the residue from the weight of the coal and dividing by the d.a.f. weight of the coal. The oil (hexane-soluble) yield was determined by difference from the conversion percentages of the asphaltene and the residue.

For tests performed in naphthalene, the work-up procedure was changed slightly because the products were rather difficult to recover from the reactor using hexane as the wash solvent. Therefore, after depressurization, the contents were rinsed using THF into tared ceramic thimbles and soxhlet-extracted overnight under nitrogen. The THF was removed by rotary evaporation and the extract further

separated into asphaltene and oil by adding hexane to it and sonicating for 10 min. The hexane-soluble oils were separated from the hexane-insolubles (asphaltene) by filtration. Asphaltene and residue were dried for 6 h in vacuum at 100 °C before weighing. Conversions were calculated as usual.

7.4 RESULTS AND DISCUSSION

7.4.1 Catalyst Characterization

Table 7.1 lists the catalyst characterization results. The iron oxide synthesized by the microemulsion method possessed a surface area in excess of 100 m^2/g. The XRD spectra of the as-prepared and calcined powders are shown in Figure 7.1. Comparison against the standard pattern of hematite (10) confirmed that the most abundant phase in the calcined sample is hematite (α-Fe_2O_3). The electron micrograph of the calcined powders is shown in Figure 7.2.

The Super Fine Iron Oxide has been characterized by others (11). It is produced by thermal decomposition of an organo-iron compound (12). Compared to this method, the microemulsion route developed above has one great advantage: it uses cheap and readily available reactants. In all fairness, however, it must be mentioned here that the microemulsion route poses problems of achieving efficient solid-liquid separation. Filtration rates were typically very slow, and material losses due to the number of steps involved were quite high (up to ~ 25%).

Figures 7.3 and 7.4 show the XRD spectra of the THF-insolubles residues from coal liquefied in tetralin and naphthalene, respectively. From Table 7.2, it can be seen that the peak at 2.07 Å (2θ=43.7°) is characteristic of pyrrhotites. Thus, during reaction, all the precursors underwent sulfidation. In Figure 7.4 it can be seen that

Table 7.1
Characteristics of Catalysts Used in this Study.

Designation	Description	Source	Most abundant XRD phase	Surface area (m^2/g)
Cat. I	Iron oxide powders	Fisher	Hematite	16.2
Cat. II	Iron oxide powders	Micro-emulsion method	Hematite	112
Cat. III	Super Fine Iron Oxide	Mach I, Inc.	FeOOH [a]	> 260[a]
Cat. IV	$FeSO_4$ [b]	Fisher	$FeSO_4.7H_2O$	Not applicable

[a] Ref. 11

[b] Impregnated onto coal

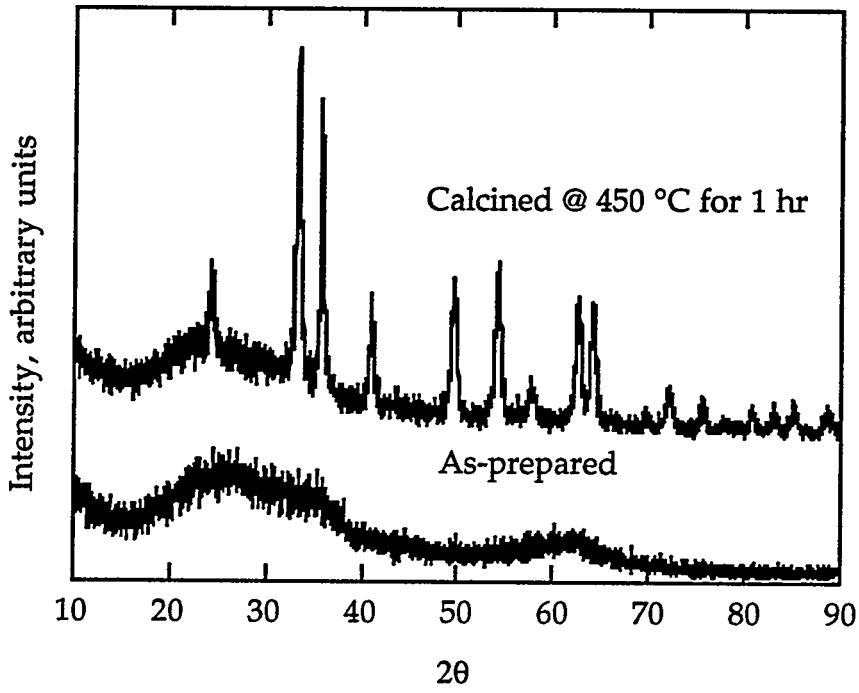

Figure 7.1
X-ray diffraction patterns of as-prepared and calcined forms of particles synthesized in microemulsions.

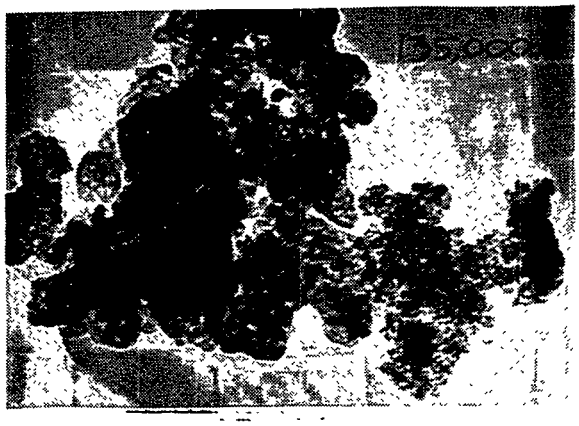

Figure 7.2
Electron micrograph of particles from the calcination of iron oxyhydroxide synthesized in microemulsions.

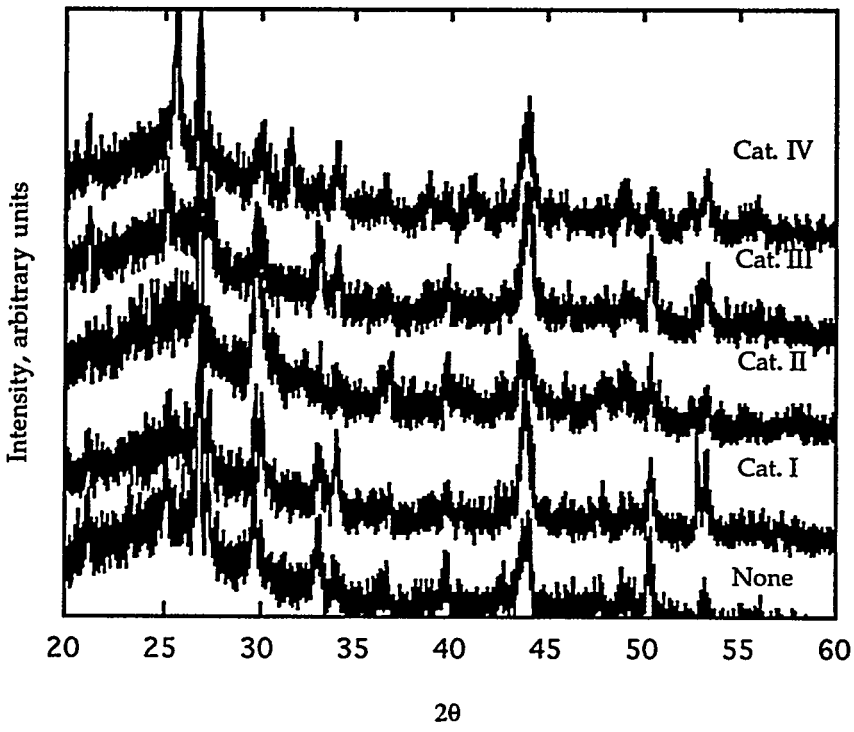

Figure 7.3

X-ray diffraction patterns of the THF-insoluble residues from Wyodak subbituminous coal liquefied in tetralin using various catalysts (see Table 7.1 for nomenclature).

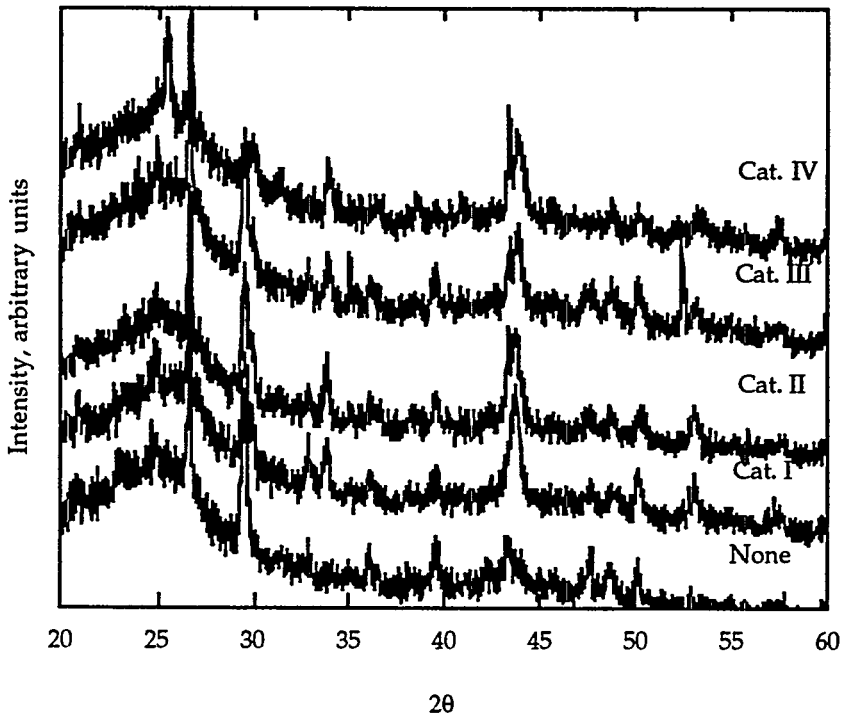

Figure 7.4

X-ray diffraction patterns of the THF-insoluble residues from Wyodak subbituminous coal liquefied in naphthalene using various catalysts (see Table 7.1 for nomenclature).

Table 7.2
Major d-spacings of Various Pyrrhotites (9).

Formula	Major d-spacings			File No.
Fe_7S_8	2.97	2.05	2.06	24-79
$Fe_{1-x}S$	2.64	2.05	2.06	29-723
$Fe_{1-x}S$	2.07	2.98	2.65	20-534
$Fe_{1-x}S$	2.07	2.65	2.99	29-726
$Fe_{1-x}S$	2.07	2.65	2.99	29-726
$Fe_{1-x}S$	2.07	2.65	2.98	25-411
$Fe_{1-x}S$	2.07	2.65	1.72	29-724
$Fe_{1-x}S$	2.06	2.64	2.98	22-1120
Fe_7S_8	2.06	2.64	2.97	24-220

Note: The literature on the iron-sulfur system is voluminous (see, for example, Ward, *Rev. Pure Appl. Chem.* **20**, 175, 1970, as well as Power and Fine, *Minerals Sci. Eng.* **8**, 106, 1976). The nomenclature that has evolved relates the superstructure of iron-sulfur compounds to multiples of the hexagonal NiAs structure. Above 308 °C and below its maximum melting point of 1190 °C, pyrrhotite exhibits a wide homogeneity range as a single solid solution $Fe_{1-x}S$, extending from the most basic pyrrhotite FeS (troilite) to a composition of approximately $Fe_{0.81}S$ (Power and Fine, op. cit.).

In the present work, the x-ray diffraction spectra were collected at room temperature. Therefore, the phases detected in the liquefaction residues are "low-temperature pyrrhotites." Irrespective of the phases found at room temperature in the liquefaction residues, there is evidence that at liquefaction temperature the solid solution $Fe_{1-x}S$ is formed and is the catalytically active phase (Udaya Rao, private communication, 1995).

for catalysts II, III and IV, there are two peaks in the region $43° < 2\theta < 44°$, as opposed to Figure 7.3, where only one peak is observed in the same region for the same catalysts. This suggests that the evolution of the catalyst precursor during liquefaction is dependent on the solvent also. Sulfidation of the catalyst precursor is believed to occur via formation of H_2S from the sulfur-bearing materials – either present in the coal, or added deliberately. Pradhan et al. (6) have pointed out that in the presence of H-donor tetralin, complete conversion of the iron catalyst precursor to the sulfided form occurs via H_2S formation in 5-6 minutes at 400 °C at 1000 psi cold H_2. Artok et al. (9) have reported that a H_2S/H_2 gas mixture is superior to pure H_2 for the transformation of ferrous sulfate to pyrrhotite. Thus, it is proposed that the iron catalyst precursors used in this work may have evolved differently in tetralin and naphthalene due to differences in H_2S availability.

7.4.2 Activities of the Iron Oxides

The conversion data in tetralin are shown in Figure 7.5. Apparently, the iron oxide catalyst precursors did not display any statistically significant differences in either total conversions or conversion to oils. Even with respect to the uncatalyzed (base) case, there are no differences. This last observation suggested that the baseline conversion of the coal was already close to the maximum before addition of catalyst. (The unreactive coal macerals are not expected to liquefy.) Evidently, the liquefaction reaction was not under kinetic control in any of these cases.

Figure 7.6 shows the results obtained using non-donor naphthalene as the solvent. Once again, the three iron oxide catalyst precursors did not exhibit significant differences either in total conversion or conversion to oils. However, relative to the base case, on average they gave approximately 15% higher total

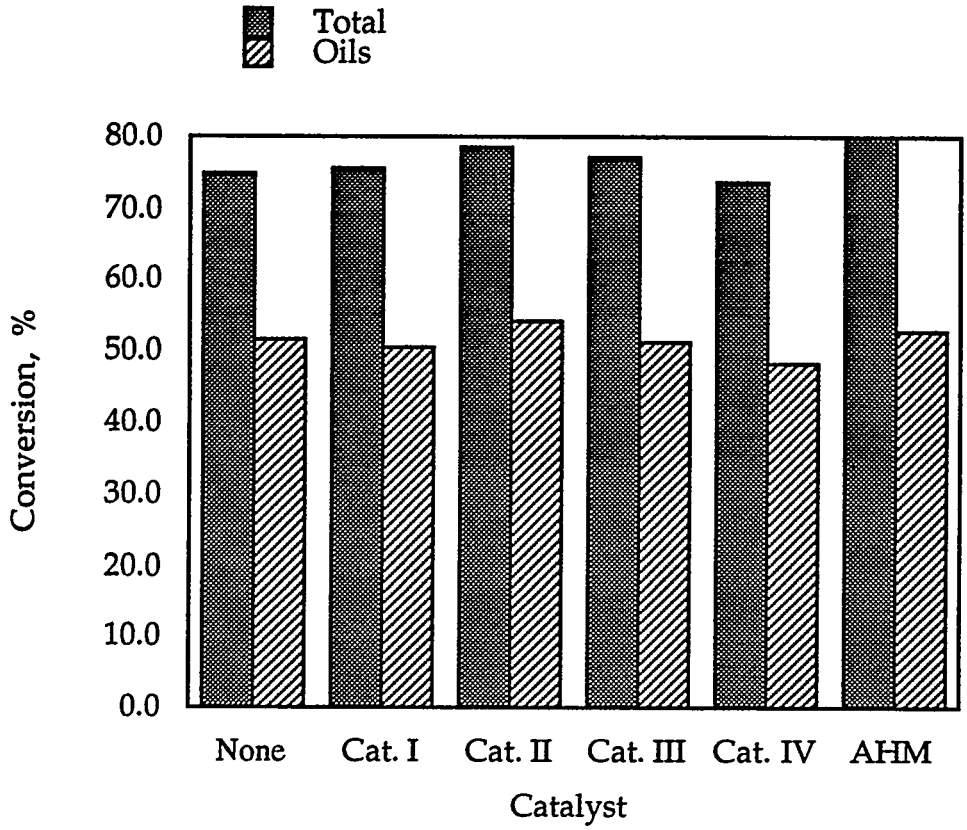

Figure 7.5
Conversion data for Wyodak subbituminous coal liquefaction in tetralin using various catalysts (see Table 7.1 for nomenclature).
(T=400 °C, P=1000 psi H_2 (cold), t=1 h, 0.7 wt% Fe catalyst, 1/2 catalyst to elemental sulfur, 2/1 solvent to coal.)

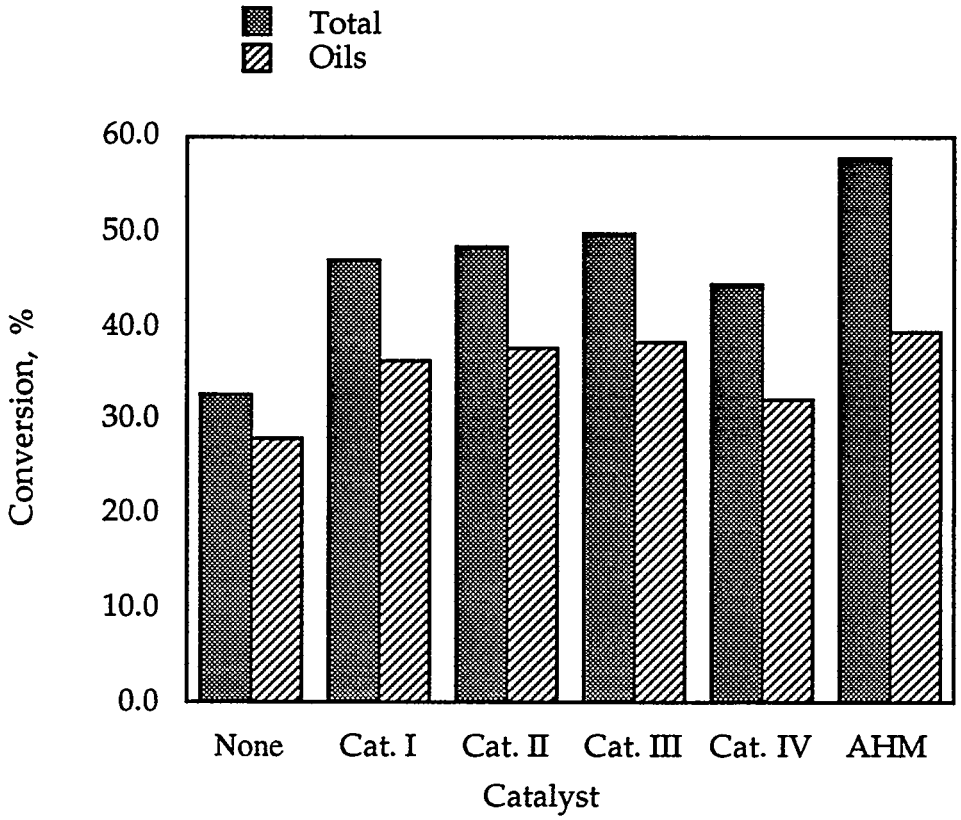

Figure 7.6
Conversion data for Wyodak subbituminous coal liquefaction in naphthalene using various catalysts (see Table 7.1 for nomenclature).
(T=400 °C, P=1000 psi H_2 (cold), t=1 h, 0.7 wt% Fe catalyst, 1/2 catalyst to elemental sulfur, 2/1 solvent to coal.)

conversions, and about 10% greater conversion to oil. The higher activity of molybdenum catalyst is also strikingly evident from the figure, as expected.

Intuitively, it might be expected that a highly dispersed iron precursor will transform to a highly dispersed pyrrhotite under liquefaction conditions. However, these results belie that expectation. Even a sixteen-fold increase in the surface area of the catalyst precursor (compare catalysts I and III) produced no significant increase in conversions. It would appear from this that the dispersion of the active form of the catalyst was independent of the (initial) dispersion of the catalyst precursor. Similar results with iron catalysts have been reported recently by Cugini et al. (13). They point out that, for iron systems, the transformation of highly dispersed catalyst precursors to highly dispersed catalysts is not guaranteed. Subsequent to activation, small catalyst particles agglomerate into larger ones, resulting in loss of activity (13, 14). Therefore, it is proposed that, during the reaction in naphthalene, the particle sizes of the iron oxide precursors used in this work were not preserved, resulting in poorly dispersed catalysts with very similar activities.

It is entirely conceivable (and probably true) that a similar phenomenon occurred during liquefaction in tetralin. However, the lack of any significant differences between the uncatalyzed and catalyzed runs makes this redundant.

7.5 CONCLUSIONS

The results of the reactions in tetralin make it evident that, to clearly discern the effect of added catalyst, it is important to work in a regime where its effects are stronger than those of temperature and solvent. From the reactions in naphthalene, it appears that iron catalyst precursors do not transform topotaxially into the active phase under liquefaction conditions. Thus, the surface area of the

precursor is not preserved after its transformation to pyrrhotite. This underscores the importance and benefit of modifying the surface of the catalyst in order to prevent sintering (5,6).

7.6 REFERENCES

1. Montano, P.A. and Granoff, B. *Fuel* **59**, 214, 1980.
2. Cugini, A.V., Utz, B.R., Krastman, D., and Hickey, R.F. *Preprints, Amer. Chem. Soc., Div. Fuel Chem.* **36** (1), 91, 1991.
3. Andrès, M., Charcosset, H., Chiche, P., Davignon, L., Mariadassou, D.G., Joly, J., and Prégermain, S. *Fuel* **62**, 69, 1983.
4. Bacaud, R. *Fuel Proc. Technol.* **28**, 203, 1991.
5. Pradhan, V.R., Tierney, J.W., and Wender, I. *Energy & Fuels* **5**, 497, 1991.
6. Pradhan, V.R., Hu, J., Tierney, J.W., and Wender, I. *Preprints, Amer. Chem. Soc., Div. Fuel Chem.* **38** (1), 8, 1993.
7. Derbyshire, F.J. *Catalysis in Coal Liquefaction: New Directions for Research,* IEA Coal Research, London, 1988.
8. Sugimoto, T. *Adv. Coll. Interf. Sci.* **28**, 65, 1987.
9. Artok, L., Schobert, H.H., and Davis, A. *Fuel Proc. Technol.* **32**, 87, 1992.
10. Joint Committee on Powder Diffraction Standards. Mineral Powder Diffraction File, p. 337.
11. Zhao, J., Feng, Z., Huggins, F.E., Shah, N., and Huffman, G.P. *Preprints, Amer. Chem. Soc., Div. Fuel Chem.* **38** (1), 196, 1993.
12. Kosowski, B.M. (Mach I, Inc.), personal communication.
13. Cugini, A.V., Krastman, D., Martello, D.V., Frommell, E.F., Wells, A.W., and Holder, G.D. *Energy & Fuels* **8**, 83, 1994.

14. Mariadassou, D.G., Besson, M., Brodzki, D., Charcosset, H., Huu, T., and Varloud, J. *Fuel Proc. Technol.* **12**, 143, 1986.

CHAPTER 8

ROLE OF COAL SURFACE CHEMISTRY IN IMPREGNATION WITH CATALYST

8.1 BACKGROUND

8.1.1 The Electrified Interface on Colloidal Surfaces

Solid surfaces possess charge or electron imbalances due to the incomplete coordination of their outermost atoms. These imbalanced sites have a tendency to interact with surrounding molecules so as to lower the electrical differences between the surface and bulk of the solid. In solution, the remaining surface charges will attract or repel ions and polar molecules. Additional charges on the surface may develop by dissociation of surface functional groups or by adsorption of ions from solution. The result is that the surface and the liquid develop equal but opposite charges, giving rise to an electrical double layer (1).

The surface charge on a microscopic particle can be measured in terms of its mobility in an electric field. There exists an electrical potential difference between the outermost surface of each moving particle and the bulk of the suspending liquid, referred to as the zeta potential. Application of a D.C. potential across the suspension will induce the movement of the particle – relative to the liquid – with a velocity proportional to its zeta potential. This effect is termed electrophoresis.

8.1.2 Development of Electric Charge at the Coal-water Interface

An electric charge develops on the surface of coal when it is immersed in water. The development of charge at the coal-water interface has been ascribed to the dissociation of surface oxygen functional groups such as –COOH and –COH (2), and surface mineral impurity groups such as Si–OH or Al–OH (3). The dissociation process and thus the magnitude and sign of the charge are pH-dependent, according to the general scheme shown below (3):

$$XOH_2^{+}{}_{surf} \overset{H^+}{\Leftrightarrow} XOH_{surf} \overset{OH^-}{\Leftrightarrow} XO^-{}_{surf}$$

Positive Surface	Neutral Surface	Negative Surface

where XOH_{surf} represents a coal surface group or a surface impurity group.

8.2 INTRODUCTION

8.2.1 Importance of Coal Surface Charge

The surface charge properties of coals have been the subject of numerous studies, particularly because of their influence on the stability of coal-water slurries (4). Of late, however, the effect of coal surface charge on the adsorption of ions from metal salt solutions has become a topic of some interest (5). This is because a popular technique for producing coal conversion catalysts involves impregnating the coal with an aqueous solution of the catalyst precursor. Thus, the magnitude and sign of the charge on a coal surface will affect the uptake of positively and

negatively charged metal species. Similar studies on the role of carbon surface charge in the preparation of carbon-supported catalysts have appeared in the literature (15).

8.2.2 Coal Liquefaction Catalysts

Unsupported, dispersed-phase catalysts have been found to be active for coal liquefaction (6). One method of introducing such catalysts is by impregnating them onto coal from aqueous solutions. The effectiveness of this method vis-a-vis others was first demonstrated in 1951 by Weller and Pelipetz (7).

However, aqueous impregnation may not be a practical method of producing highly dispersed coal liquefaction catalysts on a large scale. Its unattractiveness is due chiefly to the considerable expense and difficulty that would be associated with impregnating tons of powdered coal with any catalyst. One way to overcome this problem is to treat only a fraction of the total coal feed with the catalyst precursor. This fraction could then be mixed with the rest of the coal prior to the reaction. Such a "spiking" approach has been developed recently by Cugini et al. for FeOOH impregnated onto coal (8). Their results are reproduced in Figure 8.1. They concluded that "there appears to be a minimum quantity of impregnated coal, between 10 wt% and 20 wt%, necessary to achieve optimum catalytic effect".

Clearly, this presents a strong case for paying closer attention to the details of the catalyst loading procedure. The concept of exploiting the surface chemistry of a carrier to achieve higher catalyst dispersion via increased metal-support interactions during metal loading from solution is not a new one. It has been applied by others to the preparation of Pt/TiO_2 (9), Pt/RuO_2 (10) and MoS_2/C (15) catalysts.

In this study, the surface charge on a Wyodak subbituminous coal was monitored as a function of pH. The effect of mineral matter on the surface charge

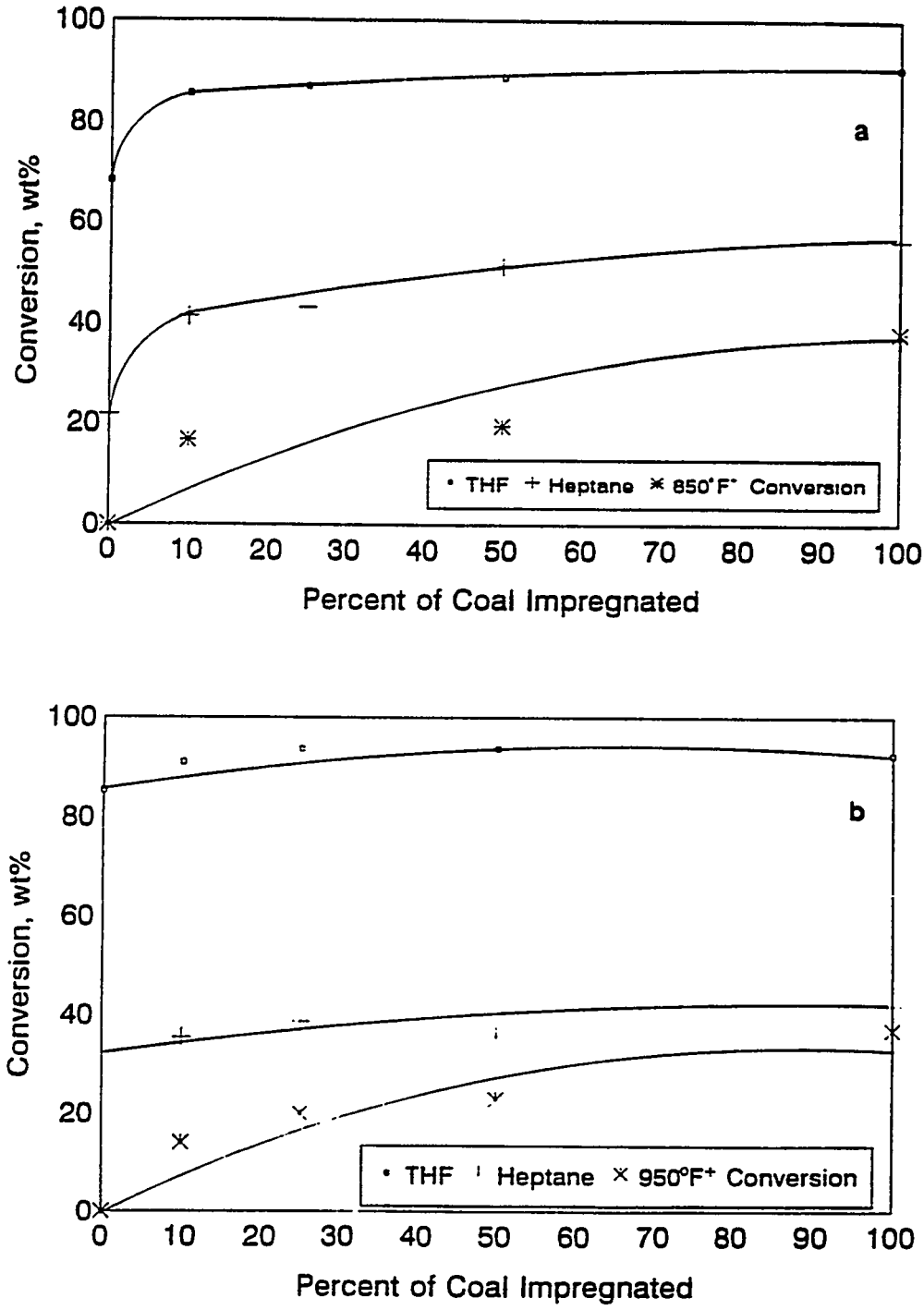

Figure 8.1
Effect of spiking (a) Black Thunder subbituminous coal (b) Illinois No. 6 bituminous coal (semi-batch operation, 1 h; 2/1 solvent (V-1074) to coal; 425°C; 2500 psig (H_2/H_2S), Ref. 6).

was also examined. The influence of coal surface charge on the adsorption of molybdate ion from ammonium heptamolybdate solutions was investigated. Finally, the implications of these studies for achieving high dispersion of molybdenum catalyst on coal via impregnation from aqueous ammonium heptamolybdate solution were examined.

8.3 EXPERIMENTAL

8.3.1 Demineralization of Coal

Table 8.1 shows the proximate and ultimate analysis for the coal investigated. The demineralization procedure employed was similar to that used by Brown et al. (11). A 5 g coal sample was warmed at 50 °C in 50 mL of conc. HF for 1 hour. The acid was filtered off and the procedure repeated twice for conc. HCl. The demineralized coal was thoroughly washed in distilled water and dried. It has been reported (11) that the residual ash yield following this procedure is typically less than 1 wt%.

8.3.2 Zeta Potential Measurements

Slurries for the electrokinetic measurements were prepared by agitating 25 mg of coal with 250 mL of 10^{-2} M KNO_3 solution (indifferent electrolyte) in Nalgene bottles for 24 hrs. Zeta potential measurements were made using a Zeta-Meter System 3.0 unit (Zeta-Meter, Inc.). Hydrochloric acid and NH_4OH were used to control the pH in the acidic and basic regions. All the experiments were conducted at room temperature ($\approx$ 25 °C).

Table 8.1

Data for Coal Sample.

Penn State Sample Bank No.	**PSOC-1401**
Seam	Canyon-Top
State	Wyoming
Country	USA
ASTM Rank	Subbit. B
Moisture (as received, wt%)	16.33
Ash (dry, wt%)	5.72
Elemental Composition	
Carbon	72.70
Hydrogen	4.62
Nitrogen	1.07
Sulfur (organic)	0.28
Oxygen (by difference)	21.38
Calcium[a]	1.20
Iron[a]	0.23
Potassium[a]	0.01

[a] dry coal basis

8.3.3 Adsorption Studies

To a 0.5 g sample of coal in a 40-mL Nalgene bottle was added 25 mL of aqueous ammonium heptamolybdate solution containing $5x10^{-2}$ mol/L of molybdenum metal. After pH adjustments with HCl or NH_4OH solution, the slurries were mechanically shaken for 24 hours at room temperature (≈ 25 °C). Aliquots were then removed for Mo and Fe analysis by inductively coupled emission plasma spectrophotometry (Leeman Labs PS3000UV) and the equilibrium pHs were measured.

8.3.4 Coal Impregnation with Catalyst

The coal was first crushed to pass a 60 mesh sieve. Impregnation with ammonium heptamolybdate (1% Mo (d.a.f), expressed as elemental Mo) was accomplished as follows: The Mo salt was dissolved in sufficient distilled water in a flat-bottom flask to give an approximate water-to-coal ratio of 1/1 (v/w), and coal was added to this solution. Several samples were prepared in this fashion, the slurry pH being adjusted in some cases using either conc. HCl or conc. NH_4OH. After stirring for 30 min, the slurry pH was measured, following which the coal was dried in vacuum for 2 h at 100 °C, removed and stored in tightly stoppered glass vials until further use.

8.3.5 Liquefaction Tests

These were conducted in 25 cc microautoclave reactors (tubing bombs) in a preheated fluidized sandbath. For each reaction, 1.5 g of coal, 1.5 g of tetralin, and 25 mg of CS_2 (ca. 2.2 times the amount of sulfur required to convert all the Mo to

MoS_2) were charged into the reactor. Air was removed by repeatedly pressurizing the reactor to 6.9 MPa, once with nitrogen and twice with hydrogen. Subsequently, the reactor was pressurized to 6.9 MPa (cold) with hydrogen. It was then plunged into the sandbath and agitated at 200 cycles per minute. Reaction temperature and residence time were 350 °C and 30 minutes, respectively. At the end of this time, the reactor was plunged into cold water to quench the reaction. After depressurizing the reactor, its contents were rinsed with hexane into a dried soxhlet thimble and extracted overnight under nitrogen. The hexane was removed from the extract by rotary evaporation. The hexane-insoluble residue was then soxhlet-extracted with THF to separate asphaltenes from the residue. The THF was removed from the extract by rotary evaporation. Asphaltenes and residue were dried for 6 h and 2 h, respectively, in vacuum at 100 °C. Conversion was calculated by subtracting the weight of the residue from the weight of the coal and dividing by the daf weight of the coal.

8.4 RESULTS AND DISCUSSION

The surface charge was monitored as a function of pH. Figure 8.2 shows the results obtained. The scatter in the data is typical for coal particles and is attributed to surface heterogeneity. The as-received coal is negatively charged over the entire range of pH studied. Similar results with another subbituminous coal (PSOC 1485) have been reported (5). Beyond pH $\approx$ 6, there is little pH dependence of zeta potential. This has been ascribed to the solubility of humic acids for which OH^- and H_3O^+ are not the potential-determining ions (2). After demineralization, the zeta potential-pH curve shifts to more positive values. This seems to indicate that

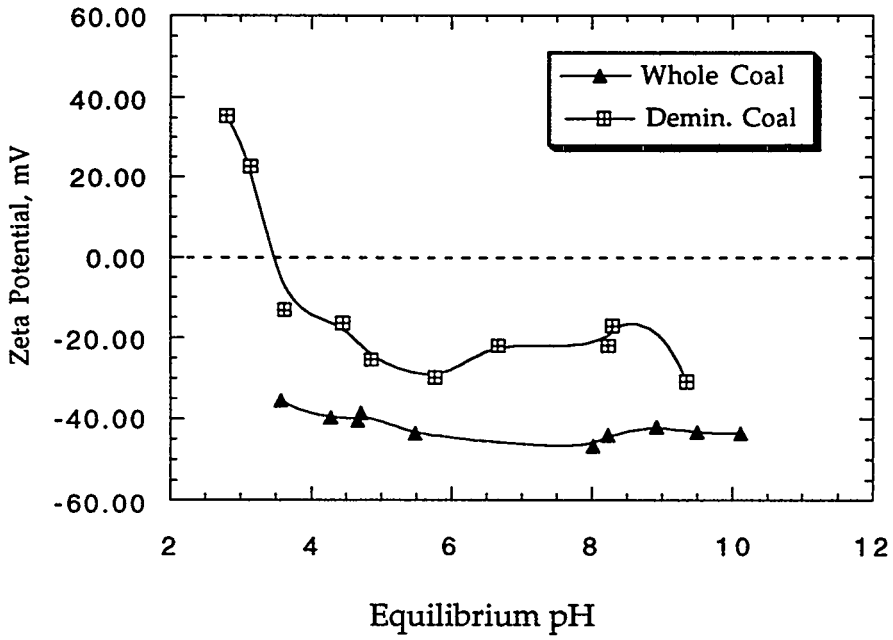

Figure 8.2
Dependence of zeta potential on coal slurry pH for Wyodak subbituminous coal.

mineral matter plays a significant role in determining the charge on a coal surface, as suggested by others (3, 12).

The uptake of molybdate ion by the as-received coal is shown in Figure 8.3. Molybdenum adsorption is favored at very low pHs, while it is negligible in alkaline solutions. A similar trend for a Montana Rosebud subbituminous B coal (PSOC 1485) has been reported by Abotsi et al. (5). However, the extent of molybdate adsorption observed in this work is somewhat lower than that found by Schroeder et al. (13) for a Wyodak subbituminous coal from the Argonne Premium Coal sample bank. This could be due to differences in experimental procedure (use of buffered solutions, lower molybdate concentrations, etc.) and/or coal composition. Interestingly, the strong pH-dependence of Mo uptake (Fig. 8.3) does not correlate well with the fact that the surface charge on the as-received coal is quite insensitive to solution pH (Fig. 8.2). Thus, the mechanism of molybdate adsorption from solution requires further study.

Coal samples impregnated with AHM at various pHs were liquefied in tubing bomb microautoclaves. Table 8.2 shows the conversion data. The reproducibility of the data was typically ± 2 wt%. It is seen from Run 78 that when the impregnating solution pH is rendered highly acidic using HCl, the oil yield decreases drastically by about a factor of four relative to the unadjusted case (Run 79, pH=5.0). On the other hand, the total conversion is nearly the same in both cases. Evidently, impregnation from highly acidic solutions has an adverse effect on the hydrogenation activity of Mo catalyst, despite the large uptake of molybdate ion by coal at low pH (Fig. 8.3). It is possible to explain this effect based on the work of Dun et al. (14) and Solar et al. (15). In both studies, no major differences in the thiophene hydrodesulfurization activity of Mo/C catalysts with varying pH were found, despite the enhancement in catalyst dispersion expected from a consideration of more favorable carbon-catalyst interactions in highly acidic AHM solutions. Solar et al.

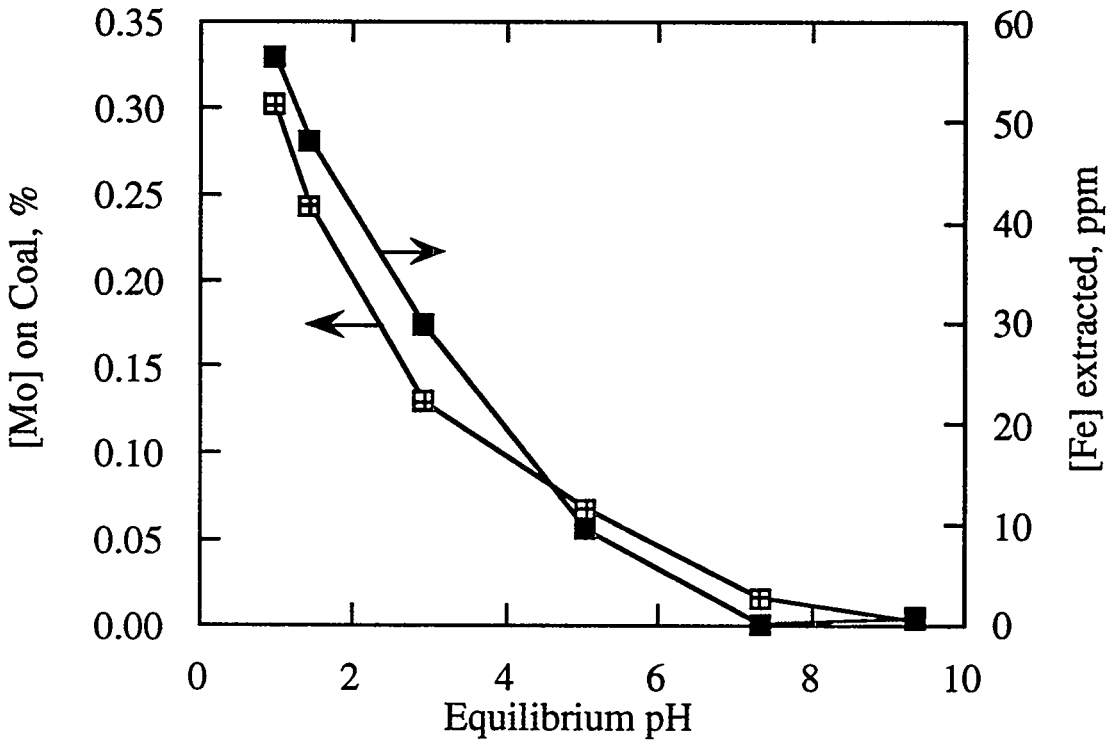

Figure 8.3
Effect of coal slurry pH on molybdenum uptake and iron extraction.

Table 8.2

Conversion Data For As-Received Wyodak Subbituminous Coal Impregnated with Mo catalyst from pH-adjusted AHM Solutions.

(T=350 °C, P= 1000 psi (cold) H_2, t=30 min, 1:1 Tetralin to Coal, CS_2 Added as Sulfiding Agent, 1 wt% Mo Catalyst.)

Run No.	Final pH of slurry	Catalyst present?	Conversion (% d.a.f.)		
			Total	Asph.	Oil
78	1.1	Yes	41.8	36.7	5.1
90	2.8	Yes	26.0	23.4	2.6
91	3.9	Yes	23.3	19.1	4.2
79	5.0	Yes	38.3	16.5	21.8
80	10.1	Yes	24.2	11.5	12.7
81	1.1	No	34.9	26.6	8.3
83	n/s*	No	27.2	16.0	11.2

* not slurried

(15) invoked the adsorption model of Cruywagen and de Wet (16) to explain this observation. According to them (Solar et al.), the enhanced dispersion due to electrostatic attraction is offset by the polymerization of molybdenum oxyanions at low pH. Polymeric Mo species may not adsorb strongly on the support, and thus be more prone to sintering upon catalyst activation. Similarly, weak interactions between the coal surface and polymeric Mo species formed at acidic pHs may have resulted in loss of activity via sintering during reaction. The higher total conversion observed in Run 78 is tentatively attributed to the formation of chlorinated mineral species during catalyst impregnation via reaction of the coal mineral matter with the HCl used to adjust slurry pH. Chlorides such as $FeCl_3$ are known to be active coal dissolution catalysts (17). An additional test (Run 81) conducted without AHM but with the slurry pH adjusted to be 1.1 using HCl lends support to this argument. The extent of iron extraction from the coal at various pHs is also shown in Fig. 8.3, and constitutes evidence for the leaching of mineral matter by HCl added to the slurry.

Impregnation from highly alkaline solutions has an extremely deleterious effect on catalytic activity (Run 80). There is virtually no difference between this run and the uncatalyzed one (Run 83). This correlates well with the negligibly small uptake of molybdate ion from highly alkaline AHM solutions (Fig. 8.3).

8.5 CONCLUSIONS

The as-received subbituminous coal is negatively charged over the whole range of pH studied. Mineral matter influences the surface charge properties of coal.

The study of coal-molybdenum interactions in aqueous solutions (and consequently of their effects in catalysed liquefaction experiments) is complicated by

two factors. First, the mechanism of molybdate interaction with the coal surface is not clear, presumably because the nature of the molybdenum species changes with changes in total concentration of Mo (VI) and pH (13). Second, attempts to control the surface properties using hydrochloric acid result in the extraction of certain mineral components into solution. Some of these components – in their chlorinated forms – may be catalytically active for coal dissolution, and thus confound the effect of *added* catalyst.

8.6 REFERENCES

1. *Electrical Phenomena at Interfaces: Fundamentals, Measurements and Applications* (A. Kitahara and A. Watanabe, Eds.), Marcel Dekker, New York, 1984.
2. Quast, K.B. and Readett, D.J. *Adv. Colloid Interf. Sci.* **27**, 169, 1987.
3. Siffert, B. and Hamieh, T. *Colloids Surf.* **35**, 27, 1987.
4. Laskowski, J.S. and Parfitt, G.D. In *Interfacial Phenomena in Coal Technology* (Botsaris, G.D., Glazman, Y.M., Eds.), Marcel Dekker, New York, 1988, p. 279.
5. Abotsi, G.M.K., Bota, K.B., and Saha, G. *Energy & Fuels* **6**, 779, 1992.
6. Utz, B.R., Cugini, A.V., and Frommell, E.A. In *Novel Materials in Heterogeneous Catalysis* (Baker, R.T.K. and Murrell, L.L., Eds.), American Chemical Society, Washington, DC, 1990, p. 289.
7. Weller, S. and Pellipetz, M.G. *Ind. Eng. Chem.* **43**, 1243, 1951.
8. Cugini, A.V., Krastman, D., Lett, R.G., Ciocco, M.V., and Erinc, J.B. Proceedings of the 1993 Direct Liquefaction Contractors' Review Meeting, Department of Energy, Pittsburgh, PA, p. 485.

9. Jaffrezic-Renault, N., Pichat, P., Foissy, A., and Mercier, R. *J. Phys. Chem.* **90**, 2733, 1986.

10. Duonghong, D., Borgarello, E., and Gratzel, M. *J. Am. Chem. Soc.* **103**, 4685, 1981.

11. Brown, H.R., Durie, R.A., and Schafer, H.N.S. *Fuel* **38**, 295, 1959.

12. Siffert, B. and Hamieh, T. *Colloids Surf.* **61**, 83, 1991.

13. Schroeder, K.T., Bockrath, B.C., and Tate, M.L. *Preprints, Amer. Chem. Soc., Div. Fuel Chem.* **38**, 512, 1993.

14. Dun, J.W., Gulary, E., and Ng, K.Y.S., *Appl. Catal.* **15**, 247, 1985.

15. Solar, J.M., Derbyshire, F.J., de Beer, V.H.J., and Radovic, L.R. *J. Catal.* **129**, 330, 1991.

16. Cruywagen, J.J. and de Wet, H.F. *Polyhedron* **7**, 547, 1988.

17. Miller, R.L., Shams, K., and Baldwin, R.M. *Preprints, Amer. Chem. Soc., Div. Fuel Chem.* **36** (1), 1, 1991.

CHAPTER 9

RESEARCH SUMMARY AND SUGGESTIONS FOR FUTURE WORK

9.1 SUMMARY

Although the microemulsion fluid phase has been used by many researchers to make a wide spectrum of particulate materials, most of the emphasis has been to demonstrate the success of synthesizing specific materials in this medium. Ours is thus one of a limited number of studies that have been conducted on the influence of the microemulsion properties (e.g., dynamics, occupancy number and nature of water) on the evolution of the materials in the surfactant aggregates.

The synthesis of MoS_3 was of primary interest. Nanosize molybdenum sulfide particles were prepared by acidification of ammonium tetrathiomolybdate in the water cores of nonionic microemulsions. The physico-chemical origins of the observed trends in particle size, size distributions, and dispersion stability were also studied. In particular, the relationships between the important microemulsion properties (e.g., the presence of free water molecules in the microemulsion fluid phase, the water-to-surfactant molar ratio, and tetrathiomolybdate occupancy number) were studied. The inverse micelles in cyclohexane (3-30 nm) were stabilized by the nonionic surfactants polyoxyethylene(5)nonylphenyl ether (NP-5), and polyoxyethylene tert-octylphenyl ether (TX-100)) and their mixtures. A unique method for extractive dissolution of ammonium tetrathiomolybdate into the water cores of the inverse micelles was developed. This method increases the reactant loading in the w/o microemulsions which is desirable if high catalyst loading is needed in coal liquefaction.

The state of the solubilized water molecules in the microemulsions (i.e., whether the water molecules are free or bound to the surfactant polar headgroups) was investigated with the aid of fluorescence spectroscopy. The water-to-surfactant molar ratio (R) at which free water appears in the microemulsion fluid phase (i.e., R_c) was obtained as $R_c = 1.75$ and $R_c = 4$, respectively, for the NP-5/cyclohexane/water and TX-100/cyclohexane/water microemulsions. For the 2/1 NP-5/TX-100/cyclohexane/water microemulsion, free water was deduced to exist at R = 2.5. Comparison of the molybdenum sulfide particles synthesized with the TX-100 and the 2/1 NP-5/TX-100 microemulsions shows that water-induced particle aggregation occurs at $R = R_c$. The phenomenon of water-induced aggregation was thus found to play a critical role in the particle growth process. To the best of our knowledge, this relationship between the presence of free water molecules and the dispersion stability of microemulsion-synthesized nanoparticles has been established for the first time.

A major controversy in the precipitation literature concerns the question of whether metal oxides and sulfides grow by monomer addition or by nuclei aggregation. An attempt was thus made to distinguish between the relative contributions of the monomer addition and particle aggregation growth mechanisms. The Poisson statistical distribution law was used to predict the number of micellar aggregates containing at least 2 tetrathiomolybdate ions. From the number of micellar aggregates in a fixed volume of microemulsion and the Poisson expression, the theoretical number of nuclei was calculated. By comparing the theoretical number of nuclei and the experimental number of particles, valuable predictions of growth mechanisms were then made. In general, it was found that molybdenum sulfide particle aggregation was important when $[MoS_4^{2-}] > 6.4 \times 10^{-6}$ M and when $R > R_c$.

The nucleation and growth processes of molybdenum sulfide in the NP-5/cyclohexane/water microemulsion were found to depend also on the molybdate occupancy number. For $[MoS_4^{2-}] = 3.2x10^{-6}$ M, the particle size was found to exhibit a minimum at R~2. For R < 2, the decrease in particle size with increasing R was attributed to an increase in the average occupancy number, and the consequent increase in the nucleation rate. It was also found that at constant R (R = 1), a doubling of the occupancy number resulted in a decrease in particle size. For R > 2, the increase in particle size with R was rationalized in terms of molybdenum sulfide particle aggregation which is related to the presence of free water molecules in the microemulsion fluid phase.

The effect of the average occupancy number on molybdenum sulfide particle size was further investigated by using a wider range of thiomolybdate concentration ($3.2\text{-}11.2x10^{-6}$ M). Also studied was the effect of the variation of sulfuric acid concentration on the molybdenum sulfide particle size. These investigations therefore examined the effects of reactant concentrations on the particle formation process. At R = 1, and $[H_2SO_4] = 1.3x10^{-3}$ M, both the particle size and the size distribution decreased with molybdate concentration to $[MoS_4^{2-}] = 4.8x10^{-6}$ M and then increased as molybdate concentration increased further. This result was rationalized using a quantitative model which is based on the monomer addition mechanism of growth. The decrease in particle size was attributed to the increasing nucleation rate of molybdenum sulfide particles which is due to the increasing occupancy number as the concentration of the thiomolybdate species was increased. For $[MoS_4^{2-}] > 4.8x10^{-6}$ M, although the occupancy number increased with the thiomolybdate concentration, the number of nuclei was found to be quasi-constant. Therefore it was concluded that, with further increase in MoS_4^{2-} concentration, a greater number of monomers not utilized in the nucleation step became available to add onto the primary particles; hence the particle size increased. Furthermore, the

TEM micrographs of the molybdenum sulfide particles synthesized at high thiomolybdate concentrations (e.g., $[MoS_4^{2-}] > 8x10^{-6}$ M), showed evidence of a bimodal distribution; this suggests that molybdenum sulfide particles also grow by aggregation. Regarding the effect of acid concentration, this study showed that the particle size remains essentially unchanged in the range $[H_2SO_4] = 0.65\text{-}1.3x10^{-6}$ M, but becomes larger at $[H_2SO_4]=2.6x10^{-6}$ M. The latter finding was attributed to a decrease in the occupancy number (caused by a decrease in droplet size).

The above analysis of particle size variations with changes in R and reactant concentrations demonstrates the usefulness of the average occupancy number as a fundamental particle synthesis parameter.

The effect of the synthesis protocol on the size of molybdenum sulfide particles was also studied. If aggregation is to be limited, the particles must be synthesized in the one-phase microemulsion domain. At relatively high water-to-surfactant molar ratios (R = 3.5-4.5), the particle size and polydispersity were found to increase with the synthesis method in the following order: acid-solubilized microemulsion plus aqueous tetrathiomolybdate < acid-solubilized microemulsion plus tetrathiomolybdate-solubilized microemulsion < tetrathiomolybdate-solubilized microemulsion plus aqueous sulfuric acid. On solubilizing tetrathiomolybdate-containing sodium hydroxide before adding aqueous sulfuric acid, the microemulsion phase-separated at a temperature of 50 °C into excess aqueous tetrathiomolybdate and dispersed droplets of aqueous tetrathiomolybdate solution stabilized by surfactant film in cyclohexane. The particles made in the phase-separated microemulsion were large, polydispersed, and had an irregular morphology, which is attributed to concurrent growth of particles in the water cores and in the conjugate aqueous phase. On the other hand, when the aqueous sulfuric acid was solubilized before the addition of aqueous ammonium tetrathiomolybdate,

there was no phase separation. The phase-separation-related particle aggregation was thus avoided and the particles formed were relatively small.

There are two approaches to the optimization of dispersion of unsupported coal liquefaction catalysts. Both were pursued in this study. In the conventional aqueous impregnation route, the catalyst preparation procedure was adjusted to the surface chemistry of the coal used. The results suggested that there are limits to this approach; the resulting catalyst dispersion (and activity) appears to be a complex function not only of the electrochemistry of the coal surface, but also on mineral matter effects and changes in metal speciation with pH. Using the microemulsion synthesis route, it was found that successful catalyst synthesis requires an important compromise in the selection of the microemulsion components in general, and surfactants and/or cosurfactants in particular. On one hand, they must prevent extensive particle growth; on the other hand, they must not act as poisons and/or promoters of retrogressive reactions. This study has shown that the latter task requires additional research efforts.

9.2 SUGGESTIONS FOR FUTURE WORK

In the work presented here, the molybdenum sulfide particles were characterized using the following techniques: chemical analysis, dynamic light scattering, transmission electron microscopy, ultraviolet/visible spectroscopy, differential thermal analysis and thermogravimetric analysis. Additional characterization of the particles is worth pursuing. It has been shown that particles which grow by aggregation are not smooth and are porous. In this study it has been established that at $R > R_c$ the molybdenum sulfide particles grow by aggregation. Thus an investigation of the effect of R on the porosity and roughness of the particle

surfaces might be helpful in distinguishing between particle growth due to aggregation and monomer addition.

Results from coal liquefaction studies show that surfactant and/or cosurfactant molecules adsorbed on the catalyst particle surface reduce catalytic activity. Thus efficient methods for separation (or "harvesting") of particles from the microemulsion fluid phase need to be developed. Possible methods are the following:

(a) Heat the catalyst-loaded microemulsion above the solubilization point to destabilize the microemulsion droplets and clean the harvested particles with tetrahydrofuran.

(b) Add a destabilizer (e.g., acetone, tetrahydrofuran) that will preferentially interact with the surfactants and hence free the surfactant molecules from the particle surfaces. Thus harvested particles can be cleaned with THF.

(c) Make the surface of particles hydrophobic by 'capping' the surface with organometallic molecules. The organic molecules should act as a barrier to aggregation. Due to their hydrophobic nature, the particles will leave the water pools and can therefore be harvested.

(d) React the harvested particles with ozone to oxidize the surfactants.

(e) Heat-treat the extracted particles at 200-400 °C to remove the surfactants by thermal decomposition.

APPENDIX I

SAMPLE CALCULATIONS

Once the water-to-surfactant molar ratio and the electrolyte concentration are fixed, the weight of catalyst produced per unit volume (or weight) of solution is automatically fixed. For example, consider the following calculation:

Micellar solution	0.4 M NP-5/tetralin/benzyl alcohol/water
$R = [H_2O]/[NP\text{-}5]$	2.0
[ATTM]	4.0×10^{-5} M (w.r. to total microemulsion)

Therefore, $[Mo] = 4.0 \times 10^{-5}$ M and thus $[MoS_3] = 4.0 \times 10^{-5}$ M. This corresponds to a particle yield of 7.7×10^{-3} g/L. This has the following implications:

(1) To harvest 1 g of MoS_3 particles, it is necessary to prepare and process 130.1 L of microemulsion.

(2) To achieve a catalyst loading of 100 ppm Mo, it is necessary to use 26 cc of the above microemulsion per gram of coal.

(3) To change the catalyst loading, it is necessary to vary the amount of microemulsion. This inadvertently changes the solvent-to-coal ratio.

APPENDIX II

REPRODUCIBILITY OF MICROAUTOCLAVE REACTOR CONVERSION DATA

A. Reproducibility of Data for *In Situ* Tests with Microemulsion-based Catalysts

Run No.	Trial	Total	Asph.	Oil
28	I	61.3	61.3	0.0
	II	59.4	66.3	- 6.9
	Mean	60.4	63.8	- 3.5
36	I	69.4	67.2	2.2
	II	75.7	65.8	9.9
	Mean	72.6	66.5	6.1

B. Reproducibility of Data for Tests with Conventional Solvents and Catalysts

Run No.	Trial	Total	Asph.	Oil
80	I	24.2	11.5	12.7
	II	27.3	11.9	15.4
	Mean	25.8	11.7	14.1
7	I	24.9	6.1	18.8
	II	25.3	4.7	20.6
	Mean	25.1	5.4	19.7

APPENDIX III

TRANSFER OF COPPER PARTICLES ONTO ACTIVE CARBON SUPPORT

Preliminary experiments were also conducted on the possibility of transferring catalyst particles synthesized in microemulsions onto a carbon support. The Cu/C system was chosen for this purpose. The synthesis of a Cu/C catalyst can be accomplished as follows:

1. Prepare a 0.4 M/AOT/cyclohexane solution.
2. In a 25 cc portion of this solution, solubilize 500 μL of 0.10 M cupric acetate solution by shaking vigorously. Microemulsion has a bluish tinge.
3. Reduce the Cu^{2+} ion to metallic copper using 500 μL of 0.8 M hydrazine solution. Color of microemulsion changes to that of metallic copper.
4. Add 0.5 g of Supersorb active carbon (78-10) to the above solution and shake for 12 h. After the carbon particles settle, it can be seen that the supernatant liquid is clear and colorless, perhaps indicating that the Cu particles have been "taken up" by the carbon.
5. Filter and wash repeatedly with tetrahydrofuran, methanol and water – in that order.
6. Dry the carbon at room temperature in vacuum.

To achieve higher loadings, it may be necessary to repeat steps 1 to 4 several times. This is because the Sodium-OT/cyclohexane system can only solubilize a limited amount of cupric ion.

APPENDIX IV

CATALYTIC GASIFICATION RESULTS WITH Cu/C CATALYSTS

Appendix III details a possible new route of catalyst synthesis. In this work, a copper-on-carbon catalyst was prepared in this fashion. For comparison, a conventional impregnation method was also used to prepare a Cu/C catalyst of similar metal loading (1 wt % Cu). Both were tested for activity in metal-catalyzed carbon gasification. The experimental conditions were as follows:

In flowing UHP N_2, approximately 5 g of the sample was

- heated from room temperature to 388 K @ 20 K/min
- held at 388 K for 2 hours
- heated from 388 K to 623 K @ 20 K/min
- held at 623 K for 2 hours.

The flow was then switched to air and the sample was

- held at 623 K for 15 minutes (~ 50% burn-off)
- heated from 623 K to 1023 K @ 20 K/min
- held at 1023 K until complete burn-off occurred.

The burnoff profiles are presented in Figure IV.1. There are two important observations that can be made about the microemulsion-based catalyst. One, it gives a higher initial burnoff rate, and two, its residual ash content is higher (8%, versus 4% for the Cu/C catalyst prepared by the incipient wetness method). The last observation suggests that all the surfactant had not been removed from the carbon. This is crucially important because the surfactant contains sodium – a good carbon gasification catalyst. Therefore, it is not possible to say whether the higher burnoff rate shown by the microemulsion-based catalyst is due to better dispersion of copper on the carbon, or an artifact of the preparation method. It is suggested that the same experiment should be tried using Copper-OT as the surfactant.

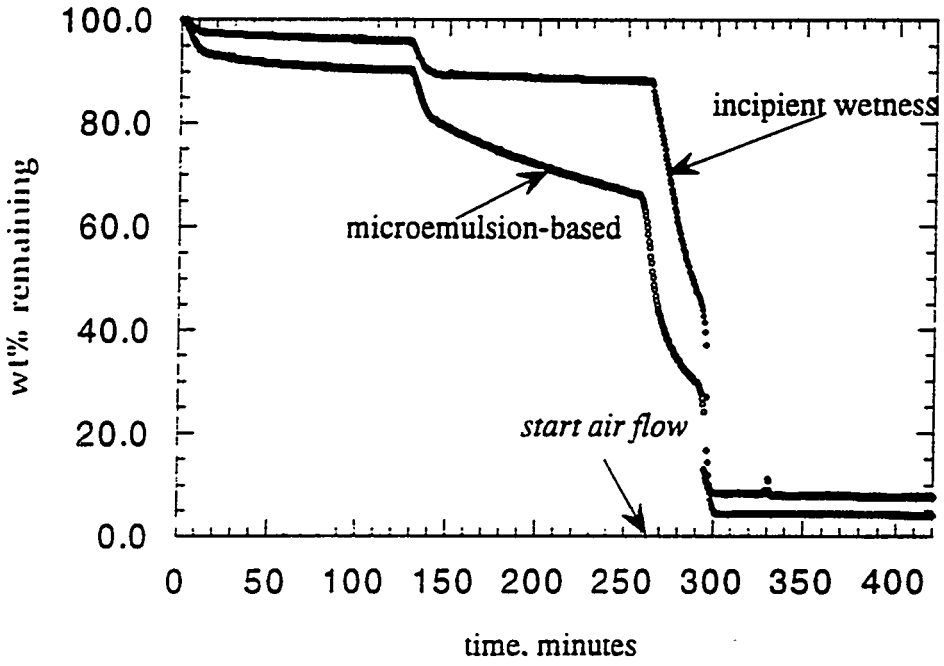

Figure IV.1
Burnoff profiles in air of Cu/C catalysts prepared by incipient wetness and microemulsion methods.

APPENDIX V
SYNTHESIS OF NANOSIZE MOLYBDENUM SULFIDE PARTICLES IN NP-5/TETRALIN MICROEMULSION SYSTEMS

1. INTRODUCTION

The synthesis of molybdenum sulfide nanoparticles in various microemulsion systems was described in detail in Chapters 2-5. Conventional solvents (e.g., cyclohexane) were used in these 'well behaved' systems. They were thus suitable for a thorough investigation of the dependence of catalyst particle size on the various synthesis conditions. Here we describe the synthesis of molybdenum sulfide particles in microemulsion systems that are directly relevant to coal liquefaction catalysis. While NP-5 was retained as the surfactant, tetralin - a widely investigated coal liquefaction model compound - was used as the solvent. The use of cosurfactants was found to be necessary in this case. Here we report the use of benzyl alcohol, methanol, propanol and hexanol. Fluorescence spectroscopy is used to determine the locale and site of solubilization of the alcohols used as cosurfactants. The solubilization data are discussed in terms of the spontaneous curvature of the interface and inter-micellar interaction.

2. EXPERIMENTAL

2.1 Materials

The following chemicals obtained from Aldrich were used as received: polyoxyethylene(5)nonylphenyl ether (NP-5), ammonium tetrathiomolybdate

(99.97%), 1,2,3,4-tetrahydronaphthalene (99%), benzyl alcohol, methanol (99.9%), propanol (99%), hexanol (98%) and tris(2,2'-bipyridyl) ruthenium(II) chloride hexahydrate.

2.2 Microemulsion Characterization

The solubilization locales of methanol and benzyl alcohol were determined by fluorescence spectroscopy using a Shimadzu RF-5000 spectrofluorometer. The spectrum was collected in the emission mode with an excitation wavelength of 460 nm. The molecule tris(2,2'-bipyridyl) ruthenium(II) chloride hexahydrate was used as the fluorescence probe. In all cases the concentration of the probe molecule was 1.45×10^{-5} M with respect to 10 mL of microemulsion.

The solubilization capacity was measured by titrating directly into each microemulsion sample under vigorous stirring. A Hamilton microsyringe was used. The quantity of aqueous species added was determined by weight difference. The onset of permanent turbidity was taken to be the limit of solubilization of the aqueous phase in the microemulsion.

2.3 Particle Synthesis

The synthesis experiments were conducted at 50 °C. The microemulsion-plus-a-second-reactant method was used. Solutions of 0.4 M NP-5/tetralin/alcohol were first made at room temperature. A number of samples containing a fixed oil-to-surfactant and oil-to-cosurfactant molar ratios with variable amounts of water were prepared. This was followed by adding 36.2 μL of 1.1 M aqueous sulfuric acid to a 10 mL solution of tetralin/alcohol microemulsion. The acid-solubilized microemulsion was deoxygenated by bubbling high-purity nitrogen gas through it. This procedure was followed by adding 36.2 μL of $1.25\text{-}7.50 \times 10^{-2}$ M ammonium

tetrathiomolybdate to the microemulsion. Nitrogen was further bubbled while molybdenum sulfide was being precipitated according to the following reaction:

$$MoS_4^{2-} + 2H^+ = MoS_3 + H_2S \qquad [1]$$

The concentrations of the reactant species were as follows: sulfuric acid, $4x10^{-3}$ M; ammonium tetrathiomolybdate, $4.5x10^{-5}$ - $3.62x10^{-4}$ M.

2.4 Particle Characterization

Samples for transmission electron microscopy were prepared by directly dropping a very small amount of molybdenum sulfide dispersion on carbon-coated copper grids and drying at room temperature. Before sampling each bottle was sonicated for one minute. Particle sizes were determined with a Philips 420 TEM operating at 120 kV with a resolution of 0.6 nm. At least 200 particles were analyzed for each sample to obtain an average particle diameter.

3. RESULTS AND DISCUSSION

3.1 Effect of R on Particle Size

Figure V.1 presents a plot of the average particle diameter versus the water-to-surfactant molar ratio (R). Figure V.2 shows TEM micrographs of molybdenum sulfide particles synthesized in the 0.4 M NP-5/tetralin/benzyl alcohol microemulsion system. The average particle diameter is about the same for R values of 1 and 1.25. As also shown in Figure 6.1, the particle size first decreases with R; above R~1.5, this trend is reversed. This trend is also similar to that observed for the 0.15 M NP-5/cyclohexane microemulsion (Figure 2.5), except that

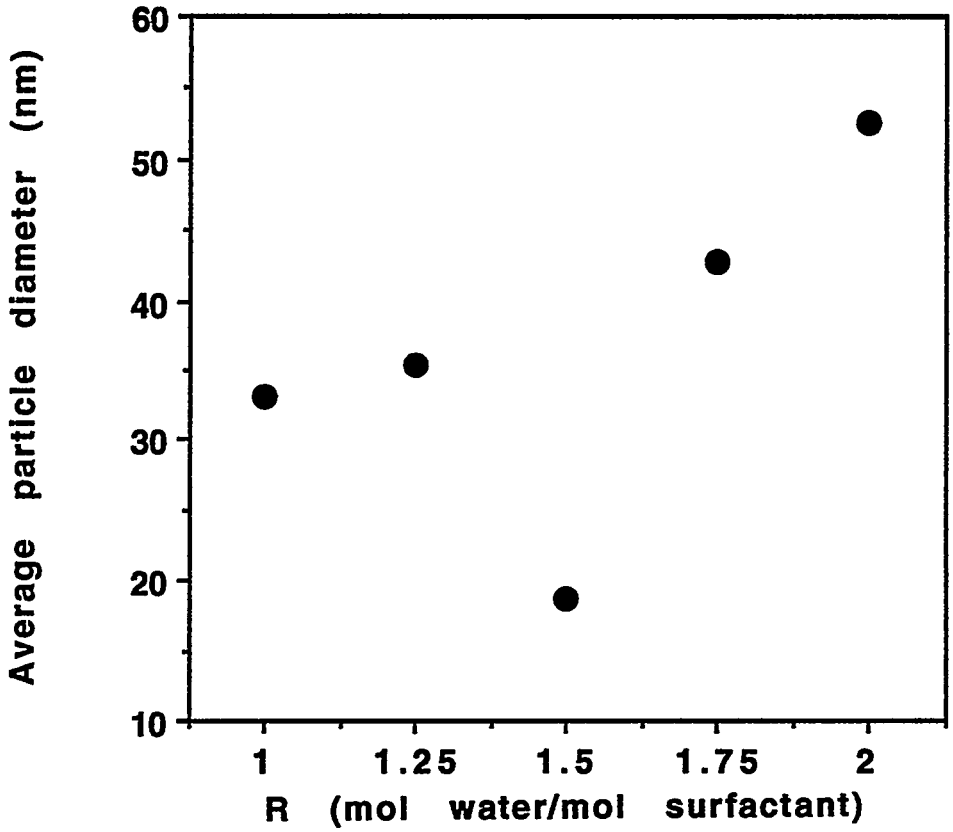

Figure V.1

Effect of water-to-surfactant molar ratio (R) on the average molybdenum sulfide particle size for the 0.4 M NP-5/tetralin/benzyl alcohol microemulsion system. ($[MoS_4^{2-}] = 4.5 \times 10^{-5}$ M; $[H_2SO_4] = 4.0 \times 10^{-3}$ M).

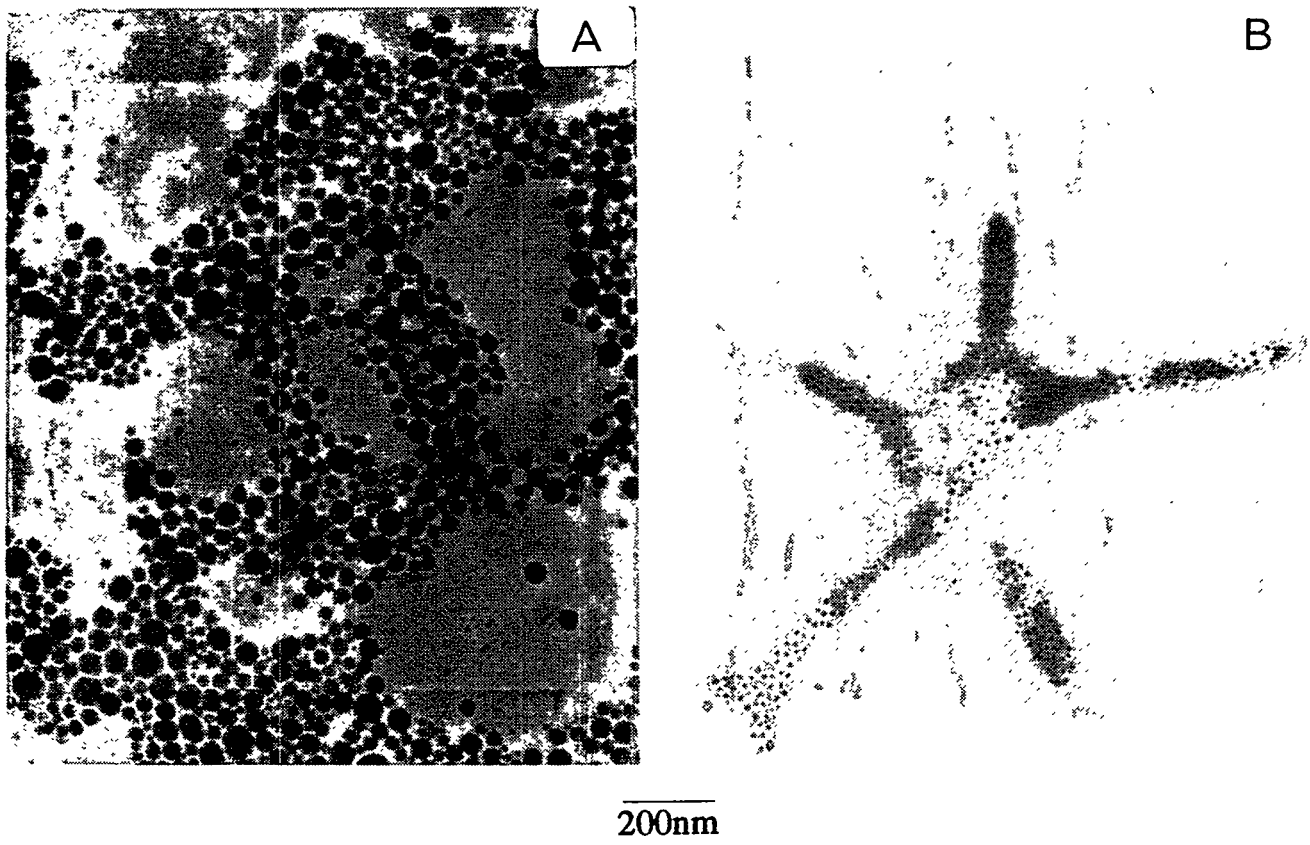

Figure V.2
TEM micrographs of molybdenum sulfide particles prepared in the 0.4 M NP-5/tetralin/benzyl alcohol microemulsion system: (A) R = 1.25; (B) R = 1.5.

the minimum occurs at a smaller R value. It is rationalized by postulating the following particle formation and growth mechanism (see Chapters 2-5): (i) ammonium tetrathiomolybdate reacts with aqueous sulfuric acid to form molybdenum trisulfide monomer; (ii) before a stable nucleus is formed, a critical number of molybdenum trisulfide monomers must combine; (iii) after a stable nucleus is formed, it grows by incorporating the molybdate ions in solution to the already formed nuclei; (iv) as a consequence of inter-micellar interactions, primary particles and/or nuclei aggregate to form bigger particles.

An important parameter in connection with the growth mechanism is seen to be the average molybdate occupancy number (i.e., the number of tetrathiomolybdate ions per inverse micelle). The aggregation number decreases as the water-to-surfactant molar ratio is decreased. For a fixed volume of microemulsion it follows that the number of inverse micelles increases. Consequently the number of tetrathiomolybdate ions per inverse micelle decreases. For very low R values, relatively few water cores contain the minimum number of monomers needed to form a nucleus. As a result, the nucleation rate is slow and the remaining ions not utilized in nuclei formation are incorporated into the already formed primary particles and/or nuclei to form bigger particles. As R increases the aggregation number increases, the micellar concentration decreases, the occupancy number increases and the nucleation rate increases. The observed decrease in particle size at $R < 1.5$ is due to the increasing occupancy number. At $R > 1.5$ the occupancy number is relatively high and hence smaller particles are expected. Contrary to expectation, however, larger particles are found. At $R > 1.5$ particle growth via fusion of nuclei or primary particles is occurring preferentially. Similar observations have been made in the synthesis of molybdenum sulfide particles in the NP-5/cyclohexane microemulsion system (Chapter 2, where TEM micrographs showed 5-nm particles aggregating to form 80-100 nm particle (Figure 2.10). An

interesting aspect of the particle aggregation phenomenon in NP-5/cyclohexane and NP-5/tetralin/benzyl alcohol microemulsions is that particle aggregation occurs at a lower R value in the latter case. Presumably, benzyl alcohol increases the fluidity of the interface and facilitates the exchange of the contents of the water pools, which favors particle aggregation and growth.

3.2 Fluorescence Spectroscopy

It has been reported that short-chain alcohols used as cosurfactants in the formulation of microemulsions partition between the inverse micellar water cores and the bulk oil phase (1,2). In addition, Atik and Thomas (3) have shown that additives such as benzyl alcohol and hexanol affect differently the transport of ions between inverse micelles. The rates of ion transport when benzyl alcohol and hexanol were used as cosurfactants were 330 and 7.5, respectively (3). Thus, obviously, the use of methanol and benzyl alcohol will affect differently the rate of ion transport between the inverse micelles and hence the exchange of solubilizates between the water pools.

Figures V.3 and V.4 represent the fluorescence spectra of tris(2,2'-bipyridyl) ruthenium(II) chloride hexahydrate ($Ru(Bpy)_3$) in the two microemulsion systems studied at various water-to-surfactant molar ratios. For the purpose of comparison, the fluorescence spectrum of $Ru(Bpy)_3$ in water is included (dashed lines). The emission maximum for the methanol-based microemulsion is seen to be about the same as that for water (615 nm). However, the spectrum of $Ru(Bpy)_3$ in the benzyl alcohol-based microemulsion peaks at 625 nm, which is red-shifted compared to that of water. These results suggest that while methanol partitions between the aqueous and the bulk organic phase, benzyl alcohol interacts with the aqueous/organic interface.

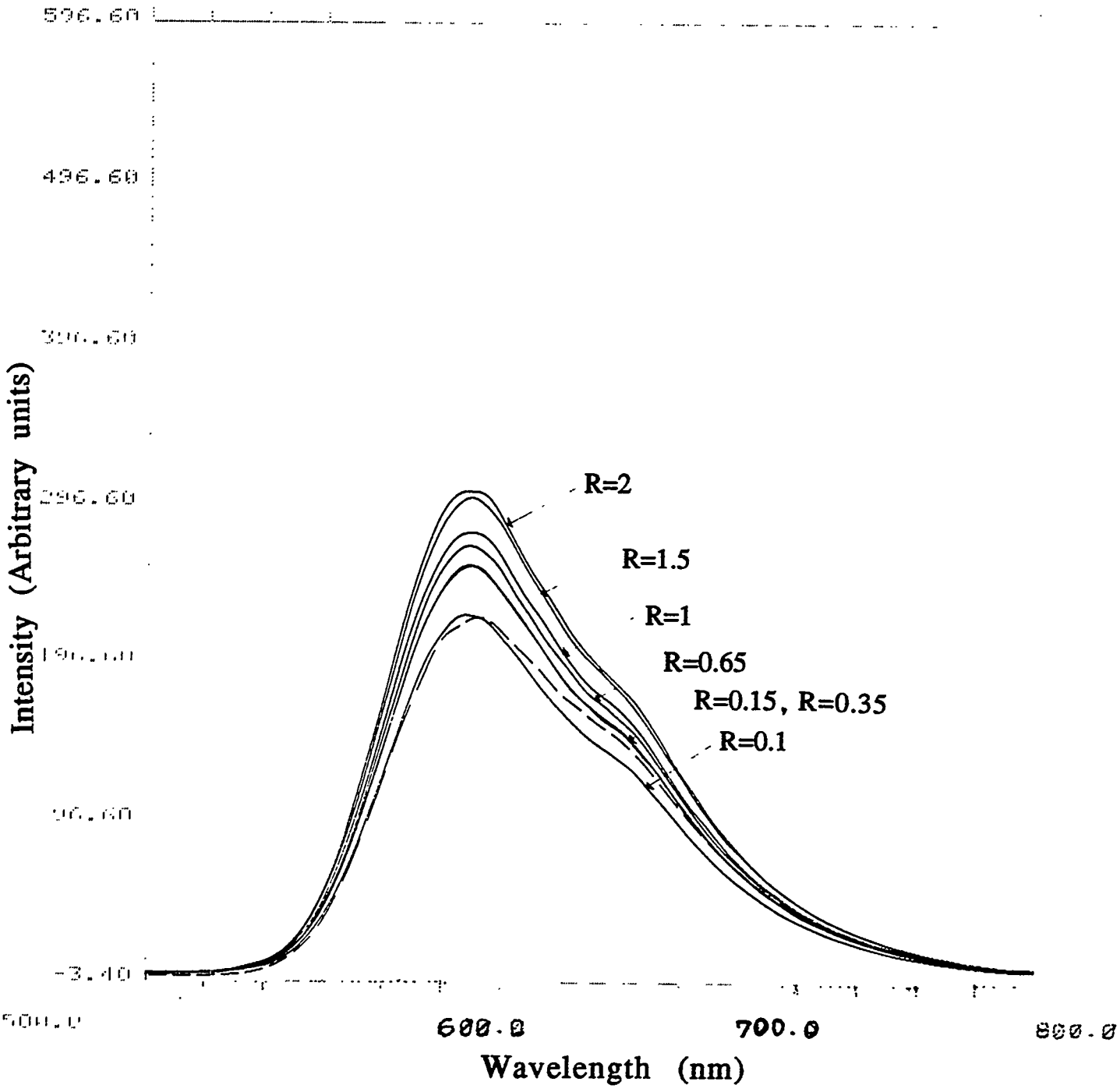

Figure V.3
Fluorescence spectra of $Ru(Bpy)_3$ solubilized in the 0.4 M NP-5/tetralin/methanol microemulsion.

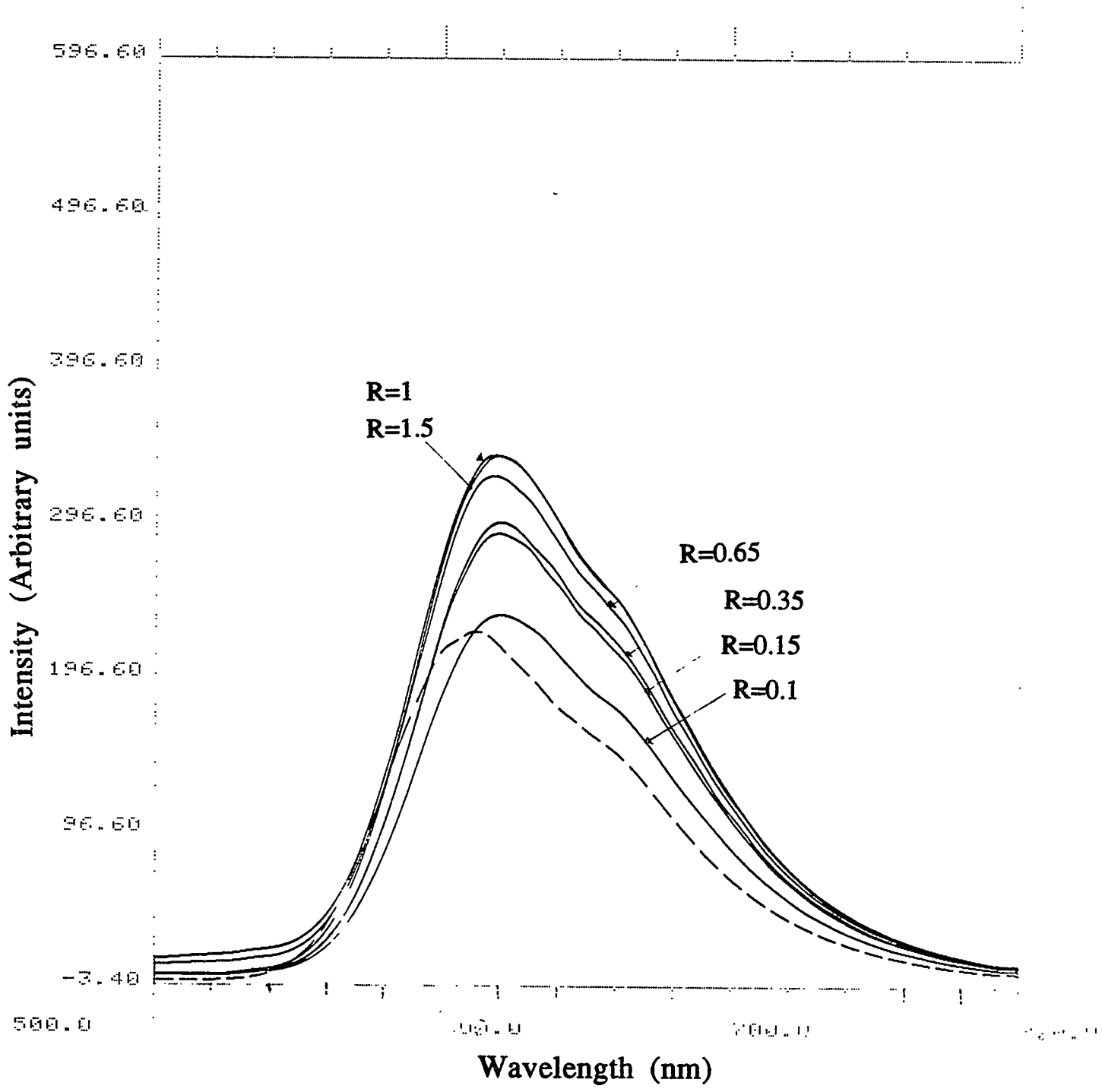

Figure V.4
Fluorescence spectra of $Ru(Bpy)_3$ solubilized in the 0.4 M NP-5/tetralin/benzyl alcohol microemulsion.

The above results are further evidence in support of the work done by Atik and Thomas (3). Benzyl alcohol, assumed to be located at the surfactant interface, causes disruption of the surfactant headgroups and thus enhances ion penetration into the reverse micelles. Also, since ions cannot interact with the organic phase, the exchange of ions occurs between inverse micelles only during collision. This means that the rate of ion transport is directly related to the rate of exchange of solubilizates between inverse micelles (K_{ex}). It follows that the K_{ex} of the microemulsion formulated with benzyl alcohol as a cosurfactant is greater than that of the microemulsion formulated with hexanol and may be greater than that of the one formulated with methanol.

3.3 Microemulsion Solubilization

Recently, Shah and coworkers (4,5) presented a model that qualitatively explains the differences in water solubility for water-in-oil (w/o) microemulsions formulated with alcohols of different chain lengths as co-surfactants. The solubility capacity also depends on the ionic strength of the aqueous domain and the oil phase. The model outlines the induction of phase separation as a consequence of (i) the curvature of the interface and (ii) the attractive interactions of the swollen inverse micelles.

The curvature effect, which applies only to relatively rigid interfaces, is said to arise from the differences in interaction between adjacent polar headgroups of the inverse micelles and those of the adjacent hydrocarbon moiety (5). It represents the tendency of the surfactant interface to bend towards the aqueous phase or the oil. The total free energy of the interface of a w/o microemulsion is represented as:

$$F = n[4\pi R^2\gamma + 16\pi K(1 - R/R^o)^2] \qquad [2]$$

where R^o is the radius of spontaneous curvature (natural radius), R is the equilibrium radius of the swollen inverse micelles, γ is the surface tension of the interface, n is the number of swollen inverse micelles and K is the curvature elasticity constant (with units of energy). The interfacial tension term is the first term in Equation 2 and the interfacial curvature term is the second term. High and low values of K correspond to rigid and fluid interfaces, respectively. The value of K is of the order of 10^{-14} erg for microemulsions (6,7). This implies that, for the curvature effect to be important, the surface tension of the interface should approach zero.

For a stable w/o microemulsion with a relatively rigid interface and low water content, the equilibrium radius is less than the natural radius ($R<R^o$). The equilibrium radius R increases as water molecules are added. In the limit when $R>R^o$ the excess water is expelled from the microemulsion droplet. At this stage there is phase separation. The composition of the system is w/o microemulsion in equilibrium with excess water. This type of phase separation is referred to as type 1 separation (4).

As the rigidity of the microemulsion interface is decreased, e.g., by adding short-chain-length alcohols, the inter-micellar interaction increases, leading to inelastic collisions and the formation of transient dimers and relatively large inverse micelles. As the fluidity is further increased, the micellar radius approaches a critical value, R^c, which represents the solubility of the water in the microemulsion. At $R>R^c$ there is phase separation. Here relatively few large inverse micelles exist in equilibrium with the continuous oil phase. This type of phase separation, which is driven by inter-micellar interactions, is referred to as type 2 separation (4).

Figure V.5 presents the results of solubilization of water and ammonium tetrathiomolybdate in the 0.4 M NP-5/tetralin/n-alcohol/microemulsion. The

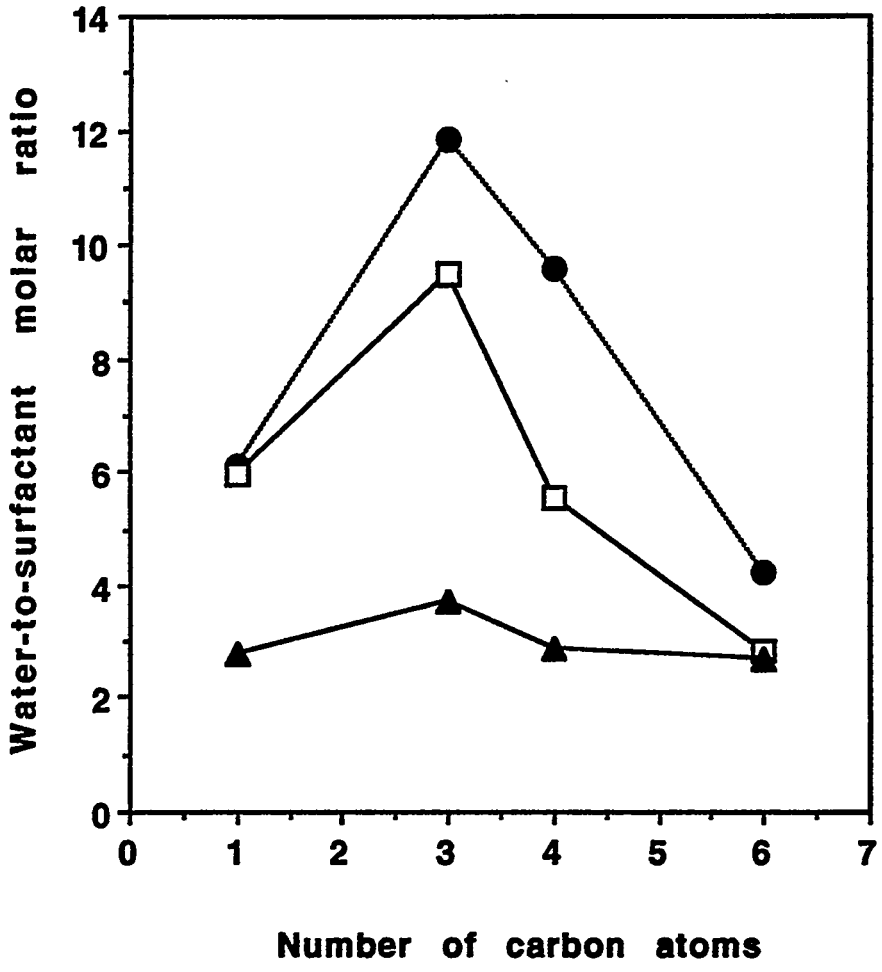

Figure V.5

Effect of alcohol chain length on microemulsion solubility:

● , water;

❑ , 0.013 M ammonium tetrathiomolybdate;

▲ , 0.05 M ammonium tetrathiomolybdate.

solubility is expressed as the water-to-surfactant molar ratio above which phase separation occurs. As the alcohol chain length is increased, the solubility first increases with the number of carbon atoms in the alcohol and then decreases. Similar results have been found for microemulsion systems formulated with cationic and anionic surfactants (5,8).

The results presented in Figure V.5 can be rationalized by invoking the model presented by Shah and coworkers (4,5). As the co-surfactant chain length is increased, the rigidity of the interface increases. Here the induction of phase separation is dominated by the curvature effect (i.e., it is limited by the natural radius R^o). However, when the fluidity of the interface is increased by using short-chain-length alcohols as co-surfactants, the natural radius of the inverse micelles increases. As a result, more water molecules will be added before the condition $R>R^o$ is reached and hence the solubility increases. As the fluidity of the interface is further increased, by using shorter-chain-length alcohols as co-surfactants, the interdroplet interaction concomitantly increases to an extent that transient dimers and relatively fewer large inverse micelles will be in equilibrium with the continuous oil phase, which corresponds to phase separation of type 2. At this stage $R>R^c$.

From the above discussion, it is reasonable that a maximum exist for the solubilization of the aqueous phase in the microemulsion: the maximum solubilization capacity corresponds to a combination of the interfacial curvature and the inter-micellar interaction effects.

For a microemulsion system with a fixed cosurfactant-to-surfactant molar ratio, one would expect the effective size of the polar headgroup to decrease (i.e., double layer contraction) as the ionic strength of the aqueous domain of the microemulsion is increased. Consequently, the natural radius of the inverse micelles should decrease as well. This corresponds to decreasing solubilization as

the condition $R>R^o$ is reached at a relatively low water content of the microemulsion compared to the case where R^o is large (i.e., no electrolyte present). In general, an increase in the ionic strength of the aqueous phase makes the interface more rigid, reduces the inter-micellar interactions, decreases the aggregation number (9,10) and reduces the solubility, as shown in Figure V.5.

3.4 Particle Synthesis

Figure V.6 presents TEM micrographs of molybdenum sulfide particles synthesized in the 0.4 M NP-5/tetralin/methanol microemulsion. A bimodal distribution is observed for particles made at each R value. Particles in the size range 2-4 nm (primary particles) and 15-50 nm (final particles) were produced. Figure V.7 presents a plot of the average particle diameter vs. R for the final particles (or aggregates of primary particles). The particle size again exhibits the characteristic minimum (see Section 3.1).

Figure V.8 presents the dependence of the average molybdenum sulfide particle diameter on the water-to-surfactant molar ratio for the 0.4 M NP-5/tetralin/benzyl alcohol system. Figure V.9 shows the corresponding TEM micrographs. In contrast to the microemulsion formulated with methanol, the particle size monotonically increases with R. (The alcohol-to-surfactant mass ratios were 3.5 and 2.5, respectively.) Also, the distribution is monomodal. The increase in particle size with R may be due to particle aggregation, as discussed previously.

An interesting question that needs to be addressed is why small particles, in the range 2-4 nm, can be made in a methanol-based microemulsion but not in the one in which benzyl alcohol is the cosurfactant. This issue was discussed in Section 3.2. While methanol partitions between the water pools and the organic phase, benzyl alcohol interacts with surfactant headgroup and hence facilitates the transport of ions between micelles. Further, it was concluded that because of this

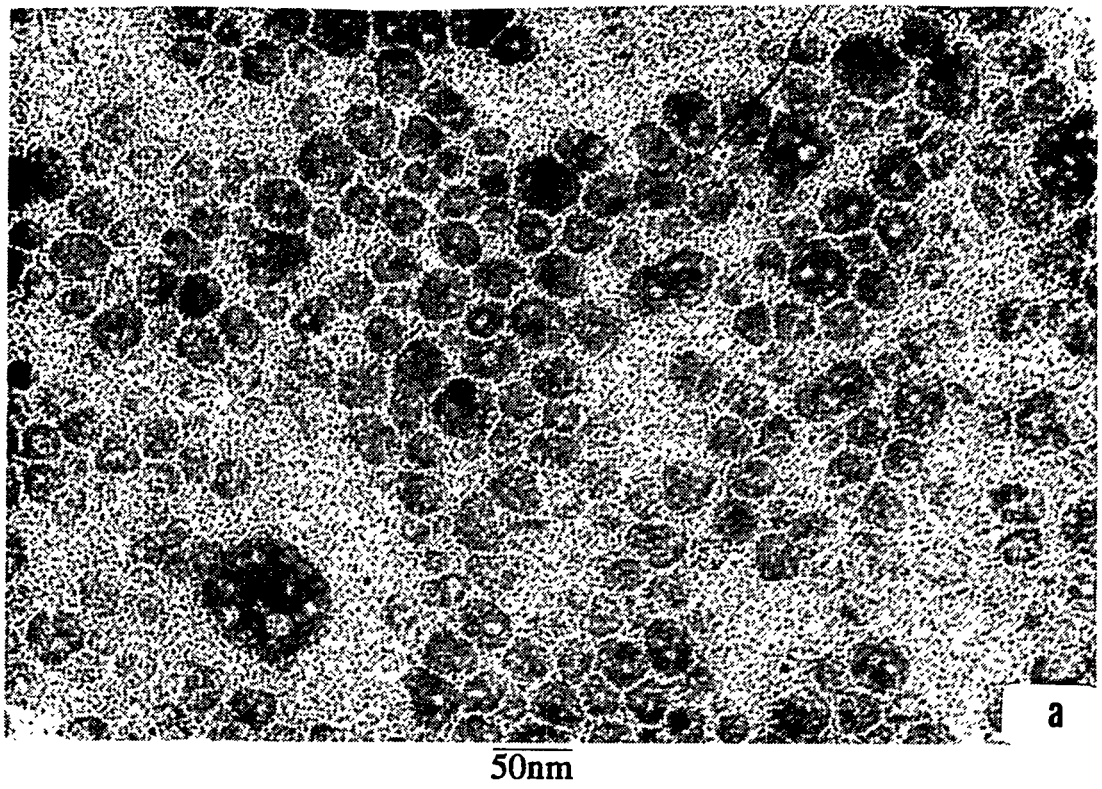

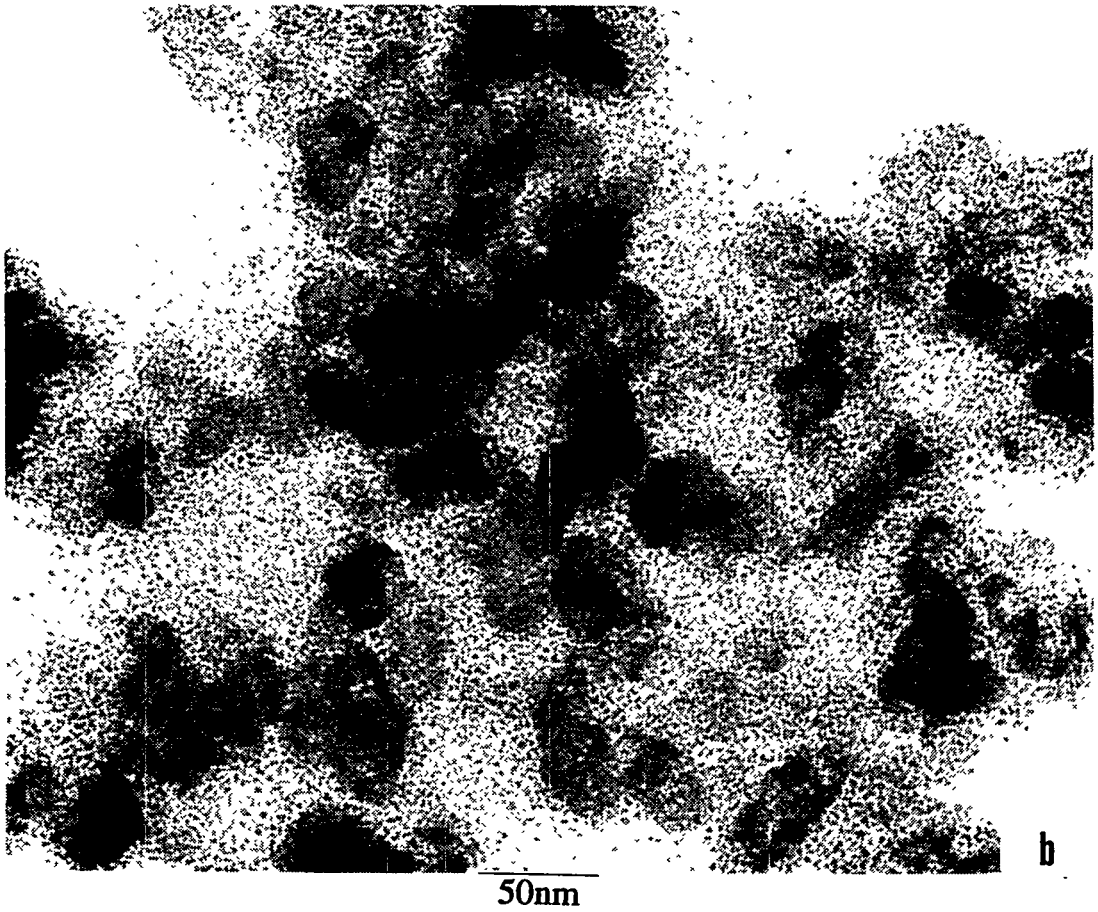

Figure V.6
TEM micrographs of molybdenum sulfide particles prepared in the 0.4 M NP-5/tetralin/methanol microemulsion system.
(a) R = 2; (b) R = 4.

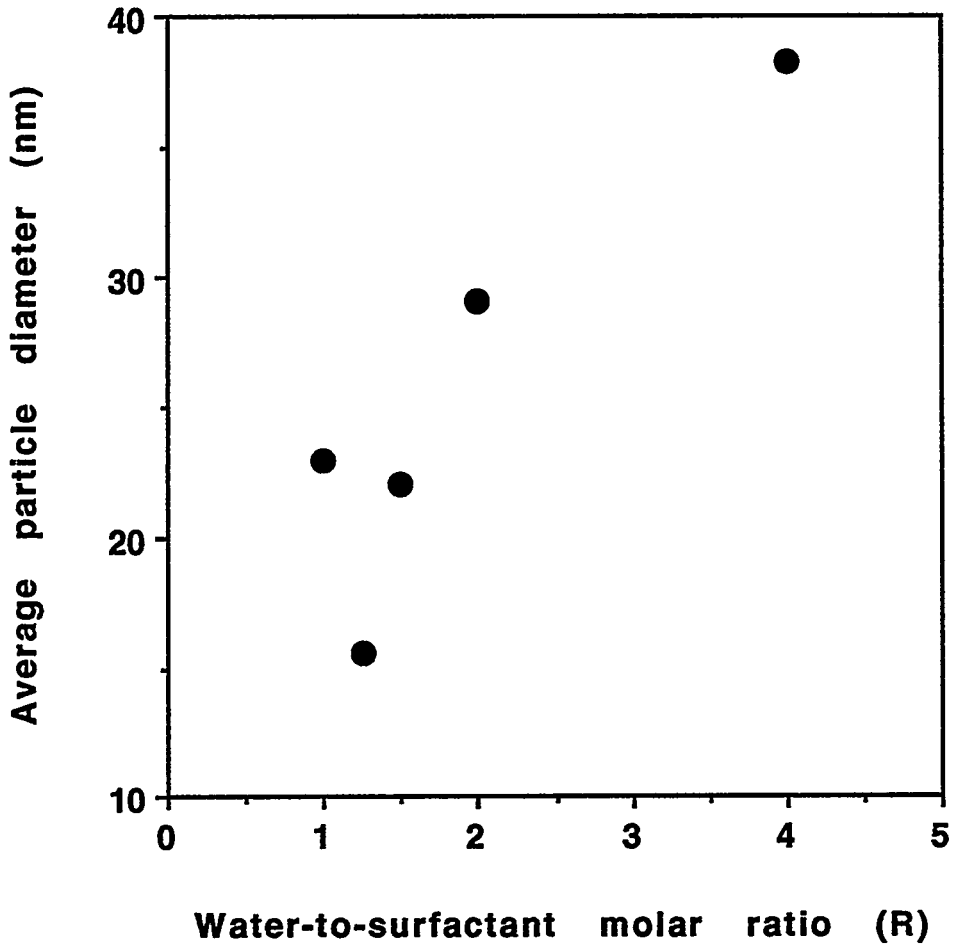

Figure V.7
Effect of water-to-surfactant molar ratio on the average molybdenum sulfide particle size for the 0.4 M NP-5/tetralin/methanol microemulsion system ($[MoS_4^{2-}]=4.5x10^{-5}$ M; $[H_2SO_4]=4.0x10^{-3}$ M).

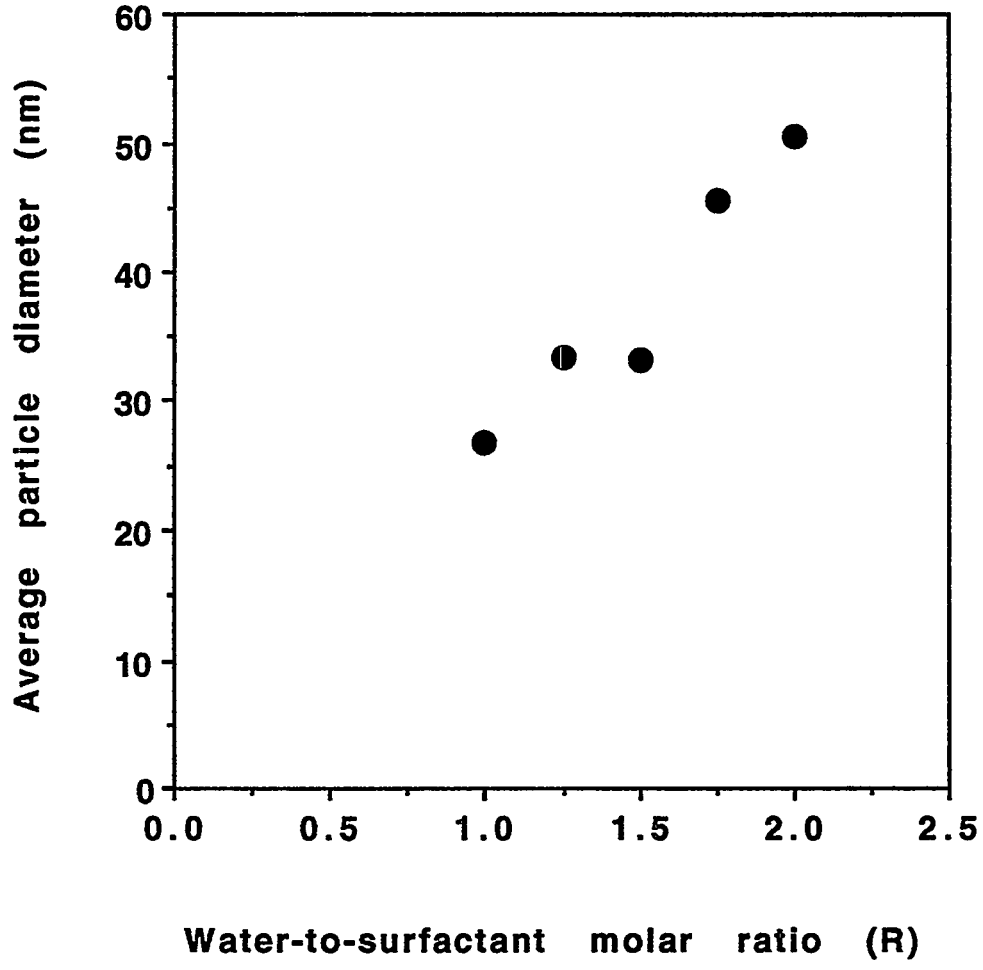

Figure V.8

Effect of water-to-surfactant molar ratio on the average molybdenum sulfide particle size for the 0.4 M NP-5/tetralin/benzyl alcohol microemulsion system ($[MoS_4^{2-}]=4.5x10^{-5}$ M; $[H_2SO_4]=4.0x10^{-3}$ M).

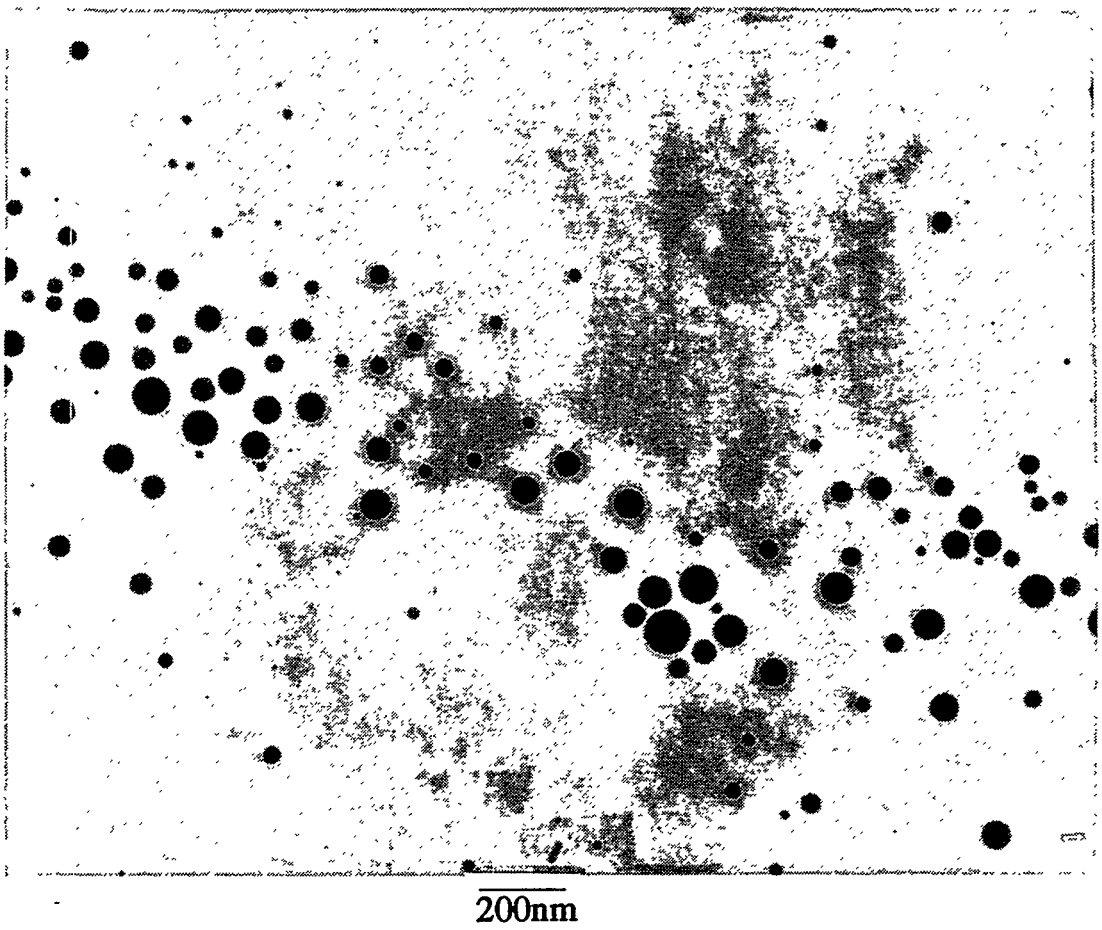

Figure V.9
TEM micrograph of molybdenum sulfide particles prepared in the 0.4 M NP-5/tetralin/benzyl alcohol microemulsion system, R=1.75.

effect, K_{ex} for microemulsions formulated with benzyl alcohol is greater than that of the microemulsion formulated with methanol. For the effectiveness of a process in which a critical number of monomers must combine to form a stable nucleus, the monomers must be retained in a specific micelle for a sufficiently long period of time. If the inter-micellar exchange of solubilizates is very rapid, then the monomers will be redistributed in other micelles before nucleation can occur. Consequently, an increase in the value of K_{ex} (e.g., for the 0.4 M NP-5/tetralin/benzyl alcohol microemulsion) may result in fewer nuclei being formed and larger particles being made. Also, as K_{ex} increases, the probability of exchange of solute species between the micelles increases. As a result, particle aggregation will increase and relatively large particles will be made.

3.5 Effect of Cosurfactant Chain Length on Particle Size

Methanol. Figures V.10 and V.11, respectively, present the TEM micrographs and a plot of average particle diameter versus the molybdate concentration of molybdenum sulfide particles synthesized in the 0.4 M NP-5/tetralin/methanol microemulsion system. The average particle diameter decreases monotonically as the thiomolybdate concentration is increased. Robinson et al. (11) have reported similar observations. This trend may be rationalized by considering the following particle formation and growth scheme (12-16): (i) When ammonium tetrathiomolybdate and sulfuric acid meet in a swollen inverse micelle, they react to form molybdenum trisulfide monomer; (ii) before a stable nucleus is formed a critical number of molybdenum trisulfide monomers must combine in a specific micelle (13); (iii) after a stable nucleus is formed, it can grow by incorporating molybdate ions and monomers in the aqueous domain via intra- and inter-micellar interactions; (iv) primary particles or nuclei may aggregate through inter-micellar interactions to form bigger particles (14,17).

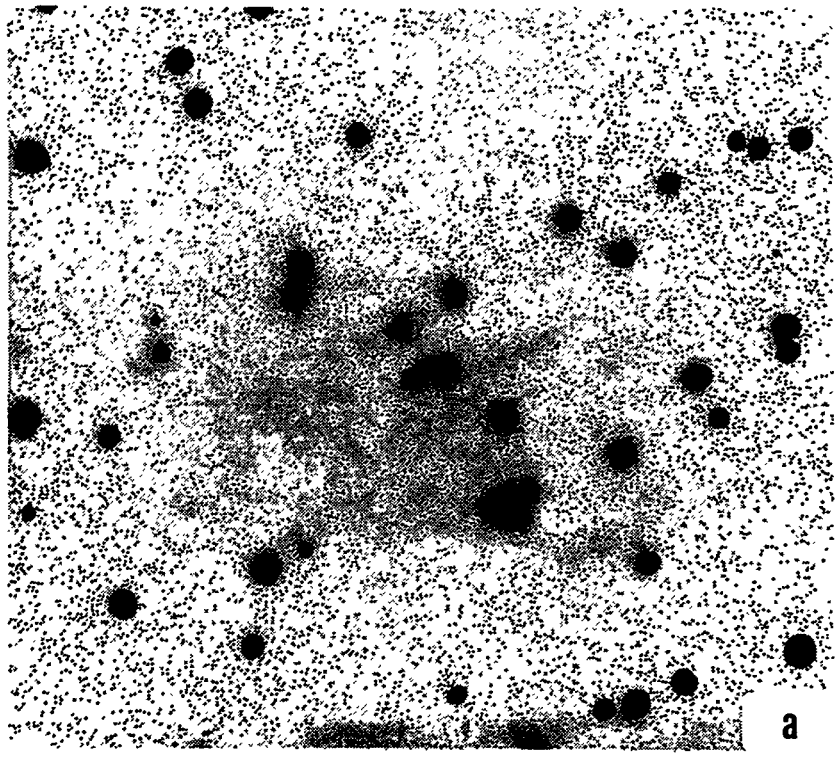

400 nm

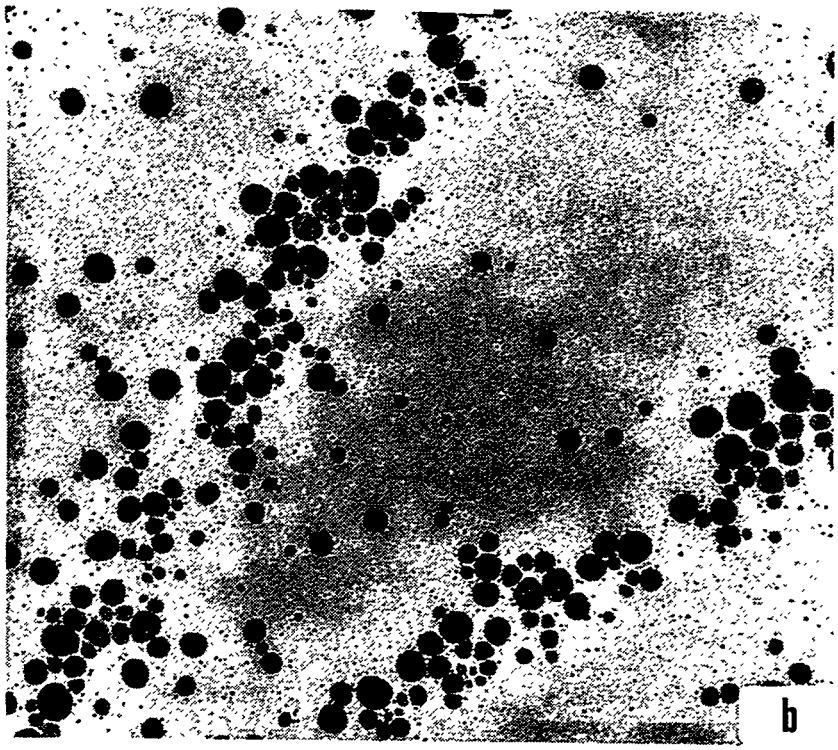

200 nm

Figure V.10

TEM micrographs of molybdenum sulfide particles prepared in the 0.4 M NP-5/tetralin/methanol microemulsion:

(a) $[MoS_4^{2-}] = 4.5 \times 10^{-5}$ M; (b) $[MoS_4^{2-}] = 1.8 \times 10^{-4}$ M.

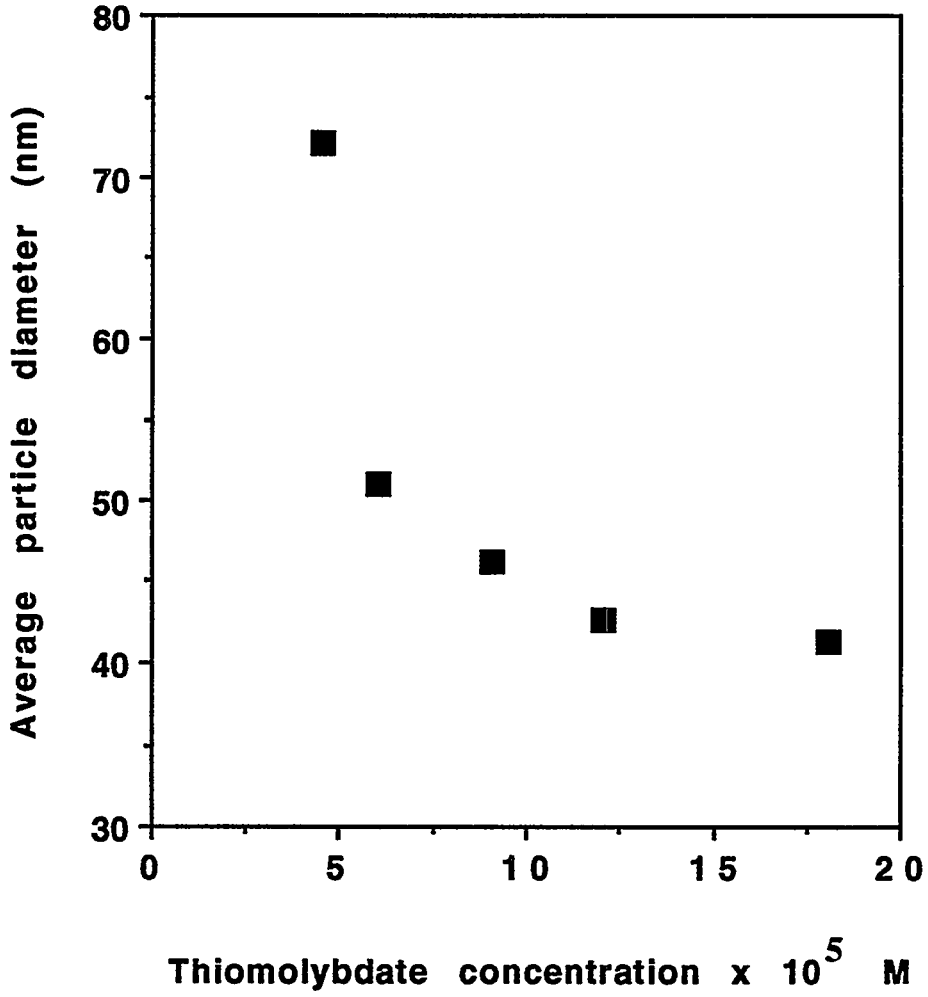

Figure V.11
Effect of ammonium tetrathiomolybdate concentration on the average molybdenum sulfide particle size for the 0.4 M NP-5/tetralin/methanol microemulsion system ($[H_2SO_4] = 4.0 \times 10^{-3}$ M).

In order to generate small and monodispersed particles, the nucleation and growth steps should occur on different time scales. To satisfy this condition, it is necessary to produce a large number of nuclei in specific inverse micelles and then transform them into particles. Furthermore, the particles should be prevented from aggregating. This condition is met if the inverse micelles act as perfect cages. This implies that the inter-micellar exchange of the particles in the micelles is controlled to a minimum extent.

From the TEM micrographs a bimodal distribution is seen to have been obtained for all concentrations of ammonium tetrathiomolybdate investigated. This may be the result of particle aggregation occurring simultaneously with ion and monomer additions. Primary particles of 2-7 nm seem to have aggregated to form particles in the size range of 40-80 nm.

Among the important observations in the solubilization studies was that, for the phase separation induced by the inter-micellar interaction (e.g., microemulsions with relatively short side chain alcohols as co-surfactants), the oil/water interface becomes relatively rigid when the ionic strength of the aqueous phase of the microemulsion is increased. This causes a decrease in inter-micellar interaction which reduces particle aggregation. Thus the decrease in particle size with increasing concentration of ammonium tetrathiomolybdate may be due to either an increase in the nucleation rate or a decrease in inter-micellar interaction.

Propanol. Presented in Figures V.12 and V.13 are the TEM micrographs and a plot of particle size versus thiomolybdate concentration of molybdenum sulfide particles synthesized in the microemulsion system 0.4 M NP-5/tetralin/propanol. The particle size exhibits a minimum as the thiomolybdate concentration increases.

This trend is also interpreted by considering the particle formation scheme presented above. For a fixed water-to-surfactant molar ratio, the thiomolybdate occupancy number increases as the ammonium tetrathiomolybdate concentration is

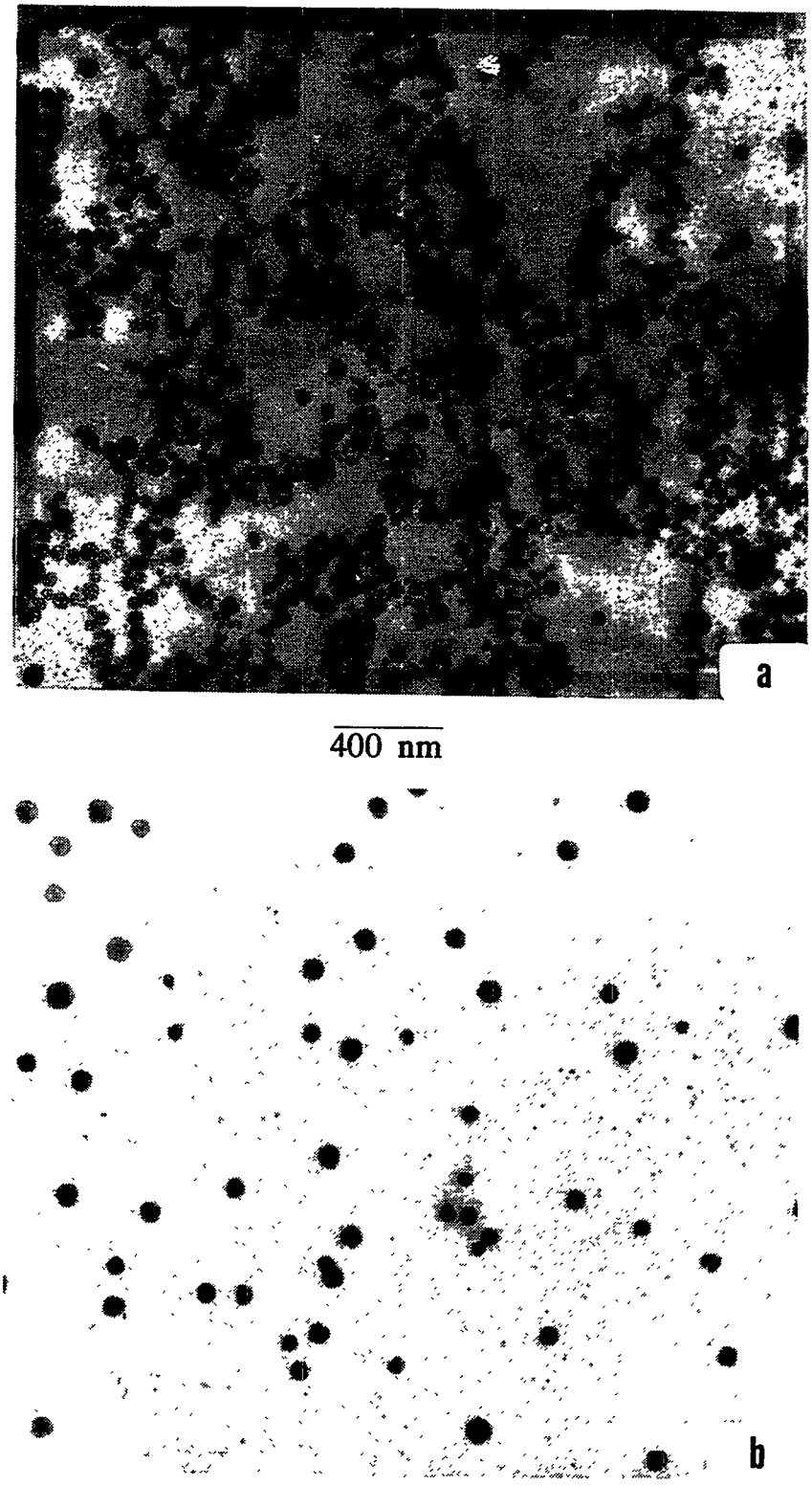

Figure V.12

TEM micrographs of molybdenum sulfide particles prepared in the 0.4 M NP-5/tetralin/propanol microemulsion.

(a) $[MoS_4^{2-}] = 4.5 \times 10^{-5}$ M; (b) $[MoS_4^{2-}] = 1.8 \times 10^{-4}$ M.

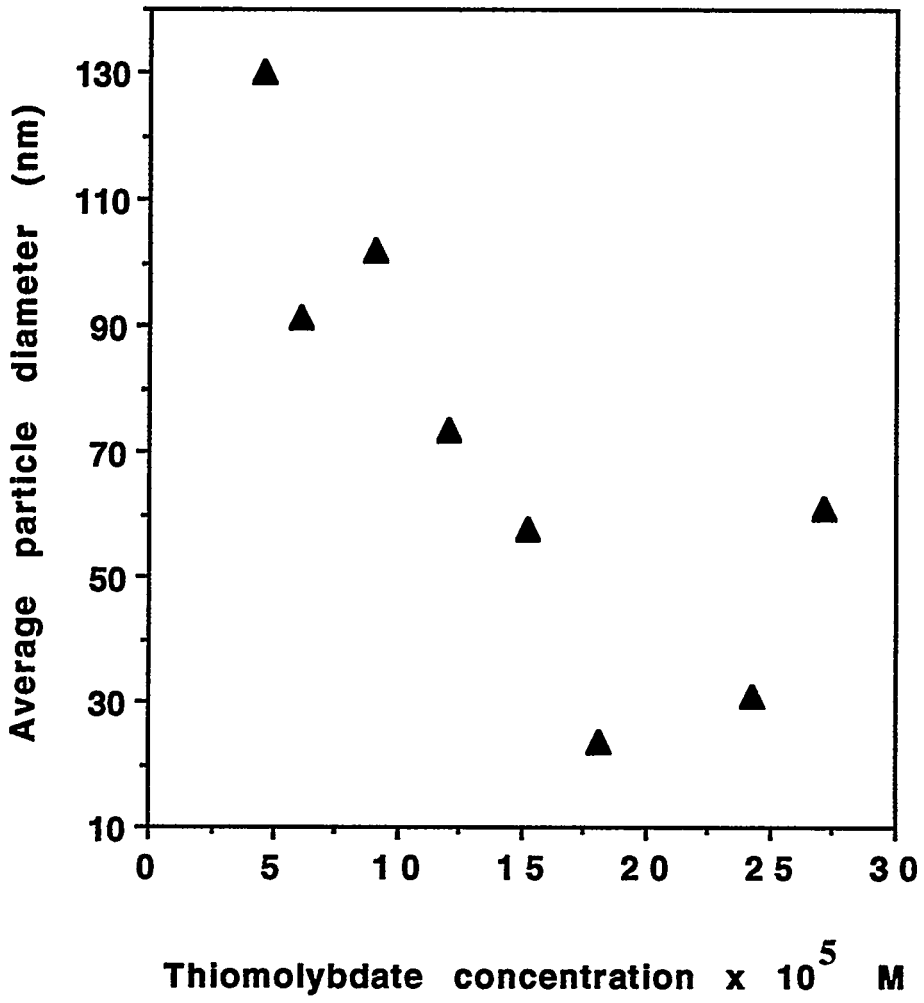

Figure V.13
Effect of ammonium tetrathiomolybdate concentration on the average molybdenum sulfide particle size for the 0.4 M NP-5/tetralin/propanol microemulsion ($[H_2SO_4] = 4.0 \times 10^{-3}$ M).

increased. The rate of nucleation increases as the thiomolybdate concentration is increased. As a result, few ions and monomers not utilized in the nucleation process contribute to the growth process. Also, as suggested in the discussion for particles made in the NP-5/tetralin/methanol microemulsion system, the water/oil interface is made relatively rigid as the ionic strength of the aqueous domain is increased (i.e., increasing thiomolybdate concentration). This reduces particle aggregation and hence small particles are made. This is confirmed by the few 2-7 nm particles seen on the TEM micrographs. Thus, for thiomolybdate concentrations less than 1.81×10^{-4} M, a decrease in the particle size may be due to an increase in the nucleation rate or a decrease in the extent of aggregation.

For thiomolybdate concentrations greater than 1.81×10^{-4} M, the average molybdate occupancy number is relatively high and hence smaller particles were expected to be made. Contrary to expectation, the particle size was found to increase as the thiomolybdate occupancy number was increased. This trend can be rationalized by considering particle aggregation.

Hexanol. Figures V.14 and V.15 present the TEM micrographs and a plot of the average particle diameter versus thiomolybdate concentration for particles synthesized in the microemulsion system 0.4 M NP/5/tetralin/hexanol. The average particle diameter decreases with increasing thiomolybdate concentration (to a concentration of 6.05×10^{-5} M) and then increases. The explanation of this trend is similar to that given for the 0.4 M NP-5/tetralin/propanol microemulsion system. For thiomolybdate concentrations $< 6.05 \times 10^{-5}$ M, the molybdate occupancy number increases as the concentration of ammonium tetrathiomolybdate is increased. As a result, the nucleation rate increases and small particles are made. For thiomolybdate concentrations $> 6.045 \times 10^{-5}$ M, particle aggregation is expected to be the principal mechanism of growth.

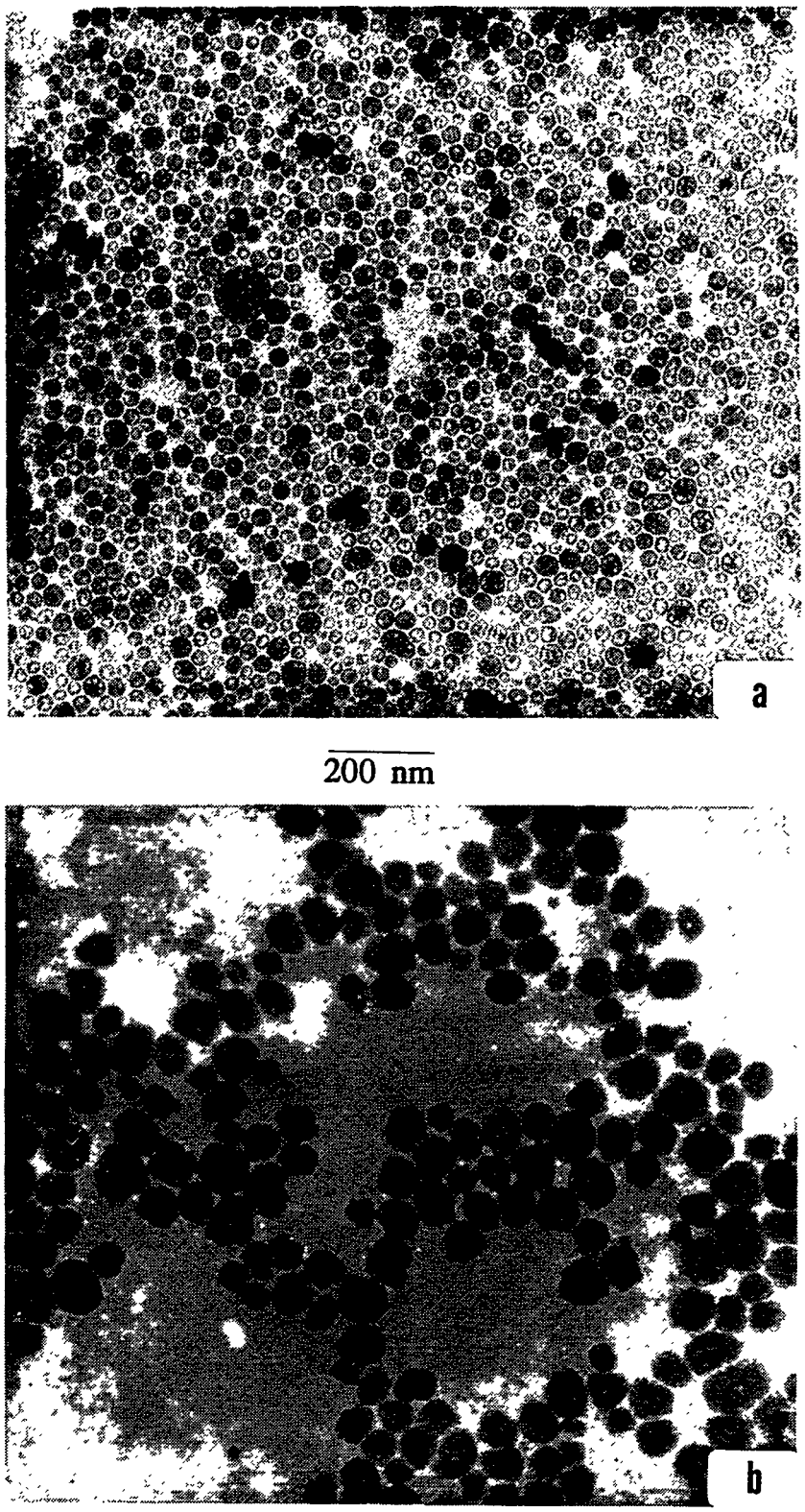

Figure V.14

TEM micrographs of molybdenum sulfide particles prepared in the 0.4 M NP-5/tetralin/hexanol microemulsion:

(a) $[MoS_4^{2-}]=4.5x10^{-5}$ M: (b) $[MoS_4^{2-}] = 1.8x10^{-4}$ M.

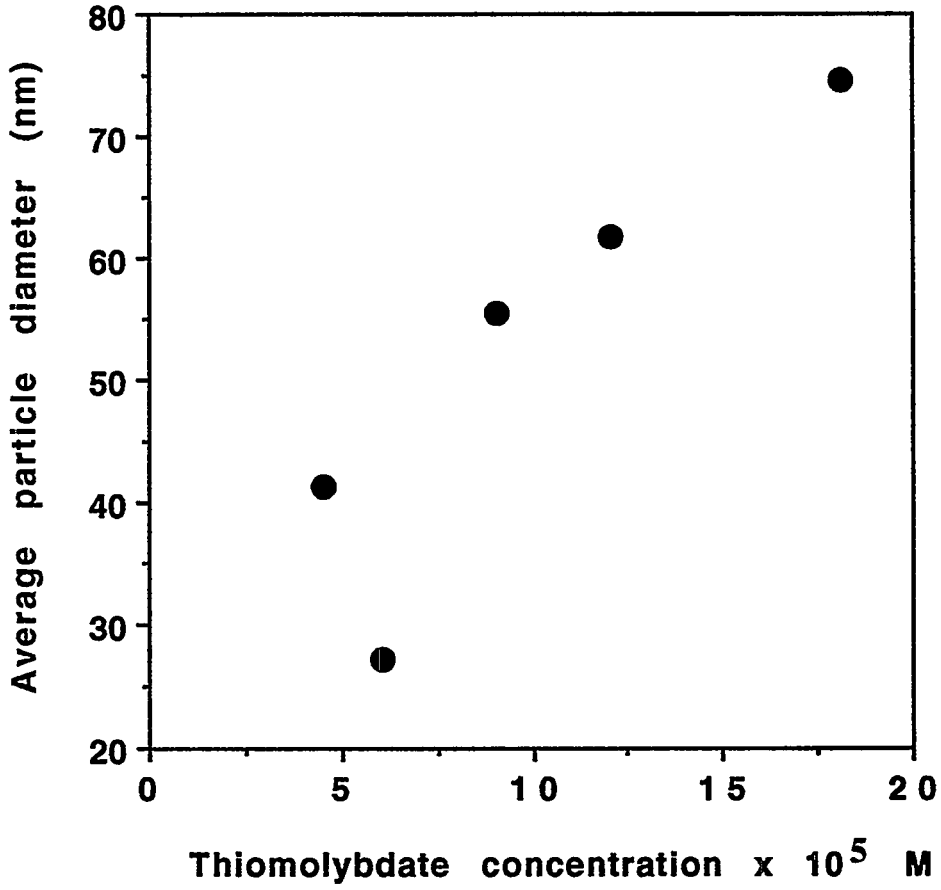

Figure V.15
Effect of ammonium tetrathiomolybdate concentration on the average molybdenum sulfide particle size for the 0.4 M NP-5/tetralin/hexanol microemulsion ($[H_2SO_4] = 4.0 \times 10^{-3}$ M).

An interesting observation worthy of special comment is that the onset of particle aggregation (i.e., the right-hand side of the minima of the plots of average particle diameter versus thiomolybdate concentration) occurs at a lower thiomolybdate concentration for the microemulsion system formulated with hexanol as a co-surfactant compared with that formulated with propanol. This may be explained by considering the interfacial curvature effect in conjunction with the concept of temporary destabilization of the microemulsion system as a result of phase separation (18,19).

For a microemulsion system formulated with a long-chain alcohol as a co-surfactant, the oil/water interface is relatively rigid. The solubilization capacity of the aqueous phase is determined by the size of the natural radius, which decreases as the ionic strength of the polar phase is increased. As discussed in the previous section, the solubilization capacity decreases with increasing ionic strength of the polar domain. Furthermore, since the condition $R>R^o$ corresponds to the onset of phase separation, the extent of temporary destabilization of the microemulsion increases as the ionic strength of the polar domain is increased, hence facilitating aggregation of particles and increasing polydispersity. Also the natural radius of the microemulsion formulated with hexanol is expected to be smaller than that of the microemulsion formulated with propanol, due to the rigidity of the interface of the former microemulsion. Therefore the induction of temporary phase separation is expected to occur at a lower thiomolybdate concentration for the hexanol-based microemulsion system. As a consequence, particle aggregation occurs at a lower thiomolybdate concentration for the former system.

4. SUMMARY AND CONCLUSIONS

Considerable progress has been made in our understanding of particle formation in microemulsions that may be suitable for *in situ* coal liquefaction catalysis. Many of the phenomena observed and explained using cyclohexane-based microemulsions (Chapters 2-5) are observed in tetralin-based microemulsions, and their rationalization follows the same patterns. Further work is required to see whether similar conclusions can be made for microemulsions formulated with coal-liquefaction-compatible surfactants and/or co-surfactants (see Chapter 6).

5. REFERENCES

1. D'Aprano, A., Donato, I.D., Pinio, F. and Turco-Liveri, V., *J. Sol. Chem.* **18**, 949 (1989).
2. Menassa, P. and Sandorfy, C., *Can. J. Chem.* **63**, 3367 (1985).
3. Atik, S.S. and Thomas, J.K., *Chem. Phys. Lett.* **79**, 351 (1981).
4. Leung, R. and Shah, D.O., *J. Colloid Interface Sci.* **120**, 320 (1987).
5. Hou, M.-J. and Shah, D.O., *Langmuir* **3**, 1086 (1987).
6. Auvray, L., *J. Physique Lett.* **46**, 163 (1985).
7. Meunier, J., *J. Physique Lett.* **46**, 1005 (1985).
8. Jada, A.J., Lang, J. and Zana, R., *J. Phys. Chem.* **94**, 381 (1990).
9. Leung, R., Hou, M.J. and Shah, D.O., in "Surfactants in Chemical/Process Engineering" (D.T. Wasan, M.E. Ginn and D.O. Shah, Eds.), Surfactant Science Series Vol. 28, 1988.
10. Shonoda, K. and Lindman, B., *Langmuir* **3**, 135 (1987).

11. Robinson, B.H., Khan-Lodhi, A.N. and Towey, T.F., in "Structure and Reactivity in Reverse Micelles" (M.P. Pileni, Ed.), Elsevier, 1989.

12. Claerbout, A. and Nagy, J.B., in "Preparation of Catalysts V" (G. Poncelet, P.A. Jacobs, P. Grange and B. Delmon, Eds.), Elsevier, 1991, p. 705.

13. Nagy, J.B., *Colloids Surf.* **35,** 201 (1989).

14. Towey, T.F., Khan-Lodhi, A. and Robinson, B.H., *J. Chem. Soc. Faraday Trans.* **86,** 3757 (1990).

15. Chew, C.H., Gan, L.M. and Shah, D.O., *J. Dispersion Sci. Technol.* **11,** 593 (1990).

16. Nielson, A.E., "Kinetics of Precipitation", MacMillan, New York (1964).

17. Hou, M.I. and Shah, D.O., in "Interfacial Phenomena in Biotechnology and Materials Processing" (Y.A. Attia, B.M. Moudgil and S. Chander, Eds.), Elsevier, 1988, p. 443.

18. Barnickel, P., Wokaun, A., Sager, S. and Eicke, H. F., *J. Colloid Interf. Sci.* **148,** 80 (1992).

19. Arriagada, F.J. and Osseo-Asare, K., *Colloids Surf.* **69,** 105 (1992).